

**Development of helix-mimetic scaffolds
as potential disruptors of the interaction between protein
kinase A and A kinase anchoring proteins**

Dissertation

to obtain the academic degree
Doctor rerum naturalium (Dr. rer. nat.)

submitted to the Department of Biology, Chemistry and Pharmacy
of Freie Universität Berlin

by

Gesa Schäfer
from Gifhorn, Germany

01.06.2011

Die vorliegende Arbeit wurde unter Anleitung von

Prof. Dr. Jörg Rademann und Priv. Doz. Dr. Enno Klußmann

in der Zeit vom November 2007 bis Mai 2011 am Leibniz-Institut für Molekulare Pharmakologie (FMP) in Berlin durchgeführt.

Tag der mündlichen Prüfung: 21.10.2011

1. Gutachter: Prof. Dr. Hans-Ulrich Reißig

2. Gutachter: Prof. Dr. Jörg Rademann

Vielen Dank an...

Prof. Dr. Hans-Ulrich Reißig für die freundliche Übernahme des Gutachtens.

Prof. Dr. Jörg Rademann für die intensive Betreuung während meiner Arbeit, die freundliche Aufnahme in seiner Arbeitsgruppe und natürlich auch für die Übernahme des Gutachtens.

Dr. Enno Klussmann und Prof. Dr. Walter Rosenthal für die Möglichkeit, die Arbeit an diesem Thema am FMP in ihrer Arbeitsgruppe durchzuführen. Ich möchte mich auch für die intensive Betreuung und die Freiheit in der Bearbeitung des Themas bedanken.

Christian Schillinger und Dr. Gerd Krause für das computer-unterstützte Design und viele fruchtbare Diskussionen und Gespräche während der letzten drei Jahre.

Dr. Peter Schmieder und Brigitte Schlegel für die Durchführung und Unterstützung von allen Protein-NMR-Messungen.

Dr. Michael Beyermann und seiner Arbeitsgruppe für die Peptidsynthesen und alle Anregungen zu demselben Thema.

die ganze AG Klußman/Rosenthal für drei Jahre spannende Zusammenarbeit, ganz besonders an die Chemie-Abteilung: Carolyn Vargas, Niko Kotzur, Jelena Milic, Adeeb El-Dashan und Sylvia Niquet. Vielen Dank auch ganz besonders an Frank Götz für die Herstellung aller Protein-Proben.

die ganze AG Rademann für alle Unterstützung, die tolle Aufnahme in der Gruppe, und alle Hilfe bei diversen Messungen, Fragen und einige lustige Abende! Vielen Dank ganz besonders an Andre Horatschek (HRMS-Messungen), Richard Raz (Mikrowelle), Katharina Koschek und Johannes Preidl (NMR)!

Zusammenfassung

AKAPs sind eine Proteinfamilie mit ungefähr 50 Proteinen. AKAPs interagieren mit der cAMP-abhängigen Protein Kinase A (PKA) und anderen Signalmolekülen. Die Interaktion mit PKA findet über eine strukturell konservierte, amphipathische α -Helix statt, die R-bindende Domäne (RBD) genannt wird.

Ein Ziel der vorliegenden Arbeit war die Bestimmung der Minimalsequenz des von AKAP18-abgeleiteten Peptids AKAP18 δ -L314E, die für eine spezifische Wechselwirkung mit PKA benötigt wird. Diese Minimalsequenz kann z.B. als zukünftige Basis für die Entwicklung von Peptidomimetika dienen. Zu diesem Zweck wurden verkürzte Peptide von dem 25-mer AKAP18 δ -L314E abgeleitet; für mehrere dieser Peptide konnte in einem *in vitro* assay gezeigt werden, dass sie PKA binden.

In einem alternativen Ansatz sollte mit der Entwicklung von kompetitiven, wirkstoffartigen Hemmstoffen der AKAP-PKA Wechselwirkung begonnen werden. Dazu wurde ein Konzept verwendet, das von Hamilton et al. entwickelt worden ist: Es wurde gezeigt, dass bestimmte aromatische oder heteroaromatische Oligomere als Mimetika des Rückgrats von α -helikalen Peptiden verwendet werden können. Basierend darauf wurde ein funktionalisiertes Quaterpyridine als potentielles α -helikales Mimetikum der RBD von AKAP18 *in silico* entworfen. Die weiteren Ziele dieser Arbeit waren die Synthese von Derivaten der Zielverbindung und die Evaluierung dieser Derivate als Mimetika der AKAP18- RBD.

Die Synthese gliedert sich in zwei Teile. Zunächst wurden die vier funktionalisierten Pyridinbausteine dargestellt. Dann erfolgte die Synthese von Bipyridin- und Terpyridinderivaten mittels Suzuki-Miyaura Kreuzkopplung der einzelnen Bausteine. Dazu wurde unter anderem eine Mikrowellen-unterstützte Prozedur für eine Eintopf Borylierung/Suzuki-Miyaura Kopplung von Bipyridylbromiden mit einem Pyridylchlorid entwickelt. In einer alternativen Synthesestrategie wurden mehrere Terpyridinderivate erfolgreich über eine Ru(II)-katalysierte [2+2+2] Cycloadditionsreaktion dargestellt.

Die bereits dargestellten Terpyridin- und Bipyridinderivate wurden auf ihre Fähigkeit zur spezifischen, AKAP-artigen Wechselwirkung mit PKA untersucht. Dazu wurden STD-NMR- und HSQC-NMR-Messungen durchgeführt. Zwei der synthetisierten Terpyridinderivate zeigten in qualitativen Messungen eine Bindung zu der PKA-Domäne, die die AKAP-Bindungsstelle enthält. Die Quantifizierung der Bindungsaffinität ist der nächste Schritt zur weiteren Charakterisierung dieser Substanzen.

Summary

AKAPs are a family of approximately 50 anchoring proteins which interact *via* specific domains with cAMP-dependent protein kinase A (PKA) and other signalling molecules. The interaction of AKAPs with PKA is mediated through a structurally conserved, amphipathic α -helix termed R binding domain (RBD).

The first aim of the thesis was to determine the minimal length of the amino acid sequence of the high-affinity peptide AKAP18 δ L314E required for specific binding to the AKAP-binding site of PKA as a basis for peptidomimetics and therapeutic exploitation. For this purpose, truncated peptides derived from AKAP18 δ L314E were tested; they retained the ability to bind RII subunits in an *in vitro* assay.

An alternative approach towards competitive disruptors of AKAP-PKA interactions could be the development of drug-like, non-peptidic mimics of RBDs using aromatic oligomers as backbone scaffolds. This concept was recently developed by Hamilton et al. who showed that a chain of certain aromatic or heteroaromatic rings can assemble in a way that allows projection of amino acid residues in a similar geometry as found as in α -helical structures. Based on this work, a highly functionalized quaterpyridine was designed *in silico* as a potential α -helical mimic of the RBD of AKAP18. The second aim of this thesis was the development of a synthesis for this ligand or derivatives thereof.

The synthesis of the derivatives was performed in two steps: First, the functionalized single pyridine building blocks were synthesized. Then, coupling of the single pyridine building blocks by sequential Suzuki-Miyaura cross-coupling reactions was performed. Several bipyridine and terpyridine derivatives of the target scaffold were successfully synthesized. A microwave-assisted two-step, one-pot borylation/Suzuki-Miyaura coupling protocol was successfully developed for the coupling of bipyridyl bromides with pyridyl chlorides. In an alternative procedure, several terpyridine derivatives were successfully synthesized with a [2+2+2] cycloaddition reaction. This procedure was employed to introduce a dihydrocyclopenta[c]pyridine moiety to a bipyridine building block using Ru(II) catalysis. The characterization of the binding ability of selected terpyridines and bipyridine derivatives to PKA was performed with STD-NMR and HSQC-NMR experiments. Qualitative measurements suggested that two terpyridine derivatives bind to the domain of PKA that contains the AKAP-binding site. The quantification of binding affinity will be the next step for the characterization of the compounds.

Contents

Contents	i
Abbreviations	vi
1 Introduction	1
1.1 Protein kinase A and A-kinase anchoring proteins	1
1.2 Structural aspects of AKAP and PKA interactions	2
1.2.1 . AKAP interactions with RII subunits of PKA	3
1.2.2 . AKAP18.....	5
1.3 Pharmacological interference with AKAP-PKA interactions.....	8
1.3.1 . Protein-protein interactions as targets for pharmacological intervention	9
1.3.1.1 Screening for PPI inhibitors.....	9
1.3.1.2 Helix-mimetic approaches.....	10
2 Aim of the thesis	16
3 Results and Discussion	18
3.1 Truncation of AKAP18 δ L314E.....	18
3.1.1 . Identification of truncated peptides which retain ability to bind PKA.....	18
3.1.2 . Characterization and Validation of identified peptides	20
3.2 Synthesis of the quaterpyridine scaffold.....	26
3.2.1 . Synthesis of terpyridines and quaterpyridines	29
3.2.1.1 Pd-catalyzed cross-couplings in the synthesis of oligopyridines	31
3.2.2 . Retrosynthetic analysis of the target scaffold	34
3.2.3 . Synthesis of functionalized pyridine building blocks	37
3.2.3.1 Synthesis of building block 6.....	37
Retrosynthetic analysis and synthetic strategy.....	37
Synthesis of building block 6.....	40
3.2.3.2 Synthesis of building block 7.....	45
Analysis and Synthetic Strategy.....	45
Synthesis of 4-alkylpyridine 7b.....	46

Contents

Alternative synthetic strategy for building block 7.....	46
3.2.3.3 Synthesis of building block 8.....	53
Retrosynthetic analysis and synthetic strategy.....	53
Synthesis of amine 8b.....	54
Retrosynthetic analysis of synthetic route A.....	55
Evaluation of synthetic route A.....	57
Retrosynthetic analysis of synthetic route B.....	62
Evaluation of synthetic route B.....	64
3.2.3.4 Synthesis of building block 9.....	67
Retrosynthetic analysis and synthetic strategy.....	67
Synthesis of 3-(benzyloxy)-2-bromo-5-propylpyridine and 3-(benzyloxy)-2-chloro-5-propylpyridine.....	68
Synthesis of 2-bromo-3-methoxy-5-propylpyridine and 2-chloro-3-methoxy-5-propylpyridine.....	72
3.2.4. Assembly of pyridine-based oligomers.....	76
3.2.4.1 Synthetic strategy.....	76
3.2.4.2 Synthesis of 3-(5-(3-(3-aminopropyl)-6,7-dihydro-5 <i>H</i> -cyclopenta[<i>c</i>]pyridin-1-yl)-2'-carbamoyl-3-methyl-2,3'-bipyridin-5'-yl)-propanoic acid.....	80
Coupling of building blocks 6 and 7.....	80
Development of two-step one-pot borylation/Suzuki-Miyaura cross-coupling procedure.....	84
Development of one-pot coupling procedure for chloride coupling.....	90
Synthesis of terpyridines 22a and 22c.....	95
Deprotection of terpyridines 22a and 22b.....	99
3.2.4.3 Synthesis of terpyridines <i>via</i> [2+2+2] cycloaddition.....	103
Analysis of synthetic strategy.....	103
Synthesis of terpyridine 24a.....	108
Re-functionalization of 12b.....	112
Sonogashira coupling of biimidyl bromides 12c and 12e.....	113
[2+2+2]-cycloaddition with 23b and succinonitrile.....	117
3.2.5 Characterization of compounds.....	121
4 Summary and Outlook.....	126
5 Experimental.....	133

Contents

5.1	Instruments	133
5.1.1	Nuclear magnetic resonance ($^1\text{H-NMR}$; $^{13}\text{C-NMR}$).....	133
5.1.2	Liquid chromatography-mass spectrometry (LC-MS)	133
5.1.3	High resolution mass spectrometry (HRMS).....	133
5.1.4	Infrared spectroscopy (FT-ATR-IR).....	134
5.1.5	Melting point determination	134
5.1.6	Microwave-assisted synthesis	134
5.2	Chromatographic methods.....	134
5.2.1	Thin layer chromatography (TLC).....	134
5.2.2	Column chromatography (CC).....	134
5.2.3	High performance liquid chromatography (HPLC).....	135
5.3	Synthesis	135
5.3.1	Ethyl 3-(6-cyanopyridin-3-yl)propanoate (6b).....	136
5.3.2	Ethyl-3-(6-cyano-5-(trimethylstannyl)pyridin-3-yl)propanoate (6c)	137
5.3.3	Ethyl-3-(6-cyano-5-(tributylstannyl)pyridin-3-yl)propanoate (6d)	138
5.3.4	Ethyl-3-[6-cyano-5-(4,4,5,5-tetramethyl-1,3,2-dioxaborolan-2-yl)pyridin-3-yl]propanoate (6f).....	139
5.3.5	2,5-Dibromo-3,4-dimethylpyridine (7d).....	141
5.3.6	3-(6,7-dihydro-5 <i>H</i> -cyclopenta[<i>c</i>]pyridin-3-yl)propanenitrile (8a)	142
5.3.7	3-(6,7-dihydro-5 <i>H</i> -cyclopenta[<i>c</i>]pyridin-3-yl)propan-1-amine (8b).....	143
5.3.8	<i>N,N</i> -dibenzyl-3-(6,7-dihydro-5 <i>H</i> -cyclopenta[<i>c</i>]pyridin-3-yl)propan-1-amine (8c)	144
5.3.9	<i>N,N</i> -dibenzyl-3-(1-bromo-6,7-dihydro-5 <i>H</i> -cyclopenta[<i>c</i>]pyridine-3-yl)propan-1-amine (8d)	145
5.3.10	<i>N,N</i> -dibenzyl-3-(1-chloro-6,7-dihydro-5 <i>H</i> -cyclopenta[<i>c</i>]pyridine-3-yl)propan-1-amine (8e)	147
5.3.11	(rac)- <i>N,N</i> -dibenzyl-3-chloro-3-(1-chloro-6,7-dihydro-5 <i>H</i> -cyclopenta[<i>c</i>]pyridine-3-yl)propan-1-amine (8l)	149
5.3.12	2,2,2-Trifluoro- <i>N</i> -(3-(6,7-dihydro-5 <i>H</i> -cyclopenta[<i>c</i>]pyridine-3-yl)propyl)-acetamide (8f).....	150
5.3.13	2,2,2-Trifluoro- <i>N</i> -(3-(4-bromo-6,7-dihydro-5 <i>H</i> -cyclopenta[<i>c</i>]pyridine-3-yl)propyl)-acetamide (8g).....	151
5.3.14	3-(4-bromo-6,7-dihydro-5 <i>H</i> -cyclopenta[<i>c</i>]pyridine-3-yl)propan-1-amine (8h)	152

Contents

5.3.15	<i>N,N</i> -dibenzyl-3-(4-bromo-6,7-dihydro-5 <i>H</i> -cyclopenta[<i>c</i>]pyridine-3-yl)propan-1-amine (8i).....	153
5.3.16	<i>N,N</i> -dibenzyl-3-(4-bromo-1-chloro-6,7-dihydro-5 <i>H</i> -cyclopenta[<i>c</i>]pyridine-3-yl)propan-1-amine (8k)	154
5.3.17	3-Bromo-5-benzyloxy pyridine (9c).....	155
5.3.18	1-Propylboronic acid.....	156
5.3.19	3-Benzyloxy-5-propylpyridine (9d).....	157
5.3.20	2-Bromo-3-benzyloxy-5-propylpyridine (9f).....	158
5.3.21	2-Chloro-3-benzoyloxy-5-propylpyridine (9g).....	160
5.3.22	3-Methoxy-5-propylpyridine (9e).....	162
5.3.23	2-Bromo-3-methoxy-5-propylpyridine (9h).....	163
5.3.24	2-Chloro-3-methoxy-5-propylpyridine (9i)	164
5.3.25	Ethyl 3-(5-bromo-2'-cyano-3,4-dimethyl-2,3'-bipyridin-5'-yl)propanoate (12a)	165
5.3.26	Ethyl 3-(6-cyano-5-(5-(3-(3-(dibenzylamino)propyl)-6,7-dihydro-5 <i>H</i> -cyclopenta[<i>c</i>]pyridin-1-yl)-3,4-dimethylpyridin-2-yl)pyridine-3-yl)propanoate (22a)	166
5.3.27	3-(2'-carbamoyl-5-(3-(3-(dibenzylaminopropyl)-6,7-dihydro-5 <i>H</i> -cyclopenta[<i>c</i>]pyridin-1-yl)-3,4-dimethyl-2,3'-bipyridin-5'yl)propanoic acid (25a)	168
5.3.28	Ethyl 3-(5-bromo-2'-cyano-3-methyl-2,3'-bipyridin-5'-yl)propanoate (12b)..	170
5.3.29	Ethyl 3-(2'-cyano-3-methyl-5-(4,4,5,5-tetramethyl-1,3,2-dioxaborolan-2-yl)-2,3'bipyridin-5-yl)propanoate (21b).....	172
5.3.30	Ethyl 3-(2'-cyano-5-(3-(3-(dibenzylamino)propyl)-6,7-dihydro-5 <i>H</i> -cyclopenta[<i>c</i>]pyridine-1-yl)-3-methyl-2,3'-bipyridin-5'-yl)propanoate (22b).....	173
5.3.31	Ethyl 3-(5-(4-chloro-3-(3-(dibenzylamino)propyl)-6,7-dihydro-5 <i>H</i> -cyclopenta[<i>c</i>]pyridine-1-yl)-2'-cyano-3-methyl-2,3'-bipyridin-5'-yl)propanoate (22c)	176
5.3.32	3-(2'carbamoyl-5-(3-(3-(dibenzylamino)propyl)-6,7-dihydro-5 <i>H</i> -cyclopenta[<i>c</i>]pyridin-1-yl)-3-methyl-2,3'-bipyridin-5'-yl)propanoic acid (25b)	178
5.3.33	3-(5-(3-(3-aminopropyl)-6,7-dihydro-5 <i>H</i> -cyclopenta[<i>c</i>]pyridin-1-yl)-2'carbamoyl-3-methyl-2,3'-bipyridin-5'-yl)propanoic acid (26b) and 3-(5-(3-(3-(benzylamino)propyl)-6,7-dihydro-5 <i>H</i> -cyclopenta[<i>c</i>]pyridin-1-yl)-2'carbamoyl-3-methyl-2,3'-bipyridin-5'-yl)propanoic acid (26c)	180

Contents

5.3.34 Ethyl 3-(2'-cyano-5-(hepta-1,6-diynyl)-3-methyl-2,3'-bipyridin-5-yl) propanoate (23a)	183
5.3.35 Ethyl 3-(2'-cyano-5-(3-(2-cyanoethyl)-6,7-dihydro-5 <i>H</i> -cyclopenta[<i>c</i>]pyridin -1-yl)-3-methyl-2,3'-bipyridin-5'-yl)propanoate (24a)	185
5.3.36 3-(5-bromo-2'-carbamoyl-3-methyl-2,3'-bipyridin-5'-yl)propanoic acid (12d)	187
5.3.37 Ethyl 5-(2-(ethoxycarbonyl)ethyl)-3-(5-bromo-3-methylpyridin-2-yl)pyridine-2-carboxylate (12c)	188
5.3.38 Methyl 5-(2-(methoxycarbonyl)ethyl)-3-(5-bromo-3-methylpyridin-2-yl)pyridine-2-carboxylate (12e)	189
5.3.39 Ethyl 5-(2-(ethoxycarbonyl)ethyl)-3-(5-(hepta-1,6-diynyl)-3-methylpyridin-2-yl)pyridine-2-carboxylate (23b)	190
5.3.40 Ethyl 5-(3-(2-cyanoethyl)-6,7-dihydro-5 <i>H</i> -cyclopenta[<i>c</i>]pyridin-1-yl)-5'-(3-ethoxy-3-oxopropyl)-3-methyl-2,3'-bipyridine-2'-carboxylate (24b)	192
5.3.41 Ethyl 5-(3-(3-amino-3-oxopropyl)-6,7-dihydro-5 <i>H</i> -cyclopenta[<i>c</i>]pyridin-1-yl)-5'-(3-ethoxy-3-oxopropyl)-3-methyl-2,3'-bipyridine-2'-carboxylate (27).....	194
5.3.42 3-(6,7-dihydro-5 <i>H</i> -cyclopenta[<i>c</i>]pyridin-3-yl)propanamide	196
5.4 Material and experimental procedures for biological assays.....	197
5.4.1 . Material.....	197
5.4.1.1 Buffers.....	197
5.4.1.2 Peptides	198
5.4.1.3 Proteins.....	198
5.4.1.4 Equipment.....	199
5.4.2. Experimental procedures.....	199
5.4.2.1 Peptides SPOT array synthesis	199
5.4.2.2 RII overlay	199
5.4.2.3 Circular dichroism measurements.....	200
5.4.2.4 Saturation transfer difference nuclear magnetic resonance (STD-NMR) .	200
5.4.2.5 ¹ H, ¹⁵ N-heteronuclear single quantum coherence (HSQC)-NMR).....	201
6 References.....	202
List of figures.....	210
Attachment.....	215

Abbreviations

AC	adenylyl cyclase
ACN	acetonitrile
AcOH	acetic acid
AKAP	A kinase anchoring protein
AQP2	aquaporine 2
B ₂ Pin ₂	bis(pinacolato)diboron
BuLi	<i>n</i> -butyllithium
cAMP	<u>cyclic adenosine monophosphate</u>
cat	catalytical
CD	circular dichroism
Cp	cyclopentadienyl
Cp*	pentamethylcyclopentadienyl
cod	cyclooctadiene
d	doublet
δ	chemical shift
DCC	dicyclohexylimide
1,2-DCE	1,2-dichloroethane
DCM	dichloromethane
D/D domain	dimerization and docking domain
DEE	diethyl ether
DMAE	<i>N,N</i> -(dimethylamino)ethanol
DMAP	4-(dimethylamino)-pyridine
DMF	dimethylformamide
DMSO	dimethylsulfoxide
eq	equivalents
ESI-MS	electrospray ionisation-mass spectrometry
EtOAc	ethyl acetate
EtOH	ethanol
GPCR	G protein coupled receptor
HPLC	high performance liquid chromatography
HMBC	heteronuclear multiple bond coherence
HMQC	heteronuclear multiple quantum coherence

Abbreviations

HRMS	high resolution mass spectrometry
HSQC	Heteronuclear Single Quantum Coherence
λ	wavelength
LDA	lithium diisopropylamide
LC	liquid chromatography
KOtBu	potassium- <i>t</i> -butoxide
M	molarity
m	multiplet
MeOH	methanol
MS	mass spectrometry
NBS	<i>N</i> -bromosuccinimide
NEt ₃	triethylamine
NMR	nuclear magnetic resonance
PCy ₃	tricyclohexylphosphine
PDB	protein database
PDE	phosphodiesterase
pH	potentia hydrogenii
PKA	protein kinase A
PPh ₃	triphenylphosphine
ppm	parts per million
P(<i>t</i> Bu) ₃	tri- <i>t</i> -butylphosphine
RBD	R binding domain
RIIBD	RII binding domain
R _f	retention factor
rt/RT	room temperature
s	singlet
Ser	serine
SPhos	2-Dicyclohexylphosphino-2',6'-dimethoxybiphenyl
SPPS	solid phase peptide synthesis
STD	saturation transfer difference
t	triplet
TFA	trifluoroacetic acid
THF	tetrahydrofuran
Thr	threonine

Abbreviations

TLC	thin layer chromatography
TMP	2,2,6,6-tetramethylpiperidine
t_R	retention time
XPhos	2-Dicyclohexylphosphino-2',4',6'-triisopropylbiphenyl

1 Introduction

1.1 Protein kinase A and A-kinase anchoring proteins

Protein kinase A (PKA) is a cAMP-dependent kinase that is ubiquitously expressed in all cell types and tissues. PKA is a Ser/Thr kinase and phosphorylates a number of target proteins containing PKA phosphorylation consensus sequences.^[1-4]

The enzyme plays a central role in cAMP-dependent signal transduction pathways which are vital for transducing stimuli from the cellular environment into a specific cellular response. In general, the cAMP pathway is activated upon binding of an agonist to a G-protein coupled receptor (GPCR), which in turn leads to activation of adenylyl cyclases (AC).^[5;6] This results in an increase in the concentration of the second messenger cAMP^[2;5;6] which activates PKA and other signaling molecules.^[1;7]

The PKA holoenzyme is a hetero-tetramer which consists of a dimer of regulatory subunits and two catalytic subunits.^[3;4] Upon cooperative binding of four cAMP molecules to the R subunit dimer the catalytic subunits are released from the holoenzyme and phosphorylate target substrates.^[3;4;8] In figure 1.1 a schematic view of the R subunit structure is depicted. R subunits consist of a dimerization and docking (D/D) domain followed by a linker region with a PKA inhibitor site that maintains the catalytic subunits inactive, and a tandem repeat of cAMP binding domains.^[9;10]

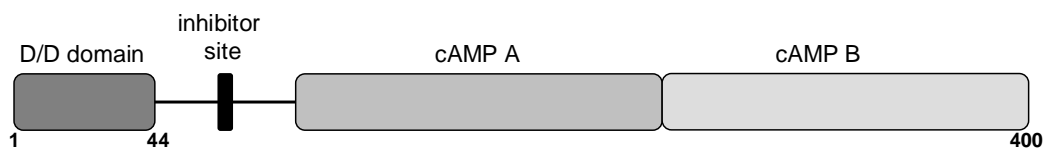


Figure 1.1: Schematic representation of the structure of an R subunit protomer. Adapted from ^[9].

There are two types of R subunits termed RI and RII which can be further divided into α - and β -subtypes; these R isoforms differ e.g. in tissue distribution and biochemical properties. RII subunits are preferentially localized at distinct cellular loci^[1;11] while RI subunits are usually considered to be localized in the cytosol.^[12]

The cAMP/PKA pathway controls a plethora of physiological processes. Therefore, a tight spatiotemporal control of PKA-activity is vital in order to ensure a specific cellular response to each of the different stimuli cells perceive.^[1;7] It is believed that this tight control of PKA activity is ensured through compartmentalization of PKA by A-kinase anchoring proteins (AKAPs).^[1;11;13]

AKAPs are a family of scaffolding proteins with around 50 members. These proteins localize PKA to distinct sites within the cell. The defining characteristic of an AKAP is the presence of an R-binding domain (RBD). The RBD is an amphipatic α -helix of 14 to 18 amino acids that binds to the D/D domain of the R subunit dimer.^[1] Apart from an RBD, AKAPs possess an anchoring domain that targets the AKAP to a specific subcellular location. AKAPs can be placed roughly into three categories: RI-specific, RII-specific or dual-specific depending on their specificity for the different PKA R subunit isoforms.^[8;9]

In addition to PKA-anchoring, several AKAPs have been suggested to serve as scaffolding proteins that coordinate signaling processes. For this purpose, AKAPs form supramolecular complexes through interactions with other signaling molecules/proteins.^[7;13] This co-localization of proteins and molecules that are involved in the regulation of cAMP-dependent signal transduction is an additional mechanism contributing to the specific control within this pathway.

1.2 Structural aspects of AKAP and PKA interactions

Structural data on full length AKAP proteins are very scarce. This is due to the large size of many AKAPs, e.g. AKAP450 (450 kDa) or AKALbc (309 kDa). In addition, AKAPs are often associated with membranes and other proteins. Therefore, additional signaling molecules may be required in order for an AKAP protein to adopt an ordered structure which would be a prerequisite for a structural analysis. Today there is only one resolved full length AKAP structure known, that of the protein GSKIP which was recently identified as an AKAP by our group.^[14;14;15] The structure of GSKIP was resolved by NMR analysis by the Northeast Structural Genomics consortium (PDB code: 1SGO).^[14;15]

The molecular determinants of AKAP-PKA interactions were studied mostly using AKAP-derived peptides comprising only the RBD of an AKAP and the D/D domain of RII α or RI α subunits. In the following chapter only the interaction of the RII α D/D

domain with RBD-derived peptides will be discussed, because AKAPs interact preferentially with RII subunits.

1.2.1 AKAP interactions with RII subunits of PKA

The RII-binding domains (RIIBDs) of AKAPs have no obvious consensus sequence and a low sequence identity of <30%; instead there is a unifying secondary structural motif as a conserved feature in different AKAPs.^[16]

AKAP		Sequence
AKAP1	(D-AKAP1)	GLDRNEEIKRAAFQIISQVISEATE
AKAP2	(AKAP-KL)	DDPLEYQAGLLVQNAIQQAIAEQVD
AKAP3	(AKAP110)	NLVIAMARKEINEKIDGSENKCVYQ
AKAP4	(AKAP82)	SIDDLFSFYVNRSLSLVIQMAHKEIK
AKAP5	(AKAP79/75/150)	YETLLIETASSLVKNAIQLSIEQLV
AKAP6	(mAKAP)	KDAEDCSVHNFVKEIIDMASTALKS
AKAP7	(AKAP18)	PEDAELVRLSKRLVENAVLKAVQQY
AKAP8	(AKAP95)	KETPEEVAADVLAEVITAAVRAVDG
AKAP9	(AKAP350)	YQEQLIEEVAKVIVSMSIAFAQQTE
AKAP9	(Yotiao)	NLQKIVEEKVAAALVLSQIQLEAVQE
AKAP10	(D-AKAP2)	GNTDEAQEELAWKIAKMIVSDVMQQ
AKAP11	(AKAP220)	VNLDKKAVLAEKIVAEAEIEKAEREL
AKAP12	(Gravin)	GILELETKSSKLVQNI IQTAVDQFV
AKAP13	(AKAP-Lbc)	KGADLIEEAASRIVDAVIEQVKAAG
AKAP14	(AKAP28)	TQDKNYEDEL TQVALALVEDVINYA
GSKIP		TDMKDMRLEAEAVVNDVLFVNNMF
MAP2		ETAEEVSARIVQVVTAEAVAVLKGE
Rab32		NINIEEAARFLVEKILVNHQSPNE
AKAP-IS	(peptide)	QIEYLAKQIVDNAIQQA
SuperAKAP-IS	(peptide)	QIEYVAKQIVDYAIHQQA
RIAD	(peptide)	LEQYANQLADQIIKEATE

Table 1.1: Alignment of RII-binding domains of the indicated AKAPs. The conserved hydrophobic aliphatic amino acid residues are indicated in grey. AKAP-IS, SuperAKAP-IS and RIAD are peptides that were identified through a combination of *in silico* design and substitution analysis as AKAP-like high-affinity binders of R subunits. Adapted from ^[13].

When aligning R-binding regions of known AKAPs, a common pattern of alternating pairs of hydrophobic and hydrophilic residues that have a high probability to form amphipathic α -helices emerges. In an ideal α -helix, one turn of the helix consists of 3.6 amino acids. Therefore, the amino acid residues i , $i+4$, $i+7$, $i+11$ and so forth are usually placed on the same face of the α -helix. Amphipathic helices are characterized by having an hydrophobic face on one side of the helix which is made up by unpolar

amino acid residues and a hydrophilic face that is made up by polar or charged residues. The amphipathic nature of an α -helical peptide can be visualized by helical wheel analysis in which the amino acids are rotated around the helical axis successively in a 100° angle to each other. *In silico* helical wheel analysis was used to identify regions with high probability to form an amphipathic α -helix in order to find potential RIIBDs on AKAPLbc (Ht31 and Ht21). Peptides representing the anticipated RIIBDs were shown to bind RII α subunits of PKA.^[16]

It was validated by NMR and crystallographic analysis that the AKAP-derived peptides adopt α -helical secondary structures in complex with the RII α D/D domain.^[8;9;17;18] The structural analysis of the interaction with the D/D domain of RII α was performed with peptides comprising the RIIBD of AKAPLbc (residues 493-515), of AKAP79 (residues 392-413), of D-AKAP2 and with the peptide AKAP-*IS* which has been designed *in silico* as a RII-binding peptide with high-affinity.

The structures showed that the two protomers of the D/D domain form an X-type four-helix bundle that creates a shallow, hydrophobic groove into which the AKAP peptides dock. The protomers are arranged antiparallel to each other as depicted schematically in figure 1.2.^[8;9;17;18]

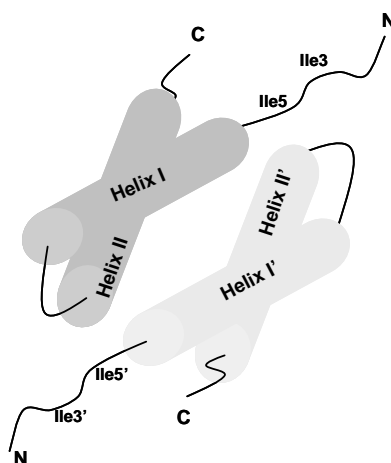


Figure 1.2: A schematic view on top of the AKAP-binding site of the D/D domain of RII α . Two protomers depicted in light and dark grey are arranged in an antiparallel manner thereby forming the characteristic X-type four-helix bundle. Also displayed are the unordered N-terminal tails of the protomers as well as the residues Ile3, Ile3', Ile5 and Ile5' which are involved in binding of RIIBD-derived peptides. Adapted from ^[9].

The RIIBD-derived peptides are positioned diagonally over one face of the D/D domain and the interaction surface between both interaction partners is shielded from the solvent (figure 1.3).

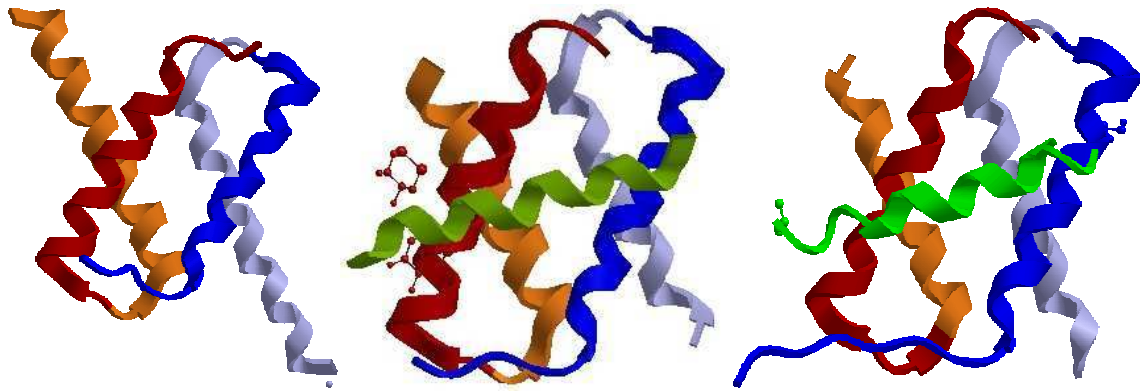


Figure 1.3: Models derived from the corresponding x-ray structures showing the D/D domain from RII α with different AKAP peptides. *Left:* apo structure (PDB code 2IZY). *Middle:* D/D domain and AKAP-IS (PDB code 2IZX). *Right:* D/D domain and D-AKAP2 peptide (PDB code 2HWN). The two RII α protomers are shown in red and blue respectively, RIIBD peptides are depicted in green.

Binding into the hydrophobic groove of the D/D domain is mediated by hydrophobic aliphatic residues which validated the earlier helical wheel analysis of RIIBDs.^[16] Binding of an AKAP peptide to the D/D domain induces asymmetry into the complex through the interaction of the peptide with one of the N-terminal tails. The N-terminal tails of the RII α D/D domain are not ordered in the absence of an RIIBD-derived peptide. Through the interaction with the AKAP peptide, amino acids Ile3 and Ile5 of one N-terminal tail become ordered while the amino acids stay unstructured in the N-terminus of the second protomer.^[8;9]

For the peptide AKAP-IS in addition to hydrophobic interactions with the D/D domain also several H-bonding interactions (Asp14/Thr10'; Gln19/Gln14; Asn15/Thr10') and intramolecular salt bridges that stabilize the peptide helix are proposed from analysis of the x-ray data^[8] while there is no evidence for H-bonding found for the AKAP-derived peptides Ht31, AKAP79 and D-AKAP2.^[9;17;18]

X-ray and NMR analysis indicate that only side chain residues of RBD-derived peptides mediate the interaction and contributions from the backbone through helix-helix interactions appear negligible.^[8;9;17;18]

1.2.2 AKAP18

The AKAP18 protein family consists of the splice variants α , β , γ and δ that contain a conserved RIIBD. AKAP18 isoforms are involved in a variety of different cellular processes including the arginine vasopressin-induced (AVP) AQP2-shuttle in renal

cells (AKAP18 δ) or glucose-stimulated insulin release (AKAP18 α and γ). AKAP18 δ has been shown to be also involved in the control of cellular processes in the heart in cardiac myocytes.^[13;19]

The isoform AKAP18 δ is a 353 amino acid long high-affinity AKAP and recently, a partial crystal structure which contains amino acids 76 to 292 of the protein has been resolved (AKAP18 δ^{CD} ; PDB code: 2VFL).^[20] This structure did not contain the RIIBD of the protein. Therefore, there is no information on secondary or tertiary structure assumed by the RBD in its native environment. Sequence alignments suggested that AKAP18 δ^{CD} contains a His-X-Thr motif which is a characteristic of the 2H-phosphoesterase family. Co-crystallization with 5'AMP and 5'CMP revealed binding of these nucleotides to the His-X-Thr motif suggesting that it has some physiological relevance.^[20] However, the function of this motif in AKAP18 δ needs further elucidation.

The RIIBD of AKAP18 δ comprises amino acid residues 292 to 321. Peptides containing this sequence as well as an N-terminally truncated AKAP18 δ protein (residues 124 – 353) bind with higher affinity to RI α than the full length protein AKAP18 δ .^[21-23] This suggested that in order for AKAP18 δ to bind to PKA, the protein has to undergo a conformational change. This conformational change might involve the N-terminal domain of AKAP18 δ ; for example, to make the hydrophobic and therefore probably partially buried RIIBD accessible for binding.^[13]

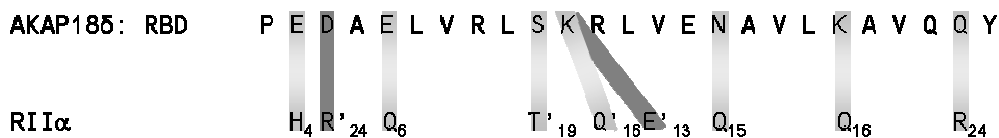


Figure 1.4: A schematic representation of potential H-bonding interactions (depicted in shaded light grey) and salt bridges (depicted in dark grey) between the RIIBD of AKAP18 and the D/D domain of RI α . The residues of the two protomers of the D/D domain are distinguishable by presence and absence of apostrophes. Adapted from ^[13].

The RIIBD of AKAP18 binds RI α subunits with subnanomolar affinity ($K_D = 0.4$ nM). Sequence alignments showed a similar number and distribution of hydrophobic amino acid residues as found in other AKAPs that bind RI α with significantly less affinity. Therefore, it seemed likely that hydrophobic contacts were not the only type of interaction contributing to this high-affinity binding.^[21]

1 Introduction

Peptides comprising the RII binding sequence of AKAP18 δ were studied using peptide spot array technology and RII-overlay techniques in order to elucidate the role of non-hydrophobic interactions to binding with RII α .^[21] The results confirmed the critical role of small, aliphatic residues for binding of the RIIBD of AKAP18 to RII α . Moreover, binding was diminished upon introduction of helix-distorting Pro residues. Based on the results from the substitution analysis, from *in vitro* assays of several AKAP18 δ -derived peptides and based on the data from the NMR structures of the RII α D/D domain with various other AKAP-derived peptides, a model structure was calculated. In Figure 1.4 amino acid residues from AKAP18 δ and RII α are highlighted that potentially form H bonds or salt bridges with each other thereby probably contributing to high-affinity binding.^[21] In addition, it was found in this study that an exchange of the hydrophobic residue Leu-314 (number of the amino acid residue is based on the position of that amino acid in full length AKAP18 δ) with a more hydrophilic Glu residue yields a peptide with similar affinity to RII α and an increased solubility in aqueous solutions as compared to the wildtype peptide.

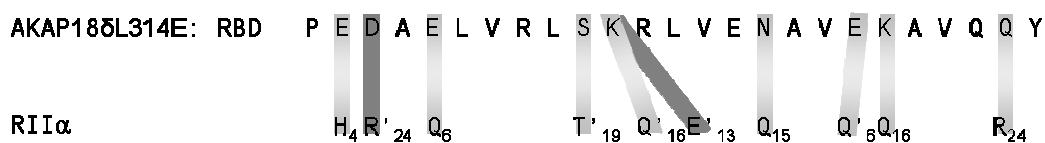


Figure 1.5: A schematic representation of potential H-bonding interactions (depicted in shaded light grey) and salt bridges (depicted in dark grey) between the peptide AKAP18 δ -L314E and the D/D domain of RII α . The residues of the two protomers of the D/D domain are distinguishable by presence and absence of apostrophes.

The interaction of the peptide AKAP18 δ -L314E with the D/D domain of RII α was also modeled. In Figure 1.5, amino acid residues from the peptide AKAP18 δ -L314E and RII α are highlighted that have been proposed to contribute to binding via H-bonding or salt bridges.^[21] In addition to the interactions proposed for the RIIBD of AKAP18 δ , one additional H-bonding interaction of Glu-314 is predicted based on the calculated structure.^[21]

1.3 Pharmacological interference with AKAP-PKA interactions

In order to understand the role of AKAP-PKA interactions in the cellular response to different extracellular stimuli several studies have employed the above described AKAP-derived peptides. RII binding peptides were used *in vivo* and *in vitro* assays as tools that prevent PKA anchoring.^[1;13;24] For example, the open-probability of L-type Ca^{2+} channels in cardiac myocytes increases when they are phosphorylated by PKA. This takes place in response to β -adrenergic stimulation of the cells and leads to an intracellular increase in Ca^{2+} -concentration. Upon treatment of cardiac myocytes with the AKAP-derived peptides Ht31 and AKAP18-derived peptides this increase in intracellular Ca^{2+} -concentration after β -adrenergic stimulation was prevented. This suggested that PKA-anchoring is required for the specific cellular response in this pathway.^[21-23] Similar studies with AKAP-derived peptides established the role of PKA-anchoring in various other cellular functions in different types of cells and tissues.^[1;13;25]

One of the major drawbacks of using peptides as pharmacological tools is their susceptibility to proteolytic degradation. In addition, peptides are highly charged, high-molecular weight compounds that usually do not readily penetrate plasma membranes.^[26] This makes their applicability as pharmacological tools in cell-based assays and animal models difficult.

Nonetheless, the use of peptidic disruptors of AKAP-PKA interactions has revealed the relevance of this interaction in several pathological processes, and suggested that inhibition of AKAP-PKA interactions is a potential new therapeutic approach, for instance towards treatment of chronic heart failure.^[27] In order to study the functional role of AKAP-PKA interactions in animal models and to validate these interactions as drug targets, the identification of non-peptidic, small molecules that inhibit the interaction between AKAPs and PKA would be desirable. Moreover, small molecules could be useful starting points for the development of drugs targeting PKA-AKAP interactions.

1.3.1 Protein-protein interactions as targets for pharmacological intervention

The interaction between AKAPs and PKA is one example for a protein-protein interaction (PPI). Protein-protein interactions are an emerging target class for the development of potentially highly-specific pharmacological tools and drugs. The term small or drug-like molecules in this work refers to compounds that in principle follow Lipinski's rule of five; i.e., molecular weight < 500 Da, max. 5 H-bond donors and 10 H-bond acceptors, $\text{clog}P < 5$ (in octanol/water).^[28]

Compared to the classic targets of drug intervention like enzymes, receptors, ion channels and ion pumps with defined binding pockets for endogenous ligands which can be used as a structural basis for drug-like molecules^{[29],[30]}, targeting PPI with small molecules is less straightforward. The interaction surface and binding contacts of two proteins are usually spread over a larger surface and often no deep, restricted binding pockets as found e.g. in enzymes are present. Instead, the interaction surface is shallow, amphiphilic, without specific features and often flexible.^[26;28;31] Nonetheless, it has been found for many PPIs that the major binding free energy of an interaction stems from a few key amino acid residues, the so-called binding hot spots of the interaction.^[32]

Several strategies have been successfully employed for the development of different types of protein-protein interaction inhibitors. For PPI involving α -helical interaction partners these approaches can be divided into (1) screening approaches^[29] and (2) helix-mimetic approaches.^[33;34] With both strategies small molecules that exhibit drug-like properties and inhibit PPIs have been identified.

1.3.1.1 Screening for PPI inhibitors

Screening methodologies have been widely established in drug discovery and have also been shown useful for PPI-targets.^[28;29] High-throughput screening (HTS) has been successfully used to identify hit compounds for the design of PPI inhibitors. For example, the interaction between the proteins p53-*hDM2* has been suggested as a potential target for novel cancer therapeutics.^[26;28] Small-molecule inhibitors of this interaction, the so-called nutlins, were initially found by HTS.^[26;28]

For cases in which no detailed structural information about the respective PPI is available, HTS can be a useful starting point for hit discovery. With regard to AKAP-PKA interactions this could be an appealing approach, because not much structural information on full length AKAP proteins is available.^[13] Indeed, successful identification of small molecule AKAP-PKA interaction inhibitors using an ELISA-based screening of a library with 20,000 compounds was reported recently.^[27]

In fragment-based drug discovery, libraries containing small molecules (100-300 Da) are screened for weak affinity binders that are subsequently chemically linked yielding ideally a higher-affinity ligand.^[26;35;36] Fragment-based screening usually employs biophysical methods for screening, like X-ray crystallography or 2D-NMR methods ("SAR-by-NMR")^[37] in which ligand binding is detected. Biophysical methods are usually supported with data from biochemical and if necessary cell-based assays at every optimization step.^[29;35]

Screening approaches can be especially valuable tools to identify allosteric inhibitors of PPIs. Allosteric inhibitors of PPIs might not be accessible using structure-based drug design approaches as binding cavities for allosteric inhibitors may not be predictable by structure-based approaches. They might not be localized close to the actual interaction site or they are inducible upon binding only and not easily localized from e.g. static crystal structures.^[29;38]

An *in silico* screening of virtual ligand libraries requires solid structural data for predicting binding pockets and for reliable docking of small molecules into the target structure. Therefore, this approach is structure-based. It has been successfully applied for example as a starting point for the development of sulfonamide-based small molecule inhibitors of the interaction between p53 and hDM2.^[26]

1.3.1.2 Helix-mimetic approaches

All helix-mimetic approaches are structure-based and detailed information about the binding interface of the protein-protein interaction that is to be targeted is required. With regard to AKAP-PKA interactions, there are structural data available, although it is restricted to the direct interaction between the D/D domain of R subunits and AKAP-derived peptides.^[8;9;17;18]

The basic idea behind an helix-mimetic approach is that the binding epitope of one of the interaction partners is transferred from the corresponding protein onto another scaffold that is considered to be suitable as pharmacological tool or drug.^[34] For this purpose, a motif that allows a spatial arrangement of the binding epitope as found in the native structure has to be identified.^[38;39]

The most straightforward way to achieve this is to use a short peptide as scaffold that contains the hot spot amino acids. Although peptide secondary structure is usually lost when taken from the surrounding protein onto short peptides of 15-20 amino acids,^[39] α -secondary structure can often be induced in a short peptide upon binding to the target protein. An example for the successful use of short peptides derived from one of the binding partners as PPI inhibitors are the RIIBD-derived peptides described in the previous chapter.^[40-42] Some of these peptides have even better affinity to the target protein than the original binding partner.^[21]

As already mentioned, one of the major drawbacks when using peptides as pharmacological tools, is their susceptibility to proteolytic degradation. In several recent examples this problem has been successfully overcome: For example, Torheim et al. showed that introduction of non-natural amino acids into certain positions of a peptide that binds to RI subunits of PKA increased stability in serum about 50-fold as compared to the unmodified peptide.^[25]

Introducing conformational restraints to strengthen the α -helical structure of short peptides is another approach to increase stability and affinity in many cases. Through suitably arranged intramolecular linkers with e.g. lactam or disulfide bridges between side chain residues, sterically restrained macrocyclic peptides can be generated.^[38;39] In one example, an alkene-linker between two amino acids was placed on the same, non-interacting face of the helix. Closing of the tether was achieved by Ru-catalyzed metathesis of two reactive, terminal alkenes that are incorporated into the peptide through corresponding α,α -disubstituted amino acids.^[43;44] This approach yielded peptidomimetic structures for inhibition of different PPI with increased potency and proteolytical stability as compared to the original peptides.^[45;46]

Apart from standard peptides other oligomeric scaffolds with increased proteolytic and metabolic stability have also been applied or designed as potential α -helix mimetics. For example, retro-inverso peptides, peptoid or β -hairpin scaffolds yielded PPI inhibitors for the p53-*hDM2* interaction.^[26;34;47] Another potential oligomeric

scaffold for helix mimetics are β -peptides consisting of β -amino acids. β -amino acids contain an additional methylene group between the carboxylic acid and the amino functionality. A careful arrangement of constrained and acyclic β -amino acids can create well-defined, distinct structures.^[48] β -peptides as well as chimeric α/β - and $(\alpha/\beta+\alpha)$ -peptides have been used as backbone scaffolds for helical PPI inhibitors.^[48;49]

All of the described oligomeric scaffolds stabilize secondary structure, show an increased resistance towards enzymatic degradation and their synthesis is generally established and automatable. However, the resulting molecules are still highly charged, have a high molecular weight and usually do not penetrate plasma membranes.^[26] This makes their applicability as pharmacological tools in cell-based assays and animal models difficult.

Recently, the concept of employing linear, aromatic oligomers for mimicking recognition patterns of helical peptide sequences was reported.^[50] The initially designed 3,2',2''-trisubstituted terphenyl derivative is - as compared to previously reported oligomers - a reduced, small-molecule type of scaffold. It was confirmed in computational studies and x-ray analysis that substituents are arranged in a way similar as found for residues i , $i+3/4$ and $i+7$ on one face of an α -helix, with the aromatic rings placed in a staggered conformation.^[50] The terphenyl scaffolds were assembled using Negishi or Suzuki-Miyaura cross-coupling.^[51]

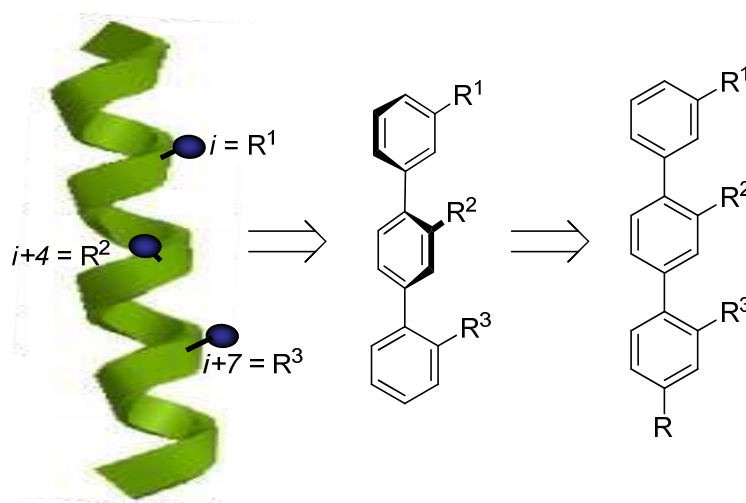


Figure 1.6: Schematic representation of the terphenyl scaffold that has been employed as α -helix-mimic. Adapted from ^[52].

With the original terphenyl scaffold depicted in figure 1.6 different PPIs were successfully targeted.^[50;51;53;54] For example, the p53-*hDM2* and the Bcl-X_L/Bak interaction were inhibited both *in vitro* and in cell culture experiments.^[55] The interaction of Bcl-X_L/Bak is involved in regulation of apoptosis and has been suggested as target for novel cancer therapeutics.^[53] Due to their hydrophobicity, selectivity of these compounds should be carefully evaluated in order to exclude unspecific binding to hydrophobic areas of random proteins.^[26]

Several new scaffolds were developed based on this idea. They were designed to exhibit a better profile with regard to hydrophobicity/solubility and synthetic accessibility. Some of the additional backbones have, for example, a more polar backbone, like the pyridine-based oligomer^[52] **1a** or terphthalimide^[53] and benzoylurea^[56] scaffolds **1c** and **1d** which are depicted in figure 1.7. For the latter two, polar H-bonding networks were included in the structure that form a similar geometric projection of substituents as in α -helices. These scaffolds have also the advantage of better synthetic accessibility.

A terphthalimide-based PPI-inhibitor has also been successfully used in a cell-based assay for inhibition of the Bcl-X_L/Bak interaction.^[53] Also, a diphenylindane scaffold was developed to mimick additional side chain residues as compared to the terphenyl scaffold.^[57]

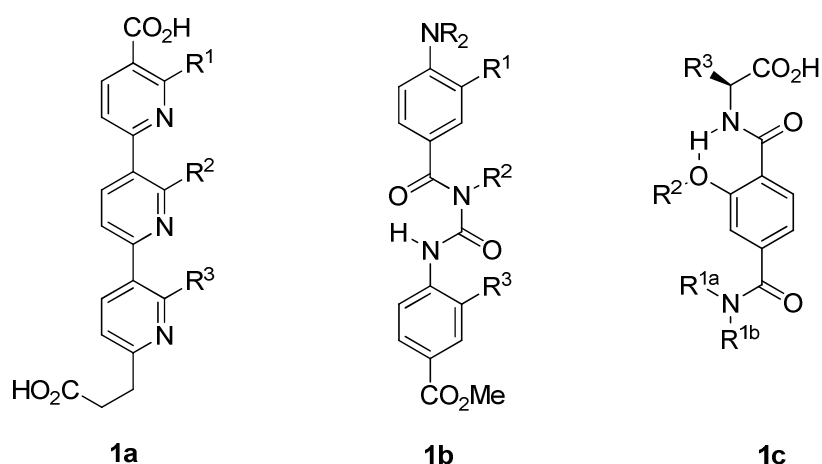


Figure 1.7: Backbone scaffolds that were proposed as potential mimetics of the peptidic α -helix. The scaffolds depicted in this scheme were developed by Hamilton et al.^[52;53;56]

Further research resulted in the identification or suggestion of other types of aromatic oligomers and hetero-oligomers (i.e., containing different aryls as central scaffold) as α -helix mimetics, some of which are depicted in figure 1.8.

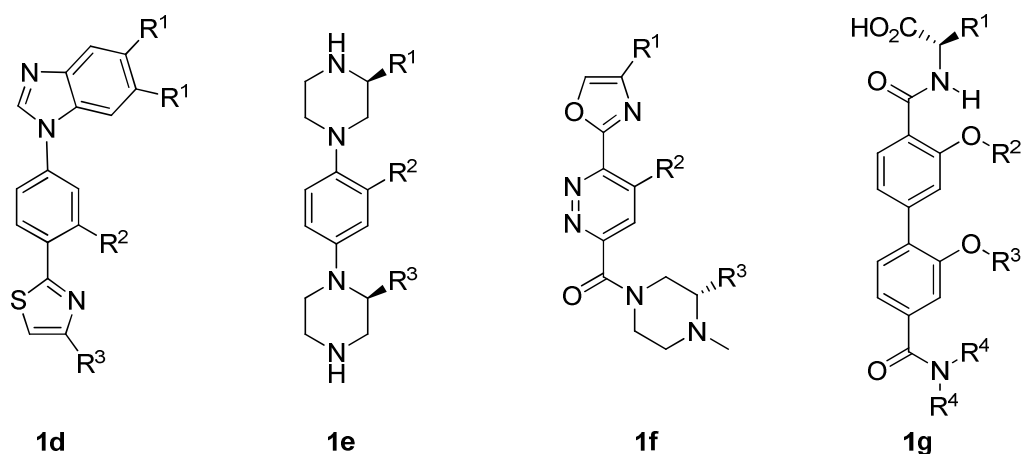


Figure 1.8: Backbone scaffolds that were proposed as potential mimetics of the peptidic α -helix with lower hydrophobicity as compared to the terphenyl scaffold. These types of compounds were developed by Hamilton et al. (**1d**, **1g**),^[58;59] Rebek et al. (**1f**)^[60] and König et al. (**1e**).^[34]

For example, several hetero-oligomeric structures were developed with lower hydrophobicity and easier synthesis as compared to the terphenyl scaffold. Rebek et al. developed pyridazine-based amphiphilic scaffolds **1f** with an hydrophobic face for protein binding and a hydrophilic face for interaction with solvent ("wet-edge") to increase solubility and decrease entropic penalty upon binding.^[60;61] Some derivatives showed inhibitory potency for the Bcl-X_L/Bak interaction, although in a weaker range as found for the terphenyl-based compounds. The Hamilton group reported 5-6-5 imidazole-phenyl-thiazole and biphenyl-4,4'-dicarboxamide scaffolds **1d** and **1g** with the latter being useful to mimic extended helices (residues *i*, *i*+3, *i*+7 and *i*+11).^[58;59;62]

In addition, based on structural analysis, several backbone scaffolds were suggested by the groups of Koenig, Rebek and Marshall which have so far not been further evaluated against PPI targets. In addition to improved synthetic accessibility and hydrophobic profile as compared to the terphenyl scaffold, stereocenters can be introduced into the piperazine-containing scaffolds **1e** and **1f** which could lead to better or more specific ligands later on since PPI targets are inherently chiral.^[34;63]

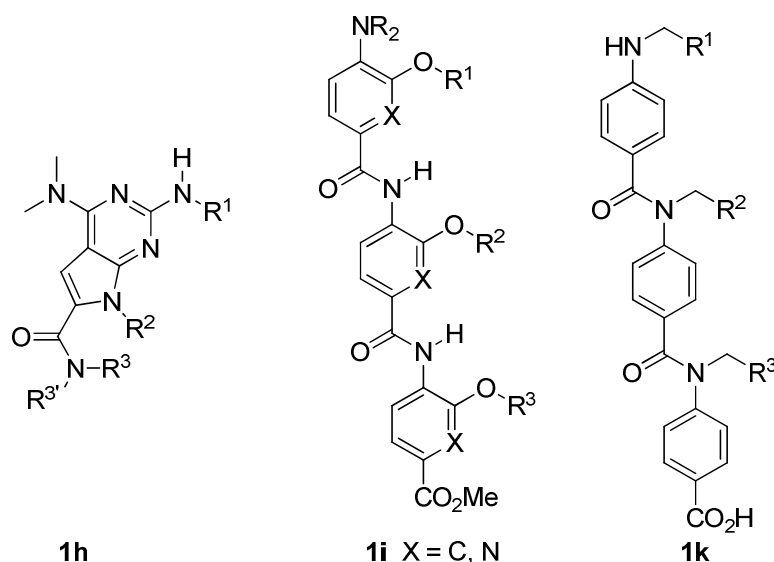


Figure 1.9: Backbone scaffolds that were proposed as potential mimetics of the peptidic α -helix with proposed better synthetic accessibility as compared to the terphenyl scaffold.

Pyrrolopyrimidine-based scaffold **1h** was used in a solid phase approach with which a library of 900 compounds was synthesized to target p53-*hDM2*; some derivatives were found with activity *in vitro* and in a cell-based assay.^[64] Oligoarylamides **1i** were also reported by several groups as useful scaffolds with good synthetic accessibility yielding active compounds against different PPI targets.^[65-68] In addition, a solid phase synthesis approach for library design has been developed for structurally related N-alkylated aromatic oligoamides **1k**.^[69] Ko et al. expanded this approach and suggested the design of generic libraries of peptidomimetic structures for HTS by developing oxazoline- and bis-triazole-based peptidomimetics for amino acid pairs.^[70]

2 Aim of the thesis

The aim of this work was to employ structure-based approaches as starting points for the development of selective PKA-AKAP interaction inhibitors.

The interaction between AKAPs and PKA is mediated by a PKA binding domain called RII-binding domain because AKAPs preferentially interact with regulatory RII subunits of PKA. RII binding domains are structurally conserved amphipathic α -helices which dock into the dimerization and docking domain of RII subunit dimers.

The first aim of the thesis was to determine the minimal length of the amino acid sequence of the high-affinity peptide AKAP18 δ -L314E required for specific binding to the D/D domain of RII α as a basis for peptidomimetics and therapeutic exploitation.

An alternative approach towards competitive disruptors of AKAP-PKA interaction could be the development of drug-like, non-peptidic mimics of RIIBDs using aromatic oligomers as backbone scaffolds. With an aromatic backbone scaffold all influences on binding related to the backbone of the peptide is lost, for example any influence of the helix dipole to the interaction.^[39] However, in the case of the interaction between D/D domain with AKAPs (or AKAP-derived peptides) it has been proposed that binding is mediated mostly through side chain interactions.^[8;9] Therefore this approach appears reasonable for the development of drug-like mimics of the RIIBD of AKAP18 δ .

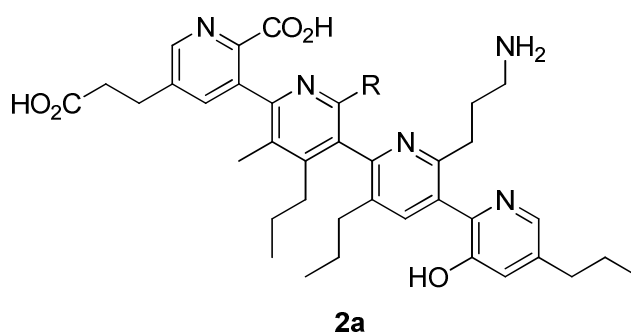


Figure 2.1: Proposed mimic of the RIIBD of AKAP18.

For this purpose, selected basic scaffolds^[52;53;56] were virtually docked using MOE software (Molecular Operating Environment; Chemical Computing Group) into the proposed binding site of the peptide AKAP18 δ -L314E within the D/D domain of RII α ;

they were functionalized on the basis of the peptide AKAP18 δ -L314E and ranked for binding potential.

The pyridine-based oligomer **2a** is based on work from Hamilton et al.^[52] and was designed *in silico* by Christian Schillinger (AG Krause, FMP Berlin). The second aim of this thesis was the development of a synthetic strategy for target scaffold **2a** depicted in figure 2.1.

The synthesis of the highly functionalized quaterpyridine **2a** was expected to be difficult and probably different synthetic strategies have to be evaluated before finishing the synthesis.

Therefore the principal goal of this thesis was to synthesize a small library of intermediate bipyridine and terpyridine derivatives that can be subjected to biological testing. The results of which can then be used to assess potential of pyridine oligomer **2a** or intermediates as a lead structure for the development of drug-like molecules targeting the AKAP-PKA interaction site.

Accordingly, the third aim of the thesis was an initial examination of the ability of bipyridine and terpyridine intermediates of **2a** to bind specifically to the RII α D/D domain. The initial round of testing can be performed by NMR-based techniques that have been already established as a means to determine binding of substances to full length RII α or to the D/D domain of RII α .^[27]

3 Results and Discussion

3.1 Truncation of AKAP18δL314E

It has been shown that peptides derived from RII-binding domain (RIIBD) of AKAP18δ bind with subnanomolar affinity ($K_D = 0.4$ nM; SPR-measurements) to RII subunits of PKA. Thereby these peptides inhibit interaction of PKA with AKAPs^[21;22]. The peptide AKAP18δL314E (PEDAELVRLSKRLVENAVEKAVQQY) inhibits AKAP18α-PKA interaction with an IC_{50} in the low nanomolar range.

One aim of this thesis was to evaluate whether truncated peptides based on AKAP18δL314E retain ability to bind specifically to RIIα as a basis for peptidomimetics and therapeutic exploitation.

3.1.1 Identification of truncated peptides which retain ability to bind PKA

The minimal binding motif of an AKAP for binding to the RIIα subunit is an amphipatic α-helix of usually 14 to 18 amino acids in length.^[1] In order to determine the minimal amino acid sequence of AKAP18δ-derived peptides required for specific binding to RIIα, peptides of 14 amino acids in length were tested for binding to the D/D domain. The amino acid sequence of AKAP18δL314E which is 25 amino acids in length was used as starting point for the truncated peptides. A total of 12 14-mer peptides derived from AKAP18δL314E were spot-synthesized by the Beyermann group (FMP Berlin) on a cellulose membrane.

The membrane containing the peptide sequences was then subjected to an RII overlay assay: The membrane was probed with ³²P-labelled RIIα subunits. Binding of RIIα to the amino acid sequences was detected by autoradiography. This type of approach (spot-synthesis of peptides in combination with RII overlay) has been successfully used to identify RII-binding peptides and to optimize amino acid sequences for binding by performing peptide substitution arrays.^[8;21;41;71] Results of autoradiography experiments with AKAP18δ-derived 14-mer peptides are depicted in figure 3.1. It was determined by LC-MS analysis that synthesis of the peptide sequence termed **1** did not work, therefore, results for that peptide are not shown.

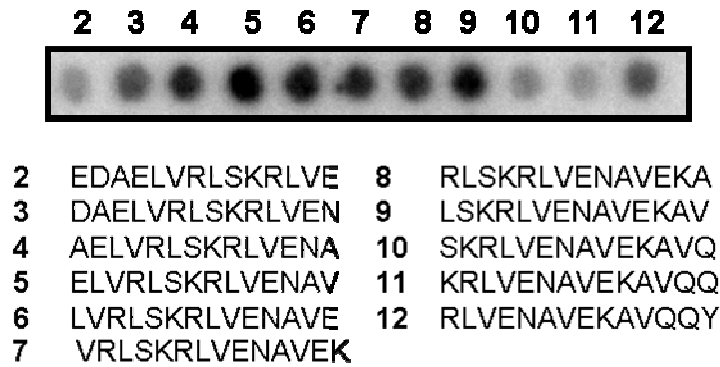


Figure 3.1: Results of autoradiography of 14-mer peptides after incubation with ^{32}P -labeled RII α . The indicated peptides were SPOT-synthesized on a cellulose membrane and probed with ^{32}P -labelled RII α subunits. Signals were detected by audio radiography. A representative experiment is shown.

As can be seen, binding of RII α to 8 out of 11 peptides is detected as judging from this assay. One problem that was encountered with this assay was the choice of appropriate positive and negative controls of binding to RII α . As negative control peptide sequences containing helix-distorting Pro residues were synthesized on the membrane (not depicted). Based on signal intensity of these sequences, peptides **4** to **9** were considered as RII α -binding. Peptides **4** to **9** contain each at least two of the four pairs of short, aliphatic residues that are proposed to make the hydrophobic interactions of AKAP18 δ with RII α .



Figure 3.2: Results of autoradiography of 10-mer peptides after incubation with ^{32}P -labeled RII α . The indicated peptides were SPOT-synthesized on a cellulose membrane and probed with ^{32}P -labelled RII α subunits. Signals were detected by audio radiography. A representative experiment is shown.

Since 14-mer peptides tested by RII overlay appeared to bind RII α , further truncated peptides of 10 amino acids in length were also subjected to an RII overlay assay. The results of these experiments are depicted in figure 3.2. Only amino acids 3 to 22 from AKAP18 δ L314E were tested. Similarly to the 14-mer peptides, Pro-containing

peptides were synthesized on the membrane as negative control (not depicted). Based on signal intensity of these sequences, peptides **1** to **3** were considered as potential binders of RII α .

However, since no appropriate positive control was available, HSQC-NMR measurements were performed to confirm specific binding of the peptides to the D/D domain of RII α .

3.1.2 Characterization and Validation of identified peptides

In order to determine the specificity of binding and to rule out unspecific hydrophobic interactions between the short peptide sequences and the spacious RII α subunits, the truncated peptides were characterized by CD-spectroscopy and binding was validated in an NMR-based assay.

For this purpose, the 14-mer peptides **4** to **9** depicted in figure 3.1 as well as a Pro-mutant of 14-mer **5** as negative control and the 10-mer peptides **1-3** and **9** (as negative control) depicted in figure 3.2 were chosen for further characterization. The designation and amino acid sequences of the chosen peptides are depicted in table 3.1. The peptides were synthesized by the Beyermann group (FMP Berlin) using standard SPPS chemistry. In addition to the 10-mer and 14-mer peptides, three longer AKAP18 δ L314E-derived peptides of 16, 18 and 22 amino acids in length were synthesized that contain all proposed pairs of amino acids mediating the hydrophobic interaction between AKAP18 δ L314E and the AKAP-binding site of RII α (table 3.1).

Designation	Sequence	Designation	Sequence
AKAP18 δ L314E_4-13	AELVRLSKRL	AKAP18 δ L314E_6-19	LVRLSKRLVENAVE
AKAP18 δ L314E_5-14	ELVRLSKRLV	AKAP18 δ L314E_7-20	VRLSKRLVENAVEK
AKAP18 δ L314E_6-15	LVRLSKRLVE	AKAP18 δ L314E_8-21	RLSKRLVENAVEKA
AKAP18 δ L314E_12-21	RLVENAVEKA	AKAP18 δ L314E_9-22	LSKRLVENAVEKAV
AKAP18 δ L314E_4-17	AELVRLSKRLVENA	AKAP18 δ L314E_6-21	LVRLSKRLVENAVEKA
AKAP18 δ L314E_5-18	ELVRLSKRLVENAV	AKAP18 δ L314E_5-23	ELVRLSKRLVENAVEKAQ
AKAP18 δ L314E_5-18-PP	ELVRLSPPLVENAV	AKAP18 δ L314E_3-25	DAELVRLSKRLVENAVEKAQQY

Table 3.1: Designation and amino acid sequences of AKAP18 δ L314-derived peptides.

RIIBDs of AKAPs have α -helical secondary structure; therefore specific RIIBD-derived peptides must be able to form α -helices as well.

3 Results and Discussion

In order to test whether helicity can be induced in the peptides depicted in table 3.1, CD-measurements in presence of the helix-stabilizing agent trifluoroethanol were carried out. This method is a means for estimating the induceability of α -helicity in short peptides.^[21;72]

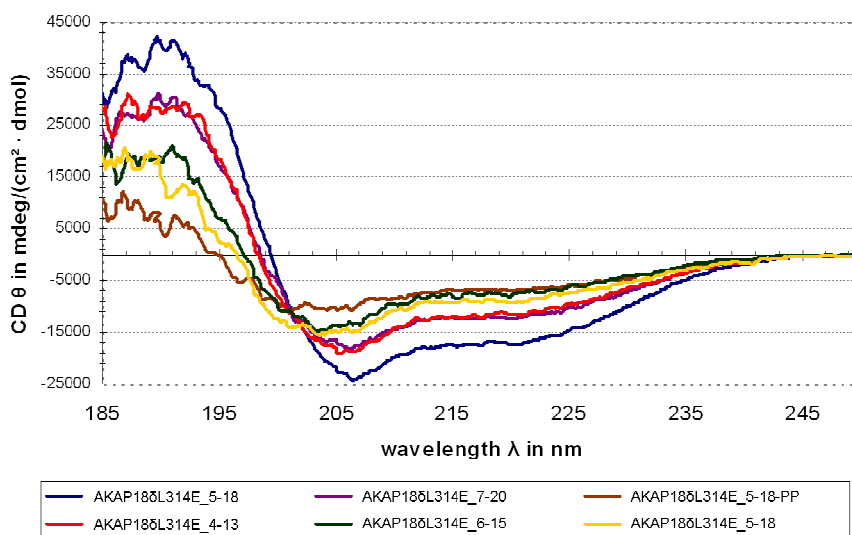


Figure 3.3: Depiction of circular dichroism spectra of selected AKAP18 δ L314E-derived peptides in CD buffer/TFE (1:1, v/v). The Peptide concentration in each sample was 100 μ M.

From the CD-spectrum of a given peptide or protein in the far UV-region (190-250nm) one can deduce the overall secondary structure found in the sample. Different types of secondary structures in a given sample give rise to characteristic CD-spectra.

In CD-measurements of the peptides in the presence of 50% trifluoroethanol the spectra of all peptides tested showed characteristic features of an α -helical structure: double negative maxima around 208 and 222 nm and a positive maximum near 191 nm. CD-spectra of selected peptides in 50% trifluoroethanol are depicted in figure 3.3.^[73]

The validation of specific binding to RII α was performed by two-dimensional $^{15}\text{N}/^1\text{H}$ heteronuclear correlation (HSQC) experiments which is a target-based NMR technique.^[37] This means that binding of a ligand to a target protein is detected through a change of chemical shifts of protein signals upon titration of the ligand to the protein sample.^[74;75] In this example, shifting of signals from the amide groups of the protein backbone and also of NH-containing side chains is detected. In order to determine whether differences in chemical shifts occur, two sets of HSQC-spectra are

3 Results and Discussion

recorded, one of the protein in buffer alone (the reference spectrum) and one spectrum of the protein in the presence of the ligand. Superimposing the processed spectra allows recognition of chemical shift changes which in turn indicate binding of the tested ligand.^[75]

The HSQC experiments were performed in cooperation with Brigitte Schlegel (FMP Berlin) and Dr. Peter Schmieder (FMP Berlin). For the HSQC experiments with the AKAP-derived peptides, ¹⁵N-labeled D/D domain was used as target protein. As discussed in chapter 1, the D/D domain contains the AKAP binding site of RII α . Therefore, binding of the truncated peptides to the D/D domain is a suitable indicator for an AKAP-like, specific interaction of these peptides with RII α . In addition, the D/D domain can be readily expressed and purified^[8;9;17;18] and is, due to its smaller size, more suitable for HSQC experiments than full length RII α .^[74]

The results from HSQC experiments are summarized in table 3.2. With none of the tested 10-mer peptides shifting of peaks was detected. This suggested that binding observed in the RII overlay was the result of an unspecific hydrophobic interaction between peptide and protein.

Designation	Activity in HSQC
AKAP186L314E_4-13	-
AKAP186L314E_5-14	-
AKAP186L314E_6-15	-
AKAP186L314E_12-21	-
AKAP186L314E_4-17	not tested
AKAP186L314E_5-18	+
AKAP186L314E_5-18-PP	-
AKAP186L314E_6-19	+
AKAP186L314E_7-20	-
AKAP186L314E_8-21	-
AKAP186L314E_9-22	+
AKAP186L314E_6-21	+
AKAP186L314E_5-23	+
AKAP186L314E_3-25	not tested

Table 3.2: Results of HSQC-NMR measurements of indicated peptides with ¹⁵N-labeled D/D domain of RII α . +: shifts of peaks in presence of the peptide as compared to original spectrum. -: no shifts in presence of the peptide as compared to original spectrum.

3 Results and Discussion

Six 14-mer peptides were tested for binding in the HSQC experiment including AKAP18δL314E_5-18-PP which was designed as a negative control. As can be seen in table 3.2, for three peptides peak shifting was observed and with three peptides including the negative control no binding to the D/D domain was observed. With peptides covering amino acids 5-18, 6-19 and 9-22 binding was detected, while peptides covering amino acids 7-20 and 8-21 did not appear to bind the D/D domain. This suggested that unspecific binding was observed for these two peptides in the RII overlay. To confirm these results further in vitro assays should be performed.

The loss/gain of binding upon shifting the basic peptide sequence by one amino acid could be caused by either the loss/gain of an amino acid critical for binding to the D/D domain or by a significant change of stability of α -helical secondary structure.

For further analysis, experiments in a second assay need to be performed to confirm the results from the HSQC experiments. For example, K_D -values or k_{on}/k_{off} rates of binding have not been determined.

When comparing the spectra of the 14-mer peptides (AKAP18δL314E_6-19 and AKAP18δL314E_9-22, figure 3.4 and 3.5) with the ones from the longer peptides (16-mer and 18-mer, figure 3.5) one can see that the differences in chemical shift upon addition of the peptide were greater with the longer peptides.

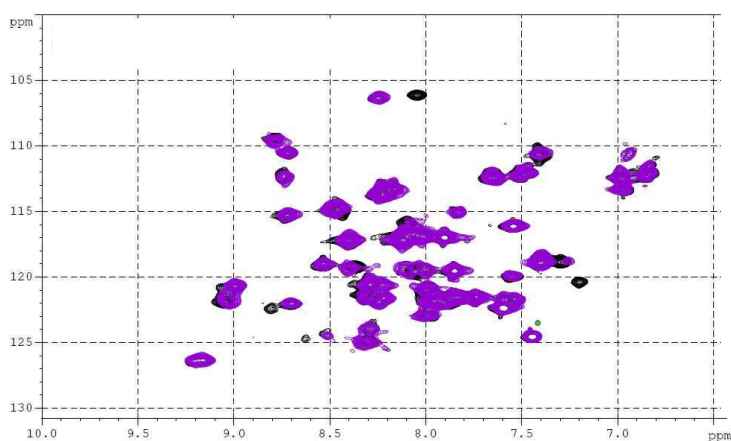


Figure 3.4: HSQC spectra of D/D domain. Black: ^1H - ^{15}N HSQC of 100 μM ^{15}N -labeled D/D domain of RII α . Violet: ^1H - ^{15}N HSQC of 100 μM ^{15}N -labeled D/D domain of RII α incubated with 800 μM of AKAP18δL314E_6-19.

3 Results and Discussion

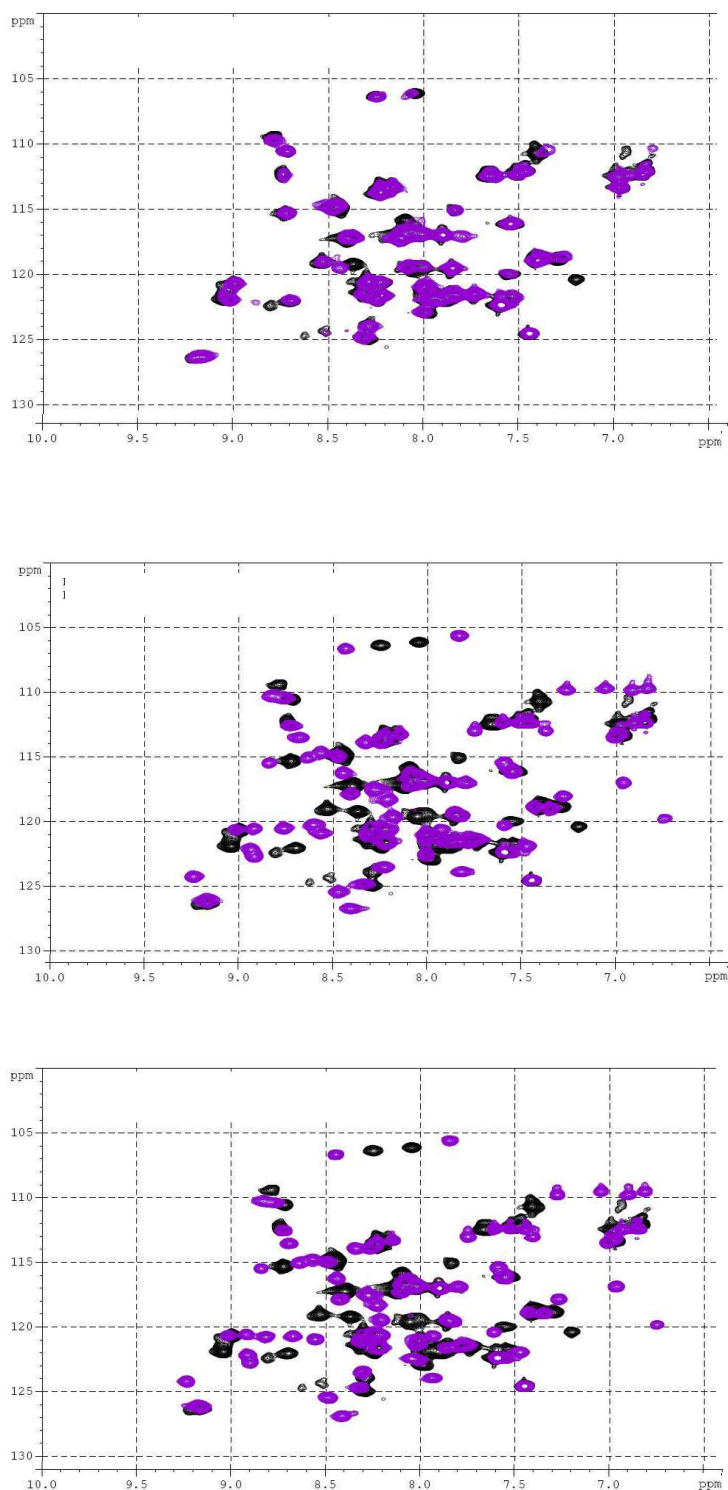


Figure 3.5: HSQC spectra of D/D domain. Black: ^1H - ^{15}N HSQC of $100\ \mu\text{M}$ ^{15}N -labeled D/D domain of RII α . Violet: ^1H - ^{15}N HSQC of $100\ \mu\text{M}$ ^{15}N -labeled D/D domain of RII α incubated with $800\ \mu\text{M}$ of peptide. Top: 14-mer AKAP18 δ L314E_6-19. Middle: 16-mer AKAP18 δ L314E_6-21. Bottom: 18-mer AKAP18 δ L314E_5-23.

This indicated that through binding of the longer peptides the whole protein is affected. The exact extend of conformational/chemical change upon binding cannot

be determined from this experiment. Therefore, the results of this experiment cannot be compared with the structural information from x-ray crystallography in which no apparent conformational change of the D/D domain itself upon binding of an AKAP peptide was observed.^[8] It also suggested that the longer peptides bind tighter and/or with higher affinity to the D/D domain. In order to quantify the difference in binding, further experiments need to be performed; for example titration HSQC experiments with different concentrations of active ligands or ITC experiments to determine K_D /binding affinity and to calculate entropic and enthalpic contributions to binding.

In conclusion, truncated peptides derived from AKAP18 δ L314E were identified that retained the ability to bind to the D/D domain of RII α . Peptides shorter than 14 amino acids do not appear to specifically bind to the D/D domain. Whether the diminished binding of shorter peptides is only dependent on loss of critical interaction partners or due to lower stabilization of the required helical secondary structure is not clear yet. Further experiments are required to distinguish between influences from side chains and helicity to binding. In order to increase α -helical content a stabilization of the helical structure by introducing conformational restraints to the non-binding peptides could be tried.

So far, the ability of these shorter peptides to inhibit the interaction of AKAP18 δ or other AKAPs and PKA has not been determined. This would be the next step in the evaluation process and is ongoing.

3.2 Synthesis of the quaterpyridine scaffold

The second aim of this thesis was the development of a synthetic strategy for ligand **2a** which was designed *in silico* by AG Krause (FMP Berlin) as a potential non-peptidic mimic of the RIIBD of AKAP18 δ . Modeling was performed with MOE software (Molecular Operating Environment; Chemical Computing Group). The general design of **2a** was based on work from Hamilton et al. in which the peptidic backbone is replaced by a chain of aromatic rings.^[52;53;56] Three backbone scaffolds which were designed by the Hamilton group, terpyridine-, terphthalimide- and benzoylurea-based oligomers, were chosen for an *in silico* evaluation as backbone scaffolds mimicking AKAP18 δ L314E when docked to the AKAP-binding site of PKA.

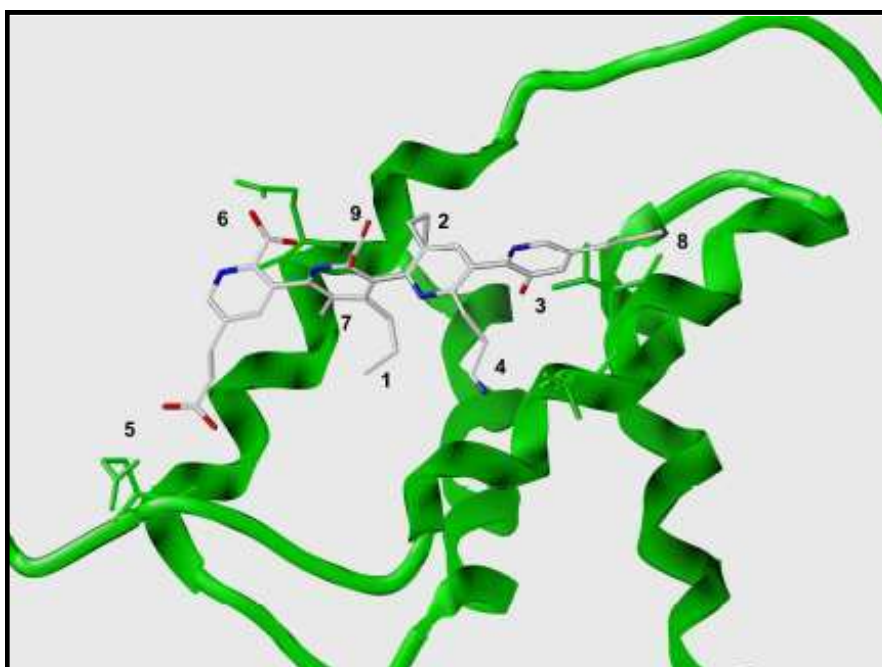


Figure 3.6: View of ligand **2a** docked into the D/D domain of the RIIBD of AKAP18 δ (depicted in green).

The best overlap between AKAP18 δ L314E and a potential mimic was found with a 2,3'-linked quaterpyridine as backbone scaffold, as can be seen in figures 3.6 and 3.7. In cooperation with AG Krause (FMP Berlin), some modifications to quaterpyridine **2a** were introduced in order to simplify the synthesis, resulting in target structure **2b** which is depicted in figure 3.8.

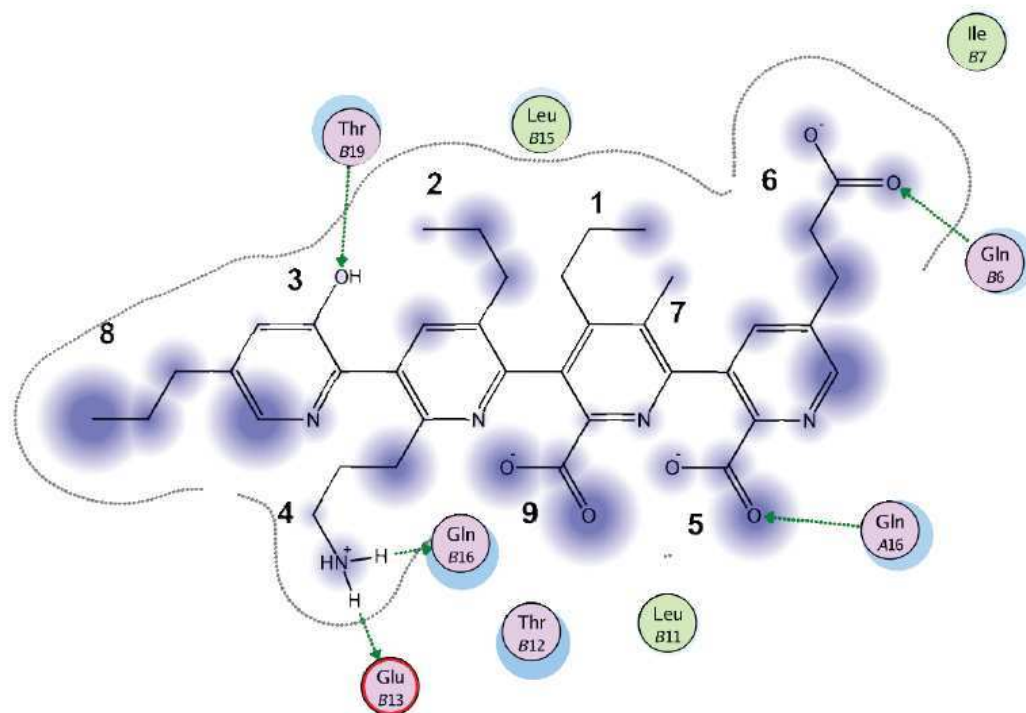


Figure 3.7: Schematic view of the proposed interaction of ligand 2a and its binding site within the D/D domain of the RII α -subunit of PKA. The depicted numbered amino acids correspond to the residues of the natural ligand that are being mimicked by the ligand.

The hydrophilic residue 9 that was originally introduced to increase water solubility of the final product was removed from the structure. No major solubility issues were anticipated for the final ligand due to the hydrophilic nature of the pyridine backbone.

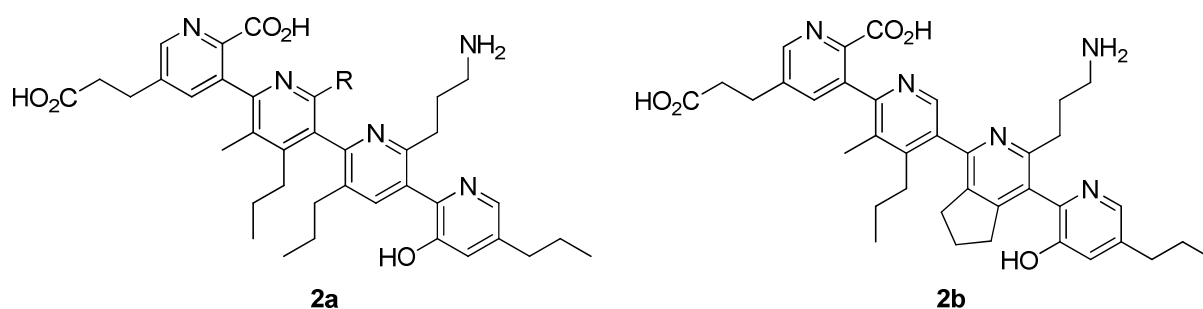


Figure 3.8: Quaterpyridine ligands 2a and derivative 2b.

In addition, residue 2 from figure 3.7 was replaced by a fused cyclopentyl group attached to C-3 and C-4 of the pyridine in order to simplify the synthesis and allow for easy modifications at this position later on.

Formation of atropisomers of the target compound **2b** cannot be excluded. For formation of atropisomers usually tri- or tetra-substitution with spacious functionalities

is required at the ortho positions around the chiral biaryl axis in order to block free rotation around the axial single bond sufficiently.^[76] If a formation of atropisomers is observed, racemic resolution of the racemic mixture would be required or an asymmetric synthesis would have to be developed in order to determine the biological activity of the different atropisomers.

Another subject with this scaffold that has to be investigated is the basicity of the pyridine N-atoms of the target ligand. Protonation at the pyridine-N-atom could occur at one or several positions. The corresponding pyridinium ions might have a different binding ability as compared to the molecule with unprotonated pyridine N-atoms. Since pH values in the performed biological assays (e.g. HSQC-NMR, STD-NMR) were basic (pH 7.5) it would be expected that only a subset of the pyridine-N-atoms is protonated under these conditions. In order to calculate this percentage, pK_A-values of the corresponding pyridinium ions have to be determined in order to estimate if pyridinium-ion formation occurs in buffer, and if so, at which positions of the target compound. Basicity of pyridine derivatives in general depends on their substitution pattern. For example picolines and lutidines are more basic than pyridine (pK_As: pyridine: 5.25, picolines: between 5.63-5.96, lutidines: between 6.15-6.99).

3.2.1 Synthesis of terpyridines and quaterpyridines

IUPAC/Hantzsch-Widman nomenclature of heterocycles is used for pyridine and dihydrocyclopenta[*c*]pyridine derivatives as depicted in figure 3.9 for clarification.^[77]

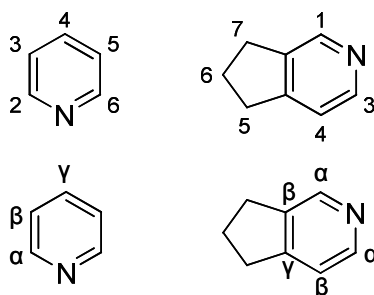


Figure 3.9: Nomenclature of pyridine and cyclopenta[*c*]pyridine derivatives. According to Hantzsch-Widman rules (top) and according to positioning of pyridine carbon atoms with respect to the pyridine nitrogen (bottom).

Pyridines are a class of heteroaromatic compounds that are ubiquitously found for example as important building blocks in many pharmaceuticals or in natural products like niacin (vitamin B₃) and pyridoxine (vitamin B₆) or in the alkaloid nicotine.^[78;79]

Pyridine derivatives serve as catalysts in chemical synthesis, e.g. DMAP (acylation) or in biological systems, e.g. NADP⁺/NADPH (involved in different redox processes) and have many other functions in chemical synthesis and in other applications.^[79;80]

Pyridine is an electron-deficient 6n-heteroaromatic compound due to presence of the electronegative nitrogen atom. Pyridines have an unequal distribution of electron density at the different carbon atoms of the aromatic system:^[78] The α - and γ -positions have the lowest electron density, therefore nucleophilic attacks occur preferentially at these positions, while the less electron-deficient carbon atoms in β -position preferentially undergo reactions with electrophiles.^[78] The pyridine nitrogen atom has the highest electron density in the aromatic ring and undergoes reactions with electrophiles or reacts as base *via* its electron lone pair, both of which result in formation of *N*-pyridinium salts. Basicity of pyridine derivative depends on their substitution pattern, with electron-donating substituents increasing and electron-withdrawing ones decreasing basicity as compared to pyridine (pK_a of $C_5H_6N^+$ = 5.2).^[78] There are a plethora of reactions for *de novo* synthesis of pyridine derivatives available, for example cyclocondensations (e.g. Hantzsch pyridine synthesis for the

synthesis of symmetrical 2,4,6-substituted pyridines)^[78] or cycloaddition reactions like transition-metal catalyzed [2+2+2] cycloadditions of alkynes and nitriles.^[79;81]

Pyridine oligomers are an important compound class themselves. 2,2'-bipyridines and 2,2':6',2''-terpyridines can stably coordinate metal ions and are frequently employed ligands in metal complexes of e.g. Ru(II), Fe(II), Pd(II), Pt(II), Zn(II).^[82] The metal complexes are used for example in catalysis, for asymmetric transformations, for applications in supramolecular chemistry, as potential therapeutics or biological tools and in others fields.^[82-84] 2,3'-linked oligopyridine cores are e.g. found in liquid crystals^[84] or in natural products, for example in nemertines which are a class of neurotoxines. One example from this compound class that has been recently synthesized is nemertelline (3,2':3',2'':4'',3'''-quaterpyridine).^[85;86]

Regarding the synthesis of terpyridines and quaterpyridines different strategies have been developed for the synthesis of symmetric and non-symmetric derivatives. For example, [2+2+2] cycloaddition reactions have been successfully used to synthesize symmetric C-2-linked 2,2'-bipyridines as well as corresponding terpyridines and quaterpyridines from diynes and cyanoalkynes or from tetraynes and nitriles.^[87] Symmetric 2,2'-oligopyridines are also accessible by several other reactions, e.g. metal-mediated homo-coupling like the Ullmann reaction.^[83]

Pd-catalyzed cross-coupling reactions have become an important tool for the synthesis of non-symmetric 2,2'-bipyridines and corresponding ter- and quaterpyridines.^[83;88;89] Similarly, non-symmetric 2,3'-bipyridines have been successfully synthesized by Pd-catalyzed cross-coupling using Suzuki,^[90-93] Stille,^[84] or Negishi^[83] conditions. Another strategy towards 2,3'-bipyridines that has been reported is a catalyzed [2+2+2] cycloaddition of pyridyl-diynes and nitriles; the development of a strategy employing this type of reaction for the synthesis of the target compound is further analyzed and discussed in chapter 3.2.4.3.^[94]

A synthetic strategy towards symmetric or non-symmetric 2,3':6',3''-terpyridines has been reported from the Hamilton group who developed this scaffold as α -helix mimic.^[52] For their synthesis, the pyridine rings were synthesized de novo by Bohlmann-Rahtz heteroannulation from a ketoalkyne, ammonium acetate and a β -ketoester; they developed a procedure in which the terpyridine scaffold is built up by sequential Bohlmann-Rahtz reactions.^[52]

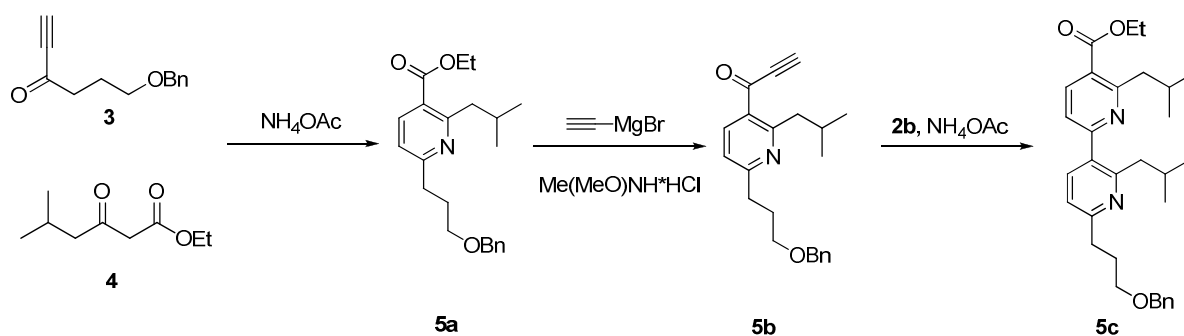


Figure 3.10: Schematic overview of sequential Bohlmann-Rahtz heteroannulation reaction towards oligopyridines.

As depicted in figure 3.10, this synthesis has a limited pattern of substituents and functionalities on the pyridines that can be incorporated into the final compound. For example, no substituents can be placed on the remaining β -carbon atoms of the newly formed pyridine ring, as required for substituents 2, 3, 6 and 7 of quaterpyridine **2b** (figure 3.7 and 3.8). It was therefore not applicable for the synthesis of the higher functionalized quaterpyridine **2b**.

Iterative Pd-catalyzed cross-coupling reactions appeared as the most straightforward way for assembling the non-symmetric quaterpyridine **2b** from functionalized single pyridine building blocks.

3.2.1.1 Pd-catalyzed cross-couplings in the synthesis of oligopyridines

Recently, synthesis of symmetric and non-symmetric 2,3':6',3''-terpyridines and the un-functionalized quaterpyridine nemertelline was achieved by sequential Pd-catalyzed cross-coupling with Suzuki-Miyaura conditions of corresponding (di)halopyridines and (halo)pyridyl boronic acids.^[85;86;90;95] In principle, using an all-Suzuki-Miyaura coupling sequence would also be desirable for the synthesis of quaterpyridine **2b** due to the low toxicity associated with this procedure as compared to e.g., Stille conditions. Stille cross-coupling conditions have been successfully employed for the synthesis of 2,3'-bipyridines and terpyridines.^[84] Negishi coupling or other types of Pd-catalyzed coupling reactions were not applied and evaluated during the work on this thesis; but they could be valuable alternatives for assembling pyridine-based oligomers.^[83;96]

3 Results and Discussion

The catalytic cycle is similar for all types of Pd-catalyzed cross-couplings and is depicted in figure 3.11. The catalytic cycle consists of three major steps: Oxidative addition of the Pd(0) species into a C-X bond of the first coupling partner Ar¹-X. X is usually a halide or pseudohalide with the general scheme of reactivity being I>OTf>Br>>Cl, according to the relative stability of the corresponding C-X bond.^[96-98]

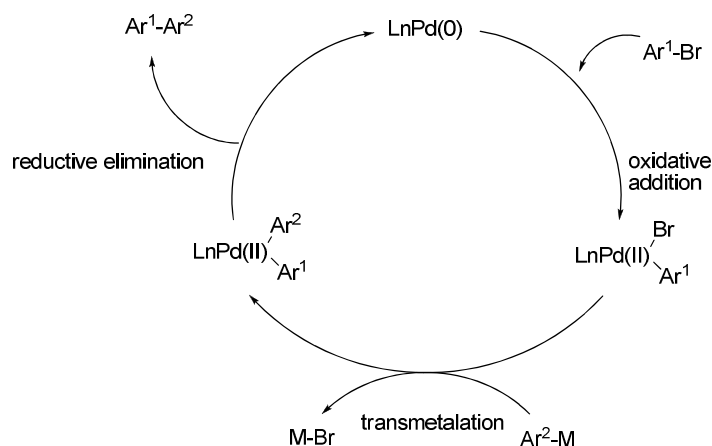


Figure 3.11: Scheme of the general catalytic cycle of Pd-catalyzed cross-couplings of aryls.

The resulting LnPd(II)-(Ar¹)(Br) complex undergoes transmetalation with an organometalate Ar²-M which yields a LnPd(II)-(Ar¹)(Ar²) complex. Upon isomerization to the corresponding *cis*-complex, the catalytically active Pd(0) species is regenerated by reductive elimination releasing the coupling product Ar¹-Ar².^[96-98]

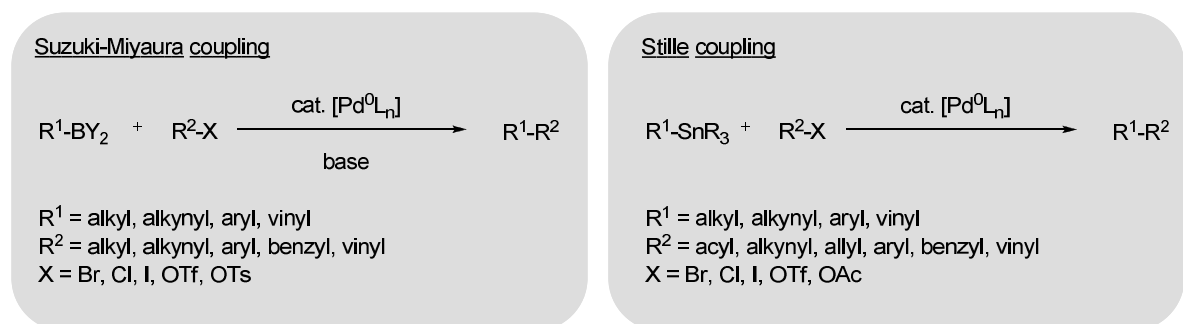


Figure 3.12: Commonly utilized Pd-catalysed cross-coupling reactions for oligopyridine synthesis. The figure was adapted from Nicolaou et al.^[83;99].

The main difference between different types of Pd-coupling is the nature of the organometalate used as nucleophilic component of the given cross-coupling as depicted in figure 3.12. In Stille couplings stannanes are employed as transmetalation

group.^[83;89;100] For Suzuki couplings, organoboron compounds are used as transmetalation group. For Suzuki reactions presence of a base in the reaction mixture is required. The base probably forms a borate-complex with the organoboron compound rendering it nucleophilic enough for the transmetalation reaction with $L_nPd(II)-(Ar^1)(X)$.^[98]

For synthesis of 2,3'-pyridine-based oligomers an important aspect is regioselectivity of Pd-catalyzed cross-couplings of dihalopyridine building blocks. It has been reported that for example 2,5-dibromopyridine undergoes Pd-coupling regioselectively at the α -C-2 position; the resulting coupling product can then undergo a second coupling to a different coupling partner.^[85;90;95;97] The reason is that Pd(0) inserts faster into the more polarized α -C-Br bond by oxidative addition. This regioselectivity can be overcome by introducing a more reactive halide to the β -position, in this case for example iodine.^[85;90;95] This is a general trend in Pd-cross-couplings of arylhalides: electron-poor aryl halides react more readily in Pd-couplings as compared to more electron rich aryl halides.^[101]

Pyridine and also other types of electron-poor heteroaryls are considered challenging substrates when used as nucleophilic component in Pd-catalyzed couplings, especially in Suzuki-Miyaura couplings: They are less nucleophilic and undergo transmetalation slower than more electron-rich aryl metalates.^[93;96]

Stability of pyridyl metalates depends on the type of metal used and its position with regard to the pyridine nitrogen atom.^[96] Pyridyl boronic acids and esters are prone to undergo competing protodeboronation in cross-couplings.^[102] 2-Pyridyl metalates often have a reduced stability as compared to 3- or 4-pyridyl metalates.^[96] Especially for boronic acids protodeboronation is probably facilitated by the neighboring pyridine nitrogen atom.^[83;102] Syntheses of stable 2-pyridylstannanes and more recently of certain types of 2-pyridyl boronic acid esters and other organoboron coupling partners have been reported.^[83;96;103;104] For the assembly of the target ligand from the single pyridine building blocks it was therefore decided to preferably follow a strategy in which Pd-catalyzed cross-couplings are performed between 3-pyridylmetalates and 2-pyridyl halides.

3.2.2 Retrosynthetic analysis of the target scaffold

As can be seen in figure 3.13, the retrosynthesis of target ligand **2b** can be roughly divided in two parts:

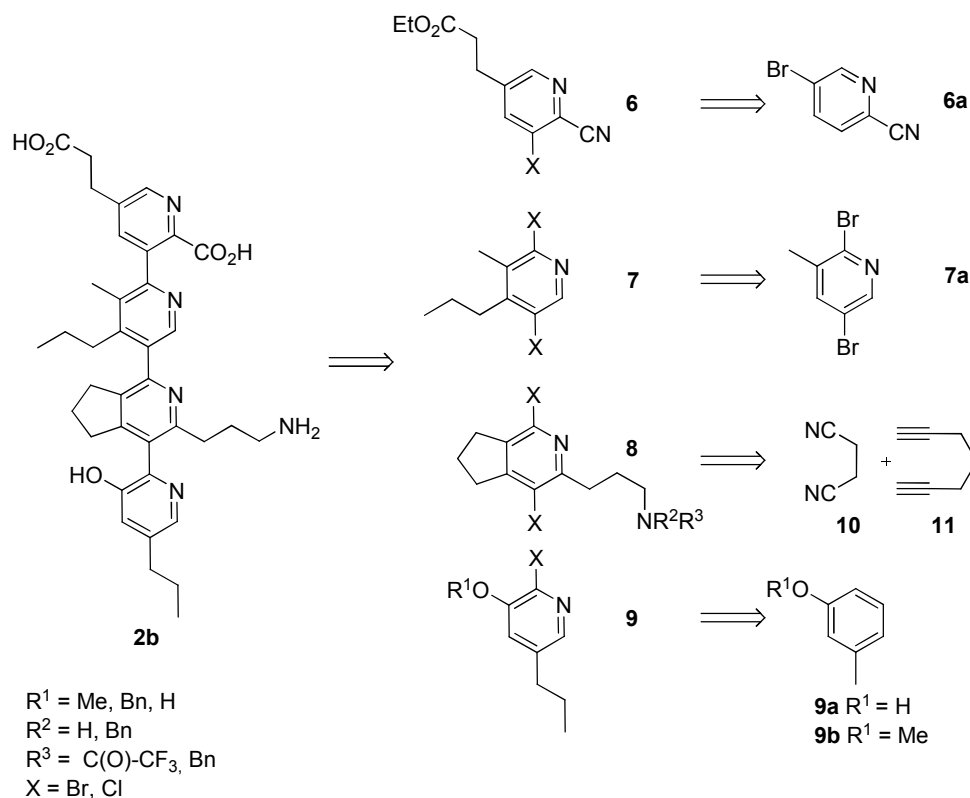


Figure 3.13: Schematic overview of the retrosynthesis of quaterpyridine **2b.**

1. Assembly of the single pyridine moieties to form the target compound by Pd-catalyzed cross-coupling.
2. Synthesis of single pyridine building blocks from depicted commercially available precursors.

As depicted in figure 3.13, the hydroxy- and amino- functionalities as well as the both carboxylic acids of quaterpyridine **2b** were protected during the synthesis in order to avoid side reactions. Side reactions from all or some of the functional groups were expected during Pd-catalyzed cross-coupling reactions or during earlier steps in the synthesis. The protection strategy is discussed in appropriate detail in the

corresponding chapters describing the synthesis of the single pyridine building blocks.

A convergent strategy which should maximize the final yield for the assembly of the target quaterpyridine from single pyridine building blocks is depicted in figure 3.14: The pyridines **6/7** and **8/9** are coupled to form bipyridines **12** and **13** which could then be coupled to give quaterpyridine **2b**.

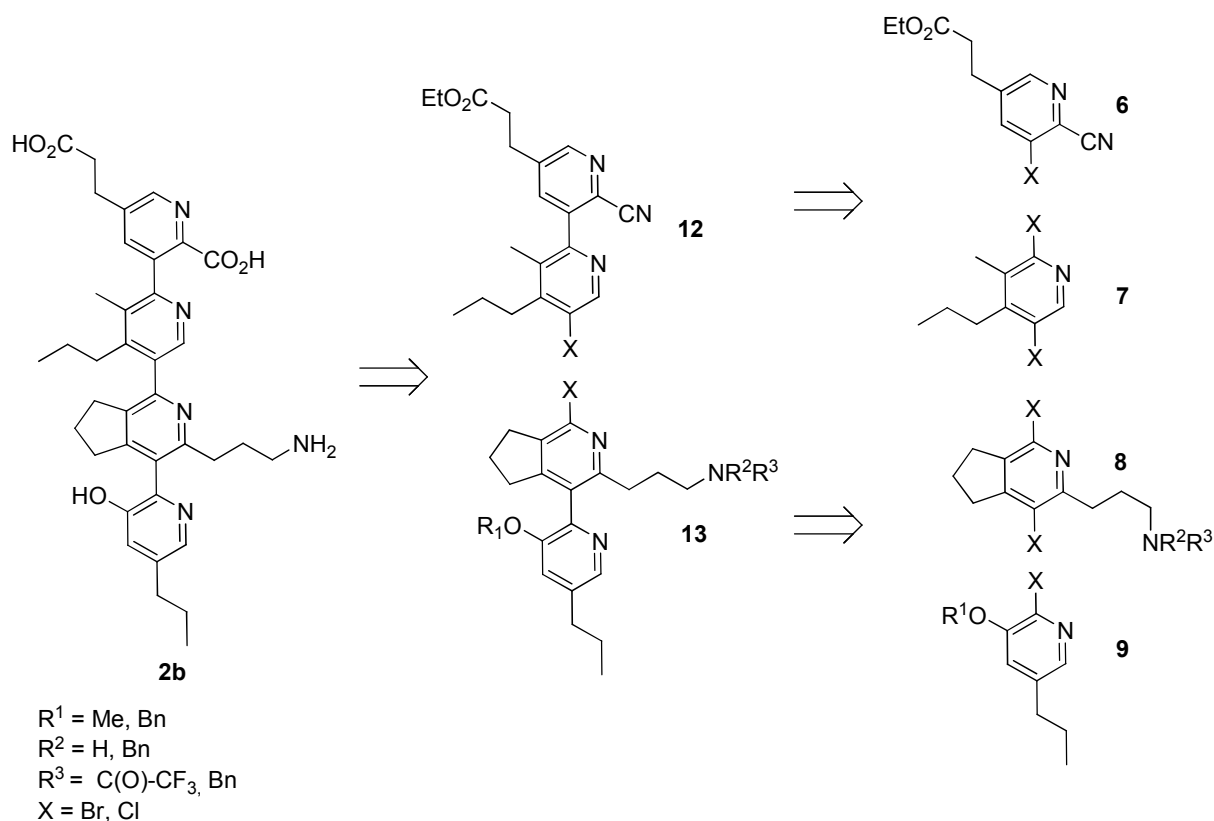


Figure 3.14: Retrosynthetic analysis of the quaterpyridine 2b: Proposed assembly of the single pyridine building blocks by Pd-catalyzed cross-coupling with a convergent strategy.

Potential difficulties regarding regioselectivity could arise during the Pd-catalyzed cross-coupling between pyridines **8** and **9** with homocoupling of dihalide **8** as a potential side reaction. Therefore, non-identical halide substituents on pyridine **8** and pyridine **9** would be required allowing oxidative addition of $L_n\text{Pd}(0)$ into the $\beta\text{-C-X}$ bond of pyridine **9** over addition into the $\alpha\text{-C-X}$ bond of pyridine **8**. There would be different combinations possible as discussed during synthesis of building block **8**.

A non-convergent and therefore less favourable synthetic pathway is depicted in figure 3.15. Regarding regioselectivity, there were no problems expected, since

halogen substitutions are found in the right order to avoid homocoupling side reactions.

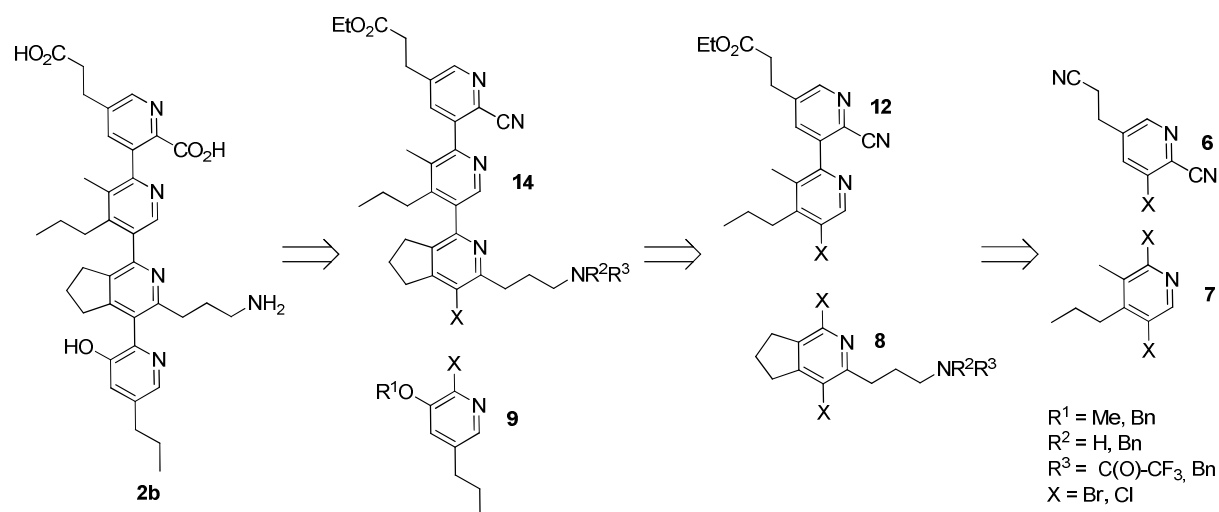


Figure 3.15: Retrosynthetic analysis of the quaterpyridine 2b: Proposed assembly of single pyridine building blocks by Pd-catalyzed cross-coupling with a non-convergent strategy.

Additional non-convergent strategies are conceivable which were, however, not further considered at this point because they did not offer any synthetic advantage but rather more potential difficulties were expected with regard to regioselectivity of the coupling reactions.

In the next chapters, the synthetic strategies for the single pyridine building blocks are analyzed and evaluated. After a short summary of the results, the synthetic strategy for the assembly of the target ligand and of relevant intermediate structures based on the results from the first chapters is discussed and then evaluated. Finally, some initial results from *in vitro*-tests obtained from synthetic intermediates of the target compound are presented and discussed.

called donor-metalation group (DMG) activates carbon atoms in neighboring *ortho*-positions by increasing acidity of its proton through inductive effect and/or by formation of a chelate complex with the lithiating reagent, thereby directing it to the neighboring carbon as depicted in figure 3.17.^[108]

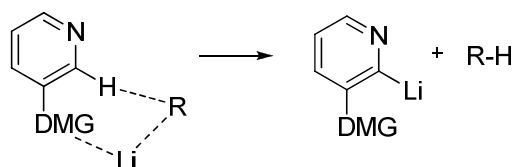


Figure 3.17: General scheme of *ortho*-directed metalation of pyridine derivatives.

A number of functional groups have been used as *ortho*-directing groups for the metalation of pyridine derivatives, e.g. carboxamides,^[109] carboxylic acid^[110;111], halides^[108] and methoxy groups^[112].

The resulting organolithium compounds can then be functionalized *in situ* by electrophilic substitution with a number of electrophiles including tributylstannyl chloride and triisopropylborate as depicted in figure 3.18, giving the corresponding stannanes^[113] or boronic acids^[114] after hydrolysis.

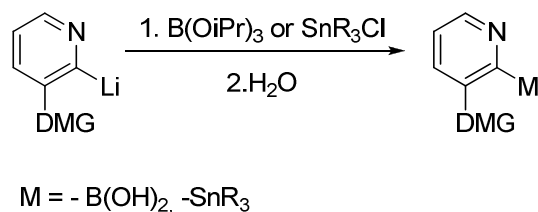


Figure 3.18: General scheme of the transmetalation of pyridyl lithium derivatives.

For the functionalization of **6b**, a procedure reported by Cailly et al.^[114;115] for the regioselective metalation of the C-3 position of 2-cyanopyridine **15** using LiTMP as lithiating agent could be used. Here, the nitrile functionality at the C-2-position serves as *ortho*-directing group.

Since 2 equivalents of lithiating reagent were required for efficient functionalization of the starting material, the authors proposed that LiTMP adds reversibly to the nitrile function generating intermediate **16** depicted in figure 3.19, while the other equivalent is required for lithiation of the *ortho*-position.^[115]

3 Results and Discussion

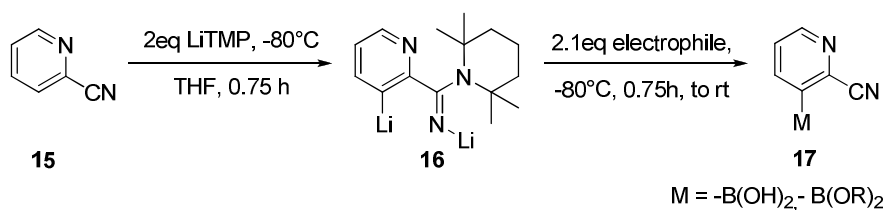


Figure 3.19: Scheme of the synthesis of pyridyl boronic acid and esters from 2-cyanopyridine.^[114;115]

This DoM reaction had not been applied to pyridines substituted with benzylic groups or aliphatic esters, both of which can undergo side reactions with LiTMP. One side reaction that was expected is lithium enolate formation of the ester as depicted in figure 3.20. It could not be excluded that the formed ester enolate will undergo side reactions, such as intermolecular condensations. Unchanged ester groups could undergo condensations with the ester enolate or the pyridyl lithium species. Transmetalation of the lithium ester enolate by the Lewis-acidic electrophiles (stannyl chlorides or borates) could also not be ruled out as a potential side reaction (transmetalation of Li-enolates with B(OiPr)₃ had been reported with aldehydes^[116]), the resulting Lewis acid complexes were, however, expected to be formed reversibly and to undergo hydrolysis during acidic work-up.^[117]

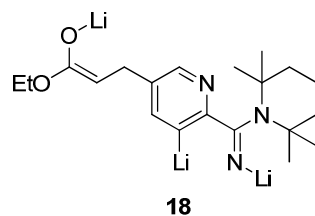


Figure 3.20: Proposed intermediate 18 during the functionalization of 6b.

Since the resulting anion is not easily stabilized due to presence of the neighboring enolate, deprotonation at the benzylic position of C-3 of **6b** as potential side reaction was not expected. In addition to this, LiTMP has been reported to not react with β -benzylic position in 3-picoline, it only deprotonates more acidic α - and γ -benzylic positions in the corresponding picolines.^[118;119]

Synthesis of building block 6

Ethyl propionate was coupled to the C-5 position of commercially available 5-bromo-2-cyanopyridine **6a** using the procedure described by Battistuzzi et al. (figure 3.21).^[107]

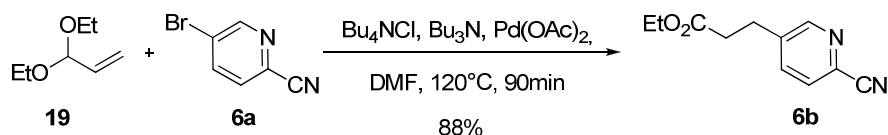


Figure 3.21: Scheme of the synthesis of **6b**.

Pyridine **6b** was obtained in very good yield of 88%. In the next step, the C-5 carbon of pyridine **6b** was functionalized *via* metal-hydrogen exchange reaction as depicted in figure 3.22.^[115]

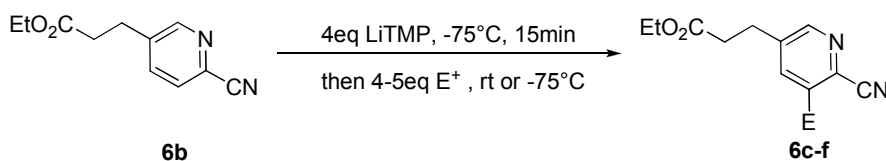


Figure 3.22: Scheme of the functionalization of **6b**.

Reaction conditions were adapted from Cailly et al., in our case 3-4 equivalents of LiTMP were employed in order to ensure complete lithiation of the nitrile functionality, lithium enolate formation and lithiation of pyridine in position C-5.

Pyridyl stannanes have been widely used as coupling partners in Stille couplings with aryl halides and they are generally considered being more stable and robust than pyridyl boronic acids.^[96] Therefore it was decided to establish this procedure for the synthesis of 3-pyridyl stannanes first.

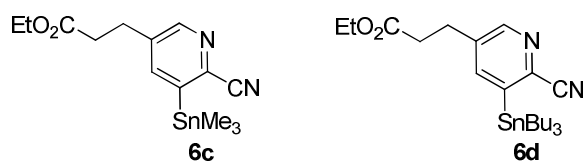


Figure 3.23: Pyridyl stannanes **6c** and **6d**.

3 Results and Discussion

Trimethylstannane **6c** and tributylstannane **6d** depicted in figure 3.23 were synthesized using the respective chlorides as electrophiles. As shown in table 3.3, **6c** was initially synthesized using 3 equivalent of LiTMP. Since after purification about 30% of the starting material was recovered, the amount of LiTMP employed was increased. This gave the products in moderate yield of 39% or 38% (entry 1 vs. entry 2/3, table 3.3).

entry	solvent	Base	T	t	E ⁺	results
1	THF	3.0eq LiTMP	-75°C	60min	4eq SnMe ₃ Cl	18% ^(a)
2	THF	4.0eq LiTMP	-75°C	60min	4eq SnBu ₃ Cl	39% ^(a)
3	THF	4.0eq LiTMP	-75°C	20min	5eq SnMe ₃ Cl	38% ^(a)

Table 3.3: Reaction conditions and results for the stannylation of 6b. ^(a)Preliminary isolated yield after column chromatography from one experiment.

No formation of side condensation products was observed under the reaction conditions employed. According to LC-MS analysis, the only compounds detected in the reaction mixture were starting materials and product as can be also seen in figure 3.24.

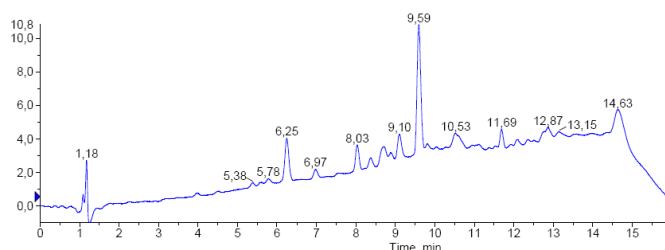


Figure 3.24: LC chromatogram of crude 6c (254nm). 6.25: 6b, 9.59: 6c. 9.10: HSnMe₃.

1D-NMR and 2D-NMR measurements were performed to confirm structure of stannanes **6c** and **6d**. ¹H-NMR of **6c** depicted in figure 3.25 and ¹³C-NMR (not depicted) confirm addition of the stannane functionalities to one of the pyridine C-atoms and show the intact ester group. Spin-spin coupling between Sn^[120] and neighboring protons including H-4 (³J [¹¹⁹Sn-¹H]: 38.8 Hz; ³J [¹¹⁷Sn-¹H]: 34.8 Hz) is observed in the ¹H-spectrum, suggesting regioselective addition of the stannyl group to C-5. This was also confirmed by HMQC and HMBC measurements. Some of the results are highlighted in figure 3.26.

3 Results and Discussion

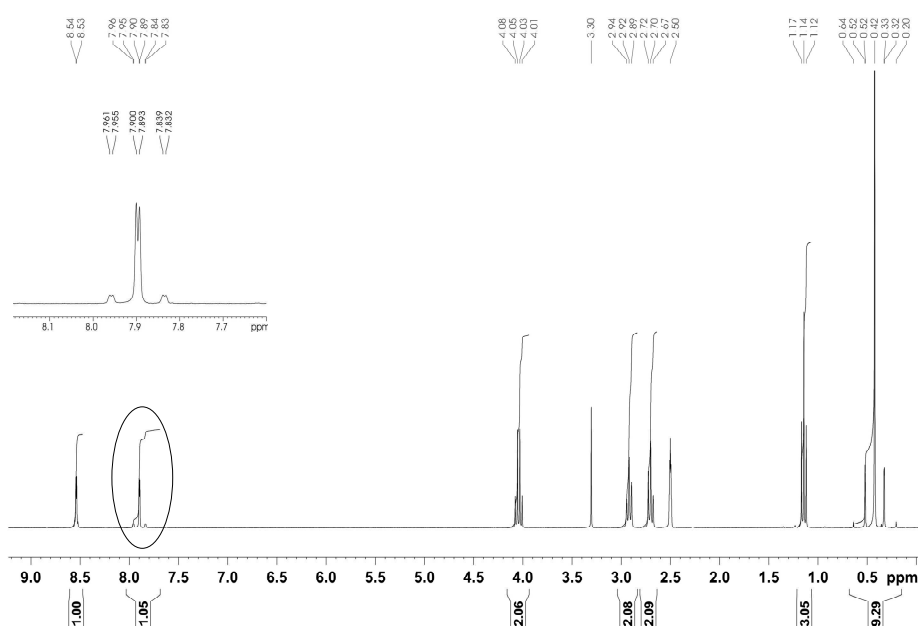


Figure 3.25: $^1\text{H-NMR}$ spectrum of trimethylstannane **6c** in $d_6\text{-DMSO}$. Top: Magnified view of the H-4 signal in which 4J -spin-spin coupling with H-2 (major peak) and 3J -spin-spin coupling with tin isotopes ^{119}Sn and ^{117}Sn is detected.

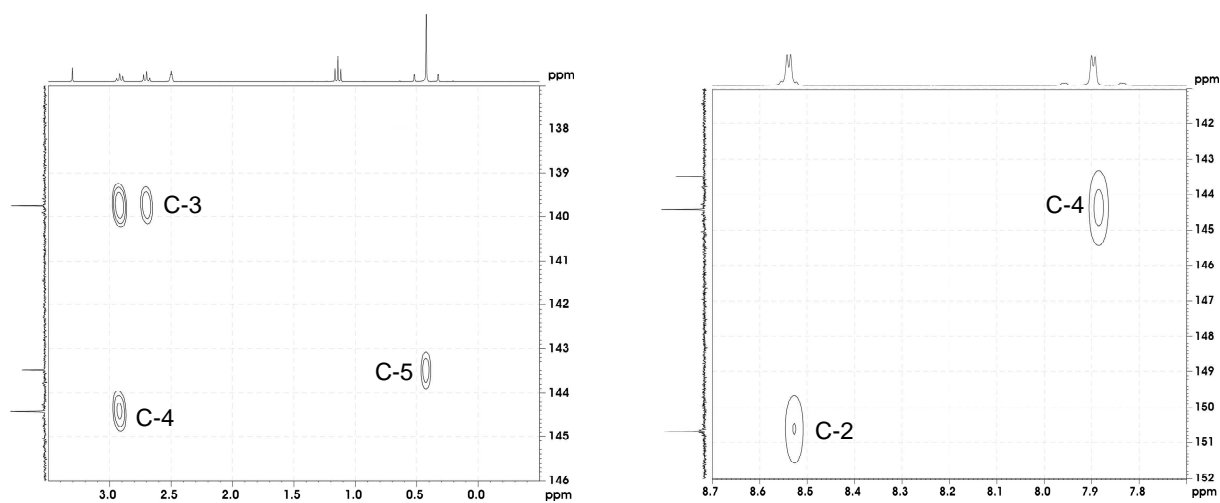


Figure 3.26: Magnified view of sections of the 2D-spectra of **6c**. Right: Detail of the HMBC spectrum depicting the correlation of aliphatic protons with C-3, C-5 and C-4. Left: Detail of the HMQC spectrum depicting the correlation between H-2 and C-2 as well as between H-4 and C-4.

It was also attempted to synthesize the boronic acid derivative **6e** using triisopropyl borate as electrophile. When the reaction mixture was quenched with $\text{H}_2\text{O}/\text{EtOAc}$ 60 minutes after addition of the electrophile and samples were taken at -75°C , LC-MS analysis showed formation of the desired product (entry 1, table 3.4).^[102]

3 Results and Discussion

The product, however, appeared to undergo protodeboronation upon warming up the crude mixture to room temperature according to LC-MS analysis. Trying to quench the reaction at room temperature and shortening the metalation time did not change the outcome of the reaction (entry 2 and 3, table 3.4).

entry	solvent	LiTMP	T	t	E ⁺	results
1	THF	3.0eq	-75°C	60min	4eq B(OiPr) ₃	product formation at -75°C ^(a)
2	THF	3.0eq	-75°C	45 min	4eq B(OiPr) ₃	no product formation ^(a)
3	Et ₂ O	3.0eq	-75°C	30 min	4eq B(OiPr) ₃	no product formation ^(a)
4	THF	4.0eq	-75°C	15min	5eq B(OiPr) ₃ / 5.1eq pinacol	used as crude product

Table 3.4: Reaction conditions used for the borylation of 6b. ^(a)according to LC-MS analysis.

This was surprising since successful synthesis of (2-cyano)pyrid-3-yl boronic acid in good yield using similar conditions has been reported^[114]. It was later found that the isolated boronic acid - obtained after HPLC purification of the corresponding pinacol ester - is sufficiently stable at room temperature for 1D- and 2D-NMR measurements. Therefore, the lability of the boronic acid must be facilitated by the reaction conditions, e.g. the higher amount of base/electrophile employed as compared to the reported conditions or the presence of the reactive lithium ester enolate.

It was then decided to trap the boronic acid *in situ* as boronic acid pinacol ester. In general boronic esters are considered to be more stable than boronic acids.^[114] Recently, Alessi et al. described the one-pot synthesis of pyridyl boronic acid pinacol esters from boronates (obtained from the corresponding lithium intermediates using LDA as lithiating agent) by simple addition of pinacol to the reaction mixture.^[121] Adapting these reaction conditions, pinacol boronate **6f** was synthesized using the one-pot sequence also depicted in figure 3.27: Regioselective lithiation of pyridine **6b** was followed by transmetalation and *in situ* esterification by addition of pinacol to the reaction mixture at -75°C and subsequent warming to 40°C.

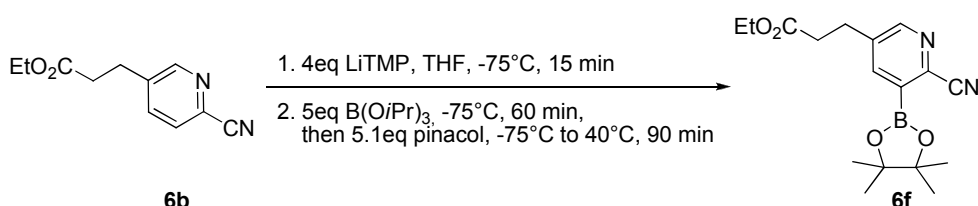


Figure 3.27: Scheme of the synthesis of pinacol pyridyl boronic acid ester 6f.

3 Results and Discussion

The reaction mixture was then subjected to an acidic work-up in order to hydrolyze metalated intermediates and to remove excess of base and electrophile from the reaction mixture. Unfortunately, deboronation of the pinacolester was observed during purification by crystallization or column chromatography. Therefore, crude pinacol boronate **6f** was used in the next reaction step.

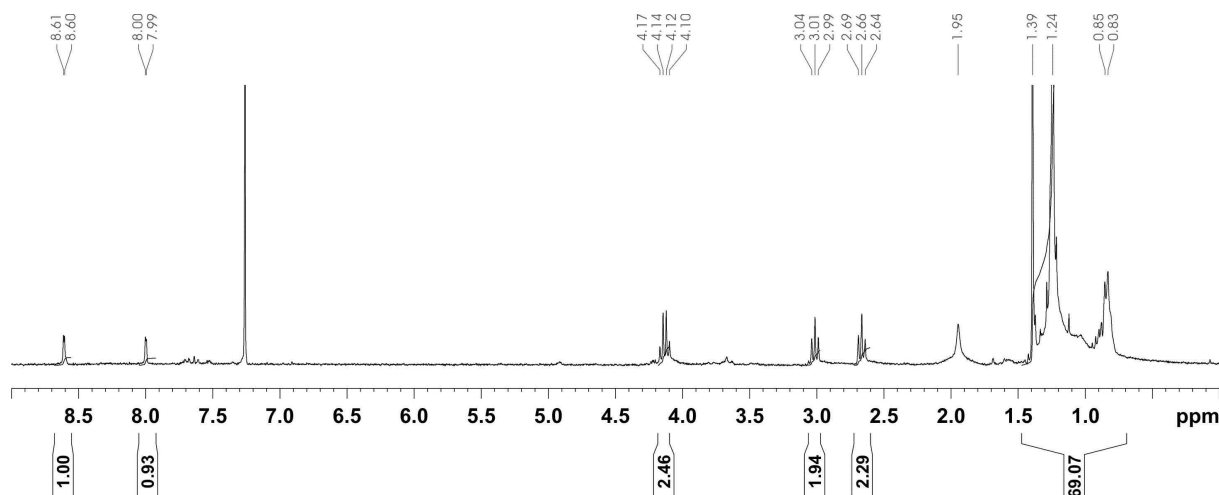


Figure 3.28: $^1\text{H-NMR}$ spectrum of crude **6f** in CDCl_3 after lyophilization in $\text{H}_2\text{O/ACN}$.

$^1\text{H-NMR}$ spectroscopy of crude boronic acid ester **6f** confirms functionalization similar as for stannane **6c** as depicted in figure 3.28. As can be seen in the LC-chromatogram of crude **6f** depicted in figure 3.29 most of the starting material **6b** was converted to pinacol boronate **6f**.

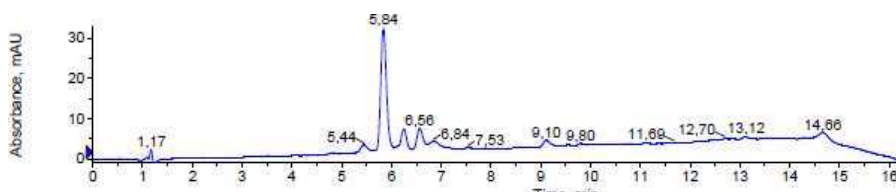


Figure 3.29: LC chromatogram of crude **6f** (254nm). 5.84: **6f**. 6.25: **6b**.

Good conversion of starting material **6b** was also confirmed by Suzuki-coupling of crude pinacol boronate **6f** with 2,5-dibromo-3-methylpyridine **7a** which gave the corresponding coupling product bipyridine **12b** in 74% yield (calculated back to **6b**) under optimized conditions as discussed in more detail in chapter 3.2.4.2.

3.2.3.2 Synthesis of building block 7

Analysis and Synthetic Strategy

As described in chapter 3.2.2 and depicted in figure 3.30, the pyridine building block **7** is a 3-methyl-4-propylpyridine derivative. As discussed in chapter 3.2.2, two functional groups were required for regioselective, sequential coupling between the C-2-position of pyridine **7** to building block **6**, followed by coupling of the C-5-position of the resulting bipyridine **12** to building block **8**. The corresponding 2,5-dibromo derivative depicted in figure 3.30 would allow the desired regioselective coupling of carbon C-2^[97] that could be followed by metalation of the remaining bromide at the C-5-position for generation of the nucleophilic component of the second Pd-catalyzed coupling.^[96]

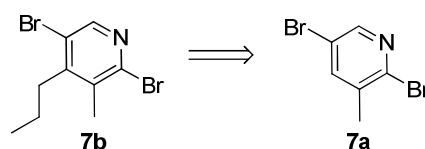


Figure 3.30: Retrosynthetic analysis of building block 7.

For the proposed reaction sequence, commercially available 2,5-dibromo-3-methylpyridine **7a** was used as starting material because it contains all but one of the required functionalities. For introduction of the propyl functionality into the 4-position of pyridine **7a** it was attempted to convert the compound to its *N*-pyridinium salt which should be susceptible to nucleophilic addition of Grignard reagents. It has been reported that with spacious reagents for the quaternization of the pyridine nitrogen, C-2 and C-6 positions can be shielded from nucleophilic attack.^[122;123] Different reagents have been used for quaternization of the pyridine nitrogen, including ethyl chloroformate or *t*-butyldimethylsilyl triflate.^[124] In this case, the synthesis of the corresponding 1-ethoxycarbonylpyridinium chloride was attempted followed by selective alkylation of the C-4 position with propyl cuprate. Propyl cuprate should be synthesizable *in situ* from the corresponding Grignard reagent and a Cu(I) salt. The resulting 1,4-dihydropyridine could then be oxidized yielding 4-alkylpyridine **7b**.^[122]

Synthesis of 4-alkylpyridine 7b

Initially formation of the required pyridinium salt **20** depicted in figure 3.31 was attempted by addition of ethyl chloroformate to the starting material at -75°C applying reported conditions.^[122] However, no product formation was observed by LC-MS and TLC analysis. It was then tested, whether use of different temperatures would result in pyridinium salt formation, but again only unreacted starting material was found. In order to confirm this result, the nucleophile propyl cuprate - which was formed *in situ* before the addition from propylmagnesium chloride and copper(I) iodide - was added to the mixture at different temperatures according to literature procedures. Again, only unreacted **7a** was found in LC-MS and TLC analysis.

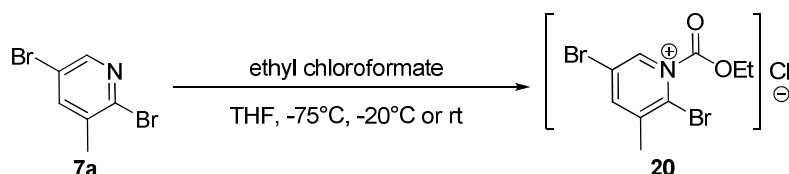


Figure 3.31: Scheme of the proposed synthesis of pyridinium salt **20**.

Control reactions performed with pyridine under the same reaction conditions showed formation of the 1-ethoxycarbonylpyridinium ion at every temperature tested in LC-MS analysis. This indicates an inherent problem of the reaction when using 2,5-dibromo-3-methylpyridine for this reaction. Whether addition of ethylchloroformate is hindered sterically by the spacious bromo-atom at C-2 or the pyridine-N-atom is too electron deficient for a successful electrophilic attack due to the electron-withdrawing bromo-substituents or a mixture of both factors was not further examined.

Alternative synthetic strategy for building block 7

Another way to functionalize C-4 of 2,5-dibromo-3-methylpyridine **7a** would be by directed *ortho*-metalation followed by electrophilic substitution, as already described in chapter 3.2.3.1. Regioselective lithiations of C-4 of 3-bromopyridine using LDA in THF as lithiating reagent have been described.^[125;126] Metalations of heteroaromatic compounds occur at the most acidic site, therefore presence of the acidic methyl

group at C-3 might result in lithiation at the methyl group similar as found when reacting 3-picoline with LDA.^[127] There are, however, also reports on successful metalation of the pyridine ring by LDA for the 3-picoline derivatives 2-chloro-3-fluoro-5,6-dimethylpyridine and 2-fluoro-5-methylpyridine.^[108] In these cases, increase of acidity of C-4 or C-3 in the latter case by the neighboring fluorine substituent was high enough for selective deprotonation of the indicated positions in the presence of the acidic methyl substituents. It was therefore decided to try this procedure on 2,5-dibromo-3-methylpyridine **7a** expecting that presence of the bromine functions might increase the acidity of the C-4 proton via inductive effects.^[128] Due to the lower electronegativity of bromine as compared to fluorine, activation of acidity at C-4 was expected to be significantly less pronounced in this system as compared to the reported examples.

If selective C-4 lithiation could be accomplished, one synthetic route to 4-propylpyridine **7b** could be trapping of the pyridyl lithium with iodine followed by Suzuki-coupling for introduction of the propyl functionality.

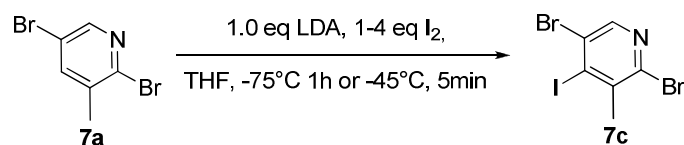


Figure 3.32: Scheme of the proposed synthesis of pyridyl iodide 7c.

Initially, reaction conditions as reported by Baxter et al. for the functionalization of 3-bromopyridine were applied.^[125] LC-MS analysis showed formation of a product with the expected product mass as well as a number of other products, including the unreacted starting material. It was then tried to scale-up the reaction and isolate the compounds found in the crude reaction mixture. Purification was, however, difficult and it was not possible to isolate clean compounds after column chromatography or kugelrohr distillation.

entry	solvent	Baes	T	t	E ⁺	results
1	THF	1eq LDA	-75°C	60min	1eq I ₂	conversion
2	THF	1eq LDA	-65°C	60 min	1eq I ₂	conversion

Table 3.5: Reaction conditions for the lithiation of 2,5-dibromopyridine 7a.

3 Results and Discussion

Further purification by preparative HPLC also did not give pure product required for characterization of the compound. However, $^1\text{H-NMR}$ (figure 3.33) of the product purified by preparative HPLC indicated that iodination took place at the pyridine ring and not at the methyl group.

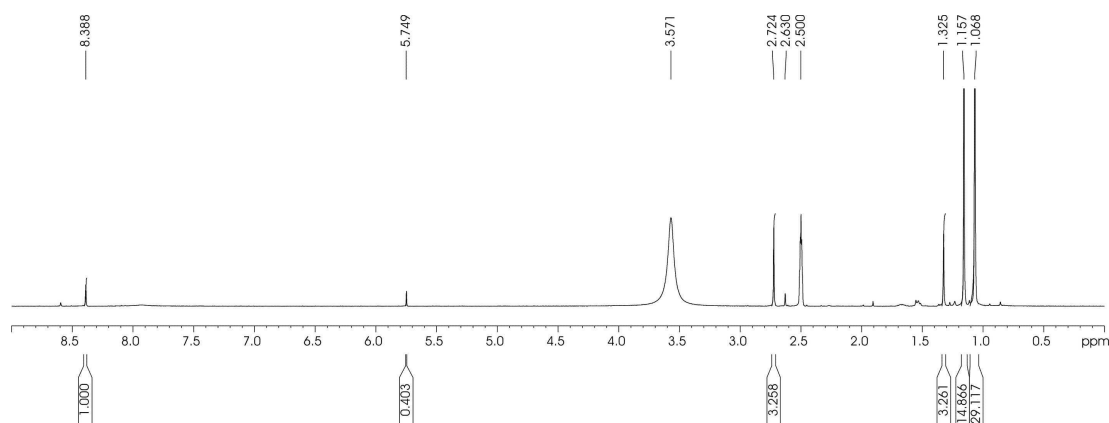


Figure 3.33: $^1\text{H-NMR}$ spectrum of **7c** after preparative HPLC in $\text{d}_6\text{-DMSO}$.

It was then tried to introduce the propyl functionality using Suzuki coupling. However, no product formation was observed by LC-MS analysis. Hypothesizing that the compound is the one expected, Suzuki coupling at C-4 might still be difficult due to severe steric hindrance by the methyl moiety and the spacious bromine atom in neighboring *ortho*-positions.

At this point it seemed reasonable to use a different approach for the synthesis of building block **7**. Synthesis of the required 2,5-dihalo-3-methyl-4-propylpyridine moiety is expected to be tedious with any synthetic strategy. The main goal at this point was to determine the potential of target compound **2b** or appropriate synthetic intermediates as a lead structure for RIIBD peptidomimetics. Therefore simplifying the building block was considered as a more reasonable approach for the time being than development of a new synthesis. In cooperation with AG Krause (FMP Berlin), one additional modification was introduced onto the target compound; the 4-propyl functionality of building block **7** was replaced with a methyl group.

It was decided to use 2,5-dibromo-3-methylpyridine **7a** again as starting material and to introduce the C-4 methyl group by DoM with the same conditions as earlier using in this case methyl iodide as electrophile as depicted in figure 3.34.

3 Results and Discussion

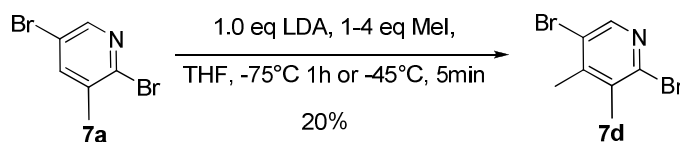


Figure 3.34: Scheme of the synthesis of 2,5-dibromo-3,4-dimethylpyridine **7d**.

Initially reaction conditions were adapted from the synthesis of **7c** (entry 1 in table 3.5). Under these conditions a mixture of products was obtained, containing starting material, 10% of product **7d** as well as several side products. The only identifiable side product was 2,5-dibromo-3-ethylpyridine, which was obtained in 5% yield. This by-product was probably formed from lithiation and subsequent methylation of the acidic methyl group. Initially, purification was performed by column chromatography. Since the three identified compounds are all very similar in polarity further purification by preparative HPLC was required for characterization of the compounds. It was later found that purification by kugelrohr distillation gave a better separation of the crude product.

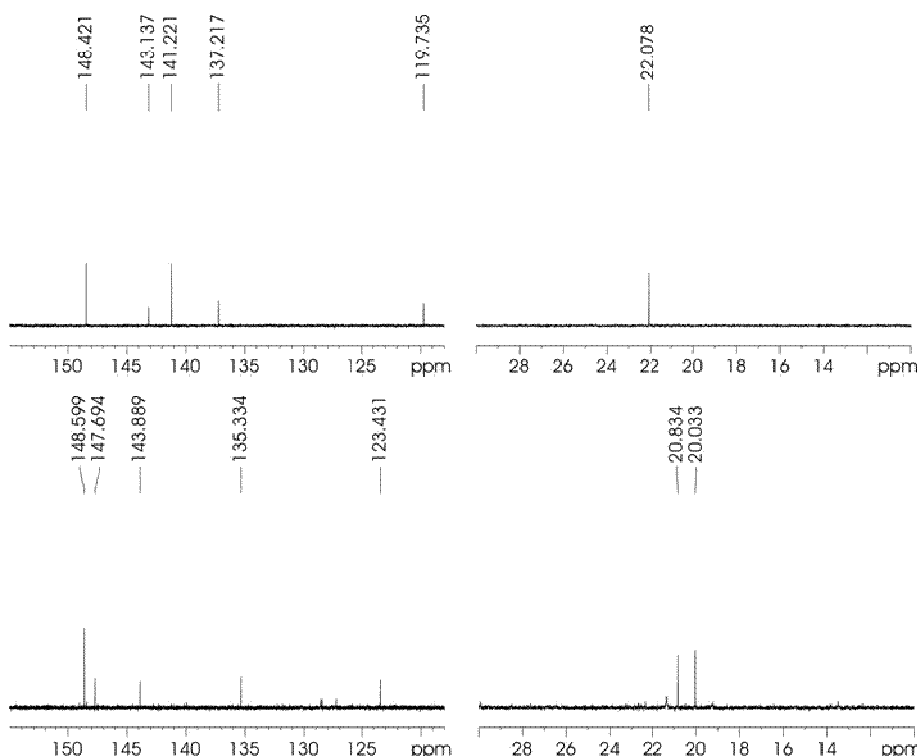


Figure 3.35: Enlarged sections of the ¹³C-NMR spectra of 2,5-dibromo-3-methylpyridine **7a** (top) and product **7d** (bottom) in CDCl₃.

3 Results and Discussion

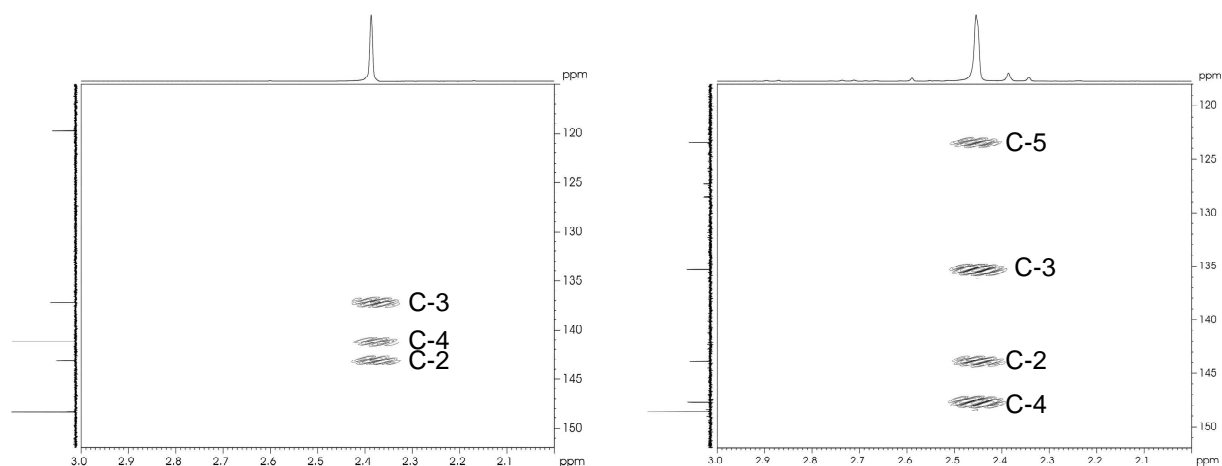


Figure 3.36: Enlarged sections of the HMBC spectra of 2,5-dibromo-3-methylpyridine (left) and product **7d (right).** The correlation of the methyl protons with pyridine carbon atoms is shown. Left: H-atoms show correlation with C-3, C-4 and C-2. Right: H-atoms show correlation with C-5, C-3, C-2 and C-4. The protons of methyl groups of 2,5-dibromo-3,4-dimethylpyridine are detected as one singlet with the expected intensity. HMQC analysis confirms correlation of the singlet with both aliphatic signals detected in the ^{13}C -NMR spectrum.

As can be seen in figure 3.35, 1D-NMR measurements confirm insertion of the methyl group into the pyridine as exemplified in ^{13}C -spectra of pyridine **7d** in comparison to the starting material. Some results of 2D-NMR measurements are depicted in figure 3.36, they confirm that the methyl group is in the C-4 position: When comparing HMBC spectra of the methyl protons with pyridine C-atoms of the starting material with **7d**, peaks are detected for both compounds with C-2, C-3 and C-4. As expected the product shows an additional interaction with C-5 that is not observed for the starting material.

It was then tried to optimize the reaction conditions on analytical scale by LC-MS monitoring in order to increase the yield. For this purpose, the influence of several factors with regard to product formation was checked. Initially, higher amounts of base were tested in order to reduce the amount of unreacted starting material found in the reaction mixture (entry 2, table 3.6).

The main product found under these conditions was a compound where double methylation occurred, e.g. at C-4 and the benzylic position, that was however not further validated. Formation of double-methylated product could be due to formation of a bi-anionic species. Another possibility is that, after addition of methyl iodide, residual LDA deprotonated already formed 3,4-dimethylpyridine **7d** and the resulting pyridyl lithium reacted again with methyl iodide.

In order to increase metalation efficiency, deprotonation was performed at higher temperatures, but for shorter periods (entry 4 and 5, table 3.6).

3 Results and Discussion

entry	solvent	LDA	T	t	E ⁺	product yield
1	THF	1.0eq	-65°C	60 min	1eq MeI	10% ^(a)
2	THF	2.0eq	-65°C	60 min	2eq MeI	mixture of products
3	THF	1.0eq	-50°C	15min	1eq MeI ^(b)	mixture of products
4	THF	1.0eq	-45°C	5 min	2eq MeI ^(b)	mixture of products
5	THF	1.0eq	-45°C	5 min	4eq MeI ^(b)	mixture of products
6	THF	1.1eq	-45°C	5 min	4eq MeI ^(b)	20% ^(c)
7	THF	1.2eq	-45°C	5 min	4eq MeI ^(b)	13% ^(c)

Table 3.6: Optimization of reaction conditions for the synthesis of 7d. ^(a)isolated yield after column chromatography of one experiment. ^(b)addition at -75°C. ^(c)isolated yield after kugelrohr distillation of two experiments.

In addition, the amount of electrophile used was increased in order to drive methylation of the starting material to completion and to quench remaining LDA in the mixture (entry 4-6, table 3.6).

According to LC-MS analysis of the crude mixtures under all conditions tested mixtures of different products were obtained. During the up-scaling of the reaction, shorter deprotonation time and higher temperatures (entry 6 and 7, table 3.6) were applied and the product was synthesized with the highest yield of 20%.

These results show that acidity of C-4 is increased by the bromine on the C-5 position thereby activating the position for deprotonation as compared to 3-picoline.^[119;127] However, acidity is not increased sufficiently to significantly favour deprotonation at C-4 over deprotonation of the benzylic position. Instead, both lithium intermediates appear to be present in equilibrium. In analytical test reactions after prolonged reaction times (>90 minutes, -65°C) only formation of 2,5-dibromo-3-ethylpyridine was detected in LC-MS analysis, suggesting that formation of the benzylic lithium intermediate is thermodynamically favored. It has not been examined so far, how pronounced solvent effects are on reaction outcome. By switching to less polar or non-coordinating solvents like DEE or hexane one could for example study if there is an influence of the aggregative state of LDA on its selectivity with the studied compound.^[129]

Nonetheless, it was decided to continue the synthesis with this low-yielding reaction step. Until the use of this scaffold as RIIBD mimetic is supported by experimental data, it seemed more reasonable not to spend more effort on developing another synthetic strategy. Instead, the synthesis of the target scaffold was established with

commercially available 2,5-dibromo-3-methylpyridine **7a** as building block **7**. The optimized reaction sequence should then be easily applicable to dimethyl-derivative **7d**, thereby reducing the required amount of this compound.

3.2.3.3 Synthesis of building block 8

Retrosynthetic analysis and synthetic strategy

As described in chapter 3.2.2 and depicted in figure 3.37, for the synthesis of the target compound a 6,7-dihydro-5H-cyclopenta[*c*]pyridine derivative was required as building block. The cyclopenta[*c*]pyridine is functionalized with a 3-propylamine at the C-3 position which needed to be protected as *N,N*-dibenzylamine or *N*-trifluoroacetamide during the synthesis. In addition, at the C-1 and C-4 position halide functions had to be introduced that could undergo Pd-catalyzed cross-coupling reactions with building block **9** and bipyridine building block **12**.

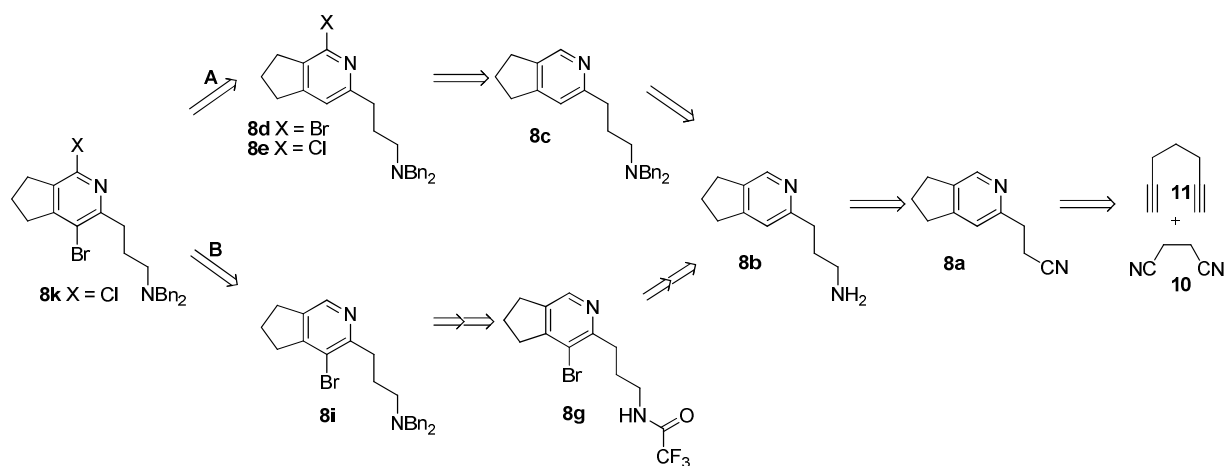


Figure 3.37: Scheme depicting the retrosynthetic analysis of building block 8.

Two different synthetic routes were investigated that differ in order of addition of the halides. For route A it was planned to attempt introduction of both halides *via* lithium-hydrogen exchange in the order depicted in figure 3.37. For route B, it was attempted to introduce the halide at C-4 by electrophilic substitution, and at C-1 by lithium-hydrogen exchange. Both synthetic strategies will be discussed in more detail in the corresponding chapters.

In both synthetic routes the amine **8b** was used as precursor. It was planned to synthesize **8b** in a two-step procedure. In the first step it was attempted to synthesize dihydrocyclopenta[*c*]pyridine **8a** *de novo* applying a Ru-catalyzed [2+2+2]-cycloaddition procedure developed recently^[80;130]. The authors described the use of Cp^{*}Ru(cod)Cl as a new catalyst^[131] for the synthesis of this type of scaffold from

different dialkynes and nitriles carrying electron-withdrawing groups in the α -position.^[132] Also, several nitriles with EWGs in β - or γ -position were successfully employed including succinonitrile which was one of the starting materials used for the synthesis of nitrile **8a**.^[130] Ru-catalyzed [2+2+2]-cycloaddition reactions of this type will be discussed in more detail in chapter 3.2.4.3. After reduction of the nitrile function with standard literature procedures, the corresponding amine **8b** could then be used as precursor for synthetic routes A and B.

Synthesis of amine **8b**

For the synthesis of building block **8**, the pyridine moiety was synthesized *de novo* by [2+2+2]-cycloaddition from 1,6-heptadiyne **11** and succinonitrile **10** with a Ru-based catalyst using conditions reported by Yamamoto et al.^[130]

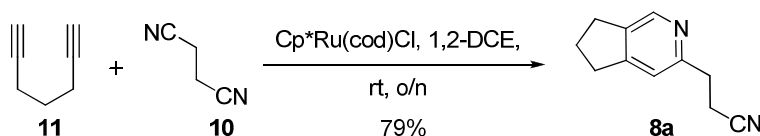


Figure 3.38: Scheme of the synthesis of **8a.**

The desired nitrile **8a** depicted in figure 3.38 was synthesized in good yields of up to 79%. The reaction was successfully up-scaled to multigram scale without reduction of yield, as shown in table 3.7.

mmol diyne	cat	yield ^(a)
66	1.3mol%	71%
271	1.3mol%	79%
175	1.0mol%	59%

Table 3.7: Reaction scales for the synthesis of nitrile **8a.** ^(a)isolated yields from at least 2 different experiments.

Lowering loading of the expensive Ru(II)-catalyst resulted in a significant drop in yield. **8a** was then reduced to give amine **8b** as depicted in figure 3.39 using BH₃*SMe₂ as reducing agent adapting reported conditions^[133] which gave the crude product in good yield of 86%.

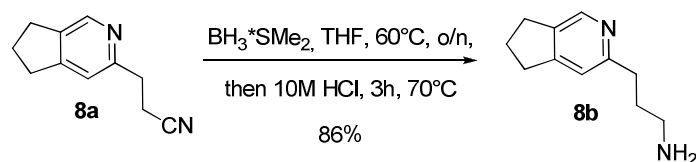


Figure 3.39: Scheme of the synthesis of amine 8b.

This reaction step was successfully scaled-up to multigram scale (max. 10 g starting material, ~60 mmol) without loss in yield.

Retrosynthetic analysis of synthetic route A

As already mentioned, functionalization of C-1 and C-4 was attempted by lithium-hydrogen exchange reaction. Protection of the amine **8b** was required under the strongly basic conditions used for the regioselective metalations, in this case the amine can be protected as *N,N*-dibenzylamine. Since pyridines are more acidic due to their lower π -electron density as compared to benzenes^[78;134], the benzyl group was expected to be inert to the metalation conditions. The protecting group should be removable under mild conditions by hydrogenolysis.^[106;135]

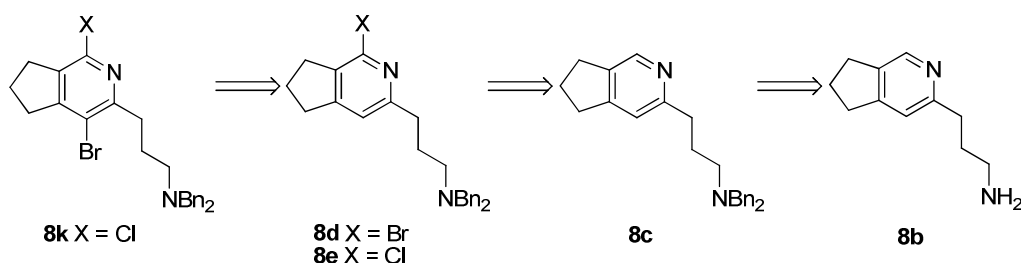


Figure 3.40: Scheme of the retrosynthetic analysis of building block 8.

The next reaction step was regioselective deprotonation of C-1 of dibenzylamine **8c**. As can be seen in figure 3.40, no substituent is present on **8c** that could facilitate regioselective lithiation by DoM. The electron-donating alkyl groups attached to α -, β - and γ -positions were expected on the one hand to deactivate the pyridine core for deprotonation^[128] and on the other hand potentially undergo lithiation at one of benzylic positions (lateral lithiation) with common lithiating agents LDA, LiTMP and *n*BuLi.^[136] In addition, it has been reported that *n*BuLi can react by nucleophilic addition to the azomethine bond of pyridines.^[137] Whether lateral lithiation or

nucleophilic addition takes place depends on the reaction conditions employed when reacting $n\text{BuLi}$ with alkyipyridines.^[138] Therefore, regioselective lithiation of C-1 of pyridine **8c** was attempted using the unimetal superbases $n\text{BuLi/LiDMAE}$ depicted in figure 3.41. This superbases consists of a 1:1 mixture of n -butyllithium and lithium- N,N -dimethylaminoethoxide. When used in non-coordinating solvents like hexane or toluene, an aggregated mixture of not-yet defined composition is formed that has been successfully used for pyridine ring functionalization of non-activated pyridine derivatives.^[139]

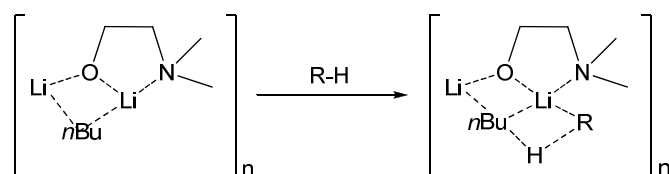


Figure 3.41: Simplified view of the composition of $n\text{BuLi/LiDMAE}$ aggregates and potential activation of the aggregate with an acidic reactant R-H .^[140]

For example, regioselective deprotonation of the C-2 position of pyridine,^[140] 3-picoline,^[137;138] 4-picoline,^[138] 3,5-lutidine^[141] and 3,4-lutidine^[138] have been described. None or only little lateral lithiation was observed as side reaction.

As already mentioned, the exact composition and aggregative state of the active reagent is not completely clear. This is also true for other Li-bases, since the amount of aggregation is dependent on a number of factors, including temperature, solvent, presence of additives, and the nature of the reactant.^[129;142] For the superbases $n\text{BuLi/LiDMAE}$, it is assumed that the formation of sterically hindered aggregates inhibits nucleophilicity of $n\text{BuLi}$ while basicity is increased by complexation, thereby preventing nucleophilic addition of the reagent to pyridine.^[136] Regioselectivity likely originates from chelation of the base with the pyridine nitrogen as depicted in figure 3.42.^[109]

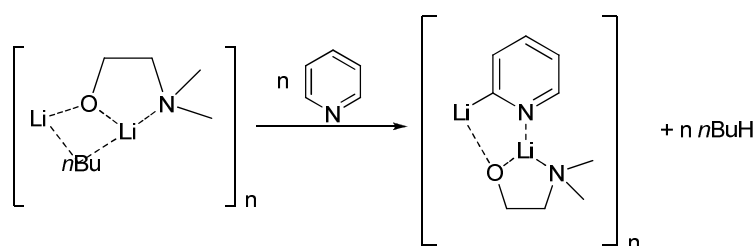


Figure 3.42: Scheme of the proposed mechanism of C-2 lithiation of pyridine by chelate formation.^[109]

There is some evidence suggesting that for 3-alkylpyridines lithiation takes place initially at the acidic side chain followed by lithium migration to C-6 which is facilitated by the complex between base and pyridine-N-atom.^[113] This has not been studied for other, more complex systems.

Following lithiation of C-1, the required pyridyl halide should be accessible by electrophilic quenching with CBr₄ or C₂Cl₆ yielding the corresponding bromide **8d** or chloride **8e**.

The final step of synthetic route A was regioselective lithiation of C-4 of building block **8**. This reaction was attempted with the chloride **8e**, since the corresponding bromide was expected to be more prone to undergo halogen-lithium exchange under metalation conditions.^[134] Again, presence of the acidic alkyl functions might lead to lateral lithiation only. The superbases *n*BuLi/LiDMAE has not been used for lithiation of non-activated β-positions of pyridine derivatives as found in this example. Some activation of acidity of C-4 was expected from the C-1 chloro- function,^[128] therefore several lithiating agents were screened for their potential in C-4 lithiation.

Evaluation of synthetic route A

The protection of amine **8b** as *N,N*-dibenzylamine **8c** was the first step. Benzyl bromide was used as alkylating agent for the synthesis of **8c**. NaH was initially used as a base, but only about 5% of product was isolated.

entry	solvent	Base	T	t	results
1	DMF	2.2 eq NaH	0°C to rt	o/n	5% ^(a)
2	ACN	2.2eq Na ₂ CO ₃	reflux	24h	no product formation
3	ACN	2.0eq K ₂ CO ₃	rt	3h	5% ^(a)
4	ACN	2.0eq K ₂ CO ₃	40°C	3h	completed ^(b)
5	ACN	2.0eq K ₂ CO ₃	rt	1.5h	5% ^(a)
6	ACN	2.0eq NEt ₃	rt	24h	51% ^(c)
7	ACN	2.0eq NEt ₃	60°C	3h	48% ^(c)

Table 3.8: Reaction conditions for the synthesis of 8c. ^(a)isolated yield from one experiment. ^(b)analytical test reaction. ^(c)isolated yield from at least four experiments.

It was then decided to use weaker bases. No product formation was observed with sodium carbonate,^[143] and only low product yields were obtained when using

potassium carbonate (entry 3-5 in table 3.8) as base. When switching to a procedure with less basic triethylamine, **8c** was obtained in modest yield of 48-51% (entry 6-7, table 3.8).^[144] This reaction step was successfully scaled-up to multigram scale (max. 10 g starting material, ~60 mmol) without loss in yield.

The next reaction step was regioselective functionalization of **8c** in position C-1 as depicted in figure 3.43.

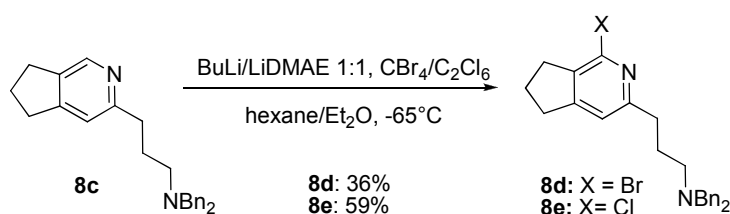


Figure 3.43: Scheme of the synthesis of halides 8d and 8e.

Initially reaction conditions for C-2 lithiation of pyridine were employed (entry 1, table 3.9),^[139] no conversion of the starting material was observed by LC-MS analysis of the reaction mixture. An increase in the amount of base to 4 equivalents (entry 2, table 3.9) gave the same result. The problem when performing the reaction in hexane is probably poor solubility of the starting material in this solvent. When performing the reaction in THF, unlike predicted from the literature, some product formation was observed (entry 3). Maybe aggregate formation of the base in hexane is so strong that lithiation of the starting material is prevented by steric hindrance at C-1 from the alkyl group at C-7'. This is supported by the finding that 3-picoline is deprotonated preferably by *n*BuLi/LiDMAE at C-6.^[137] It was, however, not further examined whether solubility or aggregate formation was the critical factor by e.g. performing the same reaction in the more polar, but also non-coordinating solvent toluene^[140] for which better solubility of the starting material can be expected.

In order to optimize the observed partial functionalization of C-1, it was decided to try to perform the reaction in mixtures of hexane and 10% THF (entry 4, table 3.9). In an initial test reaction on analytical scale, consumption of starting material and product formation was observed (entry 4, table 3.9). However, formation of a precipitate during addition of the electrophile was visible, clogging up the reaction mixture. This resulted in incomplete conversion of the starting material and only about 10% yield when up-scaling the reaction (entry 6, table 3.9).

3 Results and Discussion

entry	solvent	BuLi/LiDMAE	T	t	E ⁺	results
1	hexane	2eq	-75°C	60 min	CBr ₄	no conversion
2	hexane	4eq	-75°C	30 min	7eq CBr ₄	no conversion
3	THF	2eq	-75°C	60 min	CBr ₄	some conversion
4	hexane/THF	4eq	-75°C	30 min	7eq CBr ₄	complete conversion
5	hexane/THF	4eq	-75°C	30 min	7eq CBr ₄	conversion
6	hexane/THF	4eq	-75°C	30 min	7eq CBr ₄	<10%, not completed.
7	hexane/Et ₂ O	4eq	-75°C	30 min	7eq CBr ₄	28% ^(a)
8	hexane/Et ₂ O	4eq	-65°C	30 min	5eq CBr ₄	36% ^(b)
9	hexane/Et ₂ O	4eq	-65°C	30 min	5eq C ₂ Cl ₆	59% ^(b)

Table 3.9: Reaction conditions for the halogenation of pyridine **8c.** ^(a)preliminary yield from one experiment. ^(b)isolated yields from at least three different experiments.

When performing the reaction in hexane with 25% Et₂O instead of THF, complete consumption of the starting material was observed. The reaction mixture did not clog up despite formation of precipitate and the product was isolated in low yield (entry 7, table 3.9). Further optimization of the reaction gave bromide **8d** in 36% yield and chloride **8e** in 59% yield when performing the deprotonation at -65°C and reducing the amount of electrophile employed. The respective halides **8d** and **8e** were successfully obtained by regioselective lithiation/halogenation from **8c** after optimization of the reaction conditions. Regioselective addition of the halide functions was confirmed by 1D- and 2D-NMR measurements, the ¹H-NMR spectrum of chloride **8e** is depicted in figure 3.44.

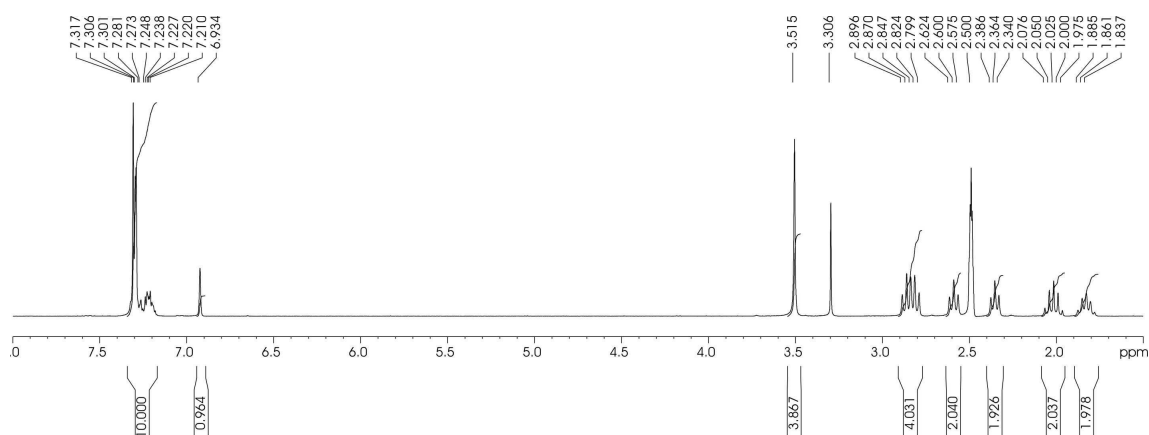


Figure 3.44: ¹H-NMR spectrum of chloride **8e in d₆-DMSO.**

3 Results and Discussion

It was shown that *n*BuLi/LiDMAE not only tolerates acidic alkyl groups at pyridine β - and γ - but also in α -positions.^[136] As expected from the literature, no formation of nucleophilic addition product or of a product from lateral lithiation was observed. It was found that the reaction does not proceed in hexane alone and that addition of more polar and coordinating etheral solvents THF or Et₂O was required. Whether this is necessary for sufficient solvation of the starting material or for formation of less tight or less spacious aggregates has not been further examined.

It was then tried to also functionalize C-5 of chloride **8e** using metal-hydrogen exchange. As already mentioned, it was not clear whether the chloro-substituent would sufficiently activate the C-4 position for metalation. There were no similar successful types of metalations found in the literature. Nonetheless, several bases were tried out in analytical test reactions under conditions depicted in table 3.10 and analyzed by LC-MS. Initially, the reaction was attempted using *n*BuLi/LiDMAE as lithiating agent with different temperatures and with the electrophiles SnM₃Cl, C₂Cl₆, CBr₄ and B(OiPr)₃ (entry 1-2, table 3.10).

entry	solvent	Bases	T	results
1	hexane/Et ₂ O	4eq BuLi/LiDMAE 1:1	-70°C	no conversion
2	hexane/Et ₂ O	4eq BuLi/LiDMAE 1:1	-60°C	some Cl-Li-Br exchange, no product formation
3	THF	1.2eq LDA	-75°C	no conversion
4	THF	LiTMP	-75°C	no conversion
5	Et ₂ O	2eq BuLi/KOtBu 1:1	-75°C	33% isolated yield ^(a)

Table 3.10: Reaction conditions for the functionalization of **8e.** ^(a)isolated yield after column chromatography from two experiments.

However, no conversion of the starting material was observed. In general, *n*BuLi/LiDMAE was reported to tolerate C-Cl bonds in pyridine substrates in α -, β - and γ -positions.^[113] This seemed to be highly temperature-dependent at least for chlorides in α -position: When performing deprotonation at -60°C and using CBr₄ as electrophile, formation of bromide **8d** was observed (but not further quantified). This was probably due to chloride/lithium exchange which suggests at this temperature C-Cl bonds become reactive towards *n*BuLi/LiDMAE. Switching to lithium amide bases LDA and LiTMP and conditions depicted in entry 3 and 4 of table 3.10 did not result in any conversion of the starting material. Formation of a compound with the expected

mass was observed when using the superbases LiCKOR as base in DEE (entry 8). LiCKOR is made up of 1:1 mixture of *n*BuLi and KO^tBu. The compound was isolated in 33% yield, but 1D- and 2D-NMR spectroscopy show that halogenation occurred at the C-3/ α -benzylic position, as depicted in figure 3.45 and 3.46.

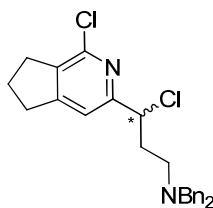


Figure 3.45: Compound 8l.

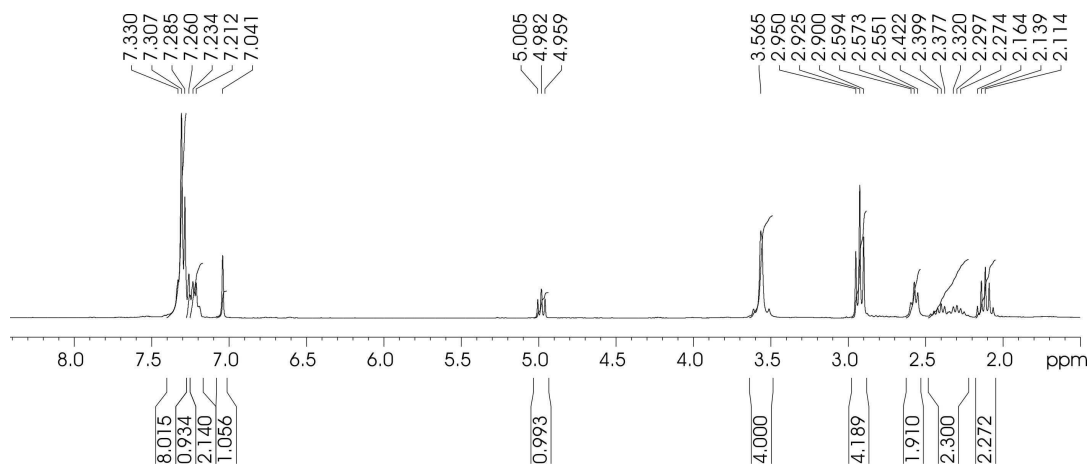


Figure 3.46: $^1\text{H-NMR}$ spectrum of 8l in CDCl_3 .

In conclusion, no selective lithiation of ring carbon atoms of the pyridine **8e** was accomplished. Nonetheless the successfully synthesized halides **8e** and **8d** are valuable compounds: They can be coupled to bipyridine **12b** giving rise to an intermediate structure of the target compound. These bipyridyl-dihydrocyclopenta[*c*]pyridines can be deprotected and evaluated for their use as RIIBD mimetics (chapter 3.2.4). The chloride **8l** can be coupled to bipyridine **12b** and evaluated as RIIBD mimetic.

Retrosynthetic analysis of synthetic route B

In an alternative approach to synthesize building block **8**, the halogen at position C-4 was supposed to be introduced by electrophilic substitution. It was decided to attempt the synthesis as bromide **8g**. The reason was on the one hand that the required reagent was already available in the lab and on the other hand that it seemed the best choice for the following Pd coupling steps: The bromide in the C-4/ β -position can be expected to undergo Pd-catalyzed borylation more rapidly than a chloride function in the C-1/ α -position. As depicted in figure 3.47, for the Pd-catalyzed cross-coupling reaction with pyridyl bromide **9h**, selective coupling of pyridine **8k** to bromide **9h** can be expected while coupling of **8k** with itself should be negligible.^[97]

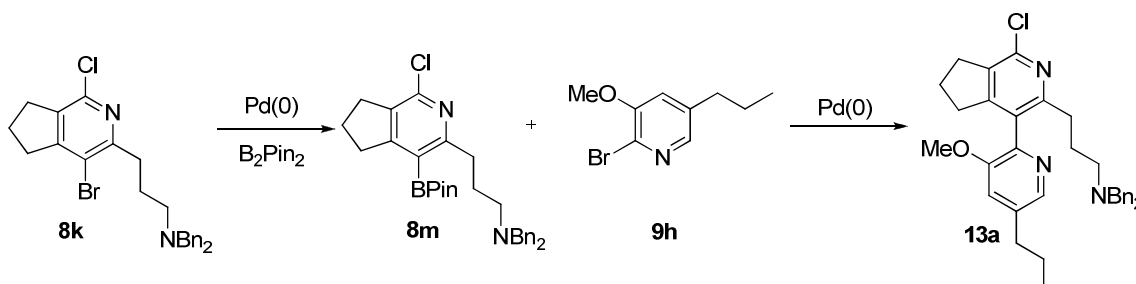


Figure 3.47: Scheme of a potential one-pot borylation-Suzuki coupling procedure with **8k (see also chapter 3.2.4).** B_2Pin_2 : bis(pinacolato)diboron, BPin: 4,4,5,5-tetramethyl-1,3,2-dioxaborolane.

In general, electrophilic substitutions of pyridines require harsh reaction conditions. The reason is the low π -electron density of pyridine due to the electron-withdrawing nitrogen atom.^[78] In this case the reaction was attempted with conditions reported for the bromination of 2,4,6-trimethylpyridine.^[145] 2,4,6-Trimethylpyridine was expected to have a comparable π -electron density as the present scaffold since they have the same number of alkyl substituents.

Unfortunately, strategy B required the use of a different, more exhausting protection strategy for the amine group. Protecting the amine as *N,N*-dibenzylamine under electrophilic substitution conditions would most likely result in halogenation of the benzyl groups which have a higher π -electron density as compared to pyridines or quaternization of the amine functionality.^[78] It was decided to protect the amine as *N*-trifluoroacetamide, which should be cleavable under basic conditions^[146] and was

expected to be stable under the strongly acidic conditions used for electrophilic substitution.^[106]

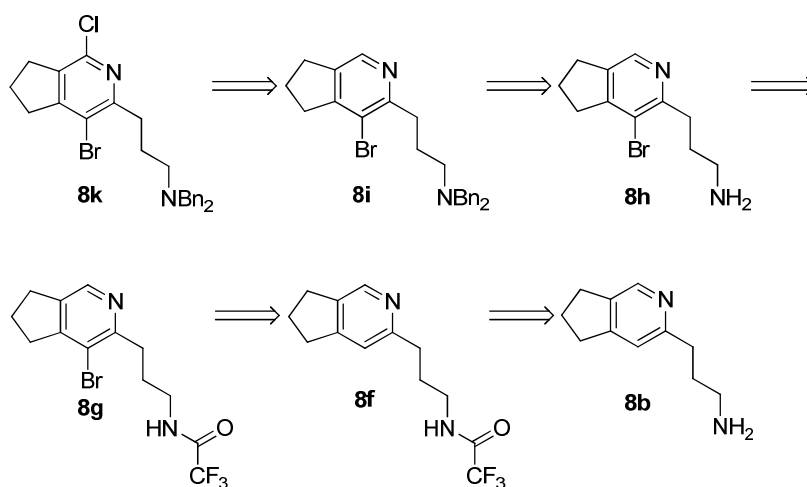


Figure 3.48: Scheme of the retrosynthetic analysis of dihalo-pyridine **8k**.

Following electrophilic substitution to obtain bromide **8g**, it was attempted to re-protect the amine functionality as *N,N*-dibenzylamine using conditions established for the synthesis of **8c**. This re-protection was required in order to avoid side reactions during the lithium-hydrogen exchange reaction that was to be employed for introduction of the halide function to the C-1 position. This last reaction step was attempted using the reaction conditions already established for the synthesis of halides **8d** and **8e**. This reaction step could be complicated by the presence of the bromide at C-4 which might react with the lithium base by lithium-bromide exchange thereby preventing efficient functionalization of C-1.^[134]

Evaluation of synthetic route B

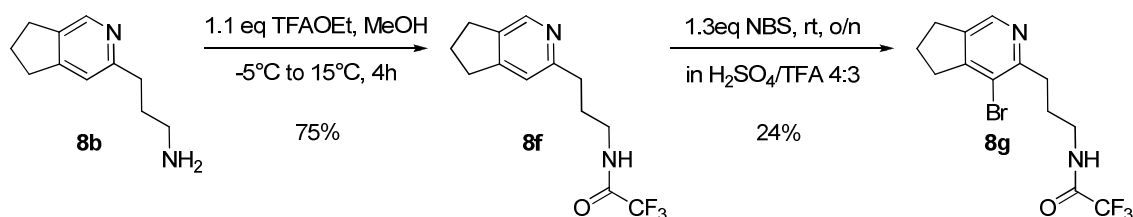


Figure 3.49: Scheme of the synthesis of 8g.

Compound **8f** was synthesized using standard conditions in good yield of 75% as depicted in figure 3.49.^[147] Electrophilic substitution of pyridine **8f** did not work very well and only low product yields of around 24% were obtained under the conditions depicted in table 3.11.^[145] Prolonging the reaction time or the amount of electrophile did not alter product yield (table 3.11). The only other isolated compound from the mixture was the starting material.

entry	solvent	electrophile	T	UV	t	yield
1	TFA/H ₂ SO ₄ 3:4	1.1eq NBS	rt	no UV	o/n	27% ^(a)
3	TFA/H ₂ SO ₄ 3:4	1.3eq NBS	rt	no UV	24h	24% ^(b)
4	TFA/H ₂ SO ₄ 3:4	1.3eq NBS	rt	no UV	36h	21% ^(a)
5	TFA/H ₂ SO ₄ 3:4	1.6eq NBS	rt	no UV	24h	23% ^(b)

Table 3.11: Reaction conditions for the synthesis of bromide 8g. ^(a)isolated yield from one experiment. ^(b)isolated yield from at least two experiments.

It was not tested, whether higher or lower reaction temperatures increase product formation. The influence of the concentration of the reactants on the equilibrium has also not been checked, nonetheless changes in both factors could improve reaction outcome.

After bromination of **8f**, the trifluoroacetamide group was removed under basic conditions to give amine **8h** using conditions adapted from Bergeron et al. with K₂CO₃ as base in a mixture of methanol/H₂O.^[146] **8h** was then protected as *N,N*-dibenzylamine **8i** with the conditions established for synthesis of *N,N*-dibenzylamine **8c** as depicted in figure 3.50. Both reaction steps gave the corresponding product in modest yields of 57% or 54% respectively.

3 Results and Discussion

Regioselectivity of lithiation/halogenation was confirmed by ^1H - and ^{13}C -NMR spectroscopy. As can be seen in figure 3.52, no pyridine proton signals are detected in the ^1H -NMR spectrum. In addition, aliphatic proton signals show the expected intensities and spin-spin couplings. Therefore, lateral lithiation can be excluded.

The side products found were a mixture of starting material **8i** (minor) and the corresponding chloride (major). This finding explains the low yield of the reaction quite well: The major side product is formed upon electrophilic substitution from the lithium species obtained after bromide/lithium exchange. It is not unexpected that the reactive C-Br bond preferably reacts with the lithiating agent, especially since quite high temperatures are required (-55°C) in order to observe any product formation at all.

entry	solvent	Base	T	t	rt ^(a) / isolated yield
1	hexane/Et ₂ O	4eq BuLi/LiDMAE 1:1	-50°C	30min	6.3min/13%

Table 3.12: Reaction conditions for the chlorination of **8i.** ^(a)rt = retention time in LC corresponding to expected product mass and isolated yield from one experiment.

In spite of being successfully synthesized, the low yield of this reaction sequence and especially of the last step did not produce the desired building block **8** in sufficient amount for use in the synthesis of target compound **2b**. An alternative approach for this reaction sequence could be electrophilic chlorination of pyridine **8h** instead of bromination. The generated chloride at C-4 position would be expected to be significantly more stable under the lithiating conditions ^[113;148] than the respective bromide.

3.2.3.4 Synthesis of building block 9

Retrosynthetic analysis and synthetic strategy

Retrosynthetic analysis of the target compounds showed that for building block **9** a pyridine ring should carry a halide function in the C-2 position for Pd-catalyzed cross-coupling, as well as a propylfunction at the C-5 position and a hydroxyfunction at C-3. The hydroxyfunction had to be protected as an alkoxyether in order to avoid side reactions during the coupling reactions and to serve as DMG for the introduction of the halide by DoM.

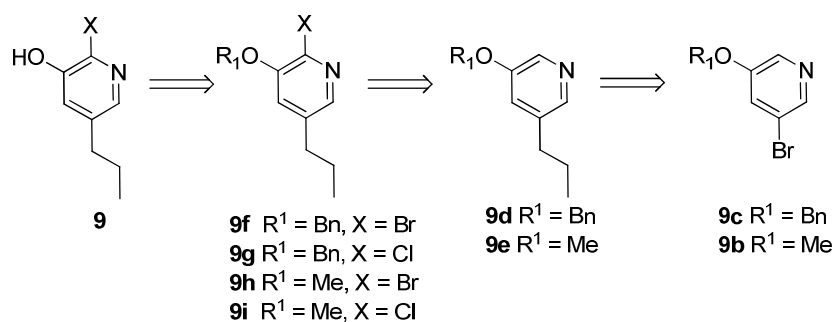


Figure 3.53: Retrosynthetic analysis of building block 9.

For introduction of the propyl group several procedures have been successfully applied with 3-bromopyridines. Therefore, commercially available 3-hydroxy-5-bromopyridine **9a** or 3-methoxy-5-bromopyridine **9b** could be used as starting materials. The 3-hydroxy derivative could be protected as benzylether **9c** using standard conditions. The propyl functionality can be introduced by an Cu(I)-catalyzed oxidative coupling procedure between pyridines **9c** or **9b** and a propylmagnesium halide.^[149] Another approach could be the introduction of the propylfunction by Suzuki cross-coupling of propylboronic acid with pyridine **9c** or **9b**.^[150]

The key step in the proposed reaction sequence was the selective functionalization of a 3-alkoxy pyridine to a 2-halide-3-alkoxy pyridine by DoM. Alkoxy pyridines have been used widely for DoM with different lithiating agents including mesityllithium,^[151] LDA,^[152] and *n*BuLi/TMEDA.^[153] A potential complication was the presence of the acidic alkyl group, therefore it was decided to employ *n*BuLi/LiDMAE as base (see also chapter 3.2.3.3). *n*BuLi/LiDMAE has been successfully used for C-2 lithiation of

3-methoxypyridine^[140] and as already described does not react with benzylic positions of alkyl substituents. Regioselectivity in this case is probably accomplished by cooperative complexation from the methoxy group and the pyridine nitrogen.^[140]

It was decided to attempt regioselective lithiation not only with methoxypyridine **9e** but also with the benzyloxypyridine **9d** for several reasons. The benzyl protecting group should be removable under mild conditions by hydrogenolysis. Also, the amine function of building block **8** was protected as *N,N*-dibenzylamine which means that both functional groups could be deprotected in one reaction step. Finally, successful lithiation of benzyloxypyridines has been reported with *n*BuLi/TMEDA in THF.^[153]

To the author's knowledge, selective deprotonations of *n*BuLi/LiDMAE with benzyloxy groups as DMG have not been described in the literature. Therefore, it was decided to compare both methoxypyridine **9e** and benzyloxypyridine **9d** as precursors in DoM-reactions with *n*BuLi/LiDMAE.

Synthesis of 3-(benzyloxy)-2-bromo-5-propylpyridine and 3-(benzyloxy)-2-chloro-5-propylpyridine

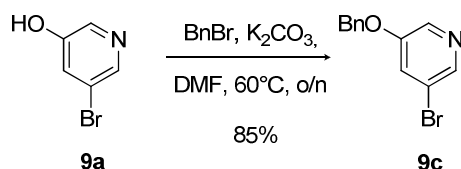


Figure 3.54: Scheme of the synthesis of benzyloxyether **9c**.

For the synthesis of pyridine **9c** depicted in figure 3.54, commercially available 3-bromo-5-hydroxypyridine **9a** was protected as benzyloxyether using standard conditions which gave the product in good yield of 85%.^[154] Introduction of the propyl functionality was tried using the Cu(I)-catalyzed procedure from Bell et al.^[149]

entry	solvent	Cu(I)salt	T	t	PrMgCl	results
1	THF	4eq CuCN	-78°C	150 min, to rt o/n	8 eq	20% yield ^(a)

Table 3.13: Reaction conditions for the synthesis of pyridine **9d**. ^(a)isolated yield after column chromatography of two experiments.

Initially, a procedure was applied using copper(I) cyanide as Cu(I) source which gave the desired product in 20% yield after column chromatography (entry 1, table 3.13).

3 Results and Discussion

In addition 40% of starting material and about 20% of reduced starting material were recovered from the reaction mixture. It was tried to optimize the product yield, e.g. by using copper(I) iodide as Cu(I)-source but this did not improve reaction outcome. Therefore it was decided to attempt introduction of the propyl moiety by Suzuki cross-coupling of pyridine **9c** with propylboronic acid as depicted in figure 3.55.

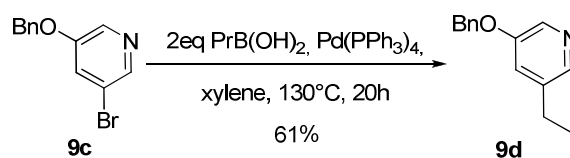


Figure 3.55: Scheme of the synthesis of pyridine 9d.

Propyl boronic acid was either bought or synthesized using standard reaction conditions giving the product in excellent yield of 91%.^[155]

entry	solvent	base	T	t	catalyst	results
1	xylene	2eq K_2CO_3	130°C	20h	1mol% $\text{Pd(PPh}_3)_4$	61% yield ^(a)
2	xylene/ H_2O	2eq K_2CO_3	130°C	20h	5mol% $\text{Pd(PPh}_3)_4$	83% yield ^(b)

Table 3.14: Reaction conditions for the synthesis of 9d. The reactions were performed with 2 eq of propyl boronic acid. ^(a)isolated yield after column chromatography of at least three experiments. ^(b)isolated yield after column chromatography of one experiment.

The propyl group was successfully coupled to **9c** using Suzuki coupling conditions from Kondolff et al., with the exception that a standard $\text{Pd(PPh}_3)_4$ catalyst system was used for the reaction.^[150] This gave the product in 61% yield and therefore the reported catalyst system which employs the so-called "tedicyp"-phosphine ligand was not tested. An initial experiment suggested that the yield of the reaction can be increased further to 83% when employing optimized reaction conditions from the synthesis of pyridine **9e** (discussed in the next chapter) when water is used as co-solvent and higher amounts of catalyst are used (entry 2, table 3.14).

The final step in this reaction sequence was the selective metalation of the C-2 position as shown in figure 3.56. The lithiated species was trapped with different halide electrophiles as depicted in table 3.15. Iodine is not well soluble in hexane and was therefore not used as electrophile in reactions at larger scale. CBr_4 and C_2Cl_6 are very well miscible with hexane.

3 Results and Discussion

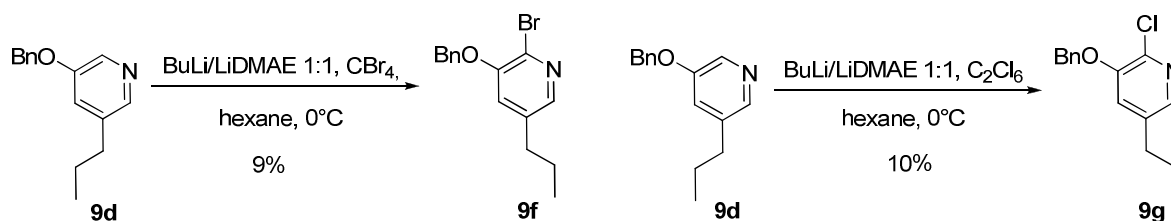


Figure 3.56: Scheme of the synthesis of bromide 9f and chloride 9g.

Initially, reactions were performed on analytical scale and analyzed by LC-MS and TLC. With conditions taken from lithiation of 3-methoxypyridine formation of product mixtures was observed.^[140] The amount of base was then increased (entry 2 and 3, table 3.15) in order to reduce the amount of unreacted starting material found, however no significant differences were observed.

entry	solvent	BuLi/LiDMAE 1:1	T	t (dep)	E ⁺	results
1	hexane	3 eq	0°C	20 min	4 eq I ₂	no product formation
2	hexane	3 eq	0°C	30 min	4 eq CBr ₄	product formation
3	hexane	4 eq	0°C	30 min	6 eq CBr ₄	product formation
4	hexane	3 eq	0°C	15 min	4 eq CBr ₄	9% ^(a)
5	hexane	4 eq	0°C	30 min	6 eq CBr ₄ ^a	9% ^(b)
6	hexane	4 eq	0°C	30 min	6eq C ₂ Cl ₆ ^(a)	10% ^(b)
7	hexane	2 eq	0°C	30 min	6eq C ₂ Cl ₆ ^(a)	5% ^(a)

Table 3.15: Reaction conditions for the synthesis of 9f and 9g. ^(a)isolated yield from one experiment. ^(b)isolated yield from at least two experiments.

Up-scaling of the reaction gave the product **9f** in very low yield of 9-10% (entry 5-6). Reducing deprotonation time or using lower amount of base (entry 4 and 7, table 3.15) did not improve final yield. There was no significant difference in final yields between chlorinated (4.7% after three steps) and brominated (5.2% after three steps) products.

1D- and 2D-NMR measurements confirmed regioselective functionalization of C-2 of halides **9f** and **9g**. As can be seen in figure 3.57, the ¹H-NMR spectrum confirms halogenation of the pyridine ring and not the benzylic positions.

3 Results and Discussion

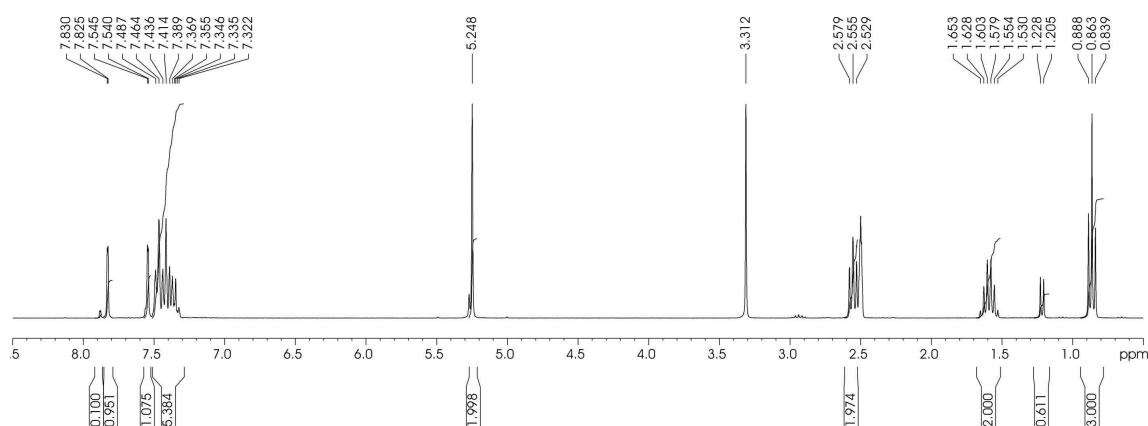


Figure 3.57: $^1\text{H-NMR}$ spectrum of chloride **9g** in $d_6\text{-DMSO}$.

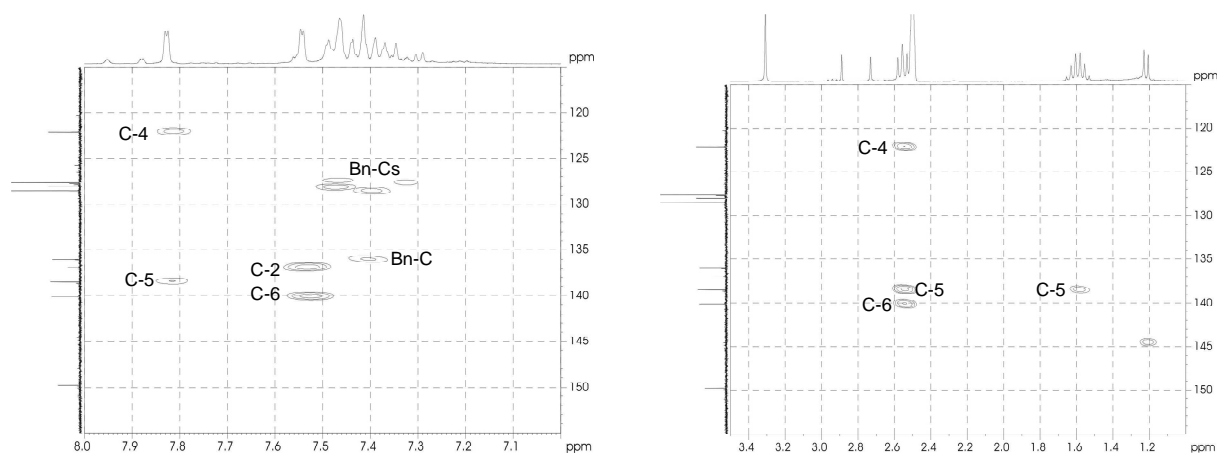


Figure 3.58: Zoom into the HMBC-spectrum of aromatic carbon atoms of chloride **9g**. Left: Cross-peaks of aromatic signals of benzyl group, H-4 and H-6 with aromatic carbon signals from the benzyl group and the pyridine core are depicted. Right: Cross-peaks of aliphatic signals of the propylfunction with aromatic carbon signals from the benzyl group and the pyridine core are depicted. Proton signals detected at 1.2 ppm, 2.7 ppm, 2.9 ppm are residual solvent peaks.

In figure 3.58 some results of 2D-NMR measurements are shown. In the depicted zoom into the HMBC spectrum of chloride **9g**, the peaks of the aliphatic proton signals of the propyl-function allow exact assignment of the correlated ^{13}C -peaks of C-5, C-6 and C-4. In addition, the expected correlation of H-4 with C-2 and C-6 is detected. H-6 shows cross peaks corresponding to C-5 and C-4 but not C-3, confirming that halogenation occurred at C-2.

The low product yields obtained suggest that regiochemical control with the benzyloxyether did not work sufficiently to activate the C-2 position for selective lithiation. The reason is probably steric hindrance from the benzyl group blocking tight

chelate formation between base and the alkoxy-oxygen. Although it was tried to optimize reaction conditions by trying different *n*BuLi/DMAE ratios and different deprotonation times, product formation was not improved.

In conclusion, isolated yields of final products were too low for further synthesis. Therefore it was decided to continue with the synthesis of the corresponding methoxypyridines **9h** and **9i**.

Synthesis of 2-bromo-3-methoxy-5-propylpyridine and 2-chloro-3-methoxy-5-propylpyridine

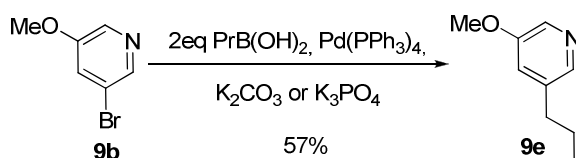


Figure 3.59: Scheme of the synthesis of 9e.

The reaction sequence was started from commercially available 3-methoxy-5-bromopyridine **9b** as depicted in figure 3.59. The propyl functionality was coupled to the C-5 position of the starting material by Suzuki coupling using the conditions established for pyridine **9d** (in the previous chapter), however, only a low yield of 26% was obtained (entry 1, table 3.16).

entry	solvent	propyl-source	T	t	Pd(PPh ₃) ₄	results
1	xylene	2eq PrB(OH) ₂	130°C	o/n	0.01eq	26% ^(a)
2	DMF	2eq PrB(OH) ₂	130°C	20h	0.05eq	completed ^(b)
3	DMF	2eq PrB(OH) ₂	130°C	20h	0.05eq ^(c)	19%, 44% red. ^(a)
4	xylene/H ₂ O	2eq PrB(OH) ₂	118°C	max. 40h	0.05eq	not completed ^(b)
5	dioxane/H ₂ O	2eq PrB(OH) ₂	98°C	max. 40h	0.05eq	not completed ^(b)
6	xylene/H ₂ O	2eq PrB(OH) ₂	130°C	40h	0.05eq ^(c)	57%, 11% s.m. ^(d)
7	dioxane/H ₂ O	2eq PrB(OH) ₂	98°C	40h	0.05eq ^(c)	48%, 30% s.m. ^(a)

Table 3.16: Reaction conditions for the synthesis of 9e. Conditions: 2eq K₂CO₃ or 3eq K₃PO₄ (entry 6 and 8) were employed as base. Amount of H₂O if used as co-solvent: 10% in indicated solvent. s.m.: starting material. ^(a)isolated yield after column chromatography of one experiment. ^(b)test reaction on analytical scale. ^(c)generated in situ from Pd(OAc)₂/PPh₃. ^(d)isolated yield after column chromatography of at least two experiments.

Therefore, reaction conditions were further optimized. For that purpose a reaction was run on analytical scale first in order to monitor progress of the reaction by LC-MS

3 Results and Discussion

and then scaled up for yield determination. At first it was decided to increase catalyst loading in all further reactions to 5 mol%. Then the influence of the solvent on reaction outcome was tested, starting with the polar solvent DMF. In DMF, the reaction was completed after 20 hours of reaction time and no starting material was isolated from the reaction mixture (entry 2 and 3, table 3.16). Product yield in DMF was low, only a yield of 20% was obtained. The main side product was reduced starting material which was recovered in more than 40% yield (entry 3, table 3.16). LC-MS data of analytical and up-scaled conditions corresponded well to each other, as can be seen in figure 3.60.

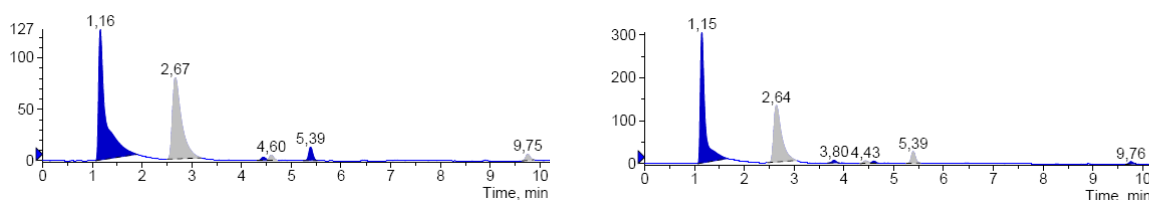


Figure 3.60: LC-spectrum of crude 9e at 280nm. Absorbance intensity is depicted as mAU. Retention time: 1.1 min: reduced starting material. 2.6 min: product. Left: LC-spectrum entry 3, table 3.16. Peak ratio: 1.1min/2.6min = 1.3:1 Right: LC-spectrum of entry 2, table 3.16. Peak ratio: 1.1min/2.6min = 1.5:1.

It was then tested whether the less polar solvents dioxane and xylene were beneficial for the reaction outcome. In these solvents, only minor amounts of reduced starting material were detected in LC-MS analysis of the reaction mixture and none was isolated after column chromatography. Analytical test reactions indicated that significantly longer reaction times of 40 hours were required as compared to DMF. Longer reaction times than 40 hours were not tested. In addition, 10% of water was added as co-solvent to the reaction mixture. This has been found to be beneficial in Suzuki couplings in some cases during the work on this thesis.

Up-scaling of the reaction gave the product **9e** in dioxane/H₂O in a reasonable yield of 48% and 30% of recovered starting material. With xylene/H₂O, the product was reproducibly obtained in 57% yield with 11% of unreacted starting material being recovered.

These results suggested that in less polar solvents the oxidative addition of Pd(0) into the pyridine-bromide bond was slower, since longer reaction times were required and unreacted starting material was recovered from the reaction mixture. The formation of reduced starting material which was observed when performing the reaction in DMF

3 Results and Discussion

was caused by hydrodebromination. This probably takes place by formation of σ -pyridine- L_n Pd(II)-H-complex (from the oxidative addition product: a σ -pyridine- L_n Pd(II)-Br-complex) which can eliminate the reduced starting material.^[97] The reason for this can be inefficient transmetalation,^[97] in this case of propylboronic acid to the pyridine- L_n Pd(II)-halide complex. Another explanation could be that propylboronic acid is unstable in DMF, e.g. undergoing β -hydride elimination,^[156] thereby reducing the amount of nucleophilic component present in the reaction mixture. In the case of dioxane and xylene, transmetalation appears to work better, no or only minor elimination of reduced starting material from the Pd(II)-complex was observed. Again, better stability of propylboronic acid in less polar solvents could add to the observed results.

Another rationalization could be a higher stability of the pyridine- L_n Pd(II)-halide complex in less polar solvents which increased probability for a productive interaction of this complex with the active alkyl boron-ate complex in the transmetalation process. An increased stability of this complex would also be an explanation for the observed suppression of dehydrobromination of the starting material in dioxane and xylene.

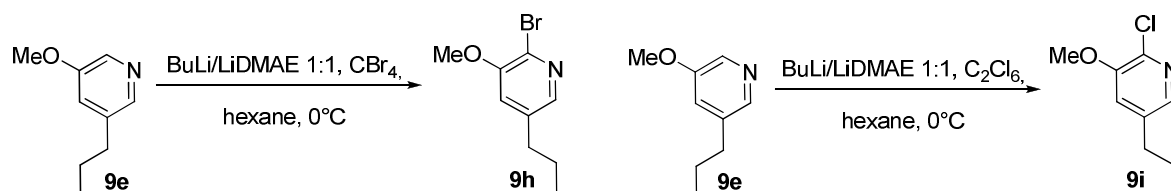


Figure 3.61: Scheme of the synthesis of bromide 9h and chloride 9i.

Selective deprotonation of 3-methoxy-5-propylpyridine **9e** worked significantly better than with the 3-benzyloxy derivative **9d**. With 4 eq of *n*BuLi/LiDMAE 41% to 57% yield of the corresponding halides were obtained (entry 3 and 5, table 3.17).

entry	solvent	BuLi/LiDMAE	T	t (dep)	E ⁺	results
1	hexane	3 eq	0°C	15 min	4eq CBr ₄ ^(a)	test run
2	hexane	2 eq	0°C	30 min	4eq CBr ₄ ^(a)	n.d. ^(b)
3	hexane	4 eq	0°C	30 min	6eq CBr ₄ ^(a)	41% ^(c)
4	hexane	2 eq	0°C	30 min	4eq C ₂ Cl ₆ ^(a)	20% ^(d)
5	hexane	4 eq	0°C	30 min	6eq C ₂ Cl ₆ ^(a)	57% ^(c)

Table 3.17: Reaction conditions for the halogenation of 9e. ^(a)E⁺ added at -75°C. ^(b)not clean, contaminated with CBr₄, therefore no yield was determined. ^(c)isolated yield after column chromatography from at least two experiments. ^(d)isolated yield after one experiment.

3 Results and Discussion

When using less *n*BuLi/LiDMAE in order to save reagent, in the case of chloride **9i** the yield dropped (entry 4, table 3.17) confirming literature reports that high amounts of the superbases were required for selective metalation.^[136] Only one product with the expected mass spectrum was found by LC-MS analysis of the crude product. Regioselectivity of lithiation/halogenation was confirmed in 1D- and 2D-NMR measurements.

As can be seen in figure 3.62, chlorination of **9e** occurred at the pyridine ring and not at the benzylic positions. Regioselective chlorination was confirmed by COSY- and HMQC-measurements of halides **9h** and **9i**.

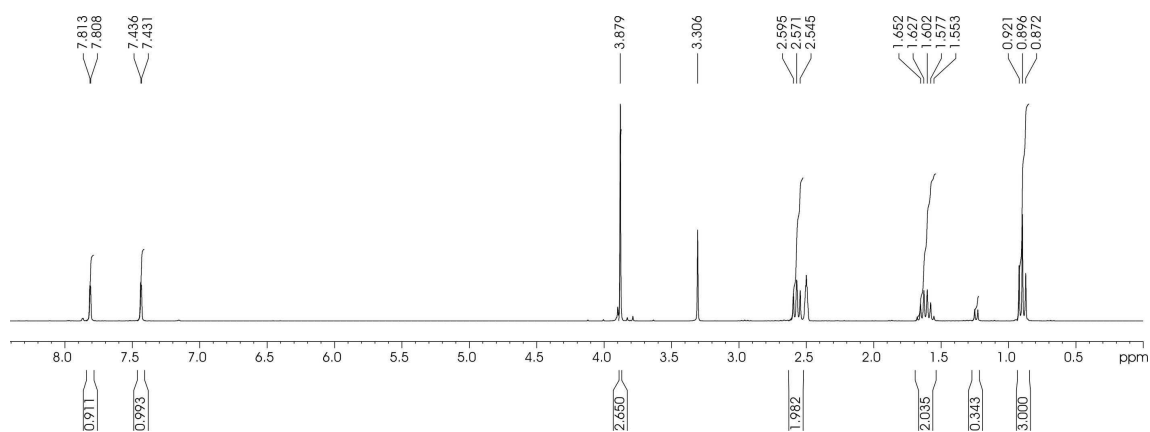


Figure 3.62: ¹H-NMR spectrum of chloride **9i** in d₆-DMSO.

3.2.4 Assembly of pyridine-based oligomers

3.2.4.1 Synthetic strategy

Having established the syntheses of the four single pyridine building blocks, the next part of the synthesis was the assembly of building blocks **6** to **9** to obtain the target scaffold **2**.

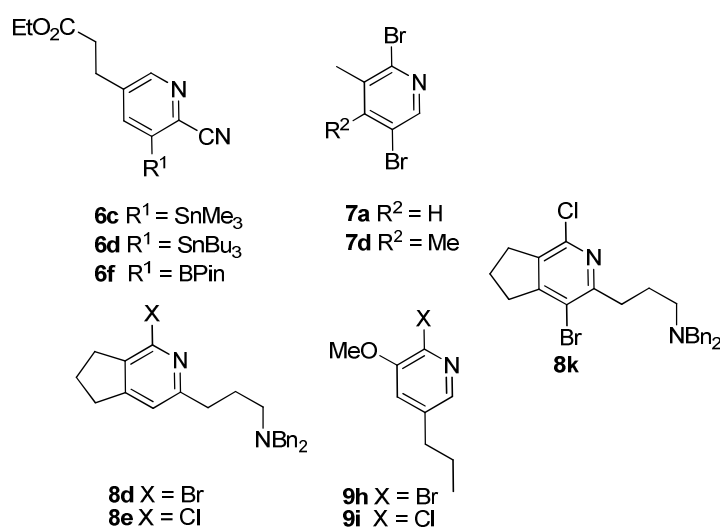


Figure 3.63: Scheme of successfully synthesized single pyridine building blocks.

Unfortunately, it was not possible to produce building block **8k** in sufficient amounts in order to construct target scaffold **2** by the initially proposed synthesis with iterative Suzuki-Miyaura coupling (route A or B, chapter 3.2.2).

compound	numer of steps	final yield	compound	numer of steps	final yield
6c	2	33.4%	8e	4	20.5%
6d	2	34.3%	8k	7	0.5%
6f	2	n.d.	9h	2	23.4%
7d	1	20.0%	9i	2	32.5%
8d	4	12.5%			

Table 3.18: Final yields of functionalized building blocks 6-9.

At this point, it was decided to synthesize the intermediate building blocks **14a** and **14b** depicted in figure 3.64. These 1-(2,3'-bipyridin-5-yl)-dihydrocyclopenta[*c*]pyridines are important precursors of quaterpyridine **2c** and

In addition, it was decided to develop a modified synthetic route to terpyridine building block **24a** in which the difficult synthesis of building block **8** was avoided. Instead, building block **8** was attached to bipyridine **12b** *via* [2+2+2] cycloaddition as discussed in detail in chapter 3.2.4.3 (figure 3.66).

3.2.4.2 Synthesis of 3-(5-(3-(3-aminopropyl)-6,7-dihydro-5H-cyclopenta[c]pyridin-1-yl)-2'-carbamoyl-3-methyl-2,3'-bipyridin-5'-yl)-propanoic acid

Coupling of building blocks 6 and 7

Both Stille^[88;89] and Suzuki^[90;102] coupling conditions have been successfully used for construction of bipyridines or terpyridines. Employing either coupling reaction is associated with certain advantages. Stannyl pyridines in Stille couplings were expected to be more stable than organoboron pyridines. In addition, Stille reactions as a whole are considered as a reliable and robust method for difficult couplings;^[83;96] the main disadvantage with this reaction is the high toxicity associated with use of equimolar amounts of tin reagents.^[161] Suzuki coupling conditions have the main advantage of employing thermally-, air- and moisture-stable boronic acids or esters,^[98] that are generally non-toxic. In addition, removal of boron-containing byproducts is straightforward.^[162]

Therefore, it was tested empirically which conditions work better for this system. Coupling with Stille or Suzuki conditions of pyridine metalates **6c-d** or **6f** was expected to take place regioselectively at the C-2-position of **7a** or **7d** by selective oxidative addition of the catalytically active Pd(0) species into the more electrophilic C-Br bond at the 2-position.^[97;163]

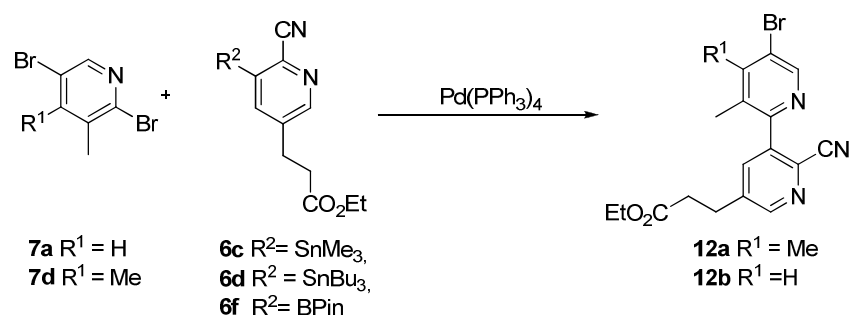


Figure 3.67: Scheme of proposed Pd-catalyzed cross-coupling of building blocks 6 and 7.

Successful synthesis of bipyridines by Stille coupling has been reported using trimethylstannylpyridine and tributylstannylpyridine, therefore both **6c** and **6d** were used as nucleophilic component in test reactions. Reaction conditions for the Stille coupling were adapted from Heller et al.^[89] (coupling of 2-tributylstannylpyridine with 2,6-dibromopyridine, entry 1, table 3.19) and Yamamoto et al.^[164] (coupling of 3-

3 Results and Discussion

trimethylstannylpyridine and 2-bromopyridine, entry 2-5, table 3.19), both of which employ a standard Pd(PPh₃)₄ catalyst. Coupling of both stannylpyridines was tested with both 2,5-dibromo derivatives **7a** and **7d**.

entry	6	7	solvent	Pd(PPh ₃) ₄	T	t	12a or b
1	d	d	toluene	3mol%	110°C	168h	-
2	d	d	xylene	1.25mol%	130°C	144h	-(^a)
3	c	d	xylene	1.25mol%	130°C	168h	+
4	d	a	xylene	1.25mol%	130°C	168h	-
5	c	a	xylene	1.25mol%	130°C	68h	+

Table 3.19: Reaction conditions of Stille coupling. Reaction mixtures were analyzed by LC-MS. Samples were taken throughout the course of the reaction in order to monitor reaction progress. +: product formation detected. -: no product formation detected. (^a)the starting materials appear to decompose over course of reaction.

As shown in table 3.19, product formation was only observed in test reactions with trimethylstannane **6c** as coupling partner. Under the conditions tested, only partial coupling of bromides **7a** or **7d** and stannane **6c** was observed even after prolonged reaction times. The best ratio of **12b/7a** observed in LC-MS analysis of the reaction mixture was 0.1:1 (determined from area of product peaks at 280 nm, from entry 5) indicating only partial coupling of stannane **6c** and bromide **7a** took place. With these results at hand, it was decided to perform further test reactions with Suzuki coupling prior to up-scaling of the reaction.

For Suzuki coupling of boronate ester **6f** and bromide **7d** depicted in figure 3.68 conditions were adapted from the literature^[90;102] for couplings of 3-pyridyl boronic acids with aryl and heteroaryl bromides (including 2,5-dibromopyridine, entry 1, table 3.20).

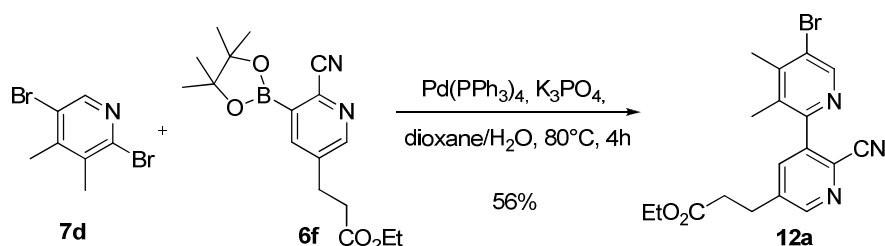


Figure 3.68: Scheme of the synthesis of bipyridine 12a by Suzuki-Miyaura coupling.

3 Results and Discussion

Although the coupling partner in this case is pyridyl boronate ester **6f**, it is assumed that the boronate ester undergoes full or partial hydrolysis under typical Suzuki conditions (H₂O as co-solvent, heat).^[165] However, when using the described conditions, no product formation was observed. When switching from dioxane/sodium carbonate to the more polar solvent DMF/potassium phosphate some product formation was observed. LC-MS analysis of the reaction mixture showed a ratio of **12a/7d** of 0.15:1 (determined from area of product peaks at 280nm) which is in a similar range as found under the Stille conditions employed earlier (entry 2, table 3.20).

entry	solvent	Pd(PPh ₃) ₄	Base	T	t	12a
1	dioxane/H ₂ O	5mol%	5eq Na ₂ CO ₃	100°C	24h	- ^(a)
2	DMF	5mol%	3eq K ₃ PO ₄	80°C	3h	+ ^(a)
3	dioxane/H ₂ O	5mol%	3eq K ₃ PO ₄	80°C	19h	+ ^(a)
4	dioxane/H ₂ O	6mol% ^(b)	3eq K ₃ PO ₄	80°C	4h	56% ^(c)
5	DMF	3mol% PdCl ₂ (dppf)	3eq K ₃ PO ₄	80°C	19h	+ ^(a)
6	dioxane/H ₂ O	Pd/PCy ₃ ^(d)	1.7eq K ₃ PO ₄	100°C	19h	- ^(a)
7	<i>n</i> BuOH	Pd/XPhos ^(e)	2eq K ₃ PO ₄	100°C	19h	- ^(a)

Table 3.20: Conditions for the synthesis of 12a. ^(a)performed under N₂-atmosphere. ^(b)formed in situ from Pd(OAc)₂/PPh₃. ^(c)performed at N₂-line with evacuation. ^(d)1mol% Pd₂dba₃/2.4mol%PCy₃. ^(e)1mol% Pd₂dba₃/4mol% XPhos. +: product formation detected by LC-MS. -: no product formation detected by LC-MS.

Switching back to the less polar dioxane/H₂O solvent system and keeping potassium phosphate as base improved product ratio as judged from LC-MS analysis to **12a/7d** 1.7:1 after 4h of reaction time (determined from area of product peaks at 280nm, (entry 3, table 3.20). The product ratio did not change after longer reaction time (up to 20h). After up-scaling, the product was isolated in 56% yield (entry 4, table 3.20).

It was also tried to increase the yield of the reaction with other catalyst systems reported for Suzuki couplings of aryls^[157] or specifically for couplings of 3-pyridyl boronic acids and esters^[91;93] (entry 5-7), however no improvement of **12a/7d** ratio was observed with the tested conditions in LC-MS analysis.

The optimized conditions for the synthesis of bipyridine **12a** were then applied to the synthesis of bipyridine **12b** as depicted in figure 3.69. **12b** was synthesized with lower yield of 43% (entry 1, table 3.21). Further optimization of reaction conditions was desired. It was found that addition of boronic ester **6f** to the reaction mixture over

3 Results and Discussion

the course of the reaction was beneficial for reaction outcome (66% yield, entry 2, table 3.21), probably by reducing deboronation of **6f** in the reaction mixture.

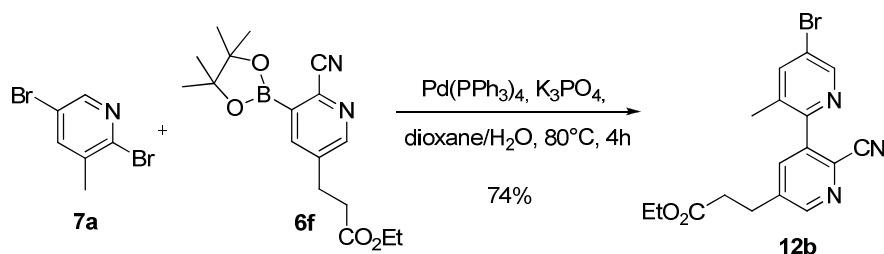


Figure 3.69: Scheme of the synthesis of bipyridine 12b by Suzuki-Miyaura coupling.

Increasing reaction time from 3h to 4h further improved reaction outcome, giving product **12b** in good yield of 74% (entry 3, table 3.21). Reduction of catalyst loading from 6 mol% to 2 mol% did not significantly change product yield (entry 4 and 5, table 3.21). The reaction was successfully adapted to multigram-scale using 6 mol% or 2 mol% of catalyst loading without affecting product yield.

entry	solvent	Pd(PPh ₃) ₄	Base	T	t	12b *
1	dioxane/H ₂ O ^(a)	6mol% ^(b)	3eq K ₃ PO ₄	80°C	3h	43%
2	dioxane/H ₂ O ^(a)	6mol% ^(b)	3eq K ₃ PO ₄	80°C	3h	66% ^(c)
3	dioxane/H ₂ O ^(a)	6mol% ^(b)	3eq K ₃ PO ₄	80°C	4h	74% ^(d)
4	dioxane/H ₂ O ^(a)	2.5mol% ^(b)	3eq K ₃ PO ₄	80°C	4h	74% ^(d)
5	dioxane/H ₂ O ^(a)	2.0mol% ^(b)	3eq K ₃ PO ₄	80°C	4h	72% ^(d)

Table 3.21: Reaction conditions for the synthesis of 12b. *depicted are isolated yields after column chromatography of at least two experiments. ^(a)dioxane/H₂O: 12:1. ^(b)formed *in situ* from Pd(OAc)₂/PPh₃, performed at N₂-line ^(c)**6f** added over course of 90 min at 80°C, reaction mixture was then stirred for 90 more minutes at 80°C. ^(d)**6f** added over course of 90 min at 80°C, reaction mixture was then stirred for 150 more minutes at 80°C, cooled down to rt and stirred o/n.

Re-applying these optimized conditions to the synthesis of bipyridine **12a** did not increase product yield of that reaction. This finding was a little surprising since both compounds are similar in structure and no differences in steric accessibility of the reaction center were present. The electron-donating methyl group at the C-4 position of **7d** might slightly deactivate the C-Br bond for oxidative addition as compared to **7a**. This was, however, not further examined by e.g. competition experiments. The expected regioselectivity of the Pd-catalyzed coupling of **6f** to bromides **7a** or **7d** was confirmed in 1D- and 2D-NMR measurements with bipyridines **12a** and **12b**.

Due to the very low product formation and long reaction times observed with Stille conditions compared to the optimized Suzuki conditions, Suzuki coupling conditions were employed for all following coupling procedures. Also, the required trimethylstannylpyridine **6c** was only obtained in modest yield. The boron-based reactants used in Suzuki couplings offer the advantage of lower toxicity and easier purification of products from metal-organic species. This is of special importance since the compounds are to be tested in biological systems.

Development of two-step one-pot borylation/Suzuki-Miyaura cross-coupling procedure

Due to the base-labile ester and nitrile functions, the 4,4,5,5-tetramethyl-1,3,2-dioxaborolane functionality was introduced to C-5 with a mild Pd-catalyzed borylation (figure 3.70) and not by a lithiation/transmetalation procedure as used for the synthesis of boronate ester **6f**.^[158;166] Pd-catalyzed borylations of aryl and heteroaryl halides are thought to proceed through the general catalytic cycle reported for other types of Pd-catalyzed cross-couplings as well: Oxidative addition of the catalytically active $L_nPd(0)$ species into the carbon-halide bond followed by transmetalation of an $L_nPd(II)$ -aryl complex by bis(pinacolato)diborane; reductive elimination regenerates the $Pd(0)$ -species and releases a pinacol areneboronate.^[166]

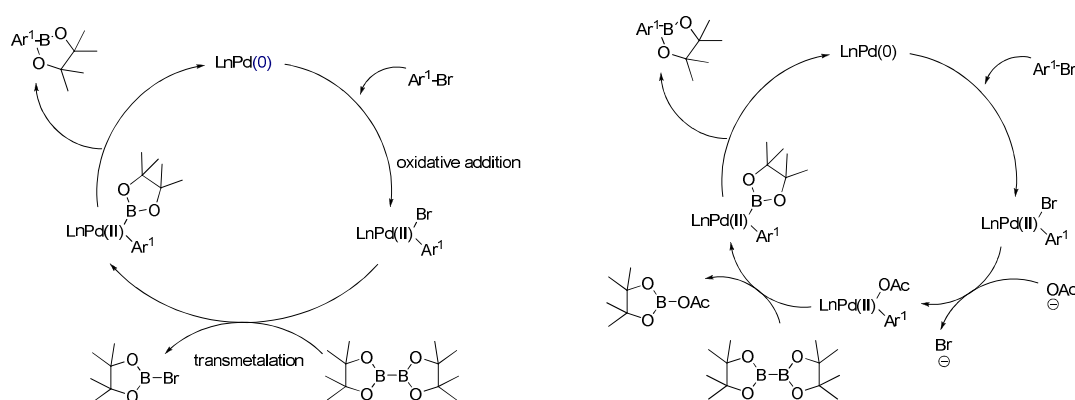


Figure 3.70: Schemes of the catalytic cycles that are proposed to be involved in Pd-catalyzed borylation of aryl halides.^[98] Left: Proposed general catalytic cycle of borylation. Right: Proposed catalytic cycle of borylation *via* $Pd(II)$ -Ar-OAc complex. Adapted from ^[98;158;166]

Potassium acetate is usually employed as base in borylation reactions. It has been found empirically that use of stronger bases like potassium phosphate often results in

3 Results and Discussion

cross-coupling of the boronate ester with remaining halide.^[166;167] The reason for efficiency of potassium acetate in borylations is probably not restricted to its lower basicity but rather more mechanistically: the acetate ion seems to replace the halide from the Pd(II)-complex formed after oxidative addition.^[98;166] This may facilitate transmetalation by interaction of the acetate-oxygen and the oxophilic boron-atom.

In general, borylations have been performed using similar catalyst systems as for Suzuki couplings,^[92;167] it has been reported that for aryl bromides and iodides PdCl₂(dppf) is more efficient than Pd(PPh₃)₄.^[166]

Borylation of bipyridines **12a** and **12b** was initially attempted using Pd(PPh₃)₄ as catalyst. Under these conditions complete conversion of the starting material was observed in LC-MS analysis of the reaction mixture. Up-scaling of the reaction gave the products in low yield of 19% after column chromatography. The low yield of the reaction was explained by instability of the boronate ester. During column chromatography, significant deboronation of the product was observed. This was surprising since it had been reported that boronic acid pinacol esters can be purified by flash chromatography.^[98]

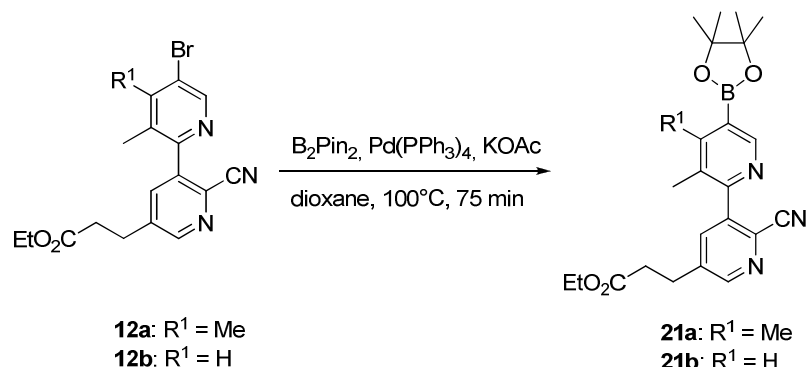


Figure 3.71; Scheme of the synthesis of boronate esters 21a and 21b.

When re-examining purification procedures of pyridine pinacol esters in the literature, it was found that other purification methods (re-crystallization, kugelrohr distillation) were used; Leblanc et al. reported similar stability problems during column chromatography with pinacol pyridyl boronates.^[92;168;169] The reaction and purification conditions for boronate ester **21a** and **21b** were not further optimized. Instead further work focused on development of a two-step one-pot coupling procedure in which *in situ* formed boronate esters **21b** or **21a** are coupled directly to 2-pyridyl bromide **8d**, thereby avoiding the isolation of the boronates.^[92;157]

Successful one pot couplings of two halides via Pd-catalyzed *in situ* conversion of one coupling partner to a pinacol boronate ester as nucleophile have been reported. The procedures were used with (hetero)aryl bromides or iodides using PdCl₂(dppf) or Pd(PPh₃)₄ as catalyst.^[157;170;171] The corresponding biaryls were obtained in modest to good yields. In addition, Billingsley et al. recently reported that a Pd-catalyst based on dialkylbiaryl phosphine ligand SPhos has been successfully used for the synthesis of unsymmetrical biaryls in a one pot borylation/Suzuki coupling procedure from deactivated aryl and heteroaryl chlorides.^[92] To the author's knowledge, until earlier this year^[172] no successful synthesis of a bipyridine or terpyridine applying a Pd-catalyzed borylation/Suzuki one pot protocol had been reported. This was attributed to the general problems associated with Suzuki-Miyaura coupling of two electron-poor heteroaromatic compounds that have been described in chapter 3.2.1.1.^[96;173]

A prerequisite for a successful one-pot coupling of bromide **12b** with bromide **8d** as depicted in figure 3.72 was that conditions could be found that allow both steps, borylation of **12b** and subsequent Suzuki coupling to **8d**, to take place with good efficiency. Prior to establishing reaction conditions for a one-pot coupling procedure of bipyridine **12b** and bromide **8d**, it was decided to use the already isolated boronate ester **21b** to find suitable conditions for the coupling to bromide **8d**. The results of these tests were then applied to the development of the one-pot procedure.

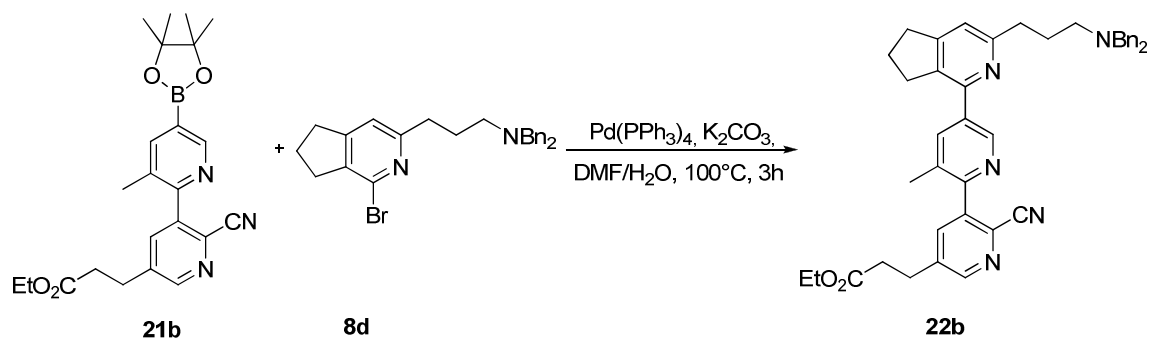


Figure 3.72: Schematic representation of the synthesis of terpyridine **22b** from boronate ester **21b** and bromide **8d**.

Pinacol boronate **21b** was used as nucleophilic component of the Suzuki coupling with bromide **8d**. Reaction mixtures of test reactions were evaluated by LC-MS analysis and are depicted in table 3.22. Initially, optimized reaction conditions established for the coupling of pinacol pyridyl boronate **6f** and 2,5-dibromopyridines

3 Results and Discussion

7a or **d** (entry 1, table 3.22) were used. However, no product formation was observed.

entry	solvent	cat	base	T	t	22b
1	dioxane/H ₂ O ^(a)	6mol% Pd(PPh ₃) ₄ ^(b)	3eq K ₃ PO ₄	80°C	o/n	-
2	DMF/H ₂ O ^(a)	6mol% Pd(PPh ₃) ₄ ^(b)	3eq K ₂ CO ₃	80°C	o/n	+
3	DMF/H ₂ O ^(a)	6mol% Pd(PPh ₃) ₄ ^(b)	3eq K ₂ CO ₃	100°C	24h	+
4	DMF/H ₂ O ^(a)	6mol% Pd(PPh ₃) ₄ ^(b)	3eq K ₂ CO ₃	100°C	3h	5% ^(d)

Table 3.22: Conditions for the synthesis of 22b. Reactions were performed with 1.2eq of **12b**. ^(a) solvent/H₂O 20:1. ^(b)from Pd(OAc)₂/PPh₃, reaction performed at N₂-line. ^(c) from 2.5mol% Pd₂dba₃/0.1eq SPhos, reaction performed at N₂-line. ^(d)purified by gradient cc starting from EtOAc/hexane 1+10 containing 1% NEt₃, product elutes at 40% to 45% EtOAc in hexane.

When switching to DMF as more polar solvent and to potassium carbonate as base, product formation was observed after 1 hour of reaction time with a ratio of **8d/22b** of 1:0.5 (determined from peak area of product peaks at 254 and 280nm, entry 2, table 3.22, figure 3.73). Increasing the reaction temperature to 100°C increased the observed ratio of **8d/22b** to 1:2 (determined from area of product peaks at 254/280nm, entry 3, table 3.22, figure 3.73) which did not change significantly after extending the reaction time to more than 3 hours.

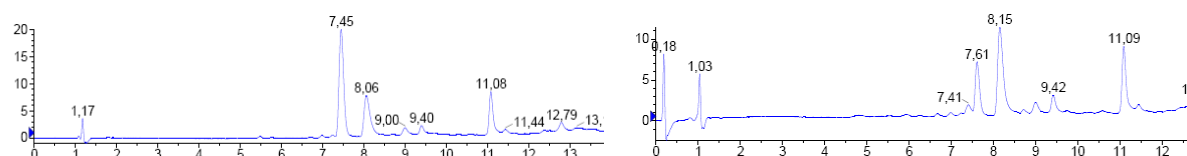


Figure 3.73: LC-chromatogram of crude 22b. Left: entry 2, reaction performed at 80°C. Right: entry 3, reaction performed at 100°C. 7.45//.61: starting material. 8.06/8.15: **22b**. 11.08: unidentified impurity from LC-MS.

Up-scaling of the reaction conditions (entry 4, table 3.22) gave the product in 5% yield after column chromatography. The low yield was explained by inefficient coupling in this particular example of the experiment, as 40% of the starting material **8d** were recovered and general difficulties with column chromatography of this type of basic scaffold. This was also observed later on during purification of this and derivatives of this compound. It was assumed that due to their four basic nitrogen functions, the compounds probably bind tightly to the silica gel and elute only partially from the column especially when using relatively unpolar eluent mixtures, as was the case in this example which was the first time that this type of terpyridine was purified.

3 Results and Discussion

As described later, optimization of purification conditions with more polar eluent mixtures and higher amount of NEt₃ as co-eluent improved outcome.

For the development of the 'one-pot' procedure, the conditions from the Suzuki-Miyaura coupling of boronate ester **21b** and bromide **8d** were applied as depicted in figure 3.74.

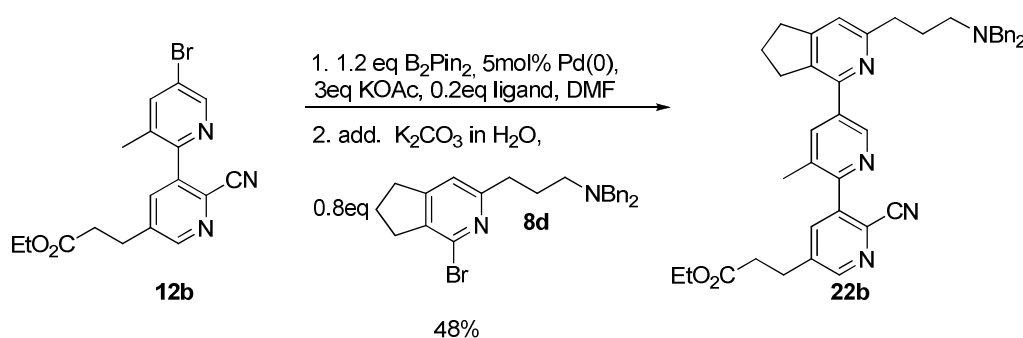


Figure 3.74: Scheme of the two-step one-pot procedure for the synthesis of terpyridine 22b.

It was decided to employ microwave-synthesis for this procedure. In microwave-assisted synthesis, dielectric heating is used for heating up reaction mixtures.^[174;175] Microwaves designed for chemical synthesis permit tight control of temperature and pressure in the reaction vessel. Reactions can be performed at higher pressure (in this case up to 20 bar) allowing superheating of mixtures to higher temperatures than under conventional conditions. This way, reaction rates can be significantly enhanced and in some cases improved reaction yields have been reported.^[175;176] Microwave-assisted synthesis has been successfully applied to Suzuki-Miyaura and other types of Pd-catalyzed cross-couplings with or without ligand support.^[174] The reaction time of the Pd-catalyzed borylation of aryl chlorides with bis(pinacolato)diboron using an Pd/NHC carbene complex was successfully reduced when applying microwave heating resulting in similar yields as found under conventional heating conditions.^[177] This suggested that a microwave procedure could be applied to the borylation/Suzuki-Miyaura coupling sequence and reduce reaction time significantly.

As already mentioned, for the coupling of boronate **21b** and bromide **8d**, DMF/potassium carbonate was established as a suitable system for the Suzuki-Miyaura coupling. This was very convenient for establishing a microwave-assisted

3 Results and Discussion

procedure since DMF is considered a very suitable microwave solvent due its polarity: Reaction mixtures containing DMF can usually be efficiently heated up by microwave irradiation in a short time to high temperatures.^[176]

In test reactions (entry 1 and entry 2, table 3.23, performed on analytical scale), progress of borylation (step 1) and afterwards of the coupling reaction (step 2) were monitored by LC-MS analysis of the reaction mixture. Borylation of bipyridine **12b** proceeded smoothly with DMF as solvent and was completed after 7 minutes at 130°C in the microwave. After addition of bromide **8d** and 1.5 eq or 2.1 eq of aqueous potassium carbonate, product formation was observed after 3 minutes/160°C in the microwave. Up-scaling of the reaction gave the product in 14% yield, which was increased to 20% after the reaction time for the Suzuki-Miyaura coupling was increased to 3.5 minutes (entry 4, table 3.23). Under thermal conditions, the product was obtained in similar low yield of 15% (entry 5, table 3.23).

entry	solvent	cat	base	T	t	22b
1	DMF/H ₂ O ^(a)	5mol% Pd(PPh ₃) ₄	3eq KOAc/	130°C/	7 min/	+
			2.1eqK ₂ CO ₃	160°C ^(b)	3 min	
2	DMF/H ₂ O ^(a)	5mol% Pd(PPh ₃) ₄	3eq KOAc/	130°C/	7 min/	+
			1.5eqK ₂ CO ₃	160°C ^(b)	3 min	
3	DMF/H ₂ O ^(a)	5mol% Pd(PPh ₃) ₄ ^(c)	3eq KOAc/	130°C/	7 min/	14% ^(d)
			1.5eqK ₂ CO ₃	160°C ^(b)	3 min	
4	DMF/H ₂ O ^(a)	5mol% Pd(PPh ₃) ₄ ^(c)	3eq KOAc/	130°C/	7 min/	20% ^(d)
			1.5eqK ₂ CO ₃	160°C ^(b)	3.5 min	
5	DMF/H ₂ O ^(a)	5mol% Pd(PPh ₃) ₄ ^(c)	3eq KOAc/	105°C/	75min/	15% ^(d)
			1.5eqK ₂ CO ₃	105°C ^(e)	3h	
6	DMF/H ₂ O ^(a)	5mol% Pd(PPh ₃) ₄ ^(c)	3eq KOAc/	130°C/	7 min/	48% ^(f)
			1.5eqK ₂ CO ₃	130°C ^(b)	40 min	

Table 3.23: Reaction conditions for the two-step one-pot synthesis of 22b. All reactions were carried out with 1.2eq of B₂Pin₂ and 0.7eq of **8d**. +: product formation detected in LC-MS analysis. ^(a)step1 in indicated solvent, H₂O is added before the 2nd step of the one pot procedure. ^(b)both reaction steps were performed in the microwave. ^(c) from Pd(OAc)₂/PPh₃, reaction performed at N₂-line. ^(d)gradient CC. ^(e)in oil bath. ^(f)isocratic CC, EtOAc/hexane 1+1 containing 2%NEt₃.

As already mentioned, purification of terpyridine **22b** and derivatives by column chromatography was difficult. It appeared that significant amounts of product stick to the stationary phase of the column, as judged from differences between crude material loaded on the column and pure material obtained from the column when using gradient column chromatography: only 55% of material was recovered. It was, however, possible to increase product yield significantly when purifying the

compound with a polar, NEt_3 -containing eluent as depicted in table 3.23. With this more polar and more basic eluent, the product probably eluted quicker from silica gel without being given time to associate with it.^[172] Similar problems with a 2,2'-6',2''-terpyridine scaffold were recently reported when trying to purify the compounds by preparative TLC.^[172] Alternative work-up strategies, like pH-dependent liquid-liquid extraction as well as kugelrohr distillation did not work for the purification of **22b**. After polar, isocratic column chromatography, **22b** was obtained in 48% yield (entry 6, table 3.23), when the 2nd step of the one-pot protocol was carried out at 130°C for 40 minutes in the microwave.

Development of one-pot coupling procedure for chloride coupling

Having successfully established a one-pot protocol for the coupling of bipyridine **12b** to the 1-bromo-dihydrocyclopenta[*c*]pyridine derivative **8d**, the next step was to expand this approach to the coupling of bipyridine **12b** with chloride **8e** as depicted in figure 3.75.

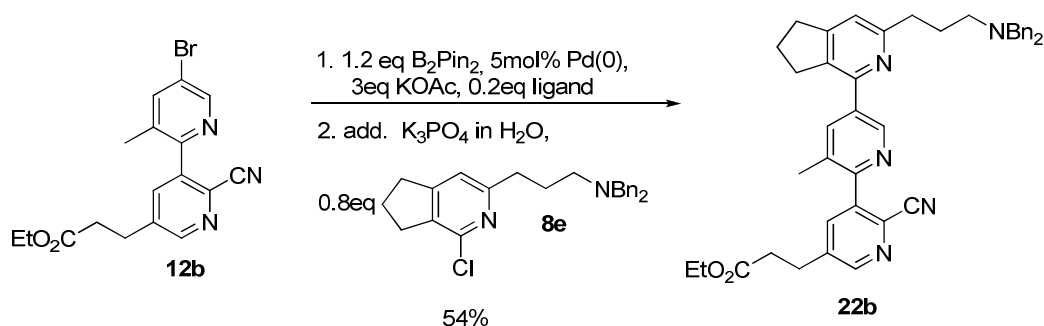


Figure 3.75: Scheme of the two-step one-pot protocol for the synthesis of terpyridine **22b with chloride **8e** as coupling partner.**

Aryl and heteroaryl chlorides are in general considered to be poor substrates for Pd-catalyzed Suzuki-Miyaura couplings due to low reactivity in these reactions under standard conditions. This has been attributed to the strength of the C-Cl bond which is thought to impede oxidative addition of the catalytically active $\text{Pd}(0)$ species into the C-Cl bond.^[101] On the other hand, 2-pyridyl chlorides like **8e** are usually activated for oxidative addition due to the polarity of the C-Cl bond placed adjacent to the

3 Results and Discussion

electron withdrawing pyridine N-atom. Therefore, successful Suzuki-Miyaura couplings of 2-pyridyl chlorides and other electron-poor aryls using standard catalysts have been reported.^[101] Avitia et al. reported earlier this year a very similar one-pot borylation/Suzuki-Miyaura coupling of 3-pyridyl bromide and 2,6-dichloropyridine using another standard catalyst - PdCl₂(dppf) - giving the desired product in modest yield.^[172] Therefore, before testing other phosphine-based catalysts, Pd(PPh₃)₄ was evaluated as catalyst for the sequential borylation/Suzuki coupling of bipyridine **12b** and chloride **8e**.

entry	solvent	cat	base	T	t	22b
1	DMF/H ₂ O ^(a)	5mol% Pd(PPh ₃) ₄	3eq KOAc/ 1.5eq K ₂ CO ₃	130°C/ 160°C ^(b)	7 min/ 3 min	-
2	DMF/H ₂ O ^(a)	5mol% Pd(PPh ₃) ₄	3eq KOAc/ 1.5eq K ₂ CO ₃	130°C/ 130°C ^(b)	7 min/ 21 min	-
3	dioxane/H ₂ O ^(a)	5mol% Pd(PPh ₃) ₄ ^(c)	3eq KOAc/ 1.5eq K ₃ PO ₄	130°C/ 130°C ^(b)	32 min/ 25 min	19% ^(d)

Table 3.24: Reaction conditions for the two-step one-pot procedure with Pd(PPh₃)₄. All reactions were carried out with 1.2eq of B₂Pin₂ and 0.8eq **8e**. -: no product formation detected in LC-MS analysis. ^(a)step1 in indicated solvent, H₂O is added before the 2nd step of the one pot procedure. ^(b)both reaction steps were performed in the microwave. ^(c)Pd(0) was generated *in situ* from 5mol% of Pd(OAc)₂/20mol%PPh₃. ^(d)isolated yield after isocratic column chromatography, average from two experiments.

As shown in table 3.24, no product formation was observed when using optimized conditions from the coupling of boronate ester **6f** with 2-pyridyl bromide **7a**, whether the 2nd step of the one-pot procedure was performed at 160°C for 3 minutes (entry 1) or at 130°C for 21minutes (entry 2). When switching bases from potassium carbonate to potassium phosphate and to the less polar solvent system dioxane/H₂O for the Suzuki coupling, product formation was observed, and the product was isolated in a low yield of 19%. Since complete conversion of the starting materials was confirmed by LC-MS analysis, no new catalyst was added for the second step of the procedure. This could be partially due to the short reaction time used in microwave-assisted synthesis, but also corresponds to a report by Miura et al. with conventional heating in which addition of new catalyst was also not required.^[170] The low yield was explained with the fact that **8e** is more electron-rich and therefore less activated for oxidative addition than unsubstituted 2-pyridyl chlorides as used by Avitia et al.

In recent years, several new ligands have been developed successfully for Pd-catalyzed cross-couplings for e.g. Suzuki-Miyaura coupling of activated and non-activated aryl and heteroaryl chlorides and also for sterically hindered substrates.

3 Results and Discussion

These ligands are usually phosphine- or CHN carbene-based.^[177;178] For this work, screening for ligands was restricted to phosphine-based ligands.

For this purpose, four ligands depicted in figure 3.76 were chosen for this screening. All of these ligands were commercially available and they can be divided in two classes: **L1** (tricyclohexylphosphine) and **L2** (tri-*t*-butylphosphine) are trialkylphosphines and were reported as efficient catalysts for Suzuki couplings with (hetero)aryl chlorides recently.^[91;167;179] The dialkyl-biarylphosphines **L3** and **L4** were also reported recently and employed successfully for the same purpose.^[165;173]

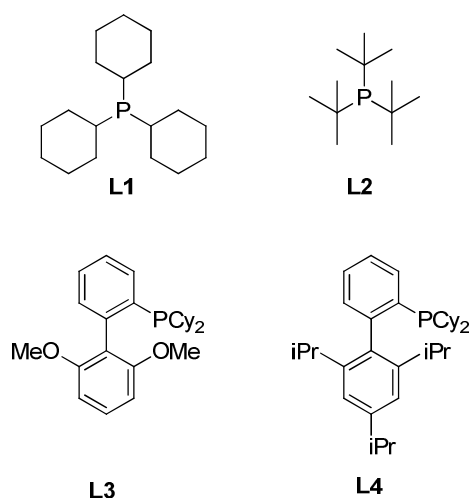


Figure 3.76: Phosphine ligands L1-L4. **L1:** tricyclohexylphosphine. **L2:** tri-*t*-butylphosphine. **L3:** SPhos. **L4:** XPhos.

The efficiency of these phosphine ligands in Pd-catalyzed cross-couplings with unactivated halides is thought to be caused by two main effects: As compared to triphenylphosphine, these ligands are more electron-rich by means of their alkylsubstituents. This facilitates oxidative addition into carbon-halides bonds.^[101;101;162;180] In addition, it is thought that the bulkiness of these ligands (in the case of **L2**: from the sterically demanding *t*Bu-groups, **L3**, **L4**: from the substituted biarylgroup) facilitates formation of mono-ligated L_1Pd -complexes in the catalytic cycle. Mono-ligated Pd-complexes are considered to be more reactive and undergo oxidative addition as well as transmetalation and reductive elimination faster than L_2Pd -species.^[162;181]

All four ligands have been successfully employed in Suzuki-Miyaura couplings of aryl chlorides with boronic acids.^[162;182] **L3**, **L4** and **L1** have been successfully employed for Pd-catalyzed borylation of heteroaryl chlorides including 3-pyridylchlorides giving

3 Results and Discussion

the corresponding pinacol boronate esters in modest to good yield.^[92;167] The four ligands were therefore expected to function well when employed for Pd-catalyzed borylation of the more reactive 5-bipyridyl bromide **12b**. Moreover, **L3** has been successfully employed in one-pot borylation/Suzuki-Miyaura couplings for the synthesis of asymmetric (hetero)biaryls from their respective chlorides.^[92] This approach has not been reported for a pyridine-pyridine coupling which employs an *in situ*-formed pyridyl boronate ester prone to undergo competing protodeboration during the reaction.

In order to shorten reaction time microwave-assisted conditions were used for the evaluation of **L1-L4** in one-pot coupling procedures. Gratifyingly, similar reaction conditions regarding solvents and bases used were reported in the literature for **L1**, **L3** and **L4** for either borylation of heteroaryls (**L4**) or both - borylation and Suzuki-Miyaura coupling - (**L1**, **L3**): dioxane/KOAc for borylation; dioxane/H₂O/K₃PO₄ for Suzuki-Miyaura coupling.^[91;92;167] Therefore, the reaction conditions applied were taken from the literature and combined with results from the already performed microwave reactions and not further optimized for the individual catalyst systems.

The evaluation of **L1-L4** was performed in two steps: 1. Determination of their potential for Pd-catalyzed borylation of the 5-bipyridyl bromide **12b**. 2. Determination of efficiency for Suzuki-Miyaura coupling of the boronate and chloride **8e**.

entry	solvent	cat	base	T	consumption*
1	dioxane	5mol% Pd(PPh ₃) ₄ ^(a)	KOAc	100°C ^(b)	1h
2	dioxane	5mol% Pd(PPh ₃) ₄ ^(a)	KOAc	130°C ^(c)	30min
3	dioxane	0.2eq L3 ^(d)	KOAc	100°C ^(b)	>20h
4	dioxane	0.2eq L3 ^(d)	KOAc	130°C ^(c)	3h
5	dioxane	0.2eq L4 ^(d)	KOAc	100°C ^(b)	1h
6	dioxane	0.2eq L4 ^(d)	KOAc	130°C ^(c)	30min
7	DMF	0.2eq L4 ^(d)	KOAc	130°C ^(c)	7min
8	DMF	0.2eq L4 ^(d)	KOAc	100°C ^(b)	1h
9	dioxane	0.2eq L1 ^(d)	KOAc	130°C ^(c)	2h
10	dioxane	0.2eq L2 ^(d)	KOAc	130°C ^(c)	2h

Table 3.25: Reaction conditions for the borylation of 12b. All reactions were carried out with 1.2eq of B₂Pin₂ and 3eq of KOAc. *consumption of **12b** is completed after indicated amount of time according to LC-MS analysis of the reaction mixture. ^(a) Pd(0) was generated from 5mol% of Pd(OAc)₂. ^(b) in oil bath. ^(c) reaction was carried out in the microwave. ^(d) Pd(0) was generated from 2.5mol% of Pd₂dba₃.

3 Results and Discussion

Results of the borylation with the different catalysts are depicted in table 3.25. All ligands tested catalyzed the borylation of the starting material in microwave-assisted reaction conditions and under thermal conditions: Borylation was completed fastest when using **L4** or PPh₃ as ligand (entry 1, 2, 4-8, table 3.25) under thermal or microwave heating, using DMF or dioxane as solvent. With **L1**, **L2** or **L3** as ligands, completion of the borylation required significantly longer reaction time, 2-3 hours in the microwave, for **L3** about 24 hours with conventional heating.

Evaluation of the catalyst systems for the Suzuki-Miyaura coupling of boronate ester **21b** with chloride **8e** confirmed **L4** as a suitable ligand in a one-pot procedure: Up-scaling of the reaction using the conditions depicted in table 3.26 gave the product in 54% yield which was more than twice as much as obtained with PPh₃ as ligand (entry 1, table 3.26).

entry	solvent	cat	base	T	t	yield*
1	dioxane/H ₂ O ^(a)	Pd- L4 ^(b)	3eq KOAc/ 1.5eq K ₃ PO ₄	130°C/ 130°C ^(b)	32 min/ 30 min	54%
2	dioxane/H ₂ O ^(a)	Pd- L4 ^(b)	3eq KOAc/ 1.5eq K ₃ PO ₄	105°C/ 105°C ^(d)	60 min/ 3h	46%**
3	DMF/H ₂ O ^(a)	Pd- L4 ^(b)	3eq KOAc/ 1.5eq K ₃ PO ₄	130°C/ 130°C ^(b)	7 min/ 21 min	25%**
4	DMF/H ₂ O ^(a)	Pd- L4 ^(b)	3eq KOAc/ 1.5eq K ₃ PO ₄	105°C/ 105°C ^(d)	60 min/ 3h	39%**
5	dioxane/H ₂ O ^(a)	Pd- L3 ^(b)	3eq KOAc/ 1.5eq K ₃ PO ₄	130°C/ 130°C ^(b)	195min/ 21 min	31%**
6	dioxane/H ₂ O ^(a)	Pd- L1 ^(b)	3eq KOAc/ 1.5eq K ₃ PO ₄	130°C/ 130°C ^(b)	110min/ 30 min	26%

Table 3.26: Reaction conditions for the synthesis of 22b. All reactions were carried out with 1.2eq B₂Pin₂ and 0.8eq **8e**. *isolated yield after isocratic column chromatography. **preliminary yield. ^(a) step1 in indicated solvent, H₂O is added before the 2nd step of the one pot procedure. ^(b) both reaction steps were performed in the microwave. ^(c) Pd(0) was generated from 2.5mol% of Pd₂dba₃ and 0.2eq of the indicated ligand. ^(d)heated in oil bath.

This confirmed that the use of a more electron-rich and bulkier ligand was beneficial for the Suzuki-Miyaura coupling of the deactivated cyclopenta[*c*]pyridyl chloride **8e** and allowed terpyridine synthesis in a convenient one-pot procedure. In addition, the microwave-assisted one-pot procedure was finished after about 1h of reaction time only.

Then control reactions using **L1-L3** as ligands were performed in order to estimate whether with **L1-L3** better results than with **L4** can be obtained for the Suzuki-Miyaura coupling step. This was not the case as judging from isolated product yields and additional LC-MS analysis of test reactions. With **L2**, less than 10% conversion of chloride **8e** was observed in LC-MS analysis of the reaction mixture, therefore this ligand was not further evaluated. With **L1**, the product was obtained with an average yield of 26% and in order for the reaction to proceed, additional Pd₂dba₃ and ligand had to be added before the second reaction step of the one-pot procedure. With **L3**, product was isolated in 31% yield in one run. This could not be reproduced, and in another run the product was obtained in less than 10% yield.

These results supported the choice of **L4** as the most suitable ligand for this coupling procedure. Performing the reaction with **L4** under thermal heating gave the product in similar yield range as the microwave-assisted procedure, although this has not been reproduced yet (entry 2, table 3.26).

Of special interest was the solvent-dependence of the reaction outcome with **L4** in microwave-assisted synthesis: Dioxane is a less favourable solvent for microwave synthesis than DMF. It does not have a permanent dipole and was therefore not efficiently heated up by the microwave irradiation in the borylation step.^[175] This was the main cause for the longer reaction times required for completion of the borylation reaction in dioxane as compared to DMF (table 3.24, table 3.26). When using dioxane as solvent, it took between 15 to 20 minutes to heat the sample to the required temperature, whereas with DMF, it only took 1 to 2 minutes. It would be advantageous, if the reaction could be performed in DMF instead of dioxane, because the reaction time could then be reduced even further. However, the use of DMF as solvent reduced isolated product yield (entry 3 and 4, table 3.26).

Synthesis of terpyridines **22a** and **22c**

Having successfully established the synthesis of the model system **22b**, the optimized conditions were applied first to the synthesis of 3,4-dimethyl derivative **22a** as depicted in figure 3.77. **22a** was synthesized in 40% yield with **L4** as ligand (entry 3, table 3.27) from bipyridyl bromide **12a** and chloride **8e** using the established microwave assisted one-pot protocol.

3 Results and Discussion

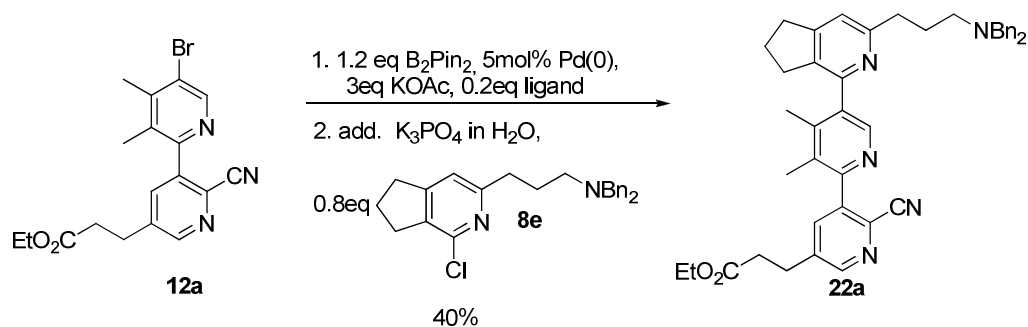


Figure 3.77: Scheme of the synthesis of terpyridine 22a.

Interestingly, when using Pd(PPh₃)₄ as catalyst, no product formation was observed under the conditions adapted from coupling of bipyridine **12b** and chloride **8e** (entry 1 and 2, table 3.27).

entry	solvent	cat	base	T	t	22a
1	dioxane/H ₂ O ^(a)	Pd(PPh ₃) ₄ ^(b)	3eq KOAc/ 1.5eqK ₃ PO ₄	130°C/ 130°C ^(c)	30 min/ 21 min	-
2	DMF/H ₂ O ^(a)	Pd(PPh ₃) ₄ ^(b)	3eq KOAc/ 1.5eqK ₃ PO ₄	130°C/ 130°C ^(c)	7min/ 21min	-
3	dioxane/H ₂ O ^(a)	Pd- L4 ^(b)	3eq KOAc/ 1.5eqK ₃ PO ₄	130°C/ 130°C ^(c)	32 min/ 30 min	40%*

Table 3.27: Reaction conditions for the synthesis of terpyridine 22a. All reactions were carried out with 1.2eq B₂Pin₂ and 0.8eq **8e**. -: no formation of product detected in LC-MS analysis. *isolated yield after isocratic column chromatography. ^(a) step1 in indicated solvent, H₂O is added before the 2nd step of the one pot procedure. ^(b) Pd(0) was generated from 5mol% of Pd(OAc)₂ and 0.2eq of the indicated ligand. ^(c) both reaction steps were performed in the microwave.

1D-NMR and 2D-NMR measurements were performed to confirm identity of the product. The ¹H-NMR spectrum of **22a** is depicted in figure 3.78.

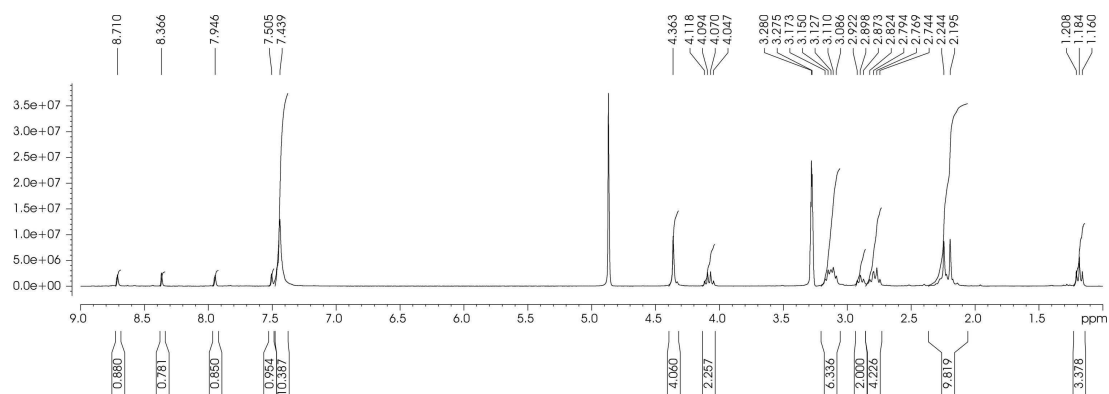


Figure 3.78: ¹H-NMR spectrum of 22a recorded in MeOD.

3 Results and Discussion

The reaction conditions were then also used for the synthesis of terpyridine **22c** from bipyridyl bromide **12b** and the di-chloropyridine derivative **8i** as depicted in figure 3.79 and table 3.28.

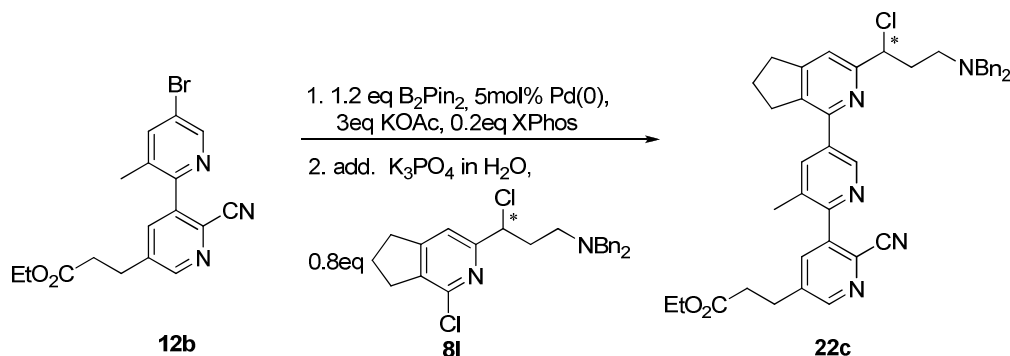


Figure 3.79: Scheme of the synthesis of terpyridine **22c**.

entry	solvent	cat	base	T	t	22a
1	dioxane/ H_2O ^(a)	Pd- L4 ^(b)	3eq KOAc/ 1.5eq K_3PO_4	130°C/ 100°C ^(c)	30 min/ 60 min	22%

Table 3.28: Reaction conditions for the synthesis of terpyridine **22c**. All reactions were carried out with 1.2eq B_2Pin_2 and 0.8eq **8e**. *isolated yield after gradient column chromatography. ^(a) step1 in indicated solvent, H_2O is added before the 2nd step of the one pot procedure. ^(b) Pd(0) was generated from 2.5mol% of Pd_2dba_3 and 0.2eq of XPhos. ^(c) both reaction steps were performed in the microwave

For the synthesis of terpyridine **22c** it was found to be beneficial to perform the reaction at maximal 100°C in the microwave or under thermal conditions. The lower yield for this reaction was explained with problems during purification since column chromatography was performed with a gradient eluent system.

When comparing the results obtained with **L1-L4**, it was shown that trialkylphosphines **L1** and **L2** appear to be less suitable ligands for the coupling: low product yields were obtained and fresh amount of catalyst had to be added for the second step of the one-pot reaction. One reason for this could be the higher susceptibility of **L1** and **L2** towards oxidation found for electron-rich phosphines as compared to e.g. triphenylphosphine.^[182;183] This could render the catalyst inactive over the course of the reaction. Whether this would be also the case when the reaction is performed in a presumably better sealed Schlenk apparatus and not in a microwave vessel was not determined. Nonetheless, **L1** has been successfully used for bipyridyl synthesis from boronate esters and chloropyridines using very similar

conditions,^[91] therefore the low yield that was obtained was still disappointing. One explanation could be that **L1** did not tolerate the higher temperature used in the microwave-assisted protocol.

Dialkylbiarylphosphines **L3** and **L4** appeared to be better suited for a one-pot protocol confirming results reported by Billingsley et al.^[92] **L3** and **L4** tolerated the higher temperatures used in microwave-assisted synthesis and no addition of fresh catalyst was needed, confirming their reported stability towards high temperatures and towards oxidation.^[162;183] For their one-pot procedure for the synthesis of asymmetric biaryls from corresponding chlorides, Billingsley et al. reported **L3** as the most suitable ligand. They did, however, not systematically apply this procedure to systems in which both coupling partners are electron-poor heteroaryls.^[92;172] The results obtained for the bipyridine-pyridine coupling between bromide **22b** and chloride **8e** suggested that **L4** might be better suited for one-pot procedures of this type. This was supported by other reports from Buchwald et al. in which **L4** has been shown to be a more suitable phosphine ligand as compared to **L3** for Suzuki-Miyaura couplings of 3- and 4-pyridyl boronic acids with heteroaryl chlorides.^[93;173] This has been attributed to the bulkier biaryl group of **L4** as compared to **L3** which could increase the concentration of the reactive L₁Pd-species in the reaction mixture.^[173] Obviously, in order to confirm this hypothesis more systematic studies with **L3** and **L4** and diverse sets of coupling partners should be performed. Unfortunately, the authors did not disclose in what way **L3** was more suitable than **L4** for one-pot borylation/Suzuki-Miyaura couplings in their study therefore further comparison and discussion of the observed results is difficult.

The lower yield obtained for terpyridine **22a** as compared to terpyridine **22b** might be accidental because the reaction for the synthesis of **22a** has only been performed twice so far. It could also be due to additional steric hindrance imposed on the reaction center by the additional C-4 methyl group. This could also explain that no product formation was observed when using Pd(PPh₃)₄ as catalyst for coupling.

In conclusion, a one pot coupling protocol was successfully applied for the coupling of bipyridyl bromides **12b** or **12a** with bromide **8d** or chloride **8e**. Similar yields were obtained when coupling bipyridyl **12b** to pyridyl bromide **8d** or to pyridyl chloride **8e** which allowed use of the cheaper chloride **8e** as coupling partner - as already done in the synthesis of terpyridine **22a**. No isolation of pinacol boronate esters **21b** or **21a**

was required. By applying microwave-assisted synthesis the reaction time was successfully reduced as compared to thermal conditions without appearing to affect product yield.

Deprotection of terpyridines **22a** and **22b**

The first step in this reaction sequence was the deprotection of the carboxylic acid functions as depicted in figure 3.80. The ester and nitrile function of terpyridines **22a** and **22b** were supposed to be hydrolyzed under basic conditions giving the corresponding di-carboxylic acids. Hydrolysis of the aliphatic ester gave the desired carboxylic acid. It was confirmed by HR-MS and IR-analysis that the nitrile function underwent only partial hydrolysis giving the corresponding amide derivatives **25a** and **25b** as depicted in figure 3.80. This was unexpected since the nitrile functionality was expected to undergo complete hydrolysis as under these conditions, the amide was considered to be more prone towards hydrolysis than the starting nitrile. The products **25a** and **25b** were obtained in 73% yield (after HPLC purification) or 80% yield (after aqueous work-up) respectively.^[105]

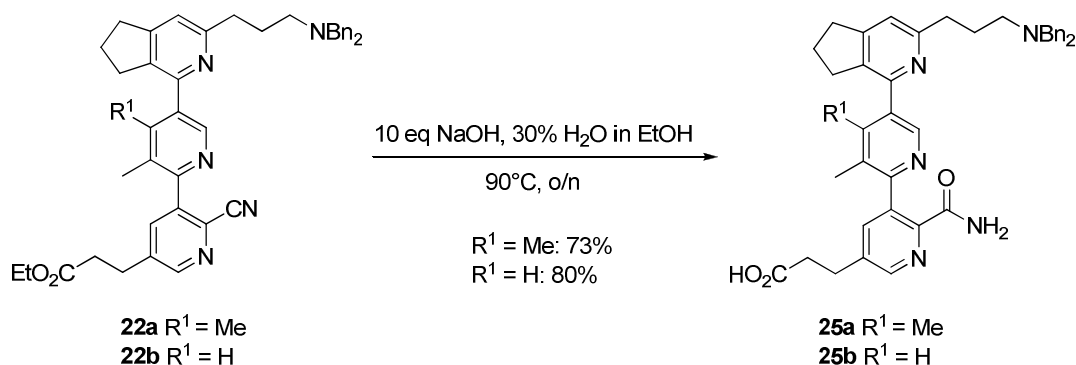


Figure 3.80: Scheme of the synthesis of terpyridines **25a** and **25b**.

After HPLC purification of the crude product, the products **25a** and **25b** eluted as trifluoroacetate salt, protonated at the dibenzylamine function as can be deduced from the ¹H-NMR spectrum of **25b** depicted in figure 3.81.

An initial characterization of the amide **25b** suggested specific binding of the compound to the D/D domain of RII α in STD-NMR and HSQC-NMR measurements as described in more detail in chapter 3.2.5. In order to estimate whether binding of this scaffold would be improved in presence of the free amine functionality as

3 Results and Discussion

predicted from the modeling study, we established the removal of the dibenzyl protecting group with this amide derivative **25b**. The synthesis of the corresponding carboxylic acid derivatives is still ongoing.

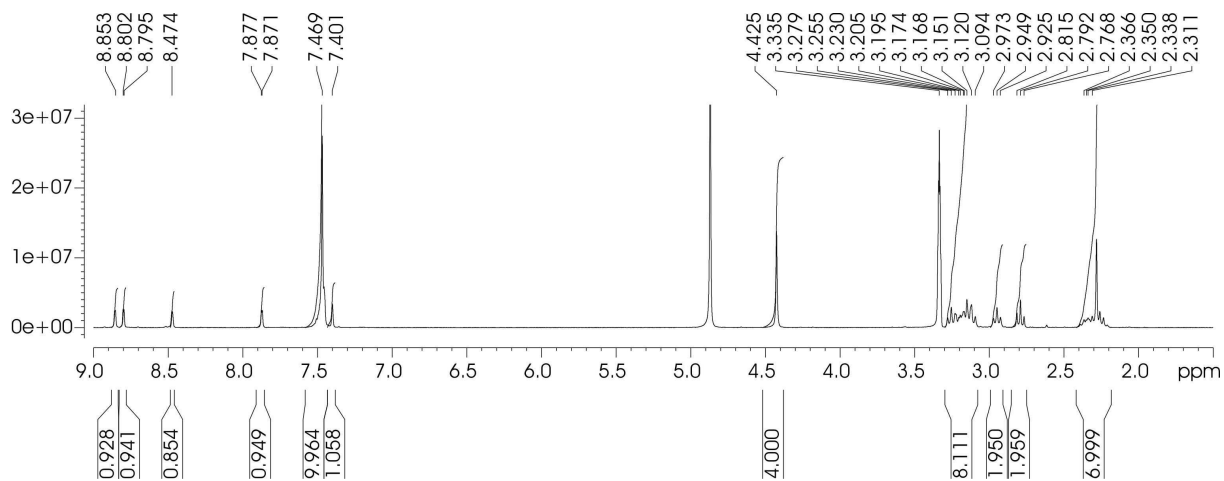


Figure 3.81: $^1\text{H-NMR}$ spectrum of terpyridine **25b** in MeOD.

The amine functionality was deprotected by hydrogenation as depicted in figure 3.82.

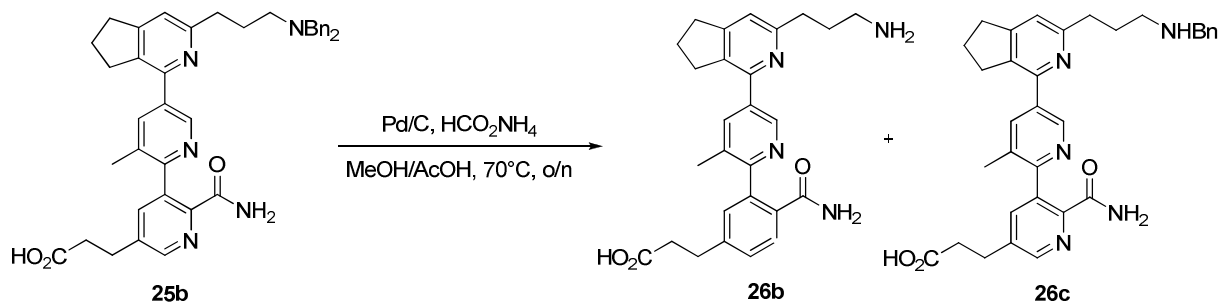


Figure 3.82: Scheme of the synthesis of amine **26b** and *N*-benzylamine **26c**.

Hydrogenation was performed using H_2 or HCO_2NH_4 as hydrogen source; the conditions that were tested are depicted in table 3.29.^[135;184] There were two problems when establishing the procedure: Finding hydrogenation conditions for reproducible reaction outcome with good yields and establishing an HPLC-based purification protocol. It was not possible to establish reliable hydrogenation with good yields as shown in in table 3.29. In addition to the product, *N*-benzylated byproduct was always obtained from the reaction in low yield of 22%. Establishing a purification protocol was difficult but successful. An overview of tested HPLC-conditions is depicted in table 3.30.

3 Results and Discussion

entry	solvent	Pd/C	H ₂ -source	T	t	26b
1	MeOH	10%	8eq HCO ₂ NH ₄	70°C	3h	product in NMR
2	MeOH/AcOH 4:1	10%	H ₂	rt	o/n	no product in NMR
3	MeOH	30%	20eq HCO ₂ NH ₄	70°C	o/n	7%
4	MeOH/AcOH 2:1	30%	20eq HCO ₂ NH ₄	70°C	o/n	6%
5	MeOH/AcOH 2:1	30%	20eq HCO ₂ NH ₄	70°C	o/n	6%

Table 3.29: Reaction conditions for the hydrogenation of 25b. Product yields refer to isolated yields after semipreparative HPLC purification.

Initially, semipreparative HPLC purification was performed with standard acetonitrile/H₂O gradient eluent systems. The pH of the eluent system was varied using the described additives. The pH for the aqueous eluent was set to the indicated pH value prior to HPLC runs. In addition, the ACN/H₂O gradient used in each run was varied.

Column	Solvents A/B	additives	pH H ₂ O	gradient % B in A	Isolatable from mixture
C18 ¹	H ₂ O/ACN	0.1% Tfa	1	5 to 99	starting material
C18 ¹	H ₂ O/ACN	0.1% Tfa	1	20 to 99	starting material, partially: monobenzylamine
C18 ¹	H ₂ O/ACN	-	5.25	5 to 99	starting material
C18 ¹	H ₂ O/ACN	-	5.25	20 to 99	starting material, partially: monobenzylamine
C18 ¹	H ₂ O/ACN	10mM AcOH	4.0	5 to 99	starting material
C18 ¹	H ₂ O/ACN	10mM AcOH	4.0	20 to 99	starting material, monobenzylamine
C18 ¹	H ₂ O/ACN	10mM AcOH	4.0	25 to 99	starting material, monobenzylamine
C18 ¹	H ₂ O/ACN	10mM AcOH	4.0	0 to 99	starting material
C18 ¹	H ₂ O/ACN	10mM AcOH/NEt ₃	7.1	5 to 99	partially: starting material
C18 ¹	H ₂ O/ACN	10mM AcOH/NEt ₃	7.1	10 to 99	partially: starting material
C18 ¹	H ₂ O/ACN	10mM NH ₃	10	5 to 99	partially: starting material
C18 ¹	H ₂ O/ACN	10mM NH ₃	10	10 to 99	partially: starting material
C18 ²	H ₂ O/MeOH	-	5.25	0 to 99	-
C18 ^{1,2}	H ₂ O/MeOH	-	5.25	20 to 99	product, starting material, monobenzylamine
C18 ²	H ₂ O/MeOH	-	5.25	35 to 99	-
Sphinx ³	H ₂ O/ACN	-	5.25	0 to 99	-
Sphinx ³	H ₂ O/ACN	0.1% Tfa	1	0 to 99	-
Sphinx ³	H ₂ O/ACN	0.1% Tfa	1	20 to 99	-
Sphinx ³	H ₂ O/ACN	10 mM AcOH	4.0	0 to 99	-

¹:Macherey&Nagel; Nucleodur C18

²:Macherey&Nagel; Nucleodur C18

³:Macherey&Nagel; EC 50/2 Nucleodur Sphinx RP, 3µm

Table 3.30: Purification of amine 26b by preparative HPLC.

However, terpyridine **26b** was not purifiable using any of the ACN/H₂O systems tested. The product eluted at the same time as the injection peak, indicating that terpyridine **26b** under the described conditions was not retained on the column and

eluted directly with other polar components of the reaction mixture. This was verified by LC-MS analysis and in selected cases with NMR-measurements which confirmed that the product was obtained with impurities from the HPLC.

It was then tried to establish a purification protocol for terpyridine **26b** with the so-called Sphinx column. Sphinx columns are designed for separation of polar compounds and are available for analytical and semi-preparative scale. Since analytical test runs with ACN/H₂O eluent systems at different pH values did not show any improvement of the purification, no semi-preparative runs were performed with that column. When switching to a MeOH/H₂O eluent system without additives, the product was isolated when using a gradient run starting from 20% MeOH in H₂O, the product eluted with a retention time of 24 minutes (run: 50 minutes, 20%MeOH to 99% MeOH in H₂O). The free amine **26b** was obtained in low yield of 6% and *N*-benzylamine **26c** was obtained in 22% yield after semipreparative HPLC and lyophilization. 1D- and 2D-NMR-measurements were performed to confirm the structure of the compounds. 1H-NMR spectra of **26b** **26c** are depicted in figures 3.83 and 3.84.

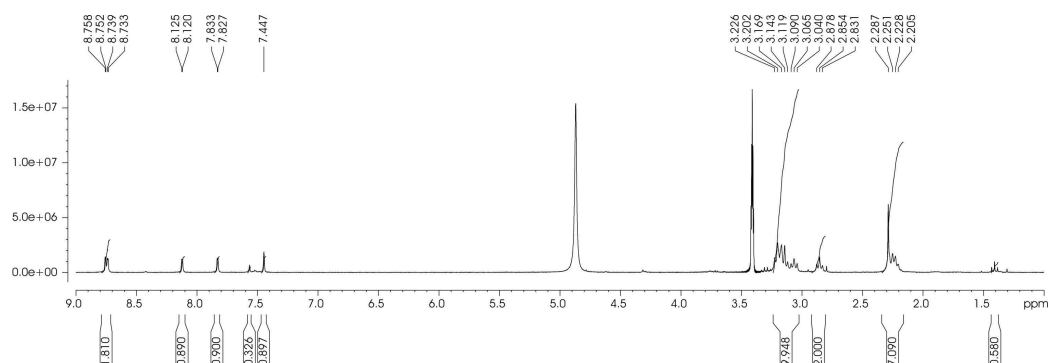


Figure 3.83: ¹H-NMR spectrum of **26b** recorded in MeOD.

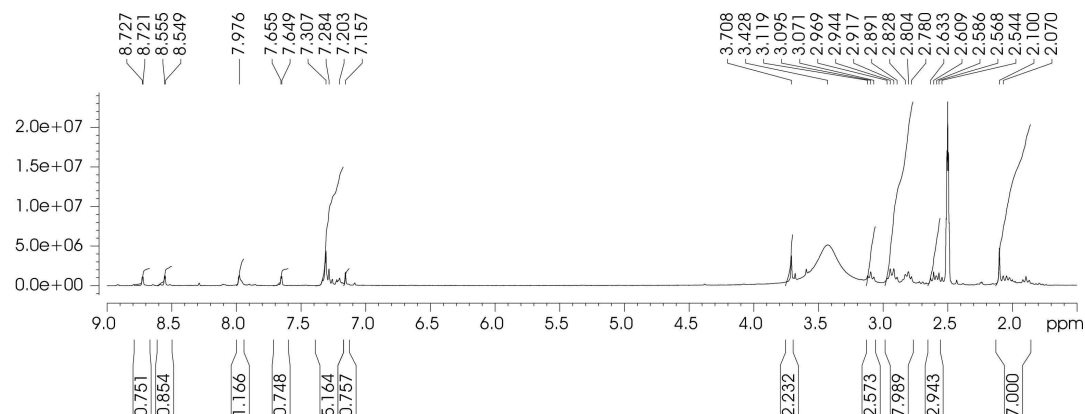


Figure 3.84: ¹H-NMR spectrum of **26c** recorded in d₆-DMSO.

3.2.4.3 Synthesis of terpyridines *via* [2+2+2] cycloaddition

Analysis of synthetic strategy

In an alternative approach it was attempted to synthesize the terpyridine scaffold differently and to avoid the tedious and ultimately low-yielding synthesis of single pyridine building block **8**. Instead it was envisioned that the depicted scaffold could be synthesized from bipyridine **12b** in two steps: Introduction of 1,6-heptadiyne to **12b** by Sonogashira coupling followed by [2+2+2] cycloaddition giving the desired scaffold **24a** (figure 3.85).

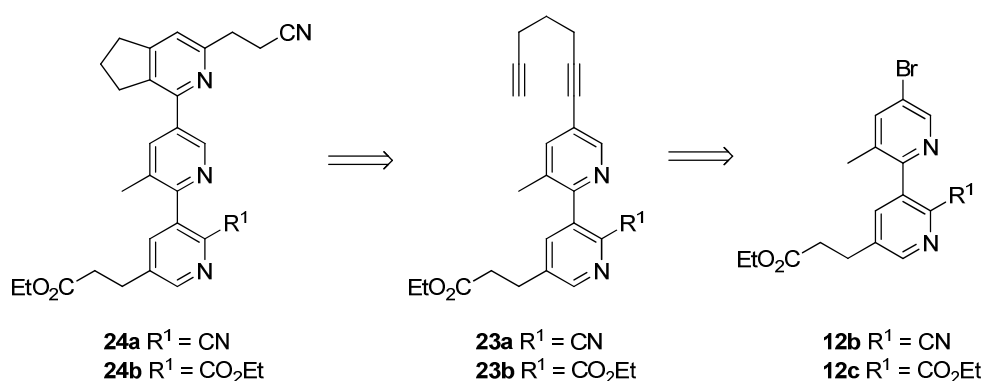


Figure 3.85: Scheme of the retrosynthesis of terpyridines **24a** and **24b** via [2+2+2] cycloaddition/Sonogashira coupling.

Since it was not clear, if and how well a cycloaddition with the sterically demanding bipyridyl group would work, a test reaction sequence was carried out using bipyridine **12b** as a model system for Sonogashira coupling and subsequent cycloaddition reaction. The resulting bipyridyl-dihydrocyclopenta[c]pyridine derivative **24a** would not be suitable for further synthesis due to the presence of two nitrile functions. These nitrile functions masked for different functional groups, a carboxylic acid and an amine and differential functionalization of them was not expected to be easily performed.

After this proof of principle, it was planned to transform **12b** into the di-ester **12c** using standard conditions,^[105;106] both derivatives could then be tested as precursors for the following reaction steps.

Sonogashira coupling is a Pd-catalyzed cross-coupling reaction for coupling of acetylides and suitable halide reaction partners requiring the presence of an amine base and additional Cu(I)-catalysis as depicted in figure 3.86.^[185] Similar to other Pd-catalyzed couplings, the Pd-catalytic cycle proceeds with the common mechanism: oxidative addition of catalytically active Pd(0) species into the C-X bond, followed by transmetalation that probably involves a copper acetylide and finally reductive elimination of the coupling product and regeneration of the Pd(0) species^[186]. The exact mechanism of the reaction is not completely understood, it is however thought that the copper acetylide is formed in a parallel catalytic cycle that possibly involves coordination of Cu(I) with the alkyne function, followed by deprotonation of the alkyne by the amine base giving the copper acetylide species.^[186]

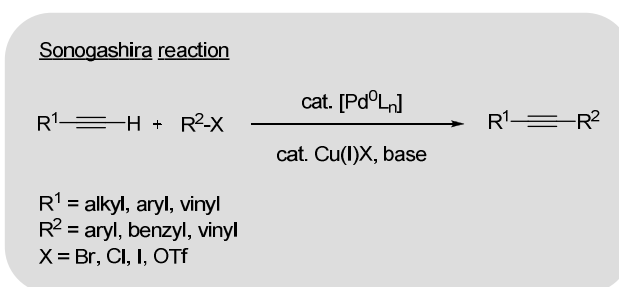


Figure 3.86: General scheme of the Sonogashira reaction. Adapted from ^[99].

Sonogashira coupling of bromide **12b** or its derivatives with 1,6-heptadiyne was expected to take place smoothly. β -bromopyridines have been shown to be suitable substrates for Sonogashira couplings with terminal alkynes in several cases.^[126;187] It was expected that double-functionalization of diynes could be avoided by choosing appropriate reaction conditions e.g. dilution, especially since the mono-functionalized diyne was not expected to be more reactive than the starting material. In addition, successful mono-functionalization of diynes by Sonogashira coupling has been reported using aryls or 2-pyridyl halides.^[188;189]

[2+2+2] cycloaddition reactions or cyclotrimerizations allow the construction of substituted pyridines or more general of (hetero)aryls in one reaction step by forming several C-C and/or C-heteroatom bonds simultaneously. Since only one transition metal catalyst is required, this can be a very nice convergent and atom-economical approach for the *de novo* synthesis of pyridines.^[80;81;94] Chemoselectivity regarding pyridine formation vs. competing cyclotrimerization of alkynes could be a problem.

However, it has been found that catalysts using e.g., Ru, Rh or Co, as metal center favour pyridine formation and only minor amounts of competing benzene formation or other side reactions have been observed.^[79;80] Nitriles have been reported to trimerize less readily than alkynes in the presence of metal catalysts.^[81]

Another issue with transition-metal catalyzed cyclotrimerizations has often been the regioselectivity of the reaction, especially when using monomeric alkynes and nitriles as reaction partners. In those cases often mixtures of differently substituted pyridines have been obtained.^[79] It has been reported that regioselectivity can be controlled in certain cases, for example, the tethered 1,6-diynes used in this work allowed synthesis of single cycloaddition products.^[80] Different transition metal catalysts have been successfully employed for [2+2+2] cycloaddition of annelated pyridine derivatives from 1,6-diynes and nitriles.

It has been reported that ruthenium(II)-based catalysts like the already mentioned Cp*Ru(cod)Cl^[190] (chapter 3.2.2.) and the cationic complex [Cp*Ru(CH₃CN)₃]PF₆^[191] require electron-deficient nitriles as reaction partners for efficient catalysis in cycloadditions. Especially dicyanides have been successfully employed for the synthesis of annelated pyridines with one of the cyanogroups staying intact through the reaction.^[190] Although a reduction in product yield as compared to malononitrile was observed, dicyanides having the second cyanide function in β- or γ-positions have been successfully used as one of the starting materials in cycloaddition reactions. This was also confirmed in this work, with the successful synthesis of **8a** from succinonitrile which gave the product in good yield under mild conditions.

These findings indicated that the electron-withdrawing character is not the major role of the second cyanofunction during the reaction. For example, based on DFT calculations it has been proposed that dicyanides or cyanides with a suitable coordinating group (e.g. α-halonitriles) play a role during the formation of the active catalyst species.^[80;191]

Complementary to Ru(II)-catalysts, Co(I)-catalysts have been shown to efficiently catalyze [2+2+2] cycloaddition reactions of 1,6-diynes with electron-rich or electron-neutral nitriles giving cyclopenta[*c*]pyridines.^[192] Several Co(I) precatalysts have been reported for this purpose, for example CpCo(CO)₂ and CpCo(cod). In addition, catalysts with substituted cyclopentadienyl rings have been developed that allow reactions in polar aqueous solvents^[81] or asymmetric synthesis of atropisomeric

biaryls.^[94] With $\text{CpCo}(\text{CO})_2$ as catalyst, cycloalka[*b*]pyridines have also been synthesized from α,ω -alkynenitriles and alkynes. Symmetrical 2,2'-bipyridines have been synthesized from two molecules of α,ω -alkynenitrile with a conjugated 1,3-diyne.

In general, different transition metal catalysts are considered to have common characteristics regarding their catalytic mechanism: In the first step of the cycloaddition cycle, the catalytically active metal species is probably formed *via* coordination to two alkyne functions. After oxidative coupling, it is believed that a metalacyclopentadiene or in the case of Ru(II)-catalysis an aromatic ruthencyclopentatriene are formed.^[130]

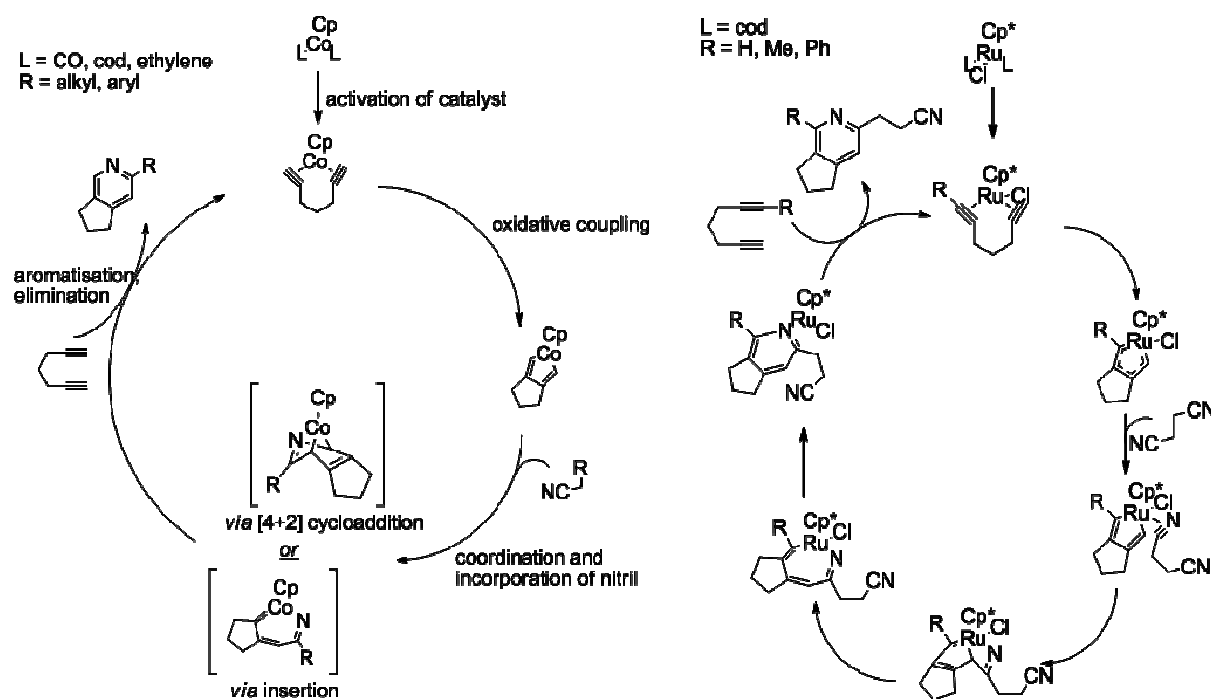


Figure 3.87: Proposed mechanism of Co-catalysed (left) and Ru-catalysed pyridines synthesis by [2+2+2] cycloaddition. Left: Catalytic cycle exemplified for synthesis of substituted cyclopenta[*c*]pyridines from substituted nitrile and 1,6-heptadiyne. Right: Ru-catalysis exemplified for the synthesis of nitrile **8a** ($R = \text{H}$). R indicates proposed regiochemistry for diynes substituted at one terminal alkyne function. Adapted from ^[80;193].

Upon coordination of the nitrile to the complex, probably an incorporation of the nitrile by a catalyst-dependent mechanism (Ru: formally a [2+2] coupling; Co: either [4+2] cycloaddition or *via* insertion) takes place.^[130] The final step is a reductive elimination from the metal center giving the final product and regenerating the active catalyst. The depicted mechanisms are based on experimental evidence as well as computational calculations; however there is still discussion about the nature of some

intermediates and exact mechanisms (see also figure 3.87, Co-catalytic cycle).^[80;81] The proposed catalytic cycles for Co(I) and Ru(II) catalysis are also depicted in figure 3.87.

As already mentioned, the proposed synthesis of the terpyridine derivatives by [2+2+2] cycloaddition reaction as depicted schematically in figure 3.88 would avoid the synthesis of pyridine **8** as a single building block. The [2+2+2] cycloaddition reaction that was performed for the synthesis of nitrile **8a** as depicted in figure 3.88 gave the desired product with complete regiocontrol. In contrast to that reaction, the introduction of the bipyridyl moiety to one of the terminal alkyne functions raised the question of regiocontrol in this type cycloaddition reaction:

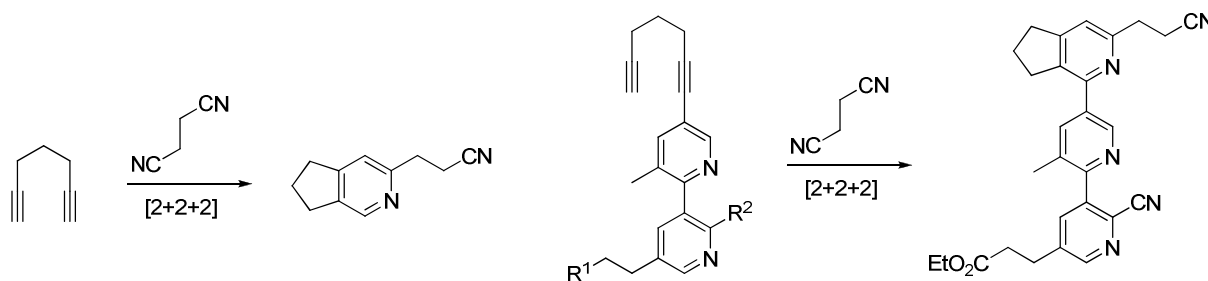


Figure 3.88: Scheme of the synthesis of nitrile **8a** and proposed synthesis of terpyridine derivatives by [2+2+2] cycloaddition.

With Cp**Ru*(cod) as catalyst, successful synthesis of 2,3,4,6-substituted pyridines over 2,3,4,5-substituted pyridines from diynes substituted on one of the alkyne termini has been reported. That means that the substituted alkyne carbon atom is placed preferentially in the α -position of the pyridine.^[190] Based on DFT-calculations, this was explained by access of the nitrile into the ruthenacycle intermediate from the sterically less hindered site as indicated in figure 3.87.^[193] However, a reduction in yield was observed. This seems to be size-dependent, as a phenyl-substituted diyne gave a lower product yield than a methyl-substituted one.^[190]

With CpCo-based catalysts the substituted terminal alkyne carbon atom has also been reported to be placed in the α -position of the final product.^[94] In addition, spacious substituents including 3-substituted pyridines and phenyls have been successfully employed - in combination with aryl nitriles - giving products in modest to good yield.

Based on these reports, formation of the desired product placing the bipyridyl moiety in the α -position of the cyclopenta[*c*]pyridine was expected when using Cp**Ru*(II)Cl-

or CpCo(I)L₂-catalysis. Both catalysts were reported to not require strictly anaerobic conditions during the reaction which made their handling convenient.^[79;194] However, based on literature reports there were potential difficulties expected with both types of metal catalysts:

It was not clear how well the cycloaddition could proceed using Cp*RuCl as catalyst due to steric hindrance from the spacious bipyridyl group.^[190] Alternatively, [Cp*Ru(CH₃CN)₃]PF₆ could be investigated as catalyst for the cycloaddition reaction,^[191] however, with this catalyst not much was known about regioselectivity. With CpCo-based catalysts problems could arise from using the dicyanide succinonitrile as reaction partner, since CpCo-based catalysts have been reported to form dipyridines from dicyanides by cocyclization with alkynes.^[81] However, presence of the spacious terpyridine in close proximity to the second nitrile function could impose sufficient steric hindrance preventing or at least delaying a reaction at this position.

There are several other potential catalysts that were not considered when starting to explore this new synthetic strategy. Nonetheless, they could be valuable alternatives or extensions when continuing to work with [2+2+2] cycloaddition reactions for the synthesis of terpyridines:

Recently, a (dppe)/(CoCl₂*6H₂O)/Zn-catalyst system has been reported that tolerates pyridine-substitution on the diyne as well as electron-rich nitriles and dinitriles.^[87;195] Similarly, a [Rh(cod)₂]BF₄/BINAP catalyst was employed for the synthesis of annelated pyridines and even fully intramolecular [2+2+2] reactions were performed giving fused, tricyclic pyridines.^[196-198] Regiocontrol with this catalyst and unsymmetric diynes needs to be further examined in order to establish a potential use for the synthesis of the required type of terpyridine scaffolds.

Synthesis of terpyridine 24a

1,6-heptadiyne was introduced to C-5 of bipyridine **12b** by Sonogashira reaction as depicted in figure 3.89. Initial trials adapted from literature procedures carried out at room temperature or at 50°C afforded only low amounts of product formation, as determined by LC-MS analysis of the reaction mixture, even after prolonged reaction time (entry 1-4, table 3.31).^[126;187]

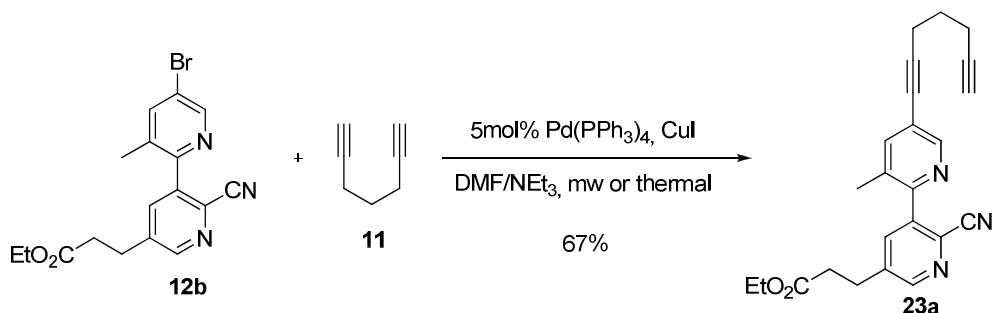


Figure 3.89: Scheme of the synthesis of diyne 23a.

This suggested that bromide **12b** was deactivated for oxidative addition as compared to the reported examples, probably resulting from the electron-donating methyl group. When increasing the reaction temperature to 100°C, the same temperature used for the Pd-catalyzed borylation of bromide **12b** at this position, conversion of bromide **12b** to diyne **23a** was observed with a ratio of **12b/23a** of 1:82 (at 254nm in LC-MS analysis of the reaction mixture).

The use of NEt₃ or a 1:1 mixture of NEt₃ and DMF appeared to be equally suitable for the reaction (entry 5 and 6, table 3.31). As depicted in table 3.31, the product was obtained in 19% yield after 40 minutes of reaction time. After reducing the reaction time to 20 minutes, the product was obtained in significantly better yield of 61% (entry 7, table 3.31). This was explained with the instability of diynes at high temperatures.

entry	solvent	cat	CuI	T	t	23a *
1	NEt ₃	5mol%PdCl ₂ (PPh ₃) ₂	5mol%	rt	40h	product
2	DMF/NEt ₃ ^(a)	5mol%PdCl ₂ (PPh ₃) ₂	5mol%	rt	40h	product
3	NEt ₃	5mol%PdCl ₂ (PPh ₃) ₂	5mol%	50°C	24h	product
4	NEt ₃	5mol% Pd(PPh ₃) ₄	5mol%	rt	24h	product
5	NEt ₃	5mol% Pd(PPh ₃) ₄	20mol%	90°C	1h	product
6	DMF/NEt ₃ ^(b)	5mol% Pd(PPh ₃) ₄	20mol%	90°C	1h	product
7	DMF/NEt ₃ ^(b)	5mol% Pd(PPh ₃) ₄ ^(c)	20mol%	100°C ^(d)	40min	19%
8	DMF/NEt ₃ ^(e)	5mol% Pd(PPh ₃) ₄ ^(c)	10mol%	100°C ^(d)	20min	61%
9	DMF/NEt ₃ ^(e)	5mol% Pd(PPh ₃) ₄ ^(c)	10mol%	130°C ^(f)	195sec	67%

Table 3.31: Reaction conditions for the synthesis of 23a. Test reactions 1-6, 10, 11 were performed using 1.2eq of 1,6-heptadiyne; entry 7-9 were performed with 1.5eq of 1,6-heptadiyne.* product formation detected by LC-MS analysis or isolated yields after column chromatography. ^(a)1.5eq NEt₃. ^(b)DMF:NEt₃ 1:1. ^(c)formed *in situ* from 5mol% Pd(OAc)₂/20mol% PPh₃. ^(d) heated in oil bath. ^(e)DMF:NEt₃ 1.3:1. ^(f) in microwave.

The reaction was easily adapted to microwave-assisted conditions (entry 8, table 3.31). **23a** was obtained after about 3 minutes reaction time in slightly higher yield

3 Results and Discussion

then observed under thermal heating. This was attributed to the shorter reaction time required that might reduce formation of side reactions that are frequently observed with terminal alkynes under Sonogashira conditions at high temperatures.^[186;199] Gratifyingly, no double-bipyridinylated diyne was obtained when using the depicted conditions.

The next step was the [2+2+2] cycloaddition of diyne **23a** and succinonitrile as depicted in figure 3.90.

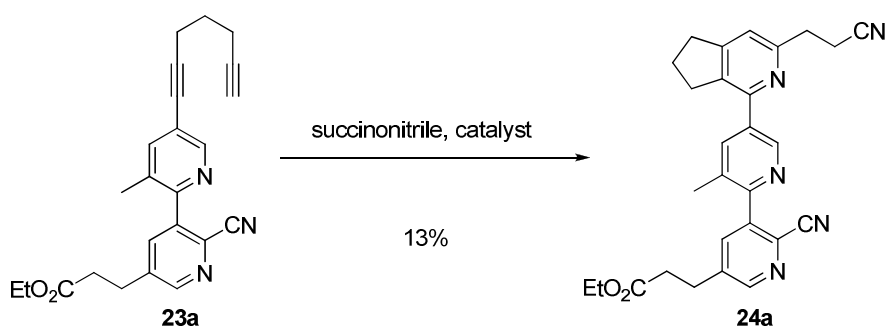


Figure 3.90: Scheme of the synthesis of terpyridine 24a.

Evaluation of two catalyst systems using different reaction conditions was done by LC-MS analysis of the reaction mixture after different reaction times. Initial test reactions with Cp^{*}Ru(cod)Cl as catalyst were performed with the reaction conditions used for the synthesis of nitrile **8a**, however no product formation was observed neither at room temperature nor at 80°C (entry 1 and 2, table 3.32).

entry	solvent	cat	T	t	results
1	1,2-DCE	1.3mol%Cp [*] Ru(cod)Cl	rt	20h	no product
2	1,2-DCE	1.3mol%Cp [*] Ru(cod)Cl	80°C	20h	no product
3	80eq SCN	20mol%Cp [*] Ru(cod)Cl	110°C	4.5h	product ^(a)
4	80eq SCN	20mol%Cp [*] Ru(cod)Cl	110°C	6h	reaction completed ^(b)
5	80eq SCN	20mol%CpCo(CO) ₂	110°C	17h	product formation
6	80eq SCN	20mol%CpCo(CO) ₂	140°C	64h	product formation
7	80eq SCN	15mol%Cp [*] Ru(cod)Cl	110°C	5.5h	4% ^(b)
8	80eq SCN	15mol%Cp [*] Ru(cod)Cl	110°C	5.5h	13% ^(b)
9	40eq SCN	10mol%Cp [*] Ru(cod)Cl	110°C	2h	not complete d

Table 3.32: Reaction conditions for the synthesis of 24a. Test reactions 1 - 6, were performed using 1eq succinonitrile(SCN)/0.66eq of diyne. ^(a)after 4.5h at 110°C, the reaction mixture was cooled down to 100°C and stirred o/n at 100°C. ^(b)purified by isocratic CC, EtOAc:hexane 1+1.

When switching from 1,2-DCE to succinonitrile as solvent and increasing the temperature to 110°C, the starting material was consumed after 5.5 hours and product formation was observed. The finding that higher temperature and higher catalyst loadings were required for product formation was not surprising since it had been reported by Yamamoto et al. that increased temperatures as well as higher catalyst loading were required when using a sterically demanding substituent on the diyne.^[190;200] The obtained yield of the isolated product was very low, with a maximum of 13% after column chromatography. It was assumed that chromatographic purification of the product lead to some loss of the product. The purification of terpyridine **24a** was not further optimized since this reaction sequence was performed as a general proof of principle only.

Expected regioselectivity of the [2+2+2] cycloaddition was confirmed by 1D- and 2D-NMR measurements of the isolated product. As depicted in figure 3.91, regioselectivity of the cycloaddition was confirmed since in the ¹H-NMR spectrum the proton signal from the newly formed pyridine is in the normal range for a proton of a pyridine β-carbon atom (singlet at 7.41 ppm in figure 3.91). An α-proton signal would be expected further downfield (8.50-9.00 ppm was the range in which the α-proton peaks from the bipyridine-moiety of the molecule were detected for example).^[78]

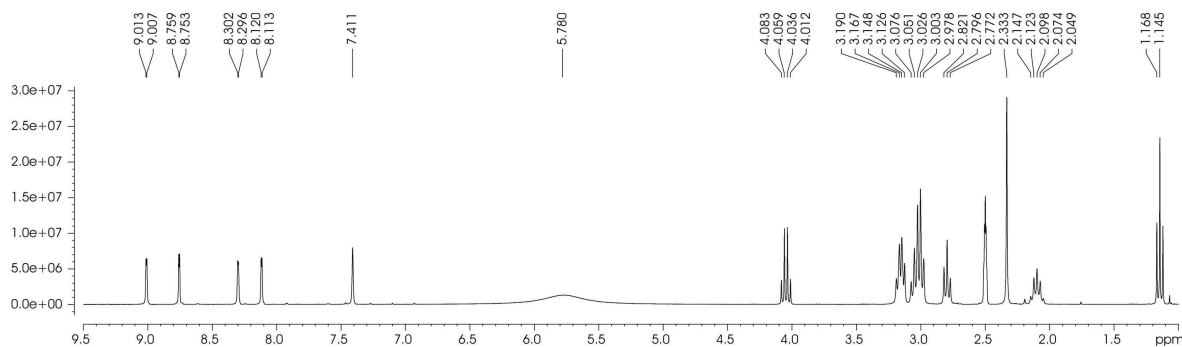


Figure 3.91: ¹H-NMR spectrum of terpyridine **24a** (obtained as pyridinium salt after HPLC purification) in d₆-DMSO. The peak detected at 7.41 ppm results from proton signal of the β-carbon atom of the dihydrocyclopenta[c]pyridine-moiety of the terpyridine. This signal is shifted downfield due to protonation at the corresponding dihydrocyclopenta[c]pyridine-N-atom; this proton was detected at 7.33 ppm in the neutral molecule. The pyridinium-proton is detected at 5.78 ppm (broad singlet).

When investigating CpCo(CO)₂ as catalyst, conversion of starting material in low amount was observed, however, the starting material was not consumed within the time frame applied. Further trials with longer reaction times have not yet been performed.

Re-functionalization of **12b**

The ester and nitrile functionalities of bipyridine **12b** were hydrolyzed under basic conditions in very good yield of 86% adapting standard conditions for the hydrolysis of nitriles (figure 3.92).^[105]

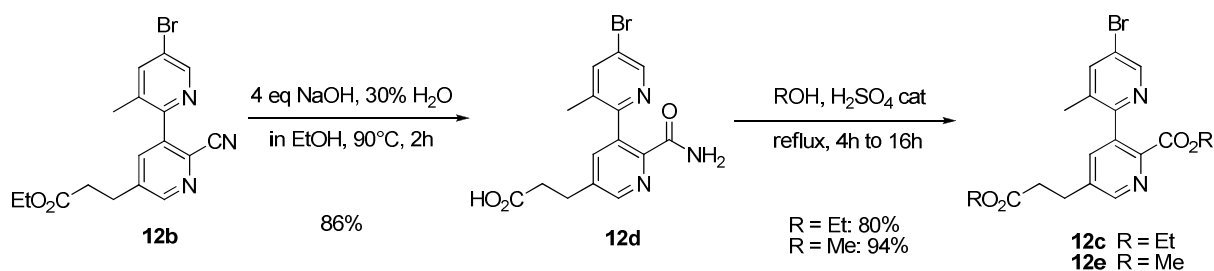


Figure 3.92: Scheme of the synthesis of 12c-e.

Since it was initially thought that the corresponding di-carboxylic acid had been obtained as judged from NMR-analysis, the synthesis of the di-methyl and di-ethyl esters of **12d** was performed with acidic catalysis (table 3.33 entry 1 and 2) employing standard conditions for the esterification of carboxylic acids.^[105] Gratifyingly, under these conditions the desired di-esters were obtained from the amide **12d**.

entry	solvent	reactants	T	t	isolated yield
1	EtOH	0.4eq H ₂ SO ₄	90°C	4h	80%
2	MeOH.	0.4eq H ₂ SO ₄	70°C	16h	94%

Table 3.33: Conditions for the esterification of di-esters 12d (entry 1) and 12e (entry 2).

Presumably, the amide functionality underwent acidic hydrolysis giving the carboxylic acid that subsequently reacted to the corresponding ester *via* esterification. For the synthesis of the di-methyl ester **12e**, longer reaction times were required as compared to di-ethyl ester **12c** in order to complete the reaction which was probably due to the lower refluxing temperatures reached in methanol. The ethyl ester **12c** was synthesized in good yield of 80% and the methyl ester **12e** was obtained in excellent yield of 94%.

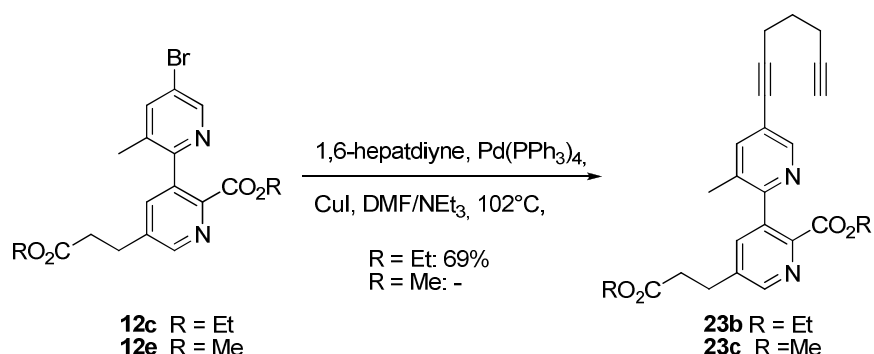
Sonogashira coupling of biimidyl bromides **12c** and **12e**

Figure 3.93: Scheme of the synthesis of diynes **23b and **23c**.**

The coupling of 1,6-heptadiyne to the C-5 position of the bromides **12c** and **12e** was performed using conditions already established for the synthesis of diyne **23a** (figure 3.93, table 3.34).

entry	solvent	cat	CuI	T	t	results
1	DMF/NEt ₃ ^(a)	5mol% Pd(PPh ₃) ₄ ^(b)	10mol%	100°C	4.5h	product
2	DMF/NEt ₃ ^(a)	5mol% Pd(PPh ₃) ₄	10mol%	110°C	4.5h	no product
3	DMF/NEt ₃ ^(a)	Pd(0)-XPhos ^(c)	10mol%	100°C	4.5h	product
4	DMF/NEt ₃ ^(a)	5mol% Pd(PPh ₃) ₄	10mol%	100°C	150min	product
5	DMF/NEt ₃ ^(a)	5mol% Pd(PPh ₃) ₄ ^(b)	10mol%	100°C	30min	product

Table 3.34: Conditions for Sonogashira for coupling of **12e.** heptadiyne: entry 1- 3: 1.2eq. entry 4- 5: 2eq. entry 6: 1.3eq. ^(a) DMF:NEt₃ 1.3:1. ^(b) formed *in situ* from 5mol% Pd(OAc)₂/20mol% PPh₃. ^(c) catalyst loading: 2.5mol% Pd₂dba₃/10mol% XPhos.

When performing the reaction with the methylester **12e** only minor amounts of product formation were observed (entry 1-3, table 3.34) when using XPhos or PPh₃ as ligand for Pd (ration of starting material to product 1:0.02 as determined from absorption peaks at 254 nm). XPhos was tested because it had been successfully employed for the Pd-catalyzed borylation of **12b** and it was assumed that it might also work in a Sonogashira coupling. In order to exclude that residual carboxylic acid in the crude product interfered with the reaction, more test reactions were performed with chromatographically purified methyl ester **12e**, however, the results did not improved (entry 4 and 5, table 3.34).

3 Results and Discussion

The ethyl ester **12c** was tested in a Sonogashira coupling reaction with 1,6-heptadiyne. When employing microwave-assisted reaction conditions from the synthesis of diyne **23a**, diyne **23b** was synthesized in low yield of about 10%. The diyne **23b** was obtained after HPLC purification as pyridinium salt. In addition, starting material and the double-functionalized heptadiyne were obtained also as pyridinium salts. In order to optimize the product yield, the reaction was performed with a greater dilution under thermal conditions (entry 2, table 3.35) to suppress formation of the di-bipyridinylated diyne.

entry	solvent	cat	Cul	[c]*	T	t	yield*
1	DMF/NEt ₃ ^(a)	Pd(PPh ₃) ₄ ^(b)	10mol%	0.113M	130°C ^(c)	195sec	22%
2	DMF/NEt ₃ ^(a)	Pd(PPh ₃) ₄ ^(b)	10mol%	0.048M	100°C	20 min	18%
3	DMF/NEt ₃ ^(a)	Pd(PPh ₃) ₄ ^(b)	10mol%	0.026M	100°C ^(d)	60 min	product
4	DMF/NEt ₃ ^(a)	Pd(PPh ₃) ₄ ^(c)	10mol%	0.111M	100°C ^(e)	30 min	49%
5	DMF/NEt ₃ ^(a)	Pd(PPh ₃) ₄ ^(c)	10mol%	0.157M	100°C ^(f)	35 min	64%
6	DMF/NEt ₃ ^(a)	Pd(PPh ₃) ₄ ^(c)	10mol%	0.159M	100°C ^(f)	40min	69%

Table 3.35: Conditions for Sonogashira coupling of 12c. Entry 1-4 were performed using 1.5eq of 1,6-heptadiyne; entry 5-6 were performed with 1.8eq of 1,6-heptadiyne.*product formation detected by LC-MS analysis or isolated yields after preparative HPLC (entry 1) or column chromatography of one experiment (entry 2,4) or at least two experiments (entry 5-6). ^(a)DMF:NEt₃ 1.3:1. ^(b)formed *in situ* from 5mol% Pd(OAc)₂/20mol% PPh₃. ^(c)in the microwave. ^(d) in oil bath. ^(e)reaction vessel charged with heptadiyne, the reaction mixture is heated up to 100°C, **12c** (in DMF) is added dropwise over 20 minutes, the reaction mixture is stirred for 10 more minutes at 100°C. ^(f)1.2eq of heptadiyne precharged, the reaction mixture is heated up to 100°C, 0.5 eq of **12c** are added dropwise over 15 minutes, then 0.6eq heptadiyne and 0.5eq of **12c** are added dropwise to the reaction mixture over 15 minutes, then the mixture is stirred for 5-10 more minutes at 100°C.

The product was isolated in 18% yield. LC-MS analysis showed that the amount of diarylated side product was reduced; the low yield of the reaction was caused by the low amount of conversion of the starting material. When performing the reaction with more dilution, the product:starting material ratio was even worse which hinted to a significant concentration-dependence of the efficiency of the reaction (entry 3, table 3.35).

Therefore, it was decided to improve the reaction by performing it in a more concentrated solution and to suppress di-functionalization of the diyne by adding the bromide **12c** over the course of the reaction (entry 4, table 3.35). The product was obtained in 49% yield using this procedure; formation of di-bipyridinylated side product was marginal. Even better product yield was obtained (entry 5 and 6, table 3.35) when increasing the amount of 1,6-heptadiyne used in the reaction, and adding

part of the excess 1,6-heptadiyne together with the bromide **23b** over the course of the reaction.

When comparing the syntheses of the diynes **23a** and **23b**, it was interesting to notice that with nitrile **12b** no formation of di-substituted diyne was observed while with di-ethylester **12c** this was a major byproduct (figure 3.94 illustrates this finding). Moreover, the reaction conditions to reach full conversion of the starting material while suppressing formation of disubstitution had to be carefully adjusted using di-ethylester **12c**. It became apparent that the reaction proceeded with very different efficiency for the two coupling partners. These differences were not easy to explain considering that both bromides were structurally very similar.

There was no obvious difference in steric accessibility of the reaction site between the derivatives. Electronic factors within the molecules explaining differences in reactivity could not be ruled out: The compounds vary in substitution of that pyridine ring of the molecules that was not involved in the Sonogashira reaction.

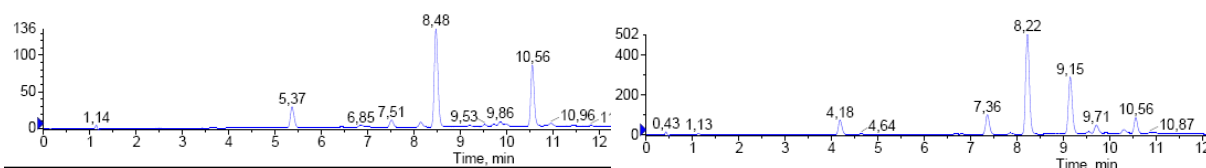


Figure 3.94: LC spectra of crude diyne 23a (left) and crude diyne 23b (right) at 280nm, absorption is depicted in mAU. The reactions were performed under similar conditions. Left: 8.48: **23a**. 7.51: starting material. 10.56: $\text{PPh}_3/\text{O}=\text{PPh}_3$. 5.37 impurity from starting material. Right: 8.22 Product. 9.15: disubstituted byproduct. 7.36: starting material. Isolated yields: **23a**: 67% (after column chromatography). **23b**: 22% (after HPLC purification).

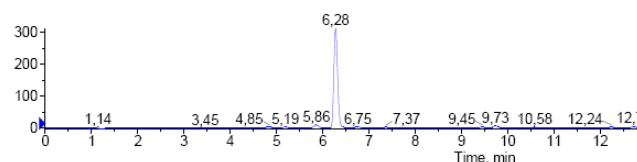


Figure 3.95: LC spectrum of the reaction mixture from the synthesis of methylester-diyne 23c; at 280 nm, absorption is depicted in mAU. 6.28: starting material bromide **12e**. Starting material was subjected to column chromatography prior to the reaction in order to remove residual carboxylic acid **12d**.

Therefore, a change in electrophilicity of C-Br bonds between the derivatives which might account for changes in the rate of oxidative addition would be possible. Both ester and nitrile functionalities are electron-withdrawing substituents, although to

different extends; with the nitrile being generally considered as more electron-withdrawing than esters. Based on these considerations one could assume that bromide **12b** is slightly more activated for oxidative addition than bromide **12c**. However, this did not readily explain that no coupling of the dimethylester **12e** was observed under conditions used for the synthesis of diyne **23a** and initially for the synthesis diyne **23b**. A significant difference in electron-withdrawing strength seemed unlikely and no literature was found that would explain the observed difference in this regard. This also did not explain the significant amount of di-substituted heptadiyne found when performing the Sonogashira coupling reaction with bromide **12c**. In order to illustrate this, in figure 3.94 and 3.95 the LC-spectra of crude **23a**, crude **23b** and the reaction mixture from methylester **12e** obtained under similar reaction conditions are depicted.

Another explanation of the observed results could be complexation or any other type of interaction of the diesters **12c** or **12e** with one of the catalytic Co- or Pd-species rendering the catalysts more inactive as compared to nitrile **12b**, or *vice versa*.

Accordingly, presence of the less sterically hindered dimethyl-ester **12e** might lead to a stronger inactivation as compared to di-ethylester **12c** resulting in almost complete deactivation of a Pd-catalytic species or a Cu(I)-catalytic species. Also the combined presence of two ester functionalities or the presence of the 2-pyridyl carboxylic acid ester moiety gave rise to a bidentate ligand that allowed a particular tight capturing of one of the catalytic intermediates. In addition, the (desired) formation of heteroaryls or heterobiaryls itself during catalyzed reactions could be a reason for inefficient catalysis in heteroaryl-synthesis: Deactivation of transition metal catalysts through coordination of the metal from the formed product or the starting materials could lead to inactivation of the catalyst over the course of the reaction.^[80;83;89;91]

In order to clarify the results observed with the performed Sonogashira reactions with methylester **12e**, additional test reactions using the optimized conditions from the synthesis of **23b** could be performed. This could clarify, whether more pronounced conversion of this bromide would possible when carefully adding them over the course of the reaction.

In addition, further experiments of the Sonogashira reaction with 1,6-heptadiyne and other derivatives containing different substituents at the C-2 position position might give valuable information about the cause of the observed results. One could try electron-donating groups with and without heteroatoms present that could form metal

complexes, e.g protected amines or alkoxides vs. alkyl substituents. In order to determine how significant differences between nitrile-, ethylester- and methylester-substituents are on electron density of the pyridine ring, one could determine basicity of the different pyridines. Basicity of pyridines is correlated to the effects of substituents on pyridine electron density. Effects of the different bromides **12b-e** onto the catalytic species would be harder to study because not all intermediate structures and their exact role for catalysis are known in Sonogashira or other types of Pd-catalyzed reactions.^[186]

[2+2+2]-cycloaddition with **23b** and succinonitrile

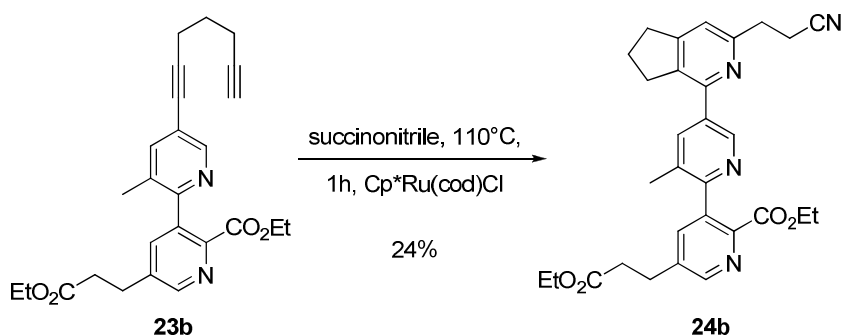


Figure 3.96: Scheme of the synthesis of terpyridine 24b.

Using reaction conditions from the synthesis of terpyridine **24a**, terpyridine **24b** was synthesized in 23% yield as depicted in figure 3.96. The reaction was completed after 1 hour at 110°C, indicating that the reaction proceeded faster than for terpyridine **23a**. Different product purification procedures were tried, however product yields remained in the same range, independent from the purification procedure tried (entry 1-4, table 3.36).

entry	solvent	cat	T	t	results
1	40eq SCN	15mol% Cp*Ru(cod)Cl	110°C	2.5h	completed, 24%
2	40eq SCN	10mol% Cp*Ru(cod)Cl	110°C	1.7h	completed, 23%
3	15eq SCN/DCE	10mol% Cp*Ru(cod)Cl	110°C	2.0h	completed, 22%
4	15eq SCN/DCE	10mol% Cp*Ru(cod)Cl	110°C	1h	completed, 24%

Table 3.36: Conditions for the synthesis of terpyridine 24b. All reactions were performed under N₂-atmosphere.

3 Results and Discussion

It was then investigated whether purification procedures that avoid column chromatography can be established. With pH-dependent aqueous work-up, it was not possible to remove the succinonitrile completely from the crude product. It was also tried to remove the succinonitrile by kugelrohr distillation, however, some of the product was distilled with the succinonitrile from the crude product.

1D- and 2D-NMR-measurements were performed to confirm regioselectivity of the cycloaddition similarly as for terpyridine **24a**: the proton signal from the newly formed pyridine was detected in the normal range for a proton of a pyridine β -carbon atom (7.30 ppm, figure 3.97).

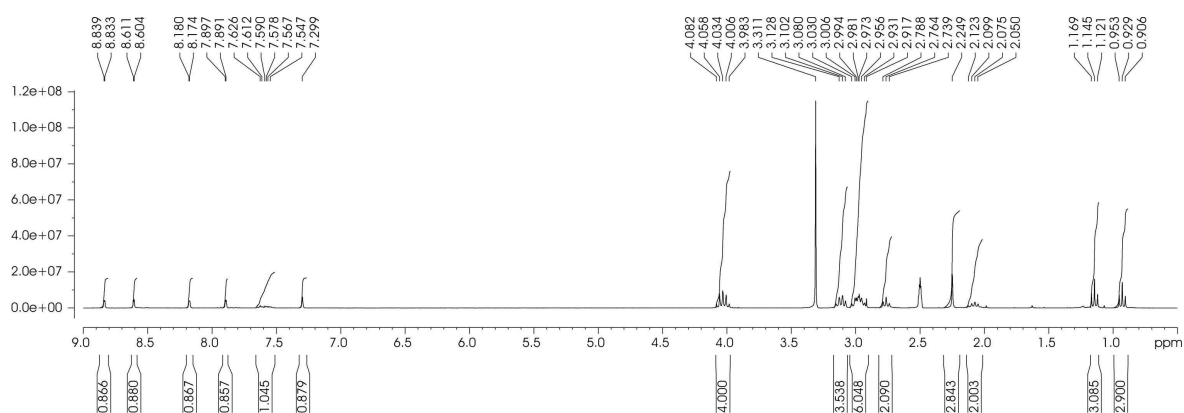


Figure 3.97: $^1\text{H-NMR}$ spectrum of terpyridine **24b** recorded in $\text{d}_6\text{-DMSO}$.

The product yield that was obtained was low, however the amount of succinonitrile employed was successfully reduced, thereby simplifying the purification procedure. A faster conversion of the starting material was observed as compared to the synthesis of terpyridine **24a**. This was attributed to the presence of the additional nitrile function on diyne **23a** which might impede the reaction rate by an additional interaction with the catalyst.

The low yield was disappointing and suggested that $\text{Cp}^*\text{Ru}(\text{cod})\text{Cl}$ was not a suitable catalyst for cycloadditions of bipyridyl-substituted 1,6-diyne. Bulkiness of the substituent probably interferes sterically with the reaction by e.g. blocking access of the catalyst to the alkyne. This corresponded to results from Yamamoto et al. who reported lower yields when performing the reaction with bulkier substituents on the diyne and the need for higher reaction temperatures as well higher catalyst loadings for good catalysis in those cases.^[200]

Therefore, the use of other catalysts should be further explored. Although $\text{CpCo}(\text{CO})_2$ as catalyst appeared not as a good choice according to the initial experiments, further testing with Co(I)-catalysis should be performed: In the initial test reaction the catalyst was activated by the use of high temperatures of 110°C or 140°C.^[189] However, this catalyst could alternatively be activated under milder conditions by an energy supply in form of visible light (300-350 nm) to the reaction mixture.^[192] This alone might be beneficial for the reaction because the thermo-sensitive diyne would be expected to be more stable, especially when long reaction times are required for a complete conversion of the starting materials.^[94] As already mentioned, CpCo(I)-based catalysts do not usually tolerate dicyanides (although no di-functionalization of succinonitrile was observed) which was why they appeared less suitable for this cycloaddition reaction than Ru-catalysts.

When attempting the selective reduction of the nitrile function of terpyridine **24b** in order to obtain the required amine in the presence of the two ester functions, no product was isolatable or identifiable using different literature procedures.^[201;202] Therefore, switching to a different nitrile as reaction partner could be an appealing new strategy for the synthesis of the terpyridine scaffold.

According to the literature, CpCo(I) catalysts appear to have a broader substrate scope with regard to the nitrile used (with the exception of electron-deficient ones)^[80;81] as well as with regard to the diynes used. In addition, with the already mentioned Rh and Co(I)/Zn catalyst systems promising alternative routes to the desired scaffold and derivatives thereof would be available.^[87;196]

One could also envision the use of di-substituted diynes in a cycloaddition reaction with nitriles thereby introducing a functional group to the β -carbon atom of the resulting cyclopenta[*c*]pyridine. For example, [2+2+2] cycloadditions have been performed with iodo-substituted diynes in the synthesis of annelated benzene derivatives.^[203] The resulting phenyl iodides were successfully used for further functionalizations. Also, boronate esters were used as substituents.^[204] One question would be, if and how well the required diynes could be synthesized. In addition, regio-control and catalyst activity with these diynes need to be examined.

Finally, an initial functionalization of terpyridine **24b** can be reported. This was performed to obtain an amide derivative of the nitrile **24b**. The primary amide **26** could be used for attempting a bromination of the β -carbon atom of the newly formed

cyclopenta[*c*]pyridine by electrophilic substitution as already performed for the synthesis for bromide **8f**. Under the strong acidic conditions used for that reaction, the nitrile function of **24b** would probably be hydrolyzed, therefore the nitrile was re-functionalized to a primary amide as depicted in figure 3.98 that would be expected to be stable under these conditions.

The nitrile function of **24b** was partially hydrolyzed in a 4:1 mixture of TFA/H₂SO₄ at room temperature to form amide **27**. In order to check that the nitrile was only partially hydrolyzed under these conditions two test reactions were performed with nitrile **8a**. In the first reaction, the nitrile **8a** was also hydrolyzed under the same conditions giving the corresponding amide. In the second reaction, nitrile **8a** was fully hydrolyzed under basic conditions. LC-MS, NMR and TLC analysis confirmed that two different products were formed under the different conditions.

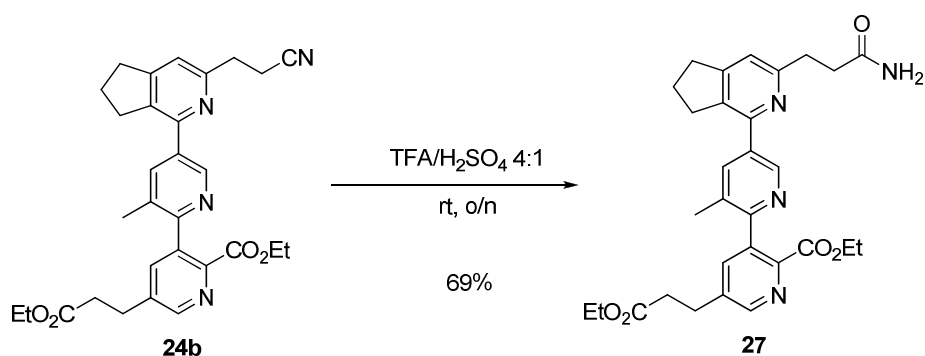


Figure 3.98: Scheme of the synthesis of amide 27.

In conclusion, initial functionalization of the nitrile **24b** to the amide **27** was successful. Amide **27** could be tested for biological activity giving additional information about the structure-activity relationship between the terpyridine scaffold and the D/D domain of RII α (chapter 3.2.5). In addition, with this scaffold, bromination by electrophilic aromatic substitution could be attempted.

3.2.5 Characterization of compounds

The first step of characterizing biologic activity and future potential of this type of scaffold as an RIIIBD mimetic was to test binding to RII α . For this purpose, six compounds depicted in table 3.37 were chosen for the first round of testing. In addition to the fully protected (**22a**) and partially deprotected terpyridine intermediates (**26b-c**, **25a-b**) of the target quaterpyridine, the bipyridine **28** was also tested.

Designation	Compound	Designation	Compound
26b		22a	
26c		25a	
25b		28	

Table 3.37: Compounds chosen for testing in STD- and HSQC-experiments.

The compounds were tested first in a saturation transfer difference (STD) NMR experiment which is a so-called ligand-based NMR technique. In STD experiments, binding between protein and ligand is detected by determining whether saturation is transferred from the protein onto the ligand. For this purpose, a so-called off-resonance ^1H -NMR spectrum is recorded (sample irradiated at a frequency outside of protein and compound signals) from a ligand-protein-buffer mixture in which normal peaks from protein (broad) and free ligand (sharp peaks since its moving free in solution) are detected. In a second experiment another, so-called on-resonance

3 Results and Discussion

^1H -spectrum is recorded in which the protein is selectively irradiated to saturation at a frequency that does not irradiate the ligand.^[75] If the ligand binds to the protein (within a certain affinity and binding kinetics range), saturation is transferred from the protein to the ligand and thereby the ligand signals in the on-resonance spectrum are attenuated as compared to the off-resonance spectrum. This is made visible in the STD spectrum by subtracting the off-resonance spectrum from the on-resonance spectrum.^[75] If peaks remain, it is assumed that saturation was transferred from the protein to the ligand which in turn would indicate that the ligand is binding to the protein. Since ligand-NMR signals are used for the determination of an interaction, STD measurements can be performed with relatively low protein amounts as compared to e.g. HSQC experiments and no expensive isotopically enriched protein is required. Usually, an excess of ligand over protein would be used in the measurement.^[205]

The NMR measurements were performed in collaboration with Dr. Peter Schmieder (FMP Berlin) and Brigitte Schlegel (FMP Berlin). For the STD experiments with the compounds depicted in table 3.38 full length RII α -His was used as the target protein. Prior to measurements of STD spectra in the presence of the target protein, the same set of experiments was performed in the absence of protein in order to confirm that no saturation of the compound signals takes place when irradiating the sample at the frequency chosen for protein irradiation. The results of the STD measurements are depicted in table 3.39.

compound	activity in STD	activity in HSQC
22a	not determined*	not tested
25a	+	not tested
25b	+	+
26b	-	-
26c	-	-
28	-	-

Table 3.38: Qualitative results from STD and HSQC experiments with the indicated compounds. *compound precipitated from solution. STD measurements were performed with 20 μM RII α -fl-His and 100 μM of compound in NMR buffer with 2% d_6 -DMSO. HSQC experiments were performed with 100 μM D/D domain and 300 μM compound in NMR buffer with 5% d_6 -DMSO.

With the partially deprotected terpyridines **25a** and **25b** a reduction in ligand peak intensity was observed, indicating binding of the compounds to RII α . No binding was detected in STD experiments with the deprotected terpyridine **26b**, partially deprotected terpyridine **26c** and bipyridine **28** which was obtained as by-product in the synthesis of **22b**. In figure 3.99, the STD-spectra of a binding compound (**25b**) and a non-binding compound (**26b**) are depicted. Fully protected terpyridine **22a** was tested in an STD experiment, however the compound crystallized from the solution and no ligand peaks were measurable by NMR.

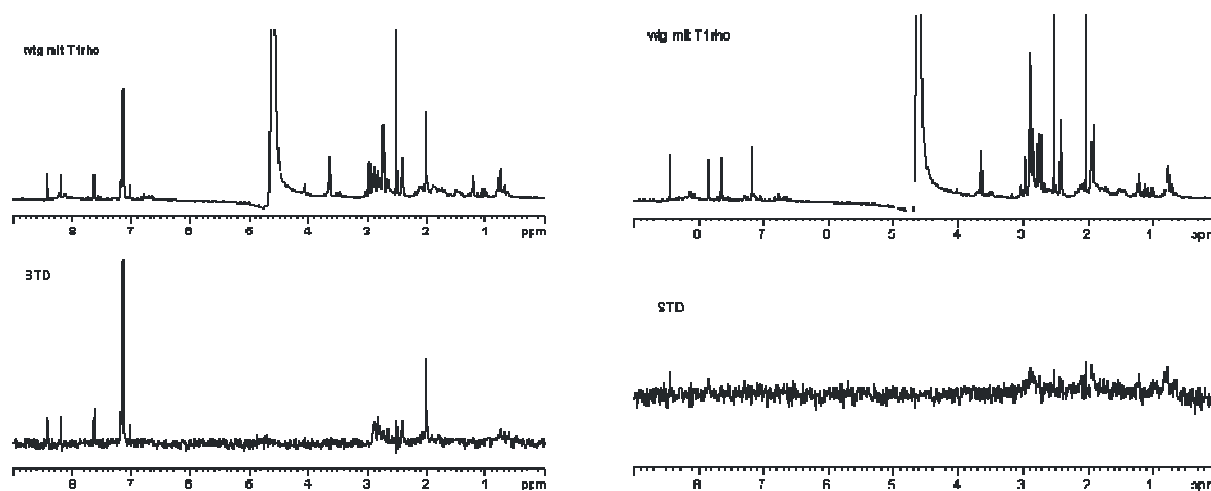


Figure 3.99: ^1H -NMR spectra from STD measurements of RIIalf-His with indicated compound. Top: off-resonance spectrum. Bottom: STD spectrum Left: **25b**. Right: **26b**.

For an estimate of binding specificity, the compounds were tested in a second NMR assay for binding to the D/D domain of RII α . As discussed in chapter 1, the D/D domain contains the AKAP binding site of RII α . Therefore, suitable small molecule mimetics of the RIIBD of AKAP18 must bind to this domain of the full length protein. In other words, binding to the D/D domain would be a good initial test for a potentially AKAP-like, specific interaction of the compounds with RII α .

For this purpose HSQC-experiments with ^{15}N -labeled D/D domain as already discussed and performed in chapter 3.1 were employed with the compounds depicted in table 3.38. The results obtained correspond to the results from the STD experiments. A change in chemical shift of D/D domain signals was observed upon addition of terpyridine **25b**, while with the other compound tested so far - terpyridines **26b**, **26c** and bipyridine **28** - no perturbation of chemical shifts was seen. In figure

3 Results and Discussion

3.100, HSQC-spectra of the D/D domain in presence and absence of **25b** are depicted.

A direct comparison between perturbation of chemical shift upon addition of AKAP18-derived peptides and the terpyridine **25b** is not easy since the longer peptides (16 amino acids and more) perturb almost all of the amino acid peaks (figure 3.101).

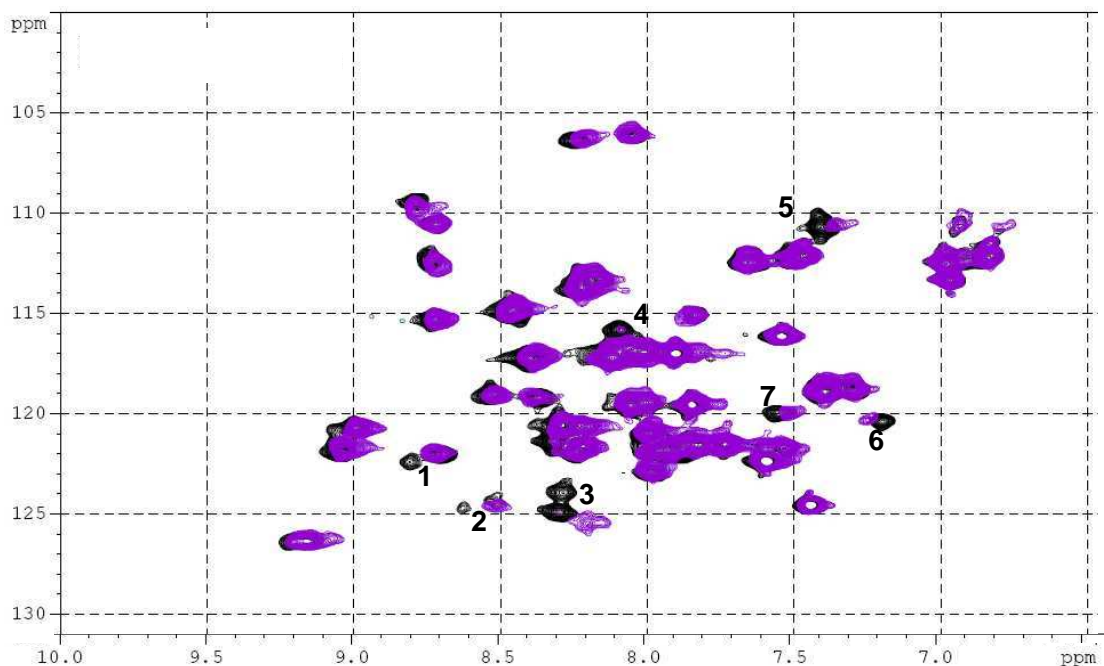


Figure 3.100: HSQC spectra of D/D domain. Black: ^1H - ^{15}N HSQC of $100\ \mu\text{M}$ ^{15}N -labeled D/D domain of RII α . Violet: ^1H - ^{15}N HSQC of $100\ \mu\text{M}$ ^{15}N -labeled D/D domain of RII α incubated with $300\ \mu\text{M}$ of **25b**.

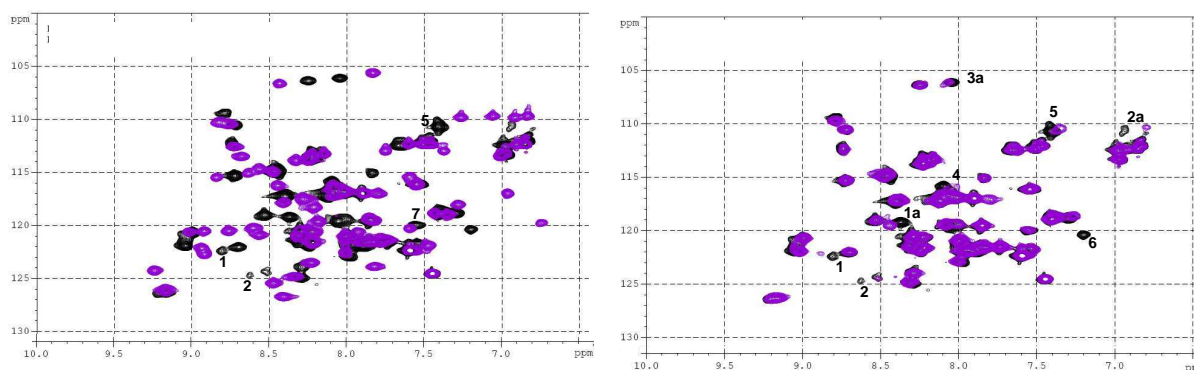


Figure 3.101: HSQC spectra of D/D domain. Black: ^1H - ^{15}N HSQC of $100\ \mu\text{M}$ ^{15}N -labeled D/D domain of RII α . Violet: ^1H - ^{15}N HSQC of $100\ \mu\text{M}$ ^{15}N -labeled D/D domain of RII α incubated with $800\ \mu\text{M}$ of peptide. Left: 16-mer AKAP18 δ L314E_6-21. Right: 14-mer AKAP18 δ L314E_9-22.

When comparing for example 14-mer peptide AKAP18δL314E_9-22 and terpyridine **25b**, one can see that some peaks are perturbed by both compound and peptide suggesting binding to the same area (peaks 1, 2, 4, 5, 6 in figure 3.100 and 3.101), but some shifts perturbed by **25b** (peak 3 and 7 in figure 3.100) are not perturbed by the 14-mer AKAP18δL314E_9-22 and vice versa. This could hint to a partially common binding site of the compounds as compared to the 14-mer peptide.

This outcome suggested that either presence of the *N,N*-dibenzylamine function is required for binding or that presence of a primary amine (**26b**) or secondary amine functionality (**26c**) in this position is detrimental for binding. Based on the nature of the binding site, which is described as a shallow hydrophobic groove, one could argue that presence of the spacious, hydrophobic benzyl groups is important for mediating binding of the terpyridines to the D/D domain. Of course, the compounds could also bind to a different binding site on the D/D domain, this has to be further investigated. It will be interesting to see whether the 3,4-dimethyl analogue **25a** also shows binding specifically to the D/D domain of RIIα in an HSQC experiment.

The next step in evaluating the terpyridines as potential lead structures should be quantification of binding of the active compounds as well as testing of other bipyridines and terpyridines that have been already synthesized. In addition, the synthesis of the corresponding carboxylic acid derivatives of **25a** and **25b** is currently ongoing in order to determine, whether binding to the D/D domain can also be achieved in presence of the carboxylic acid functionality as suggested from modeling. The exact binding sites of terpyridines **25a** and **25b** have to be mapped. For this purpose, AG Krause is currently performing computational studies to see if a potential binding site for these scaffolds can be identified.

4 Summary and Outlook

Protein kinase A (PKA) is a cAMP-dependent Ser/Thr kinase that plays a central role in cAMP-dependent signal transduction pathways. PKA consists of a dimer of regulatory (R) subunits, each of which binds one catalytic (C) subunit. The cAMP/PKA pathway controls a plethora of physiological processes. Therefore, a tight spatiotemporal control of PKA-activity is essential. One mechanism involved in the tight control of PKA activity is compartmentalization of PKA to distinct cellular sites by A-kinase anchoring proteins (AKAPs). AKAPs are a family of scaffolding proteins with around 50 members. The defining characteristic of an AKAP is an amphipatic α -helix of 14 to 18 amino acids that is called R binding domain (RBD) because it interacts with the R subunit dimer of PKA. More specifically, the RBDs of AKAPs bind to a domain of R subunits that is termed Dimerization and Docking domain (D/D domain). Most AKAPs preferentially interact with PKA RII type subunits.

Identification of Peptides that retain ability to bind PKA

Several peptides derived from the RII-binding domains of AKAPs bind with high affinity to the regulatory subunits of PKA. A 25-mer peptide derived from the AKAP18 δ , AKAP18 δ L314E, binds RII subunits with subnanomolar affinity and inhibits the interaction between PKA and AKAPs *in vitro* and in cell-based assays if coupled to stearate. The first aim of the thesis was to determine the minimal length of the amino acid sequence of the peptide AKAP18 δ L314E required for specific binding to the D/D domain of RII α as a basis for peptidomimetics that can be exploited as pharmacological tools.

Initial evaluation of the truncated peptides suggested that 10-mer peptides were too short for specific binding to the RII α D/D domain and that a length of 14 amino acids was a minimum requirement. It is not clear yet, whether amino acids important for the interaction were missing in the truncated peptides or whether the truncated peptides were not able form stable α -helices. Either factor or a combination of both could be the reason for the inability of the 10-mer and some of the 14-mer peptides to bind specifically to the D/D domain of RII α .

Based on the results from HSQC-experiments it seemed that binding of the 16-mer peptide AKAP18 δ L314E_6-19 is more pronounced than of the 14-mer peptides

tested. Thus, AKAP18δL314E_6-19 appears as the most promising starting point for further development of peptidomimetics. They could be generated e.g. by introduction of conformational restraints to strengthen helical structure and thereby potentially increasing stability and affinity.^[45;46]

No quantification of binding affinity or determination of inhibitory potential has been performed and experiments for these purposes are ongoing.

Synthesis of pyridine-based mimics of AKAP18δL314E

The second part of the work was to develop a synthesis for the quaterpyridines **2c**, **2d** or intermediate terpyridine derivatives thereof. The ligand was designed as a potential α -helical mimic of the RBD of AKAP18δ. The synthesis was performed in two stages: First the synthesis and functionalization of the single pyridine building blocks followed by Suzuki-Miyaura coupling of the building blocks to construct bipyridines and terpyridines.

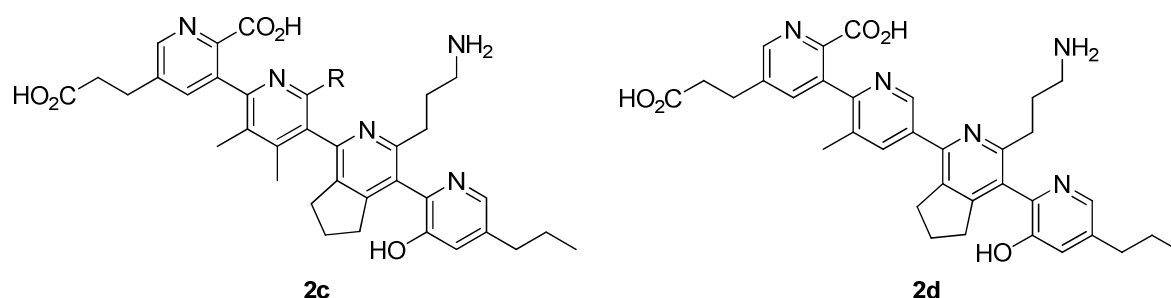


Figure 4.1: Quaterpyridines **2c** and **2d**.

Syntheses have been successfully established for the four single pyridine building blocks.

Synthesis of intermediate terpyridines and determination of their binding

Several bipyridine and terpyridine derivatives of the target scaffold were successfully synthesized. The assembly of compounds **22a-b** depicted in figure 4.2 was achieved in 9 to 10 reaction steps by sequential Suzuki-Miyaura coupling of single pyridine building blocks. This all-Suzuki approach allowed use of boron-containing nucleophiles that are in general considered to be non-toxic.

One key step in the synthesis of the terpyridine derivatives was the Pd-catalyzed cross-coupling of bipyridyl bromides and a dihydrocyclopenta[*c*]pyridyl bromide or chloride. For that purpose a two-step, one-pot borylation/Suzuki-Miyaura coupling procedure was developed successfully based on work from Billingsley et al.^[92;93] and applied for the synthesis of terpyridines **22a**, **22b** (figure 4.2) and **22c** (not depicted) using a Pd-XPhos-based catalyst system.

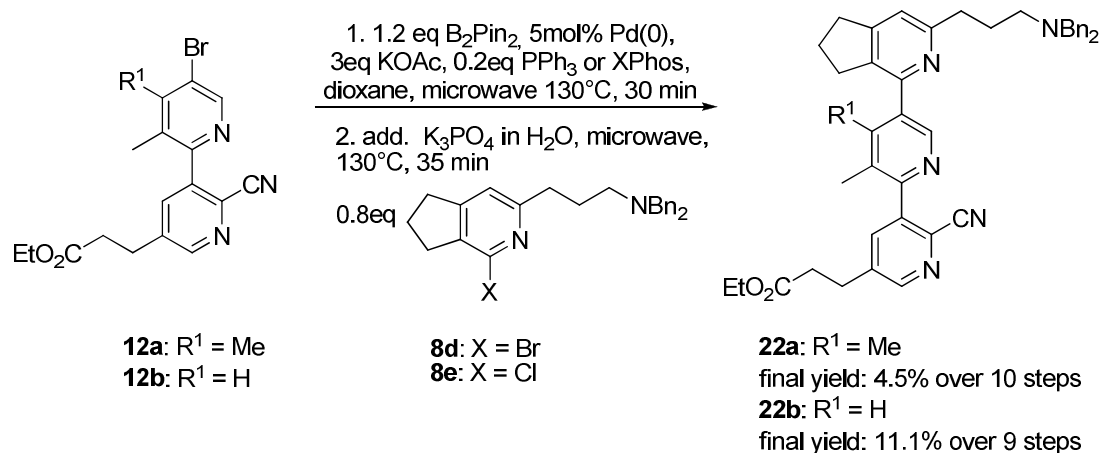


Figure 4.2: Scheme of the one-pot borylation/Suzuki coupling procedure.

No isolation of intermediate pinacol boronate esters used as the nucleophilic component in the Suzuki-Miyaura step of the procedure was required. The use of microwave-assisted synthesis reduced the reaction time to less than 70 minutes. The amount of catalyst used was quite high (5mol%), a reduction of catalyst loading has not been attempted but should be investigated in order to reduce cost of the reaction, especially for larger scale reactions.

In addition, an alternative approach towards the desired functionalized terpyridine derivatives was established. Herein, a [2+2+2] cycloaddition reaction was employed to introduce the cyclopenta[*c*]pyridine moiety to bipyridine building block **12** directly. With this strategy the synthesis of building block **8** was avoided and the corresponding terpyridine **24a** was synthesized with only 5 reaction steps in 8.5% overall yield, terpyridine **24b** was synthesized in only 7 steps in 4.9% overall yield.

Although the final yields of terpyridines obtained from the [2+2+2] cycloaddition-strategy using Ru(II) catalysis were not superior to the yields obtained with the all-Suzuki strategy, the lower number of reaction steps required for terpyridine synthesis is one advantage.

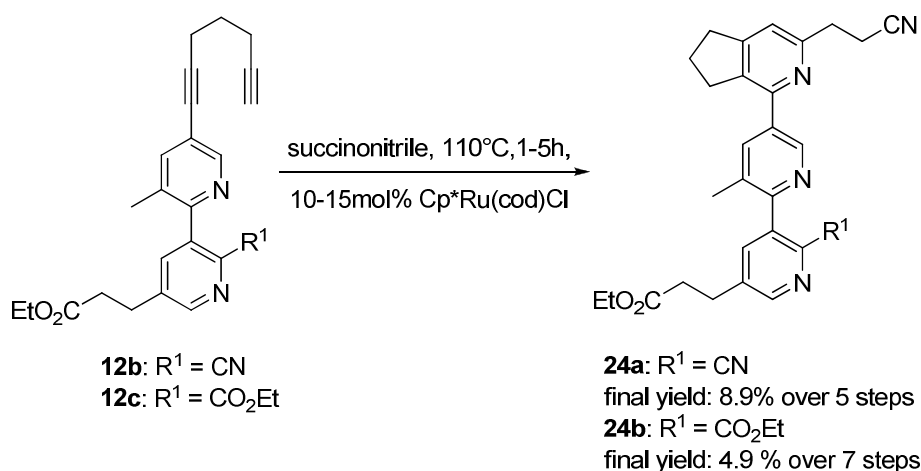


Figure 4.3: Scheme of the [2+2+2] cycloaddition reaction for the synthesis of terpyridines.

If the yield of the cycloaddition step can be increased and the reaction can be extended to other nitriles this will become an interesting complementary strategy for terpyridine synthesis. Application of a [2+2+2] cycloaddition synthesis would have the advantage of avoiding the strong basic reaction conditions required for introduction of the halide-function to building block **8**; this could be especially useful for the synthesis of terpyridine derivatives with base-labile substituents on building block **8**. For this purpose, other catalyst systems employed in the *de novo* synthesis of pyridines from alkynes and nitriles, for example CpCo(II)-based catalysts, could be investigated.

As shown in figure 4.1, in the *in silico*-designed target ligand, a carboxylic acid was suggested as suitable functionality in the C-2 position of building block **6**. However, when attempting the synthesis of the di-carboxylic acid derivatives, the amide derivatives depicted in figure 4.4 were obtained instead since unexpectedly only partial hydrolysis of the nitrile functionality took place. The synthesis for the corresponding carboxylic acids is currently being established.

The characterization of the binding ability of selected terpyridines and bipyridine derivatives to RII α was started by NMR-based techniques. Qualitative measurements suggested that the *N,N*-dibenzylamine-containing terpyridines **25a** (11 steps, 3.3% yield) and **25b** (10 steps, 8.9% yield) bind to RII α . For terpyridine **25b** binding to the D/D domain of RII α was confirmed also in a second assay using HSQC-NMR.

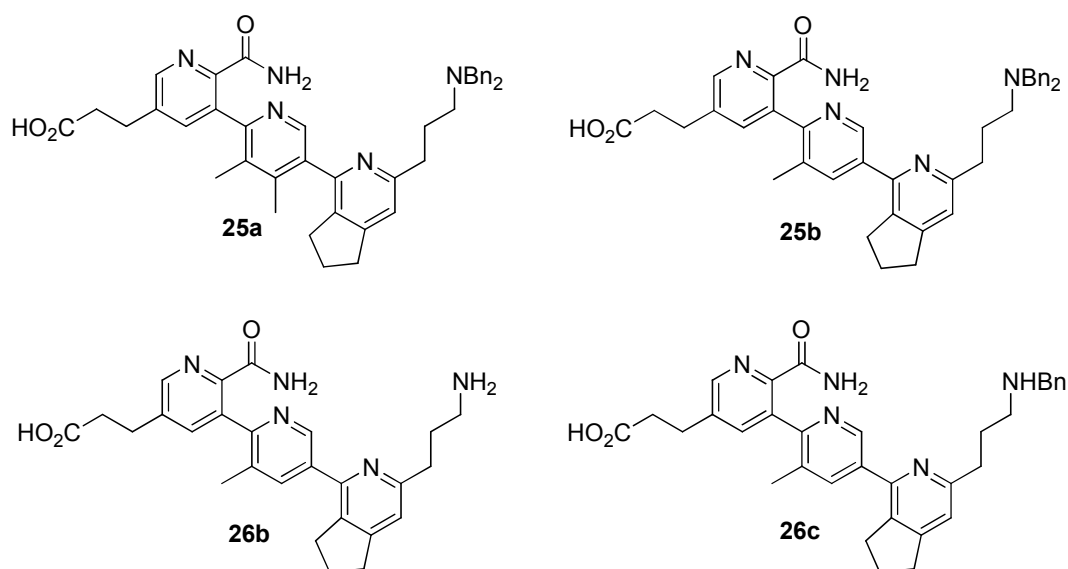


Figure 4.4: Compounds **25a** and **25b**: binding to RII α is detected in STD-NMR (**25a** and **25b**) and HSQC-NMR measurements (**25b**; **25a** not yet tested). Compounds **26b** and **26c**: no binding is detected in STD-NMR and HSQC-NMR measurements.

These results could be a first hint towards specific, potentially AKAP-like binding of the terpyridines. On the other hand, for terpyridine **26b** which contains the free amine functionality predicted as an interacting group from the modeling study, no binding to RII α or the D/D domain of RII α was detected. Also, with the *N,N*-dibenzylamine **26c** no binding was detected. It appeared therefore, that the *N,N*-dibenzylamine functionality that was originally introduced merely as a protecting group of the amine functionality is required for binding.

In order to confirm these initial results and to further assess the scope of this terpyridine scaffold as a structural basis for AKAP-PKA interaction inhibitors an additional characterization of the two hit compounds is required:

A quantification of binding affinity should be the next step followed by determination of inhibitory potential towards distinct AKAP-PKA interactions. Also, there several terpyridine derivatives left that have already been synthesized but not yet tested. Evaluation of their biological activity should give additional information about the structure-activity relationship (SAR) between the terpyridine scaffold and the D/D domain of RII α . For example, the characterization of derivative **22b** could give information whether the free carboxylate functions in terpyridines **25a** and **25b** are required for binding. In addition, binding of the carboxylic derivatives of the amides **25a** and **25b** should be determined.

In general, the specificity of the terpyridines with regard to other proteins should be examined.^[26] A very important step would be the identification of the exact binding pocket for structure-based library design and to estimate the potential of this terpyridine scaffold as a lead structure. For precise structural data and the exact binding mode, high resolution NMR- or x-ray-structures of ligand-protein complexes could be determined.^[37] In between, docking studies with accessible data have been started by AG Krause (FMP Berlin) based on the already obtained information, but more detailed information about the binding affinity of the compounds and data on the behaviour of other terpyridine derivatives similar to **25a** and **25b** might be required for reliable predictions.

Synthesis of quaterpyridines

The synthesis of quaterpyridine derivatives **2c** or **2d** depicted in figure 4.1 was not finished during this work.

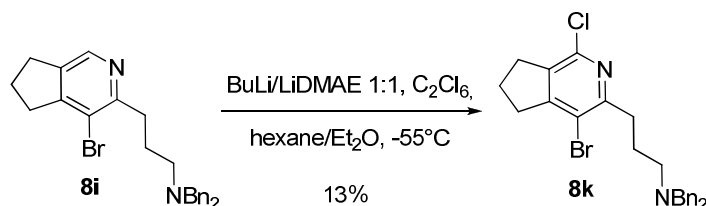


Figure 4.5: Scheme of the synthesis of di-halo building block **8k**.

One reason for this was that the dihalo-building block **8k** depicted in figure 4.5 was synthesized in very low yield (final yield: 0.5%, 7 steps) which was not sufficient for further use in the synthesis. Therefore, a modified synthesis for this building block **8** would have to be developed in order to construct target scaffold **2** by iterative Pd-catalyzed cross couplings. One problem in the synthesis of **8k** was that the last reaction step gave the product in only 13% yield. The synthesis of the di-chloro derivative of **8k** could be an alternative approach because the chloro-derivative of **8i** is expected to be more stable under similar reaction conditions.

However, as long as it has not been determined if the terpyridines **25a** and **25b** bind to the binding site proposed from the initial modeling study, focusing on the synthesis of the quaterpyridine scaffold was not the preferred strategy: The fourth pyridine building block might not be required for an increase in binding affinity and other

4 Summary and Outlook

substituents that can be easier introduced to the target scaffold might be more suitable for binding. Therefore, it appears most reasonable to focus further synthetic efforts on the synthesis of derivatives of the terpyridine scaffold to obtain more SAR data and to try to solve the structure of the best binding compound in complex with the D/D domain of RII α .

5 Experimental

5.1 Instruments

5.1.1 Nuclear magnetic resonance ($^1\text{H-NMR}$; $^{13}\text{C-NMR}$)

1D- and 2D-NMR spectra were recorded on a *Bruker AV 300* (^1H : 300 MHz, ^{13}C : 75 MHz). Chemical shifts δ are depicted in *ppm* and coupling constants *J* are depicted in Hz. The spectrometer was normalized to TMS. As internal standard, the measured NMR-spectra were normalized to the solvent peak used for recording the spectrum:

$\text{d}_6\text{-DMSO}$: ^1H : 2.50 ppm, ^{13}C : 39.51 ppm,

MeOD : ^1H : 4.87 ppm, ^{13}C : 49.15 ppm,

CDCl_3 : ^1H : 7.26 ppm, ^{13}C : 77.23 ppm.

5.1.2 Liquid chromatography-mass spectrometry (LC-MS)

All mass spectra were recorded on a *4000QTrap* (*Applied Biosystems*) connected to a Shimadzu UFLC system. Ionization was done by electrospray (ESI) of a approximately 1 μM solution of the sample in pure MeCN, MeOH or MeCN/ H_2O (1/1). All values are depicted as atomic mass units *m/z*.

The system is equipped with an *Shimadzu LC-20* system (degaser *Degasys DG-2410*, Autosampler *SIL-20A*, Controller *CBM-20A*) with a DAD-UV-detector (*SPD-M20A*). LC-MS runs were performed on an analytical Nucleodur column (100-5 C18 ec, 100 Å, 5 μm , 250 x 4 mm, Macherey-Nagel). The flow rate was set to 1 ml/min and column temperature was set to 40 Cg. Injection volumina were set between 5 μl and 20 μl with an approximate sample concentration of 50 μM .

Analytical LC-MS runs were performed with the following gradient: $\text{H}_2\text{O}/0.1\%$ TFA (v/v) (solvent A) and ACN/ 0.1% TFA (v/v) (solvent B), 5% B to 95 % B in 11 minutes. Stated retention times t_{R} of synthesized compounds refer to this gradient.

5.1.3 High resolution mass spectrometry (HRMS)

High resolution mass spectra were recorded on *Ionspec QFT-7* (*Varian*) with a Z-spray-ESI-source (*Micromass*).

5.1.4 Infrared spectroscopy (FT-ATR-IR)

FT-ATR-IR spectra were recorded on a Bruker Vector 22/Harrick. This machine is equipped with a SplitPea[®]-ATR-unit from Harrick. The compounds were pressed on Zincselenide and measured. IR spectra were recorded in a range of 500-400 cm⁻¹ with 32 scans. Background and ATR corrections were performed automatically. Carbon dioxide bands were removed from the spectra for clarity.

5.1.5 Melting point determination

Melting points of solid compounds were determined using an SMP3 machine from *Bibby Sterilin Ltd.*

5.1.6 Microwave-assisted synthesis

Microwave-assisted synthesis was performed with a Initiator[™] (Biotage). Reactions were performed in pressure-stable microwave vials with 0.2ml-20 ml reaction volume. Microwave vials were sealed with a septum. A magnetron with 15 to 300 W power generates microwave radiation with a frequency of 2.45 GHz. The temperature range of the machine can be varied from 60°C to 250°C with a heating rate of 2-5°C/sec. The maximal acceptable pressure within the reaction vessel is 20 bar. During the reaction, the temperature within the vessel is kept constant by short microwave pulses. Fast cooling of the microwave vials is achieved with compressed air.

5.2 Chromatographic methods

5.2.1 Thin layer chromatography (TLC)

TLC plates were made off aluminium foil coated with silica gel 60 (with fluorescence indicator F₂₅₄) or aluminum foil coated aluminium oxide with fluorescence indicator F₂₅₄). For detection, a UV kabinet from Lamag was used (wavelengths: 254 nm and 365 nm).

5.2.2 Column chromatography (CC)

Preparative CC was performed in glass columns with silica gel (pore size 60 Å, particle size 30-60 µm) from *J.T. Baker* as flash-chromatography with N₂-overpressure. Composition of solvents used for CC is shown in volume fractions.

5.2.3 High performance liquid chromatography (HPLC)

The preparative HPLC was made up of a *Shimadzu LC-20* system (degaser *Degasys DG-2410*, Autosampler *SIL-20A HT*, Controller *CBM-20A*) with a DAD-UV-detector (*SPD-M20A*). Analytical HPLC runs were performed on one of two columns, a Nucleodur column (100-5 C18 ec, 100 Å, 250 x 4 mm, 3µm, Macherey-Nagel) or a Nucleodur Sphinx column (15 cm x 4,6 mm 3 µm, Macherey-Nagel). In both cases the flow rate was set to 1 ml/min. Injection volumina were set between 10 µl and 100 µl with an approximate sample concentration of 50 µM.

Preparative separations were performed on a *Nucleodur C-18 RP* column (100 Å, 10 µm 300 mm x 25 mm, *Macherey-Nagel*) with the flow rate set to 9.2 ml/min.

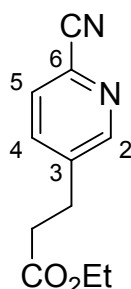
Semipreparative separations were performed on a *Nucleodur C-18* column (100 Å, 10 µm 300 mm x 25 mm, *Macherey-Nagel*) with the flow rate set to 3-4 ml/min.

5.3 Synthesis

Starting materials and solvents for synthesis were purchased from *Sigma-Aldrich*, *Fluka*, *Merck*, *J. T. Baker*, *Acros*, and *ALFA Aesar* in p.a. grade. For HPLC- and LC-MS measurements, acetonitrile and methanol (HPLC grade) from *J. T. Baker* and purified water (*Milli-Q-Plus* from *Millipore*) were used. The anhydrous solvents DMF, THF, hexane, diethyl ether, 1,2-dichloroethane, methanol, toluene, xylene and dioxane were purchased from *Sigma-Aldrich* and *Acros Organics*. Deuterated solvents for NMR spectroscopy were purchased from *Deutero GmbH*.

Compound-containing extracts in organic solvents were dried over $\text{MgSO}_4/\text{Na}_2\text{SO}_4$ and the solvent was removed with temperature of the water bath of the rotary evaporator set to 40 C. Solvent residues were removed if necessary in high vacuum ($p \leq 10^{-3}$ mbar). Compounds in aqueous solutions were freeze-dried by lyophilization with an *Alpha 1-2* lyophilizer (*Christ*). Reactions involving moisture- or air-sensitive compounds were performed in oven-dried glass flasks under N_2 -atmosphere. Anhydrous solvents were stored over molecular sieve (*Fluka UOP type 3A*, 3 Å).

5.3.1 Ethyl 3-(6-cyanopyridin-3-yl)propanoate (6b)



A 250 ml one-necked flask equipped with magnetic stir bar and condenser was charged with 5-bromo-2-cyanopyridine (2 g, 11 mmol), acrolein diethylacetal (5.08 ml, 33 mmol), *n*-tetrabutylammonium chloride (3.05 g, 11 mmol), tributylamine (5.25 ml, 22 mmol) and palladium(II) acetate (75 mg, 0.33 mmol). After addition of DMF (100 ml), the reaction mixture was heated to 120°C and stirred for 90 minutes. After the mixture was cooled down to room temperature, it was diluted with 100 ml of 2N hydrochloric acid. The aqueous phase was extracted three times with ethyl acetate, the combined organic phases were dried over MgSO₄ and the solvent was removed under reduced pressure. Column chromatography gave the crude product in 88% yield (1.98 g) as yellow solid.

¹H-NMR (300 MHz, d₆-DMSO): δ 1.12-1.16 (t, ³J = 7.1, 3H, -CH₂-CH₃), 2.72-2.74 (t, ³J = 7.4, 2H, -CH₂-CO₂Et), 2.93-2.98 (t, ³J = 7.4, 2H, -CH₂-CH₂-CO₂Et), 4.00- 4.07 (quartet, ³J = 7.1, 2H, -CH₂-CH₃), 7.94-7.95 (m, 2H, H-4, H-5), 8.66 (s, 1H, H-2).

¹³C-NMR (75,5 MHz, d₆-DMSO): δ 14.01 (-CH₂-CH₃), 27.37 (-CH₂-CH₂-CO₂Et), 33.70 (-CH₂-CO₂Et), 59.98 (-CH₂-CH₃), 117.60 (-CN), 128.58 (C-5), 130.34 (C-6), 137.40 (C-4), 141.07 (C-3), 151.51 (C-2), 171.72 (-CO₂Et).

HRMS: cal. 205.0972; exp. 205.0965 ([M+H]⁺)

ESI-MS: cal. 205.0972; exp. 205.0 ([M+H]⁺)

IR: ν [cm⁻¹] = 2984, 2233, 1729, 1565, 847.

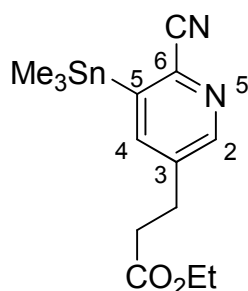
m.p. 36.4°C

R_f (TLC) 0.32 (EtOAc:hexane 1:2)

t_R (HPLC)

5.37 min

5.3.2 Ethyl-3-(6-cyano-5-(trimethylstannyl)pyridin-3-yl)propanoate (6c)



Into an oven-dried two-necked flask equipped with magnetic stir bar, nitrogen inlet and rubber septum was placed 2,2,6,6-tetramethylpiperidine (1.04 ml, 6 mmol) in anhydrous THF (20 ml) under nitrogen atmosphere. The reaction mixture was cooled down to 0°C, then 2.5 M *n*-butyllithium in hexane (2.4 ml, 6 mmol) was added dropwise via syringe and the reaction mixture was stirred for 30 minutes at 0°C. After cooling down to -75°C, **6b** (0.30 g, 1.5 mmol) in THF was added dropwise with a syringe. The reaction mixture turned orange-brown and darkened further while being stirred for 1 hour at -75°C. 1M trimethylstannane chloride in THF (5 ml, 5 mmol) was added quickly to the reaction mixture, which was then warmed up to room temperature and stirred for 2 hours. The reaction was quenched with 20 ml of water. The aqueous phase was extracted three times with diethyl ether. The combined organic phases were dried over MgSO₄ and the solvent was removed under reduced pressure. Column chromatography (EtOAc/hexane 1:4) gave the product as colorless oil in 38% yield (209 mg).

¹H-NMR (300 MHz, d₆-DMSO): δ 0.32-0.52 (m, 9H, -Sn(CH₃)₃), 1.12-1.17 (t, ³J = 7.1, 3H, -CH₂-CH₃), 2.67-2.72 (t, ³J = 7.4, 2H, -CH₂-CO₂Et), 2.89-2.94 (t, ³J = 7.4, 2H, -CH₂-CH₂-CO₂Et), 4.01-4.08 (quartet, ³J = 7.1, 2H, -CH₂-CH₃), 7.89-7.90 (d, ⁴J = 2.1, 1H, H-4) 8.54-8.54 (d, ⁴J = 2.1, 1H, H-2).

¹³C-NMR (75,5 MHz, d₆-DMSO): δ -8.61 (-Sn(CH₃)₃), 14.03 (-CH₂-CH₃), 27.47 (-CH₂-CH₂-CO₂Et), 33.93 (-CH₂-CO₂Et), 59.95 (-CH₂-CH₃), 118.92 (-CN), 136.66 (C-6), 139.75 (C-3), 143.49 (C-5), 144.43 (C-4), 150.68 (C-2), 171.82 (-CO₂Et).

HRMS: cal. 369.0622, exp. 369.0617 ([M+H]⁺)

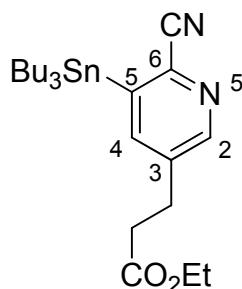
ESI-MS: cal. 369.0622, exp. 369.1 ([M+H]⁺)

IR: ν [cm⁻¹] = 2983, 2932, 2227, 1728, 1575, 778.

R_f (TLC) 0.68 (EtOAc:hexane 1:2)

t_R (HPLC) 9.62 min

5.3.3 Ethyl-3-(6-cyano-5-(tributylstannyl)pyridin-3-yl)propanoate (6d)



Into an oven-dried two-necked flask equipped with magnetic stir bar, nitrogen inlet and rubber septum was placed 2,2,6,6-tetramethylpiperidine (1.04 ml, 6 mmol) in anhydrous THF (20 ml) under nitrogen atmosphere. The reaction mixture was cooled down to 0°C, then 2.5 M *n*-butyllithium (2.4 ml, 6 mmol) in hexane was added dropwise into the flask via syringe and the reaction mixture was stirred for 30 minutes at 0°C. After cooling down to -75°C, **6b** (0.30 g, 1.5 mmol) in THF was added dropwise via syringe. The reaction mixture turned orange-brown and darkened further while being stirred for 1 hour at -75°C. Next tributylstannane chloride (1.07 ml, 4 mmol) was added quickly to the reaction mixture, which was then warmed up to room temperature and stirred for 10 minutes. The reaction was quenched with 20 ml of water. The aqueous phase was extracted three times with diethyl ether. The combined organic phases were dried over MgSO₄ and the solvent was removed under reduced pressure. Column chromatography (10% EtOAc in hexane) gave the product as colorless oil in 39% yield (289 mg).

¹H-NMR (300 MHz, d₆-DMSO): δ 0.82-0.87 (t, ³J = 7.3, 9H, -Sn(*n*Bu)₃), 1.10-1.15 (t, ³J = 7.1, 3H, -CH₂-CH₃), 1.20-1.32 (m, 12H, -Sn(*n*Bu)₃), 1.47-1.55 (m, 6H, -Sn(*n*Bu)₃), 2.67-2.72 (t, ³J = 7.3, 2H, -CH₂-CO₂Et), 2.90-2.95 (t, ³J = 7.3, 2H, -CH₂-CH₂-CO₂Et), 3.99-4.06 (quartet, ³J = 7.1, 2H, -CH₂-CH₃), 7.87-7.88 (d, ⁴J = 2.1 1H, H-4) 8.53-8.54 (s, ⁴J = 2.1 1H, H-2).

¹³C-NMR (75.5 MHz, d₆-DMSO): δ 9.64 (-Sn(*n*Bu)₃), 13.41 (-Sn(*n*Bu)₃), 14.00 (-CH₂-CH₃), 26.49 (-Sn(*n*Bu)₃), 27.43 (-CH₂-CH₂-CO₂Et), 28.36 (-Sn(*n*Bu)₃), 33.90 (-CH₂-CO₂Et), 59.90 (-CH₂-CH₃), 119.05 (-CN), 136.93 (C-6), 139.80 (C-3), 142.55 (C-5), 144.80 (C-4), 150.80 (C-2), 171.75 (-CO₂Et).

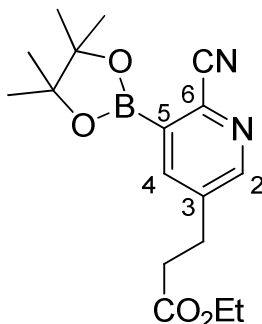
HRMS: cal. 495.2032, exp. 495.2049 ([M+H]⁺) **ESI-MS**: cal. 495.2032, exp. 495.2 ([M+H]⁺)

IR: ν [cm⁻¹] = 2925, 2226, 1736, 1633, 1534, 764.

R_f (TLC) 0.82 (EtOAc:hexane 1:2)

t_R (HPLC) 12.41 min

5.3.4 Ethyl-3-[6-cyano-5-(4,4,5,5-tetramethyl-1,3,2-dioxaborolan-2-yl)pyridin-3-yl]propanoate (6f)



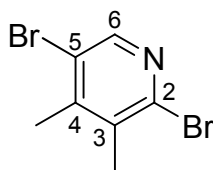
Into an oven-dried 100 ml three-necked flask equipped with magnetic stir bar, nitrogen inlet, rubber septum and bubbler was placed 2,2,6,6-tetramethylpiperidine (0.99 ml, 6.0 mmol) in anhydrous THF (10 ml) under nitrogen atmosphere. The reaction mixture was cooled down to 0°C, then 2.5 M *n*-butyllithium in hexane (2.35 ml, 6.0 mmol) was added dropwise into the flask via syringe and the reaction mixture was stirred for 30 minutes at 0°C. After cooling down to -75°C, **6b** (0.3 g, 1.5 mmol) in THF was added dropwise via syringe. The reaction mixture turned deep brown and was stirred for 15 minutes at -75°C. Neat triisopropylborate (1.7 ml, 7.5 mmol) was added quickly to the reaction mixture, which was then stirred for 1 hour at -75°C. Then, pinacol (0.89 g, 7.7 mmol) in THF (2 ml) was added quickly to the reaction mixture. The solution was warmed up in a water bath (T = 40°C) and stirred for 2 hours. The reaction was quenched with water. The aqueous phase was acidified to pH 4 with 1M hydrochloric acid and extracted three times with chloroform. The combined organic phases were dried over MgSO₄ and the solvent was removed under reduced pressure. The product hydrolyzed to the free boronic acid under conditions used in HPLC and LC-MS runs. Analytical data represent results for the boronic acid.

The product was used without further purification in the next reaction step.

HRMS: cal. 249.1043, exp. 249.1032 ([M+H]⁺)

ESI-MS: cal. 249.1043, exp. 249.1 ([M+H]⁺)

t_R (HPLC) 4.18 min

5.3.5 2,5-Dibromo-3,4-dimethylpyridine (7d)

Into an oven-dried 50 ml two-necked flask equipped with magnetic stir bar, nitrogen inlet and rubber septum was placed lithiumdiisopropylamide (1.62 ml, 3.2 mmol) in anhydrous THF (15 ml) under nitrogen atmosphere. The solution was cooled down to -45°C and then 2,5-dibromo-3-methylpyridine (**7a**) (0.75 g, 2.98 mmol) in anhydrous THF was added to the reaction mixture dropwise via syringe and the deep brown solution was stirred for 5 minutes at -45°C . After cooling down to -75°C , methyl iodide (0.84 ml, 11.9 mmol) in anhydrous THF (1 ml) was added quickly to the reaction mixture which was warmed up to room temperature after 2 minutes and stirred for 2 more hours. The reaction was quenched with water and the aqueous phase was extracted three times with ethyl acetate. The combined organic phases were dried over MgSO_4 , the solvent was removed under reduced pressure. The product was purified by Kugelrohr distillation as yellow oil in 20% yield (158 mg).

$^1\text{H-NMR}$ (300 MHz, CDCl_3): δ 2.45-2.45 (s, 6H, $-\text{CH}_3$), 8.29 (s, 1H, H-6).

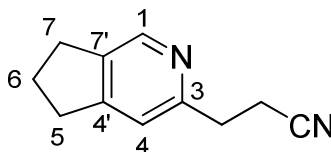
$^{13}\text{C-NMR}$ (75,5 MHz, CDCl_3): δ 20.04 ($-\text{CH}_3$), 20.87 ($-\text{CH}_3$), 123.44 (C5), 135.40 (C-3), 143.69 (C-2), 147.89 (C-4), 148.49 (C-6).

HRMS: cal. 265.8998, exp. 265.8987 ($[\text{M}+\text{H}]^+$)

ESI-MS: cal. 265.8998,, exp. 265.9($[\text{M}+\text{H}]^+$)

R_f (TLC) 0.79 (EtOAc:hexane 1:2)

t_R (HPLC) 8.08 min

5.3.6 3-(6,7-dihydro-5H-cyclopenta[c]pyridin-3-yl)propanenitrile (8a)

An oven-dried 500 ml three-necked flask equipped with magnetic stir bar, nitrogen inlet and bubbler was charged under nitrogen atmosphere with succinonitrile (10 g, 125 mmol) and Cp*Ru(cod)Cl (600 mg, 1.63 mmol) in 1,2-dichloroethane (300 ml). The reaction mixture was cooled down to 0°C and 1,6-heptadiyne (7.6 g, 82.5 mmol) in 1,2-dichloroethane (50 ml) was added slowly via dropping funnel over 30 minutes. The reaction mixture was warmed up to room temperature and stirred for 20 hours, and then the mixture was concentrated *in vacuo*. Column chromatography of the residue (EtOAc:hexane 2+1) gave the product as white solid in 79% yield (11.2 g).

¹H-NMR (300 MHz, CDCl₃): δ 2.06-2.16 (m, 2H, H-6), 2.80-2.85 (t, ³J = 7.3, 2H, -CH₂-CN), 2.89-2.94 (m, 4H, H-5, H-7), 3.05-3.10 (t, ³J = 7.3, 2H, -CH₂-CH₂-CN), 7.11 (s, 1H, H-4), 8.38 (s, 1H, H-1)

¹³C-NMR (75,5 MHz, CDCl₃): δ 17.32 (-CH₂-CN), 25.24 (C-6), 30.14, 32.84 (C-5, C-7), 33.44 (-CH₂-CH₂-CN), 119.64 (C-4), 119.74 (-CN), 139.12 (C-7'), 145.27 (C-1), 154.71, 155.35 (C-3, C-4').

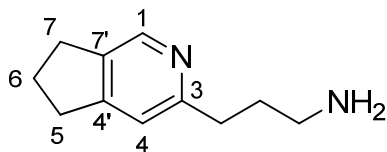
HRMS: cal. 173.1073, exp. 173.1070 ([M+H]⁺)

ESI-MS: cal. 173.1073, exp. 173.0 ([M+H]⁺)

IR: ν [cm⁻¹] = 2937, 2245, 1607, 896, 883.

m.p. 68.5°C

R_f (TLC) 0.29 (EtOAc:hexane 2+1) **t_R (HPLC)** 1.13 min

5.3.7 3-(6,7-dihydro-5H-cyclopenta[c]pyridin-3-yl)propan-1-amine (8b)

An oven-dried 500 ml three-necked flask equipped with magnetic stir bar, nitrogen inlet, condenser with bubbler and dropping funnel was charged with **8a** (5 g, 29 mmol) in anhydrous THF (200 ml) under nitrogen atmosphere. Neat $\text{BH}_3 \cdot \text{SMe}_2$ (12.6 g, 165.3 mmol) was added in one portion to the solution via dropping funnel. The reaction mixture was heated up to 60°C and stirred at this temperature over night. The solution was cooled down to room temperature, and then nitrogen inlet and dropping funnel were removed from the apparatus. 10 M hydrochloric acid was added very carefully (gas development!) until the white precipitate was completely dissolved. The reaction mixture was then heated to 70°C and stirred for 3 hours. After cooling down to room temperature, the aqueous phase was washed three times with diethyl ether. The aqueous phase was cooled down to 0°C and treated with 10 M sodium hydroxide solution to pH >11. The aqueous phase was extracted three times with chloroform. The combined organic phases were dried over a 1:1 mixture of MgSO_4 and K_2CO_3 . Removal of the solvent under reduced pressure gave the crude product as light brown oil in 86% yield (4.4 g). The product was used without further purification in the next reaction step.

$^1\text{H-NMR}$ (300 MHz, d_6 -DMSO): δ 1.65-1.75 (m, 2H, $-\text{CH}_2\text{-CH}_2\text{-NH}_2$), 1.95-2.05 (m, 2H, H-6), 2.51-2.56 (t, $^3J = 7.0$, 2H, $-\text{CH}_2\text{-NH}_2$), 2.66-2.71 (t, $^3J = 7.6$, 2H, $-\text{CH}_2\text{-CH}_2\text{-CH}_2\text{-NH}_2$), 2.80-2.85 (m, 4H, H-5, H-7), 7.11 (s, 1H, H-4), 8.29 (s, 1H, H-1).

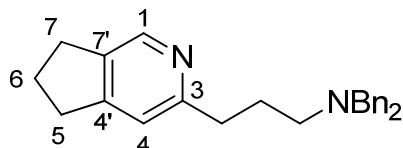
$^{13}\text{C-NMR}$ (75,5 MHz, CDCl_3): δ 25.27, 30.10 (C-6, $-\text{CH}_2\text{-CH}_2\text{-NH}_2$), 31.35, 32.83 (C-5, C-7), 35.64 ($-\text{CH}_2\text{-CH}_2\text{-CH}_2\text{-NH}_2$), 41.26 ($-\text{CH}_2\text{-CH}_2\text{-CH}_2\text{-NH}_2$), 119.40 (C-4), 138.05 (C-7'), 144.70 (C-1), 155.12, 158.54 (C-3, C-4').

HRMS: cal. 177.1386, exp. 177.1380 ($[\text{M}+\text{H}]^+$)

ESI-MS: cal. 177.1386, exp. 177.1 ($[\text{M}+\text{H}]^+$)

t_R (HPLC) 1.04 min

5.3.8 *N,N*-dibenzyl-3-(6,7-dihydro-5*H*-cyclopenta[*c*]pyridin-3-yl)propan-1-amine (**8c**)



Into an one-necked 100 ml flask was placed **8b** (1.4 g, 8 mmol), benzyl bromide (1.9 ml, 16 mmol) and triethylamine (2.23 ml, 16 mmol) in acetonitrile (75 ml). The reaction mixture was stirred for 3 hours at 60°C or for 24 hours at room temperature. The solvent was removed under reduced pressure and the residue was partitioned between brine and chloroform. The aqueous phase was extracted twice with chloroform. The combined organic phases were dried over MgSO₄; the solvent was removed under reduced pressure. Column chromatography (EtOAc/hexane 1:2 containing 2% NEt₃) gave the product as yellow oil in 51% yield (1.45 g).

¹H-NMR (300 MHz, d₆-DMSO): δ 1.80-1.90 (m, 2H, -CH₂-CH₂-NBn₂), 1.93-2.03 (m, 2H, H-6), 2.35-2.40 (t, ³J = 7.0, 2H, -CH₂-NBn₂), 2.58-2.63 (t, ³J = 7.5, 2H, -CH₂-CH₂-CH₂-NBn₂), 2.75-2.83 (m, 4H, H-5, H-7), 3.52 (s, 4H, Bn-H), 6.92 (s, 1H, H-4), 7.22-7.32 (m, 10H, Bn-H), 8.26 (s, 1H, H-1).

¹³C-NMR (75,5 MHz, d₆-DMSO): δ 24.62 (C-6), 26.51 (-CH₂-CH₂-NBn₂), 29.25 (C-7), 31.92 (C-5), 34.94 (-CH₂-CH₂-CH₂-NBn₂), 52.12 (-CH₂-NBn₂), 57.48 (Bn-C), 118.52 (C-4), 126.69 (Bn-C), 128.09 (Bn-C), 128.46 (Bn-C), 136.79 (Bn-C), 139.50 (C-7'), 144.36 (C-1), 153.35 (C-4'), 158.72 (C-3).

HRMS: cal. 357.2325 exp. 357.2329 ([M+H]⁺)

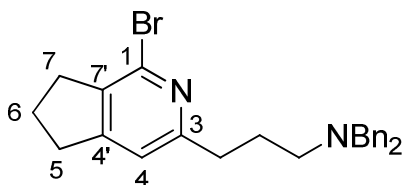
ESI-MS: cal. 357.2325, exp. 357.2 ([M+H]⁺)

IR: ν [cm⁻¹] = 2941, 2793, 1631, 1607, 742, 691.

R_f (TLC) 0.53 (EtOAc:hexane = 1:2 with 2% NEt₃)

t_R (HPLC) 2.86 min

5.3.9 *N,N*-dibenzyl-3-(1-bromo-6,7-dihydro-5*H*-cyclopenta[*c*]pyridine-3-yl)propan-1-amine (**8d**)



An oven-dried 500 ml three-necked flask equipped with magnetic stir bar, nitrogen inlet, bubbler and rubber septum was charged with 2-dimethylaminoethanol (2.3 ml, 22.5 mmol) in anhydrous hexane under nitrogen atmosphere. The reaction mixture was cooled down to 0°C and 2.5M *n*BuLi in hexane (17.9 ml, 44.9 mmol) was added to the solution by syringe. The mixture was stirred for 15 minutes at 0°C and then cooled down to -65°C. **8c** (2 g, 5.6 mmol) in diethyl ether was added to the reaction mixture by syringe. The solution turned deep red and was stirred at -65°C for 30 minutes. The mixture was cooled down to -75°C and tetrabromomethane (11.1 g, 42 mmol) in hexane (15 ml) was added quickly via dropping funnel. The reaction mixture was stirred at -75°C for 30 minutes and quenched with water. The aqueous phase was extracted three times with chloroform. The combined organic phases were dried over MgSO₄ and the solvent was removed under reduced pressure. Column chromatography (EtOAc/hexane containing 1% NEt₃: gradient starting with 0% EtOAc, product eluted at 10% EtOAc) gave the product as yellow oil in 36% yield (878 mg).

¹H-NMR (300 MHz, *d*₆-DMSO): δ 1.83-1.88 (m, 2H, -CH₂-CH₂-NBn₂), 1.96-2.07 (m, 2H, H-6), 2.34-2.39 (t, ³*J* = 6.9, 2H, -CH₂-NBn₂), 2.58-2.62 (t, ³*J* = 7.4, 2H, -CH₂-CH₂-CH₂-NBn₂), 2.77-2.82 (t, ³*J* = 7.5, 2H, H-7), 2.87-2.92 (t, ³*J* = 7.6, 2H, H-5), 3.52 (s, 4H, Bn-H), 6.95 (s, 1H, H-4), 7.22-7.32 (m, 10H, Bn-H).

¹³C-NMR (75,5 MHz, *d*₆-DMSO): δ 23.11 (C-6), 26.11 (-CH₂-CH₂-NBn₂), 32.11 (C-7), 33.14 (C-5), 34.22 (-CH₂-CH₂-CH₂-NBn₂), 51.77 (-CH₂-NBn₂), 57.48 (Bn-C), 118.66 (C-4), 126.70 (Bn-C), 128.09 (Bn-C), 128.47 (Bn-C), 137.59 (C-7'), 138.25 (C-1), 139.43 (Bn-C), 156.49 (C-4'), 160.79 (C-3).

HRMS: cal. 435.1430, exp. 435.1428 ([M+H]⁺) **ESI-MS**: cal. 435.1430, exp. 435.1 ([M+H]⁺)

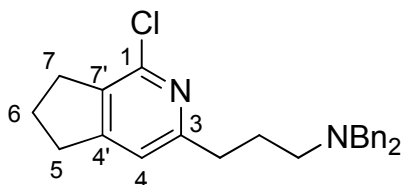
IR: ν [cm⁻¹] = 2944, 2802, 1597, 1537, 896, 745, 691.

m.p. 63.9°C

5 Experimental

R_f (TLC) 0.58 (EtOAc:hexane = 1:6 with 1% NEt₃) **t_R (HPLC)** 5.56 min

5.3.10 *N,N*-dibenzyl-3-(1-chloro-6,7-dihydro-5*H*-cyclopenta[*c*]pyridine-3-yl)propan-1-amine (**8e**)



An oven-dried 500 ml three-necked flask equipped with magnetic stir bar, nitrogen inlet, bubbler and dropping funnel was charged with 2-dimethylaminoethanol (5.8 ml, 56 mmol) in anhydrous hexane under nitrogen atmosphere. The reaction mixture was cooled down to 0°C and 2.5M *n*BuLi in hexane (44.8 ml, 112 mmol) was added to the solution by syringe. The mixture was stirred for 15 minutes at 0°C and then cooled down to -65°C. **8c** (5 g, 14 mmol) in diethyl ether was added to reaction mixture by syringe. The solution turned deep red and was stirred at -65°C for 30 minutes. The mixture was cooled down to -75°C and hexachloroethane (16.5 g, 70 mmol) in hexane (45 ml) was added in one shot by dropping funnel. The reaction mixture was stirred at -75°C for 30 minutes and quenched with water. The aqueous phase was extracted three times with chloroform. The combined organic phases were dried over MgSO₄ and the solvent was removed under reduced pressure. Column chromatography (EtOAc/hexane containing 1% NEt₃: gradient starting with 0% EtOAc, product eluted at 10% EtOAc) gave the product as white solid in 59% yield (3.2 g).

¹H-NMR (300 MHz, *d*₆-DMSO): δ 1.79-1.89 (m, 2H, -CH₂-CH₂-NBn₂), 1.98-2.08 (m, 2H, H-6), 2.34-2.39 (t, ³*J* = 7.0, 2H, -CH₂-NBn₂), 2.57-2.62 (t, ³*J* = 7.4, 2H, -CH₂-CH₂-CH₂-NBn₂), 2.80-2.90 (m, 4H, H-5, H-7), 3.52 (s, 4H, Bn-H), 6.93 (s, 1H, H-4), 7.21-7.30 (m, 10H, Bn-H).

¹³C-NMR (75,5 MHz, *d*₆-DMSO): δ 23.46 (C-6), 26.08 (-CH₂-CH₂-NBn₂), 30.38 (C-7), 32.86 (C-5), 34.27 (-CH₂-CH₂-CH₂-NBn₂), 51.78 (-CH₂-NBn₂), 57.48 (Bn-C), 118.38 (C-4), 126.70 (Bn-C), 128.08 (Bn-C), 128.48 (Bn-C), 135.27 (C-7'), 139.43 (Bn-C), 145.46 (C-1), 157.24 (C4'), 160.34 (C-3).

HRMS: cal. 391.1936 exp. 391.1930 ([M+H]⁺)

ESI-MS: cal. 391.1936, exp. 391.2 ([M+H]⁺)

IR: ν [cm⁻¹] = 2943, 2802, 1600, 1545, 745, 692.

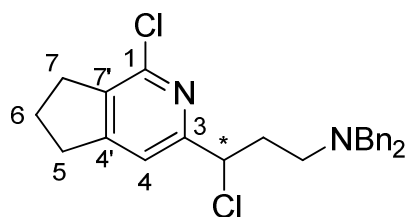
m.p. 48.7°C

5 Experimental

R_f (TLC) 0.56 (EtOAc:hexane = 1:6 with 1% NEt₃)

t_R (HPLC) 7.34 min

5.3.11 (rac)-N,N-dibenzyl-3-chloro-3-(1-chloro-6,7-dihydro-5H-cyclopenta[c]pyridine-3-yl)propan-1-amine (8l)



An oven-dried 500 ml three-necked flask equipped with magnetic stir bar, nitrogen inlet, bubbler and dropping funnel was charged with potassium *t*-butoxide (2.3 g, 20.5 mmol) under nitrogen atmosphere. Anhydrous diethyl ether (250 ml) was added, the solution was cooled down to -75°C and 2.5 M *n*BuLi in hexane (8.2 ml, 20.5 mmol) was added to the solution by syringe. The mixture was stirred for 10 minutes at -75°C . **8e** (4 g, 10.3 mmol) in diethyl ether was added to the reaction mixture by dropping funnel. The solution turned deep red and was stirred at -75°C for 60 minutes. Hexachloroethane (12.1 g, 51.3 mmol) in hexane (30 ml) was added quickly by dropping funnel. The reaction mixture was stirred at -75°C for 60 minutes and quenched with water. The aqueous phase was extracted three times with chloroform. The combined organic phases were dried over MgSO_4 and the solvent was removed under reduced pressure. Column chromatography (EtOAc/hexane containing 1% NEt_3 : gradient starting with 0% EtOAc, product eluted at 10% EtOAc) gave the product as yellow oil in 33% yield (1.4 g).

$^1\text{H-NMR}$ (300 MHz, CDCl_3): δ 2.06-2.16 (m, 2H, H-6), 2.27-2.42 (m, 2H, $-\text{CH}_2-\text{CH}_2-\text{NBn}_2$), 2.55-2.59 (t, $^3J = 6.5$, 2H, $-\text{CH}_2-\text{NBn}_2$), 2.90-2.95 (m, 4H, H-5, H-7), 3.56 (s, 4H, Bn-H), 4.96-5.01 (t, $^3J = 7.0$, 1H, $-\text{CH}(\text{Cl})-$), 7.04 (s, 1H, H-4), 7.21-7.33 (m, 10H, Bn-H).

$^{13}\text{C-NMR}$ (75,5 MHz, CDCl_3): δ 24.07 (C-6), 31.29, 33.72 (C-5, C-7), 35.77 ($-\text{CH}_2-\text{CH}_2-\text{NBn}_2$), 50.51 ($-\text{CH}_2-\text{NBn}_2$), 58.56 (Bn-C), 61.17 ($-\text{CH}(\text{Cl})-$), 117.45 (C-4), 127.04 (Bn-C), 128.36 (Bn-C), 129.08 (Bn-C), 138.51 (Bn-C), 139.54 (C-7'), 146.89 (C-1), 157.79 (C-3), 158.62 (C-4').

HRMS: cal. 425.1546, exp. 425.1540 ($[\text{M}+\text{H}]^+$)

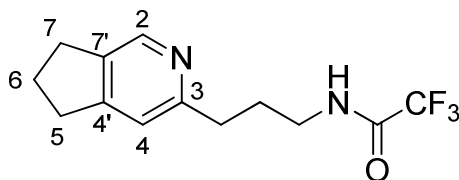
ESI-MS: cal. 425.1546, exp. 425.2 ($[\text{M}+\text{H}]^+$)

IR: ν [cm^{-1}] = 2936, 2827, 1632, 1599, 1550, 745, 736, 697.

R_f (TLC) 0.65 (EtOAc:hexane = 1:6 with 1% NEt_3)

t_R (HPLC) 6.67 min

5.3.12 2,2,2-Trifluoro-*N*-(3-(6,7-dihydro-5*H*-cyclopenta[*c*]pyridine-3-yl)propyl)-acetamide (8f)



An oven-dried 100 ml three-necked flask equipped with magnetic stir bar, nitrogen inlet, bubbler and rubber septum was charged with **8b** (1.5 g, 8.5 mmol) in anhydrous methanol (50 ml) under nitrogen atmosphere. The reaction mixture was cooled down to -5°C and ethyl trifluoroacetate (1.12 ml, 9.4 mmol) was added to the mixture via syringe. The reaction mixture was warmed up in the cooling bath over 4 hours. The solvent was removed under reduced pressure and the crude product was purified by column chromatography (EtOAc/hexane 2:1 containing 1% NEt_3). The product was obtained as white solid in 75% yield (1.7 g).

$^1\text{H-NMR}$ (300 MHz, MeOD): δ 1.93-2.02 (m, 2H, $-\text{CH}_2-\text{CH}_2-\text{N}-$), 2.10-2.20 (m, 2H, H-6), 2.78-2.84 (t, $^3J = 7.6$, 2H, $-\text{CH}_2-\text{CH}_2-\text{CH}_2-\text{N}-$), 2.94-2.99 (m, 4H, H-5, H-7), 3.33-3.37 (m, 2H, $-\text{CH}_2-\text{N}-$), 7.24 (s, 1H, H-4), 8.29 (s, 1H, H-1).

$^{13}\text{C-NMR}$ (75,5 MHz, MeOD): δ 26.30 (C-6), 30.37 ($-\text{CH}_2-\text{CH}_2-\text{N}-$), 30.89, 33.68, 35.77 (C-5, C-7, $-\text{CH}_2-\text{CH}_2-\text{CH}_2-\text{N}-$), 40.48 ($-\text{CH}_2-\text{N}-$), 115.82-119.62 ($-\text{CF}_3$), 120.83 (C-4), 139.88 (C-7'), 145.14 (C-1), 157.43 (C-4'), 158.86-159.35 ($-\text{C}(\text{O})-\text{CF}_3$), 159.62 (C-3).

HRMS: cal. 273.1209, exp. 273.1214 ($[\text{M}+\text{H}]^+$)

ESI-MS: cal. 273.1209, exp. 273.1 ($[\text{M}+\text{H}]^+$)

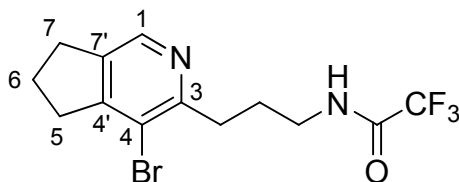
IR: ν [cm^{-1}] = 2965, 1702, 1564, 1140, 720, 692.

m.p. 84.9 $^{\circ}\text{C}$

R_f (TLC) 0.29 (EtOAc:hexane 2:1 with 1% NEt_3)

t_R (HPLC) 1.12 & 2.66 min

5.3.13 2,2,2-Trifluoro-*N*-(3-(4-bromo-6,7-dihydro-5*H*-cyclopenta[*c*]pyridine-3-yl)propyl)- acetamide (8g)



A 100 ml one-necked flask equipped with magnetic stir bar was charged with **8f** (1.59 g, 5.8 mmol). The flask was cooled with a water bath and trifluoroacetic acid (12 ml) was added slowly into the flask. Sulfuric acid (15.8 ml) and, after removal of the water bath, *N*-bromosuccinimide (1.35 g, 7.6 mmol) were added to the reaction mixture. The mixture was stirred at room temperature and under exclusion of light for 24 hours. The reaction mixture was then poured into ice and alkalinized to pH 9 using 10M NaOH. The aqueous phase was extracted twice with ethyl acetate and once with chloroform. The combined organic phases were dried over Na₂SO₄ and the solvent was removed under reduced pressure. Column chromatography (EtOAc/hexane 1+1) gave the product as light yellow solid in 24% yield (489 mg).

¹H-NMR (300 MHz, MeOD): δ 1.94-2.04 (m, 2H, -CH₂-CH₂-N-), 2.15-2.25 (m, 2H, H-6), 3.00-3.14 (m, 6H, H-5, H-7, -CH₂-CH₂-CH₂-N-), 3.38-3.42 (m, 2H, -CH₂-N-), 8.27 (s, 1H, H-1).

¹³C-NMR (75,5 MHz, MeOD): δ 25.27 (C-6), 29.01 (-CH₂-CH₂-N-), 32.21, 34.99, 36.08 (C-5, C-7, -CH₂-CH₂-CH₂-N-), 40.49 (-CH₂-N-), 129.88 (C-4), 141.52 (C-7'), 143.74 (C-1), 157.64 (C-4'), 157.71 (C-3).

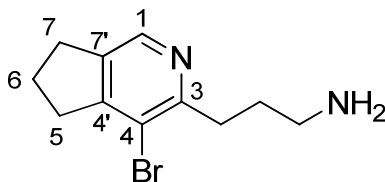
HRMS: cal. 351.0314, exp. 351.0313 ([M+H]⁺)

ESI-MS: cal. 351.0314, exp. 351.0 ([M+H]⁺)

IR: ν [cm⁻¹] = 2936, 1706, 1632, 1535, 1177, 1151, 721, 683.

m.p. 75.2°C

R_f (TLC) 0.58 (EtOAc:hexane = 2:1) **t_R (HPLC)** 5.58 min

5.3.14 3-(4-bromo-6,7-dihydro-5H-cyclopenta[c]pyridine-3-yl)propan-1-amine (8h)

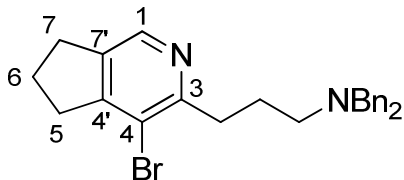
A 100 ml one-necked flask equipped with magnetic stir bar and condenser was charged with **8g** (200 mg, 0.57 mmol) and potassium carbonate (197 mg, 1.45 mmol). After addition of methanol (15 ml) and H₂O (0.75 ml), the reaction mixture was refluxed for 150 minutes. After cooling down to room temperature, the reaction mixture was concentrated *in vacuo*, diluted in water and extracted with chloroform and *n*-butanol. The aqueous phase was alkalinized to pH14 and extracted again with chloroform and butanol. The combined organic phases were dried over Na₂SO₄ and the solvents were removed under reduced pressure. The crude product was obtained in 57% yield (83 mg) and used in the next reaction step without further purification.

HRMS: cal. 255.0591; exp. 255.0479 ([M+H]⁺)

ESI-MS: cal. 255.0591, exp. 255.1 ([M+H]⁺)

t_R (HPLC) 2.44

5.3.15 *N,N*-dibenzyl-3-(4-bromo-6,7-dihydro-5*H*-cyclopenta[*c*]pyridine-3-yl)propan-1-amine (**8i**)



A 100 ml one-necked flask equipped with magnetic stir bar and condenser was charged with **8h** (129 mg, 0.51 mmol) in a 1:1 solution of acetonitrile and DMF. Benzyl bromide (0.13 ml, 1.06 mmol) and triethylamine (0.15 ml, 1.06 mmol) were added and the reaction mixture was stirred at 60°C for 2 hours. After cooling down to room temperature, the reaction mixture was concentrated *in vacuo*, diluted with water and extracted three times with chloroform. The combined organic phases were dried over Na₂SO₄ and the solvent was removed under reduced pressure. Column chromatography (EtOAc/hexane 1+20 containing 0.5% NEt₃) gave the product as yellow oil in 54% yield (120 mg).

¹H-NMR (300 MHz, d₆-DMSO): δ 1.83-1.92 (m, 2H, -CH₂-CH₂-NBn₂), 1.99-2.11 (m, 2H, H-6), 2.40-2.45 (t, ³J = 6.9, 2H, -CH₂-NBn₂), 2.79-2.90 (m, 4H, H-7, -CH₂-CH₂-CH₂-NBn₂), 2.94-2.99 (t, ³J = 7.5, 2H, H-5), 3.52 (s, 4H, Bn-H), 7.21-7.34 (m, 10H, Bn-H), 8.21 (s, 1H, H-1).

¹³C-NMR (75,5 MHz, d₆-DMSO): δ 23.61 (C-6), 25.00 (-CH₂-CH₂-NBn₂), 30.58, 33.88, 34.37 (C-5, C-7, -CH₂-CH₂-CH₂-NBn₂), 51.94 (-CH₂-NBn₂), 57.83 (Bn-C), 117.98 (C-4), 126.67 (Bn-C), 128.07 (Bn-C), 128.41 (Bn-C), 138.93, 139.38 (C-7', Bn-C), 142.90 (C-1), 154.16 (C-4'), 156.30 (C-3).

HRMS: cal. 435.1430, exp. 435.1427 ([M+H]⁺)

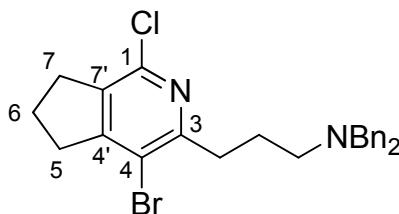
ESI-MS: cal. 435.1430, exp. 435.2 ([M+H]⁺)

IR: ν [cm⁻¹] = 2939, 2829, 1677, 1637, 1024, 700.

R_f (TLC) 0.31 (EtOAc:hexane = 1:6 with 1% NEt₃)

t_R (HPLC) 5.50 min

5.3.16 *N,N*-dibenzyl-3-(4-bromo-1-chloro-6,7-dihydro-5*H*-cyclopenta[*c*]pyridine-3-yl)propan-1-amine (8k)



An oven-dried 100 ml three-necked flask equipped with magnetic stir bar, nitrogen inlet, rubber septum and bubbler was charged with anhydrous hexane (10 ml) and 2-dimethylaminoethanol (0.1 ml, 0.92 mmol) under nitrogen atmosphere. The solution was cooled down to -5°C and then 2.5 M BuLi in hexane (0.72 ml, 1.8 mmol) was added dropwise via syringe. After stirring for 30 minutes at -5°C , the reaction mixture was cooled down to -60°C and **8i** (0.1 g, 0.23 mmol) in anhydrous diethyl ether (3 ml) were added dropwise. The solution was stirred at this temperature for 30 minutes. The reaction mixture was cooled down to -75°C and hexachloroethane (0.27 g, 1.15 mmol) in anhydrous diethyl ether was added quickly to the solution. The reaction mixture was stirred for 30 minutes at -75°C and then quenched with ammonium chloride solution. The aqueous phase was extracted three times with chloroform. The combined organic phases were dried over MgSO_4 and the solvent was removed under reduced pressure. Column chromatography (EtOAc:hexane containing 1% NEt_3 , gradient starting from 0% EtOAc, product eluted at 2.5% EtOAc) gave the product as colorless oil in 13% yield (14 mg).

$^1\text{H-NMR}$ (300 MHz, d_6 -DMSO): δ 1.81-1.90 (m, 2H, $-\text{CH}_2-\text{CH}_2-\text{NBn}_2$), 2.04-2.15 (m, 2H, H-6), 2.39-2.44 (t, $^3J = 6.8$, 2H, $-\text{CH}_2-\text{NBn}_2$), 2.76-2.81 (t, $^3J = 7.4$, 2H, H-7), 2.93-2.98 (m, 4H, H-5, $-\text{CH}_2-\text{CH}_2-\text{CH}_2-\text{NBn}_2$), 3.51 (s, 4H, Bn-H), 7.18-7.32 (m, 10H, Bn-H).

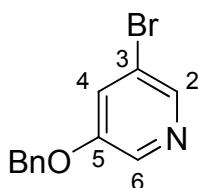
$^{13}\text{C-NMR}$ (75.5 MHz, d_6 -DMSO): δ 22.51 (C-6), 24.59 ($-\text{CH}_2-\text{CH}_2-\text{NBn}_2$), 31.84, 33.28, 35.43 (C-5, C-7, $-\text{CH}_2-\text{CH}_2-\text{CH}_2-\text{NBn}_2$), 51.58 ($-\text{CH}_2-\text{NBn}_2$), 57.42 (Bn-C), 117.01 (C-4), 126.67 (Bn-C), 128.05 (Bn-C), 128.41 (Bn-C), 137.05, 139.33 (C-7, Bn-C), 143.97 (C-1), 157.43 (C-4'), 157.70 (C-3).

HRMS: cal. 469.1041, 471.1020 exp. 469.1022, 471.1004 ($[\text{M}+\text{H}]^+$)

ESI-MS: cal. 469.1, exp. 469.1 ($[\text{M}+\text{H}]^+$)

R_f (TLC) 0.8 (EtOAc:hexane = 1:6 with 1% Net_3)

t_R (HPLC) 6.27 min

5.3.17 3-Bromo-5-benzyloxy pyridine (9c)

IA 250 ml one-necked flask was charged with 3-bromo-5-hydroxypyridine (2.5 g, 10.4 mmol), benzyl bromide (3.6 g, 21 mmol) and potassium carbonate (3.9 g, 28 mmol). After addition of DMF (150 ml), the reaction mixture was heated to 60°C and stirred over night. After the mixture was cooled down to room temperature the solvent was removed *in vacuo* and the residue was partitioned between 1N HCl and ethyl acetate. The aqueous phase was extracted twice with ethyl acetate. The organic phases were combined, washed with brine and dried over MgSO₄. The solvent was removed under reduced pressure. Column chromatography (EtOAc/hexane, 1:1) gave the product as brown solid in 85% yield (2.3 g).

¹H-NMR (300 MHz, d₆-DMSO): δ 5.21 (s, 2H, Bn-H), 7.35-7.48 (m, 5H, Bn-H), 7.79-7.81 (m, 1H, H-4), 8.29-8.30 (m, 1H, H-2), 8.36-8.37 (m, 1H, 6-H).

¹³C-NMR (75,5 MHz, d₆-DMSO): δ 70.01 (Bn-C), 119.97 (C-3), 124.08 (C-4) 127.96 (Bn-C), 128.18 (Bn-C), 128.51 (Bn-C), 135.96 (Bn-C), 137.16 (C-6), 142.25 (C-2), 155.08 (C-5).

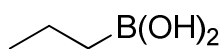
HRMS: cal. 264.0019, exp. 264.0008 ([M+H]⁺)

ESI-MS: cal. 264.0019, exp. 264.0 ([M+H]⁺)

IR: ν [cm⁻¹] = 2933, 2872, 1571, 1549, 694.

m.p. 61.8°C

R_f (TLC) 0.59 (EtOAc:hexane 1:2) **t_R (HPLC)** 7.96 min

5.3.18 1-Propylboronic acid

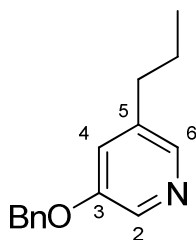
A 500 ml three-necked flask equipped with magnetic stir bar, nitrogen inlet, dropping funnel and bubbler was charged with trimethylborate (10.7 ml, 96 mmol) in diethyl ether (200 ml) under nitrogen atmosphere. The solution was cooled down to -75°C . and 2M propylmagnesium chloride (48.5 ml, 97 mmol) in diethyl ether was added via dropping funnel over 45 minutes. The white, clouded reaction mixture was stirred for 2 more hours at -75°C . The reaction mixture was warmed up to room temperature and hydrolyzed with 10% hydrochloric acid until the white solid was dissolved. The biphasic solution was stirred for 15 minutes. The aqueous phase was extracted twice with diethyl ether. The combined organic phases were dried over MgSO_4 , and the reaction mixture was concentrated under reduced pressure. The product was recrystallized from diethyl ether in 91% yield (7.7 g) as colorless solid. Analytical NMR data correspond to literature data.

$^1\text{H-NMR}$ (300 MHz, $\text{d}_6\text{-DMSO}$): δ 0.54-0.59 (t, $^3J = 7.7$, 2H, $\text{B(OH)}_2\text{-CH}_2\text{-CH}_2\text{-CH}_3$), 0.82-0.87 (t, $^3J = 7.3$, 3H, $\text{B(OH)}_2\text{-CH}_2\text{-CH}_2\text{-CH}_3$), 1.27-1.39 (m, 2H, $\text{B(OH)}_2\text{-CH}_2\text{-CH}_2\text{-CH}_3$), 7.35 (bs, $\text{B(OH)}_2\text{-CH}_2\text{-CH}_2\text{-CH}_3$).

$^{13}\text{C-NMR}$ (75,5 MHz, $\text{d}_6\text{-DMSO}$): δ 17.11 ($(\text{OH})_2\text{B-CH}_2\text{-CH}_2\text{-CH}_3$), 17.55 ($(\text{OH})_2\text{B-CH}_2\text{-CH}_2\text{-CH}_3$).

m.p. 87.5 $^{\circ}\text{C}$

5.3.19 3-Benzyloxy-5-propylpyridine (9d)



A 250 ml three-necked flask equipped with magnetic stir bar, nitrogen inlet, septum and condenser with bubbler was charged with **9c** (3.0 g, 11.4 mmol), propylboronic acid (2.0 g, 22.8 mmol), potassium carbonate (3.15 g, 22.8 mmol), palladium(II) acetate (0.13 g, 0.57 mmol) and triphenylphosphine (0.6 g, 2.3 mmol). Xylene (108 ml) and H₂O (8 ml) were added under nitrogen atmosphere and the reaction mixture was refluxed at 130°C for 20 hours. After the mixture was cooled down to room temperature, the solvent was removed *in vacuo* and the residue was partitioned in 14% ammonium hydroxide solution/ethyl acetate. The aqueous phase was extracted twice with ethyl acetate; the combined organic phases were washed with brine, and then dried over MgSO₄. The solvent was removed under reduced pressure. Column chromatography of the crude product (EtOAc/hexane, 4:1) gave the product as colorless oil in 83% yield (2.2 g).

¹H-NMR (300 MHz, CDCl₃): δ 0.92-0.96 (t, ³J = 7.3, 3H, -CH₂-CH₂-CH₃), 1.58-1.70 (m, 2H, -CH₂-CH₂-CH₃), 2.55-2.60 (t, ³J = 7.6, 2H, -CH₂-CH₂-CH₃), 5.10 (s, 2H, Bn-H), 7.10 (s, 1H, H-4), 7.34-7.44 (m, 5H, Bn-H), 8.08 (s, 1H, H-6), 8.22 (s, 1H, H-2).

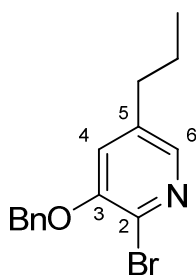
¹³C-NMR (75,5 MHz, CDCl₃): δ 13.86 (-CH₂-CH₂-CH₃), 24.32 (-CH₂-CH₂-CH₃), 35.08 (-CH₂-CH₂-CH₃), 70.58 (Bn-C), 122.38 (C-4), 127.76 (Bn-C), 128.48 (Bn-C), 128.91 (Bn-C), 135.26 (C-2), 136.46 (Bn-C), 138.90 (C-5), 142.70 (C-6), 155.09 (C-3).

HRMS: cal. 228.1383, exp. 228.1377 ([M+H]⁺)

ESI-MS: cal. 228.1383, exp. 228.10 ([M+H]⁺)

IR: ν [cm⁻¹] = 2958, 2931, 2870, 1586, 1432, 735, 695.

R_f (TLC) 0.67 (EtOAc:hexane 4:1) **t_R (HPLC)** 5.46 min

5.3.20 2-Bromo-3-benzyloxy-5-propylpyridine (**9f**)

Into an oven-dried 100 ml three-necked flask equipped with magnetic stir bar, nitrogen inlet, rubber septum and bubbler was placed 2-dimethylaminoethanol (1.8 ml, 17.6 mmol) in anhydrous hexane (30 ml) under nitrogen atmosphere. The solution was cooled down to -5°C and 2.5 M BuLi in hexane (14.1 ml, 35.2 mmol) were added dropwise via syringe. After stirring for 30 minutes at -5°C , the reaction mixture was warmed up to -2°C and **9d** (1 g, 4.4 mmol) in anhydrous hexane (5 ml) was added dropwise. The solution was stirred at this temperature for 30 minutes. The reaction mixture was cooled down to -75°C , and the *n* tetrabromomethane (8.6 g, 26.4 mmol) in hexane were added quickly. The reaction mixture was warmed up to room temperature and quenched with ammonium chloride solution. The aqueous phase was extracted three times with dichloromethane. The combined organic phases were dried over MgSO_4 ; the solvent was removed under reduced pressure. Column chromatography (EtOAc:hexane containing 2% NEt_3 , gradient starting from 0% EtOAc, product eluted at 20% EtOAc) gave the product as orange oil in 9% yield (121 mg).

For analytical purposes, the product was further purified by preparative HPLC (ACN, H_2O) on a preparative column with the following gradient: 50% ACN in H_2O to 99% ACN in H_2O in 45 minutes. **9f** eluted with $t_{\text{R}} = 35.9$ minutes and was obtained after lyophilization as white solid.

$^1\text{H-NMR}$ (300 MHz, DMSO): δ 0.84-0.89 (t, $^3J = 7.3$, 3H, $-\text{CH}_2-\text{CH}_2-\text{CH}_3$), 1.53-1.65 (m, 2H, $-\text{CH}_2-\text{CH}_2-\text{CH}_3$), 2.53-2.57 (t, $^3J = 7.4$, 2H, $-\text{CH}_2-\text{CH}_2-\text{CH}_3$), 5.25 (s, 2H, Bn-H), 7.32-7.49 (m, 6H, Bn-H and H-4), 7.82-7.83 (d, $^4J = 1.6$, 1H, H-6).

$^{13}\text{C-NMR}$ (75,5 MHz, DMSO): δ 13.36 ($-\text{CH}_2-\text{CH}_2-\text{CH}_3$), 23.53 ($-\text{CH}_2-\text{CH}_2-\text{CH}_3$), 33.38 ($-\text{CH}_2-\text{CH}_2-\text{CH}_3$), 70.11 (Bn-C), 121.67 (C-4), 127.51 (Bn-C), 128.02 (Bn-C), 128.48 (Bn-C), 129.10 (C-2), 136.05 (Bn-C), 138.73 (C-5), 141.08 (C-6), 151.02 (C-3).

5 Experimental

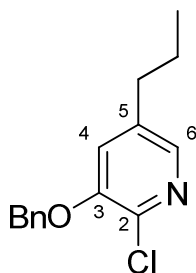
HRMS: cal. 306.0488, exp. 306.0478 ($[M+H]^+$)

ESI-MS: cal. 306.0488, exp. 306.0 ($[M+H]^+$)

IR: ν [cm^{-1}] = 2954, 2930, 2871, 1577, 1418, 730.

m.p. 61.3°C

R_f (TLC) 0.42 (EtOAc:hexane 1:10) **t_R (HPLC)** 9.24 min

5.3.21 2-Chloro-3-benzoyloxy-5-propylpyridine (9g)

Into an oven-dried 100 ml three-necked flask equipped with magnetic stir bar, nitrogen inlet, rubber septum and bubbler was placed 2-dimethylaminoethanol (0.9 ml, 8.8 mmol) in 20 ml of anhydrous hexane under nitrogen atmosphere. The solution was cooled down to -5°C and then 2.5 M BuLi in hexane (7.0 ml, 17.6 mmol) was added dropwise via syringe. After stirring for 30 minutes at -5°C , the reaction mixture was warmed up to -2°C and **9d** (0.5 g, 2.2 mmol) in 3 ml anhydrous hexane were added dropwise. The solution was stirred at this temperature for 30 minutes. The reaction mixture was cooled down to -75°C and hexachloroethane (3.1 g, 13.2 mmol) in hexane was added quickly. The reaction mixture was warmed up to room temperature and stirred for 1 hour. The reaction was quenched with ammonium chloride solution. The aqueous phase was extracted three times with ethyl acetate. The combined organic phases were dried over MgSO_4 , the solvent was removed under reduced pressure. Column chromatography (EtOAc:hexane gradient starting from 0% EtOAc, product eluted at 20% EtOAc) gave the product as yellow solid in 10% yield (58 mg).

For analytical purposes, the product was further purified by preparative HPLC (ACN, H_2O) on a preparative column with the following gradient: 60% ACN in H_2O to 99% ACN in H_2O in 45 minutes. **9g** eluted with $t_{\text{R}} = 27.2$ minutes and was obtained after lyophilization as white solid.

$^1\text{H-NMR}$ (300 MHz, DMSO); δ 0.84-0.89 (t, $^3J = 7.3$, 3H, $-\text{CH}_2-\text{CH}_2-\text{CH}_3$), 1.53-1.65 (m, 2H, $-\text{CH}_2-\text{CH}_2-\text{CH}_3$), 2.53-2.58 (t, $^3J = 7.5$, 2H, $-\text{CH}_2-\text{CH}_2-\text{CH}_3$), 5.25 (s, 2H, Bn-H), 7.34-7.44 (m, 5H, Bn-H), 7.54 (d, $^4J = 1.5$, 1H, H-4), 7.82-7.83 (d, $^4J = 1.5$, 1H, H-6).

5 Experimental

¹³C-NMR (75,5 MHz, DMSO): δ 13.35 (-CH₂-CH₂-CH₃), 23.57 (-CH₂-CH₂-CH₃), 33.42 (-CH₂-CH₂-CH₃), 70.07 (Bn-C), 122.10 (C-4), 127.64 (Bn-C), 128.07 (Bn-C), 128.49 (Bn-C), 136.02 (Bn-C), 136.88 (C-2), 138.47 (C-5), 140.12 (C-6), 149.76 (C-3).

HRMS: cal. 262.0993, exp. 262.0994 ([M+H]⁺)

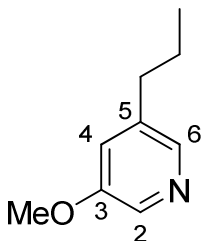
ESI-MS: cal. 262.0993, exp. 262.1 ([M+H]⁺)

IR: ν [cm⁻¹] = 2954, 2938, 2870, 1580, 1420, 724.

m.p. 43.2°C

R_f (TLC) 0.43 (EtOAc:hexane 1:10) **t_R (HPLC)** 9.01 min

5.3.22 3-Methoxy-5-propylpyridine (9e)



A 250 ml three-necked flask equipped with magnetic stir bar, nitrogen inlet, septum and condenser with bubbler was charged with 3-bromo-5-methoxypyridine (5 g, 21.3 mmol), propylboronic acid (4.8 g, 42.6 mmol), potassium carbonate (11.02, 63.9 mmol), palladium(II) acetate (0.12 g, 0.53 mmol) and triphenylphosphine (0.56 g, 2.1 mmol) and then evacuated and purged with nitrogen for three times. Xylene (200 ml) and H₂O (16 ml) were added under nitrogen atmosphere and the reaction mixture was refluxed at 130°C for 40 hours. After the mixture was cooled down to room temperature, the solvent was removed *in vacuo* and the residue was partitioned between 10% hydrochloric acid/ethyl acetate. The aqueous phase was extracted twice with ethyl acetate; the combined organic phases were washed with brine, and then dried over MgSO₄. The solvent was removed under reduced pressure. Column chromatography of the crude product (EtOAc/hexane, 1:10) gave the product as colorless oil in 64% yield (2.1 g).

¹H-NMR (300 MHz, d₆-DMSO): δ 0.87-0.92 (t, ³J = 7.3, 3H, -CH₂-CH₂-CH₃), 1.54-1.66 (m, 2H, -CH₂-CH₂-CH₃), 2.52-2.57 (t, ³J = 7.6, 2H, -CH₂-CH₂-CH₃), 3.81 (s, 3H, -CH₃), 7.20-7.21 (m, 1H, H-4), 8.01-8.02 (m, 1H, H-6), 8.10-8.11 (m, 1H, H-2).

¹³C-NMR (75,5 MHz, d₆-DMSO): δ 13.49 (-CH₂-CH₂-CH₃), 23.71 (-CH₂-CH₂-CH₃), 33.98 (-CH₂-CH₂-CH₃), 55.33 (-CH₃), 120.22 (C-4), 134.76 (C-2), 138.20 (C-5), 141.72 (C-6), 155.26 (C-3).

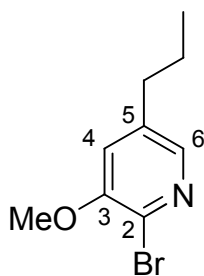
HRMS: cal. 152.1070, exp. 152.1068 ([M+H]⁺)

ESI-MS: cal. 152.1070, exp. 152.1 ([M+H]⁺)

IR: ν [cm⁻¹] = 2959, 2933, 2871, 1587, 1460, 1425, 1268, 859.

R_f (TLC) 0.31 (EtOAc:hexane 2:1) **t_R (HPLC)** 2.59 min

5.3.23 2-Bromo-3-methoxy-5-propylpyridine (9h)



Into an oven-dried 100 ml three-necked flask equipped with magnetic stir bar, nitrogen inlet, rubber septum and bubbler was placed 2-dimethylaminoethanol (0.8 ml, 7.92 mmol) in anhydrous hexane (5 ml) under nitrogen atmosphere. The solution was cooled down to -5°C and then 2.5 M BuLi in hexane (6.3 ml, 15.8 mmol) was added dropwise via syringe. After stirring for 30 minutes at -5°C , the reaction mixture was warmed up to -2°C and **9e** (0.3 g, 1.98 mmol) in anhydrous hexane (1 ml) was added dropwise. The solution was stirred at this temperature for 30 minutes. The reaction mixture was cooled down to -75°C and tetrabromomethane (3.9 g, 11.9 mmol) in hexane was added in one portion. The reaction mixture was warmed up to room temperature and stirred for 1 hour. The reaction was quenched with ammonium chloride solution. The aqueous phase was extracted three times with ethyl acetate. The combined organic phases were dried over MgSO_4 , the solvent was removed under reduced pressure. Column chromatography (EtOAc:hexane gradient starting from 0% EtOAc, product eluted at 10% EtOAc) gave the product as yellow oil in 41 % yield (187 mg).

$^1\text{H-NMR}$ (300 MHz, d_6 -DMSO): δ 0.87-0.92 (t, $^3J = 7.3$, 3H, $-\text{CH}_2\text{-CH}_2\text{-CH}_3$), 1.55-1.68 (m, 2H, $-\text{CH}_2\text{-CH}_2\text{-CH}_3$), 2.53-2.58 (t, $^3J = 7.6$, 2H, $-\text{CH}_2\text{-CH}_2\text{-CH}_3$), 3.88 (s, 3H, $-\text{CH}_3$), 7.37 (d, $^4J = 1.7$, 1H, H-4), 7.81 (d, $^4J = 1.7$, 1H, H-6).

$^{13}\text{C-NMR}$ (75,5 MHz, d_6 -DMSO): δ 13.44 ($-\text{CH}_2\text{-CH}_2\text{-CH}_3$), 23.61 ($-\text{CH}_2\text{-CH}_2\text{-CH}_3$), 33.44 ($-\text{CH}_2\text{-CH}_2\text{-CH}_3$), 56.26 ($-\text{CH}_3$), 120.15 (C-4), 128.55 (C-2), 138.90 (C-5), 140.68 (C-6), 152.04 (C-3).

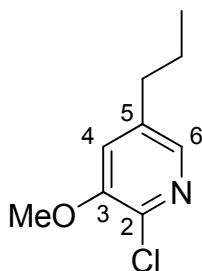
HRMS: cal. 230.0175, exp. 230.0175 ($[\text{M}+\text{H}]^+$)

ESI-MS: cal. 230.0175, exp. 230.1 ($[\text{M}+\text{H}]^+$)

IR: ν [cm^{-1}] = 2937, 2830, 1633, 1403, 1024, 669.

R_f (TLC) 0.30 (EtOAc:hexane 1:10) **t_R (HPLC)** 7.28 min

5.3.24 2-Chloro-3-methoxy-5-propylpyridine (9i)



Into an oven-dried 100 ml three-necked flask equipped with magnetic stir bar, nitrogen inlet, rubber septum and bubbler was placed 2-dimethylaminoethanol (0.4 ml, 3.96 mmol) in anhydrous hexane (5 ml) under nitrogen atmosphere. The solution was cooled down to -5°C and then 2.5 M BuLi in hexane (3.20 ml, 7.94 mmol) was added dropwise via syringe. After stirring for 30 minutes at -5°C , the reaction mixture was warmed up to -2°C and **9e** (0.15 g, 0.99 mmol) in anhydrous hexane (1 ml) were added dropwise. The solution was stirred at this temperature for 30 minutes. The reaction mixture was cooled down to -75°C and hexachloroethane (1.4 g, 5.96 mmol) in hexane was added quickly. The reaction mixture was warmed up to room temperature and stirred for 1 hour. The reaction was quenched with ammonium chloride solution. The aqueous phase was extracted three times with ethyl acetate. The combined organic phases were dried over MgSO_4 ; the solvent was removed under reduced pressure. Column chromatography (EtOAc:hexane gradient starting from 0% EtOAc, product eluted at 10% EtOAc) gave the product as colorless oil in 57% yield (105 mg).

$^1\text{H-NMR}$ (300 MHz, d_6 -DMSO): δ 0.87-0.92 (t, $^3J = 7.3$, 3H, $-\text{CH}_2-\text{CH}_2-\text{CH}_3$), 1.55-1.65 (m, 2H, $-\text{CH}_2-\text{CH}_2-\text{CH}_3$), 2.54-2.60 (t, $^3J = 7.6$, 2H, $-\text{CH}_2-\text{CH}_2-\text{CH}_3$), 3.88 (s, 3H, $-\text{CH}_3$), 7.43-7.44 (d, $^4J = 1.5$, 1H, H-4), 7.81 (d, $^4J = 1.5$, 1H, H-6).

$^{13}\text{C-NMR}$ (75,5 MHz, d_6 -DMSO): δ 13.44 ($-\text{CH}_2-\text{CH}_2-\text{CH}_3$), 23.65 ($-\text{CH}_2-\text{CH}_2-\text{CH}_3$), 33.49 ($-\text{CH}_2-\text{CH}_2-\text{CH}_3$), 56.13 ($-\text{CH}_3$), 120.57 (C-4), 136.41 (C-2), 138.63 (C-5), 139.71 (C-6), 150.77 (C-3).

HRMS: cal. 186.0680, exp. 186.0671 ($[\text{M}+\text{H}]^+$)

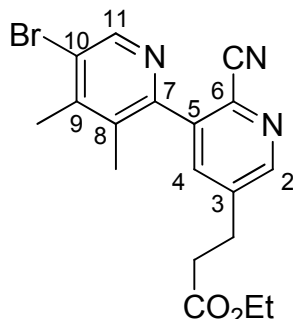
ESI-MS: cal. 186.0680, exp. 186.0 ($[\text{M}+\text{H}]^+$)

IR: ν [cm^{-1}] = 2933, 2870, 1633, 1403, 1076, 684.

R_f (TLC) 0.31 (EtOAc:hexane 1:10)

t_R (HPLC) 7.10 min

5.3.25 Ethyl 3-(5-bromo-2'-cyano-3,4-dimethyl-2,3'-bipyridin-5'-yl)propanoate (12a)



An oven-dried 250 ml three-necked flask equipped with magnetic stir bar, condenser with bubbler, nitrogen inlet and dropping funnel was charged with **6f** (4.1 g, 12.7 mmol), **7d** (2.0 g, 7.5 mmol), palladium (II) acetate (0.1 g, 0.45 mmol) and triphenylphosphine (0.5 g, 1.8 mmol). After evacuation and subsequent purging with N₂ for three times, dioxane (120 ml) and 1M potassium phosphate (5.7 ml) in H₂O were added by dropping funnel to the solution. The reaction mixture was heated to 80°C and stirred for 4 hours at this temperature. After cooling down to room temperature, the reaction mixture was diluted with brine and extracted three times with ethyl acetate. The combined organic phases were dried over MgSO₄ and the solvent was removed under reduced pressure. Column chromatography (EtOAc/hexane 1:4 containing 1% NEt₃) gave the product in 56% yield as yellow viscous liquid (1.6 g).

¹H-NMR (300 MHz, d₆-DMSO): δ 1.11-1.16 (t, ³J = 7.1, 3H, -CH₂-CH₃), 2.19 (s, 3H, -CH₃), 2.48 (s, 3H, -CH₃), 2.74-2.79 (t, ³J = 7.4, 2H, -CH₂-CO₂Et), 3.00-3.05 (t, ³J = 7.4, 2H, -CH₂-CH₂-CO₂Et), 4.00-4.07 (quartet, ³J = 7.1, 2H, -CH₂-CH₃), 7.98-7.99 (d, ⁴J = 1.9, 1H, H-4), 8.69 (s, 1H, H-11), 8.74-8.74 (d, ⁴J = 1.9, 1H, H-2)

¹³C-NMR (75,5 MHz, d₆-DMSO): δ 14.02 (-CH₂-CH₃), 16.81 (-CH₃), 19.35 (-CH₃), 27.25 (-CH₂-CH₂-CO₂Et), 33.56 (-CH₂-CO₂Et), 60.00 (-CH₂-CH₃), 116.60 (-CN), 123.79 (C-10), 129.61 (C-6) 133.18 (C-8), 137.91 (C-4), 139.76 (C-5), 140.56 (C-3), 146.71 (C-9), 148.09 (C-11), 150.92 (C-2), 151.65 (C-7), 171.74 (-CO₂Et).

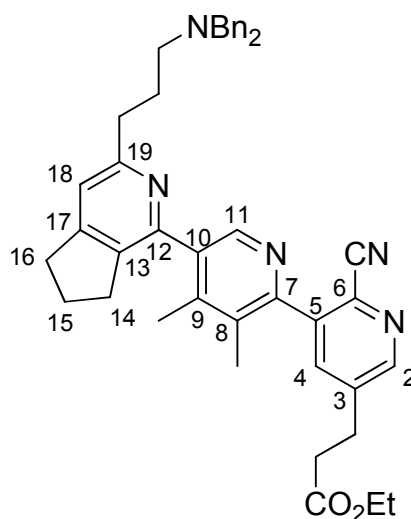
HRMS: : cal. 388.0655, 390.0637; exp. 388.0638, 390,0620 ([M+H]⁺)

ESI-MS: cal. 388.0655; exp. 388.2 ([M+H]⁺)

IR: ν [cm⁻¹] = 2984, 2236, 1716, 1369 1156, 946, 778.

R_f (TLC) 0.24 (EtOAc:hexane 1:2) t_R (HPLC)

9.07 min

5.3.26 Ethyl 3-(6-cyano-5-(5-(3-(3-(dibenzylamino)propyl)-6,7-dihydro-5H-cyclopenta[c]pyridin-1-yl)-3,4-dimethylpyridin-2-yl)pyridine-3-yl)propanoate (22a)

An oven-dried 5 ml microwave-flask equipped with magnetic stir bar was charged with **12a** (0.1 g, 0.26 mmol), potassium acetate (0.08 g, 0.39 mmol), bis(pinacolato)diboron (0.08 g, 0.31 mmol), tris(dibenzylideneacetone) dipalladium(0) (0.006 g, 0.006 mmol) and XPhos (0.025 g, 0.05 mmol) and was sealed with a microwave septum. The flask was evacuated and flushed with nitrogen. After addition of dioxane (2 ml), the reaction mixture was heated in the microwave to 130°C and stirred at this temperature for 15 minutes. After cooling down to room temperature, **8e** (0.08 g, 0.23 mmol) in dioxane (0.8 ml) and potassium phosphate (0.08 g, 0.39 mmol) in H₂O (0.3 ml) were added to reaction mixture via syringe. The reaction mixture was heated in the microwave to 130°C and stirred at this temperature for 30 minutes. After cooling down to room temperature, the reaction mixture was diluted with brine and extracted three times with ethyl acetate. The combined organic phases were dried over MgSO₄ and the solvent was removed under reduced pressure. Column chromatography (EtOAc/hexane 1:1 containing 1% NEt₃) gave the product in 40% yield (69 mg) as orange oil.

5 Experimental

The product was further purified by preparative HPLC (ACN/0.1% TFA, H₂O/0.1% TFA) with the following gradient: 30% ACN to 99% ACN in H₂O in 50 minutes. **22a** eluted at $t_R = 25.6$ minutes and was obtained after lyophilization as violet ammonium trifluoroacetate salt.

¹H-NMR (300 MHz, MeOD): 1.16-1.21 (t, $^3J = 7.1$, 3H, -CH₂-CH₃), 2.10-2.30 (m, 10H, -CH₂-CH₂-NBn₂, -CH₃, H-15), 2.74-2.82 (m, 4H, -CH₂-CO₂Et, H-14), 2.87-2.92 (t, $^3J = 7.3$, 2H, H-16), 3.09-3.17 (m, 6H, -CH₂-CH₂-CH₂-NBn₂, -CH₂-NBn₂, -CH₂-CH₂-CO₂Et, H-14), 4.05-4.12 (quartet, $^3J = 7.1$, 2H, -CH₂-CH₃), 4.36 (s, 4H, Bn-H), 7.44 (m, 10H, Bn-H), 7.50 (s, 1H, H-18), 7.95 (s, 1H, H-4), 8.37 (s, 1H, H-11), 8.71 (s, 1H, H-2).

¹³C-NMR (75,5 MHz, MeOD): δ 14.66 (-CH₂-CH₃), 16.52 (-CH₃), 17.35 (-CH₃), 24.64 (C-15), 26.04 (-CH₂-CH₂-NBn₂), 29.01 (-CH₂-CH₂-CO₂Et), 31.63 (C-14), 33.42 (C-16), 34.70 (-CH₂-CH₂-CH₂-NBn₂), 35.42 (-CH₂-CO₂Et), 52.32 (-CH₂-NBn₂), 58.56 (Bn-C), 61.93 (-CH₂-CH₃), 117.49 (-CN), 122.10 (C-18), 130.70 (Bn-C), 130.76 (Bn-C), 131.52 (Bn-C), 131.90 (C-6), 132.44 (Bn-C), 134.18 (C-8), 136.28 (C-10 or C-13), 139.62 (C-4), 141.61, 141.74 (C-5, C-10 or C-13), 142.74 (C-3), 147.53 (C-11), 148.62 (C-9), 149.86 (C-12), 152.60 (C-2), 155.08 (C-7), 157.84 (C-17), 163.16 (C-19), 173.88 (-CO₂Et).

HRMS: cal. 664.3646, exp. 664.3643 ([M+H]⁺)

ESI-MS: cal. 664.3646, exp. 664.3 ([M+H]⁺)

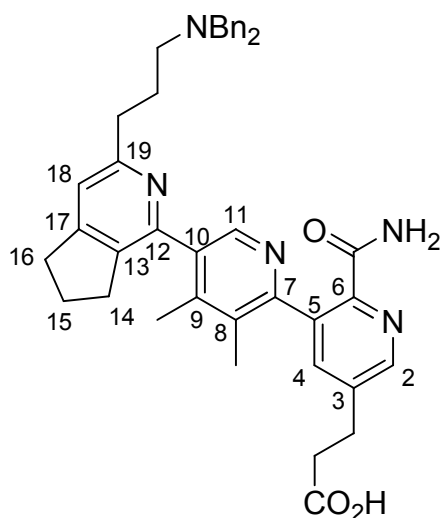
IR: ν [cm⁻¹] = 2954, 2233, 1729, 1671, 1195, 1127, 700.

m.p. 44.1°C

R_f (TLC) 0.38 (EtOAc:hexane 1:1 with 1% of NEt₃)

t_R (HPLC) 6.04 min

5.3.27 3-(2'-carbamoyl-5-(3-(3-(dibenzylaminopropyl)-6,7-dihydro-5H-cyclopenta[c]pyridin-1-yl)-3,4-dimethyl-2,3'-bipyridin-5'yl)propanoic acid (25a)



A 50 ml one-necked flask equipped with magnetic stir bar and condenser was charged with **22a** (25 mg, 0.04 mmol) and of sodium hydroxide (15 mg, 0.4 mmol). After addition of ethanol (0.7 ml) and H₂O (0.3 ml), the reaction mixture was refluxed over night. After cooling down to room temperature, the reaction mixture was concentrated under reduced pressure. The product was purified by semipreparative HPLC (ACN/0.1% TFA, H₂O/0.1% TFA) with the following gradient: 20% ACN to 99% ACN in H₂O in 60 minutes. **25a** eluted at $t_R = 14.9$ minutes and was obtained after lyophilisation as white ammonium trifluoroacetate salt in 73% yield (19 mg).

¹H-NMR (300 MHz, MeOD): 2.22-2.35 (m, 10H, -CH₂-CH₂-NBn₂, H-15, -CH₃), 2.76-2.81 (t, ³J = 7.2, 2H, -CH₂-CO₂H), 2.84-2.97 (m, 4H, H-16, -CH₂-NBn₂), 3.13-3.21 (m, 6H, H-14, -CH₂-CH₂-NBn₂, -CH₂-CH₂-CO₂H), 4.41 (s, 4H, Bn-H), 7.47-7.55 (m, 11H, H-18, Bn-H), 7.92 (s, 1H, H-4), 8.49 (s, 1H, H-11), 8.78 (s, 1H, H-2).

5 Experimental

¹³C-NMR (75,5 MHz, MeOD): δ 16.50 (-CH₃), 17.81 (-CH₃), 18.24 (C-15), 26.07 (-CH₂-CH₂-NBn₂), 28.85 (-CH₂-CH₂-CO₂H), 31.60, 33.69 (C-16, -CH₂-CH₂-CH₂-NBn₂), 34.67 (C-14), 35.36 (-CH₂-CO₂H), 52.38 (-CH₂-NBn₂), 58.57 (Bn-C), 122.23 (H-18), 130.68 (Bn-C), 130.74 (Bn-C), 131.49 (Bn-C), 132.46 (Bn-C), 134.31 (C-8), 135.12, (C-13), 140.92 (C-4), 141.15, 141.67, 141.85 (C-5, C-9, C-10), 142.60 (C-3), 143.90 (C-11), 145.58 (C-6), 151.10 (C-2), 151.91 (C-12), 155.55 (C-7), 157.98 (C-17), 162.39 (C-19), 167.20 (-C(O)NH₂), 175.72 (-CH₂-CH₂-CO₂H).

HRMS: cal. 654.444, exp. 654.3390 ([M+H]⁺)

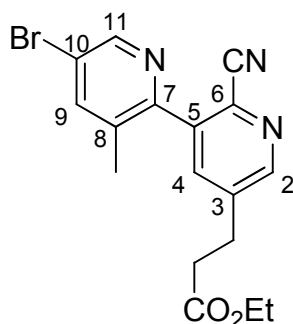
ESI-MS: cal. 655.3444, exp. 654.2 ([M+H]⁺)

IR: ν [cm⁻¹] = 2941, 1715, 1669, 1196, 1127, 701, 696.

m.p. 68.3°C

t_R (HPLC)

4.22 min

5.3.28 Ethyl 3-(5-bromo-2'-cyano-3-methyl-2,3'-bipyridin-5'-yl)propanoate (12b)

An oven-dried 250 ml three-necked flask equipped with magnetic stir bar, condenser with bubbler, nitrogen inlet and dropping funnel was charged with 2,5-dibromo-3-dimethylpyridine (2.2 g, 8.8 mmol), potassium phosphate (5.6 g, 26 mmol), palladium(II) acetate (0.46 g, 0.43 mmol) and triphenylphosphine (0.22 g, 1.7 mmol). After evacuation and subsequent purging with N₂ for three times, dioxane (45 ml) and H₂O (5 ml) were added via dropping funnel and the reaction mixture was stirred for 10 minutes at room temperature. After heating the mixture to 80°C, crude **6f** (6.6 g, about 8.8 mmol) in dioxane (15 ml) was added via dropping funnel over 90 minutes. The reaction mixture was stirred for 150 minutes at 80°C, cooled down to room temperature and stirred over night. The reaction mixture was diluted with brine and extracted three times with ethyl acetate. The combined organic phases were dried over MgSO₄ and the solvent was removed under reduced pressure. Column chromatography (EtOAc/hexane 1:4) gave the product in 74% yield (2.4 g) as yellow solid.

¹H-NMR (300 MHz, CDCl₃): δ 1.21-1.25 (t, ³J = 7.17, 3H, -CH₂-CH₃), 2.28 (s, 3H, -CH₃), 2.68-2.73 (t, ³J = 7.3, 2H, -CH₂-CO₂Et), 3.06-3.11 (t, ³J = 7.3, 2H, -CH₂-CH₂-CO₂Et), 4.09-4.16 (quartet, ³J = 7.14, 2H, -CH₂-CH₃), 7.70 (d, ⁴J = 1.9, 1H, H-4), 7.85 (d, ⁴J = 1.7, 1H, H-9), 8.64 (m, 2H, H-2, H-11).

¹³C-NMR (75,5 MHz, CDCl₃): δ 14.37 (-CH₂-CH₃), 19.14 (-CH₃), 28.19 (-CH₂-CH₂-CO₂Et), 34.75 (-CH₂-CO₂Et), 61.15 (-CH₂-CH₃), 116.47 (-CN), 121.53 (C-10), 131.31 (C-6), 134.11 (C-8), 137.80 (C-4), 139.93 (C-5), 140.21 (C-3), 141.33 (C-9), 148.85 (C-11), 151.02 (C-2), 151.69 (C-7), 171.89 (-CO₂Et).

HRMS: cal. 374.0499; exp. 374.0496 ([M+H]⁺)

ESI-MS: cal. 374.0499; exp. 374.1 ([M+H]⁺)

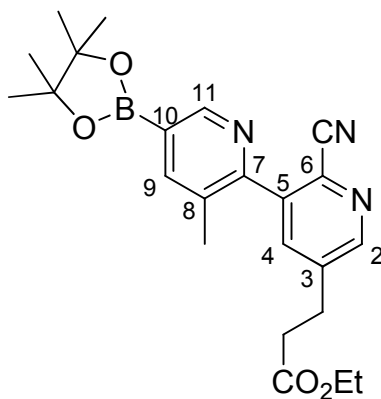
5 Experimental

IR: ν [cm^{-1}] = 2978, 2229, 1714, 1367, 1107, 946.

m.p. 45.3°C

R_f (TLC) 0.27 (EtOAc:hexane 1:2)

t_R (HPLC) 7.52 min

5.3.29 Ethyl 3-(2'-cyano-3-methyl-5-(4,4,5,5-tetramethyl-1,3,2-dioxaborolan-2-yl)-2,3'-bipyridin-5-yl)propanoate (21b)

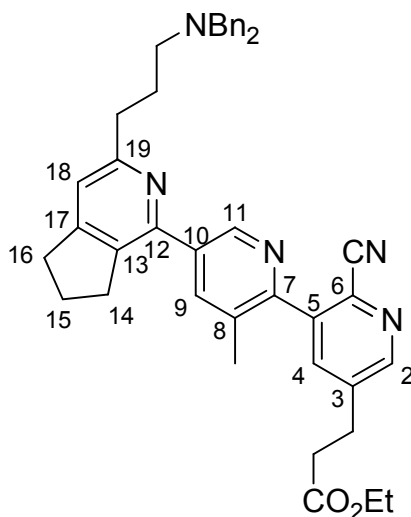
An oven-dried 250 ml three-necked flask equipped with magnetic stir bar, condenser with bubbler, nitrogen inlet and rubber septum was charged with **12b** (2.5 g, 6.7 mmol), potassium acetate (1.96 g, 20.1 mmol), bis(pinacolato)diboron (2.0 g, 8.0 mmol), palladium(II)acetate (0.075 g, 0.34 mmol) and triphenylphosphine (0.35 g, 1.3 mmol) under nitrogen atmosphere. After addition of dioxane (120 ml) the reaction mixture was heated to 102°C and refluxed for 1 hour. The reaction mixture was cooled down to room temperature and diluted with brine. The aqueous phase was extracted three times with ethyl acetate. The combined organic phases were dried over MgSO₄ and the solvent was removed under reduced pressure. Column chromatography (EtOAc/hexane 1:2) gave the product in 19% yield (536 mg) as yellow solid. The product hydrolyzed to the free boronic acid under conditions used in HPLC and LC-MS runs. Analytical data represent therefore data for the free boronic acid.

The product was used without further purification in the next reaction step.

HRMS: cal. 340.1466, exp. 340.1455 ([M+H]⁺)

ESI-MS: cal. 340.1466, exp. 340.1 ([M+H]⁺)

t_R (HPLC) 4.87 min

5.3.30 Ethyl 3-(2'-cyano-5-(3-(3-(dibenzylamino)propyl)-6,7-dihydro-5H-cyclopenta[c]pyridine-1-yl)-3-methyl-2,3'-bipyridin-5'-yl)propanoate (22b)**Procedure A: microwave**

An oven-dried 20 ml microwave-flask equipped with magnetic stir bar was charged with **12b** (0.40 g, 1.1 mmol), potassium acetate (0.32 g, 3.2 mmol), bis(pinacolato)diboron (0.33 g, 1.3 mmol), the indicated amount of Pd(0) source and phosphine ligand and was sealed with a microwave septum. The flask was evacuated and flushed with nitrogen. After addition of 12 ml of the indicated solvent, the reaction mixture was heated in the microwave to 130°C and stirred at this temperature for 7 minutes (DMF) or 32 minutes (dioxane).

After cooling down to room temperature, dihydro-5H-cyclopenta[c]pyridine halide **8d** (0.75 mmol) or **8e** (0.75 mmol) in 3 ml of solvent and 1.6 mmol of base in 1 ml of H₂O were added to reaction mixture via syringe. The reaction mixture was heated in the microwave to 130°C and stirred at this temperature for 30-40 minutes. After cooling down to room temperature, the reaction mixture was diluted with brine and extracted three times with ethyl acetate. The combined organic phases were dried over MgSO₄ and the solvent was removed under reduced pressure. Column chromatography (EtOAc/hexane 1:1 containing 1% NEt₃) gave the product as orange oil.

5 Experimental

	8d	8e
Pd(0) source	Pd(OAc) ₂ (12 mg, 0.05 mmol)	Pd ₂ dba ₃ (25mg, 0.03 mmol)
phosphine	PPh ₃ (56 mg, 0.21 mmol)	XPhos (102 mg, 0.2 mmol)
solvent	DMF	dioxane
base	K ₂ CO ₃ (0.22 g, 1.6 mmol)	K ₃ PO ₄ (0.34 g, 1.6 mmol)
yield	48% (234 mg)	54% (263 mg)

Procedure B: thermal

An oven-dried 100 ml three-necked flask equipped with magnetic stir bar, nitrogen inlet, rubber septum and condenser with bubbler was charged with **12b** (0.15 g, 0.4 mmol), potassium acetate (0.12 g, 1.2 mmol), bis(pinacolato)diboron (0.12 g, 0.48 mmol), tris(dibenzylideneacetone) dipalladium(0) (0.01 g, 0.01 mmol) and XPhos (0.04 g, 0.08 mmol). The flask was evacuated and flushed with nitrogen for at least three times. After addition of dioxane (3 ml) the reaction mixture was heated to 102°C and stirred at this temperature for 1 hour. Then, **8e** (0.1 g, 0.28 mmol) in dioxane (3ml) and potassium phosphate (0.13 g, 0.6 mmol) in H₂O (0.3 ml) were added to reaction mixture via syringe. The reaction mixture was stirred at 102°C for 3 more hours. After cooling down to room temperature, the reaction mixture was diluted with brine and extracted three times with ethyl acetate. The combined organic phases were dried over MgSO₄ and the solvent was removed under reduced pressure. Column chromatography (EtOAc/hexane 1:1 containing 1% NEt₃) gave the product in 46% yield (84 mg) as orange oil.

¹H-NMR (300 MHz, CDCl₃): 1.22-1.26 (t, ³J = 7.1, 3H, -CH₂-CH₃), 1.97-2.16 (m, 4H, -CH₂-CH₂-NBn₂ and H-15), 2.35 (s, 3H, -CH₃), 2.52-2.57 (t, ³J = 7.0, 2H, -CH₂-NBn₂), 2.69-2.74 (t, ³J = 7.4, 2H, -CH₂-CO₂Et), 2.80-2.85 (t, ³J = 7.6, 2H, -CH₂-CH₂-CH₂-NBn₂), 2.89-2.94 (t, ³J = 7.4, 2H, H-16), 3.07-3.13 (m, 4H, -CH₂-CH₂-CO₂Et and H-14), 3.59 (s, 4H, Bn-H), 4.10-4.17 (quartet, ³J = 7.1, 2H, -CH₂-CH₃), 6.93 (s, 1H, H-18), 7.19-7.38 (m, 10H, Bn-H), 7.73-7.74 (d, ⁴J = 1.9, 1H, H-4), 8.08-8.09 (s, ⁴J = 1.5, H-9), 8.63-8.64 (s, ⁴J = 1.9, 1H, H-2), 8.91-8.91 (s, ⁴J = 1.5, 1H, H-11).

5 Experimental

¹³C-NMR (75,5 MHz, CDCl₃): δ 14.39 (-CH₂-CH₃), 19.34 (-CH₃), 25.70 (C-15), 27.53 (-CH₂-CH₂-NBn₂), 28.23 (CH₂-CH₂-CO₂Et), 32.32 (C-14), 33.02 (C-16), 34.82 (-CH₂-CO₂Et), 35.95 (-CH₂-CH₂-CH₂-NBn₂), 53.15 (-CH₂-NBn₂), 58.61 (Bn-C), 61.12 (-CH₂-CH₃), 116.73 (-CN), 118.92 (C-18), 126.95 (Bn-C), 128.35 (Bn-C), 129.03 (Bn-C), 131.46 (C-6), 131.96 (C-8), 135.49 (C-13), 136.71 (C-10), 138.02 (C-4), 138.83 (C-9), 140.04 (C-3), 140.16 (Bn-C), 140.92 (C-5), 147.32 (C-11), 149.63 (C-12), 150.73 (C-2), 152.19 (C-7), 156.05 (C-17), 160.63 (C-19), 171.96 (-CO₂Et).

HRMS: cal. 650.3490, exp. 650.3491 ([M+H]⁺)

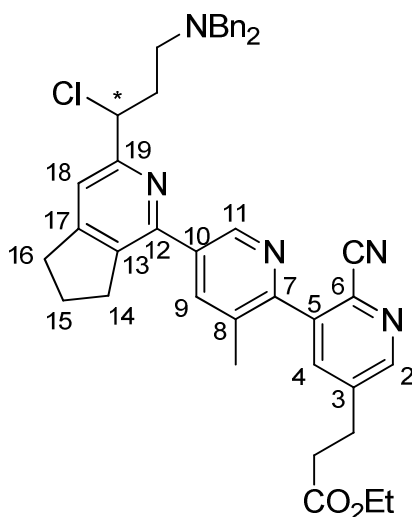
ESI-MS: cal. 650.3490, exp. 650.4 ([M+H]⁺)

R_f (TLC) 0.25 (EtOAc:hexane 1:1 with 1% of NEt₃)

t_R (HPLC)

6.11 min

5.3.31 Ethyl3-(5-(4-chloro-3-(3-(dibenzylamino)propyl)-6,7-dihydro-5H-cyclopenta[c]pyridine-1-yl)-2'-cyano-3-methyl-2,3'-bipyridin-5'-yl)propanoate (22c)



An oven-dried 20 ml microwave-flask equipped with magnetic stir bar was charged with **12b** (0.50 g, 1.3 mmol), potassium acetate (0.39 g, 4.0 mmol), bis(pinacolato)diboron (0.41 g, 1.6 mmol), tris(dibenzylideneacetone) dipalladium(0) (0.03 g, 0.034 mmol) and XPhos (0.13 g, 0.27 mmol) and was sealed with a microwave septum. The flask was evacuated and flushed with nitrogen. After addition of dioxane (12 ml), the reaction mixture was heated in the microwave to 130°C for 32 minutes. After cooling down to room temperature, **8I** (0.51 g, 1.2 mmol) in dioxane (3ml) and potassium phosphate (0.43 g, 2.0 mmol) in H₂O (1 ml) were added to reaction mixture via syringe. The reaction mixture was heated in the microwave to 100°C and stirred at this temperature for 55 minutes. After cooling down to room temperature, the reaction mixture was diluted with brine and extracted three times with ethyl acetate. The combined organic phases were dried over MgSO₄ and the solvent was removed under reduced pressure. Column chromatography (EtOAc/hexane 1:1) gave the product in 22% yield (180 mg) as orange oil.

5 Experimental

¹H-NMR (300 MHz, CDCl₃): 1.22-1.26 (t, ³J = 7.1, 3H, -CH₂-CH₃), 2.11-2.34 (m, 7H, H-15, -CH₃, -CH₂-CH₂-NBn₂), 2.62-2.74 (m, 4H, -CH₂-CO₂Et, -CH₂-NBn₂), 2.95-3.00 (t, ³J = 7.5, 2H, H-16), 3.08-3.17 (m, 4H, -CH₂-CH₂-CO₂Et, H-14), 3.58 (s, 4H, Bn-H), 4.10-4.18 (quartet, ³J = 7.1, 2H, -CH₂-CH₃), 5.13-5.18 (t, ³J = 7.0 1H, -CH(Cl)-), 7.20-7.34 (m, 11H, Bn-H, H-18), 7.74-7.75 (d, ⁴J = 1.8, 1H, H-4), 8.09-8.10 (d, ⁴J = 1.5, 1H, H-9), 8.64-8.65 (s, ⁴J = 1.8, 1H, H-2), 8.93-8.93 (s, ⁴J = 1.5, 1H, H-11).

¹³C-NMR (75,5 MHz, CDCl₃): δ 14.38 (-CH₂-CH₃), 19.35 (-CH₃), 25.70 (C-15), 28.22 (-CH₂-CH₂-CO₂Et), 32.56 (C-14), 33.10 (C-16), 34.80 (-CH₂-CO₂Et), 35.99 (-CH₂-CH₂-NBn₂), 50.73 (-CH₂-NBn₂), 58.60 (Bn-C), 61.12 (-CH₂-CH₃), 62.06 (-CH(Cl)-), 116.71 (-CN), 118.06 (C-18), 127.06 (Bn-C), 128.37 (Bn-C), 129.05 (Bn-C), 131.43 (C-6), 131.97 (C-8), 136.05 (C-10), 137.69 (C-13), 137.99 (C-4), 138.89 (C-9), 139.62 (Bn-C), 140.07 (C-3), 140.80 (C-5), 147.29 (C-11), 149.49 (C-12), 150.78 (C-2), 152.46 (C-7), 156.92 (C-17), 158.40 (C-19), 171.96 (-CO₂Et).

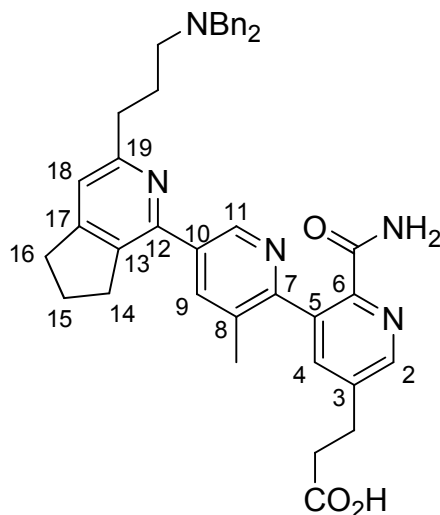
HRMS: cal. 684.3100, exp. 684.3067 ([M+H]⁺)

ESI-MS: cal. 684.3495, exp. 684.3 ([M+H]⁺)

IR: ν [cm⁻¹] = 2926, 1730, 1596, 1185, 746, 698.

R_f (TLC) 0.38 (EtOAc:hexane 4:6 with 2% MeOH) **t_R (HPLC)** 7.40 min

5.3.32 3-(2'carbamoyl-5-(3-(3-(dibenzylamino)propyl)-6,7-dihydro-5H-cyclopenta[c]pyridin-1-yl)-3-methyl-2,3'-bipyridin-5'-yl)propanoic acid (25b)



A 50 ml one-necked flask equipped with magnetic stir bar and condenser was charged with **22b** (431 mg, 0.66 mmol) and sodium hydroxide (266 mg, 6.6 mmol). After addition of ethanol (20 ml) and H₂O (6 ml), the reaction mixture was refluxed over night. After cooling down to room temperature, the reaction mixture was diluted with water and extracted three times with diethyl ether. The aqueous phase was acidified to pH 1 with 1M HCl and extracted three times with ethyl acetate. The aqueous phase was then alkalized to pH 9 with saturated NaHCO₃ solution and extracted three times with *n*-butanol. The combined organic phases from pH 9 were dried over MgSO₄ and the solvent was removed under reduced pressure. The product was obtained as white solid in 80% yield (338 mg) and used without further purification in the next reaction step.

¹H-NMR (300 MHz, MeOD): 2.00-2.07 (m, 2H, -CH₂-CH₂-NBn₂), 2.13-2.19 (m, 2H, H-15), 2.22 (s, 3H, -CH₃), 2.50-2.60 (m, 4H, -CH₂-NBn₂ and -CH₂-CO₂H), 2.80-2.84 (t, ³J = 7.2, 2H, -CH₂-CH₂-CH₂-NBn₂), 2.95-3.00 (t, ³J = 7.4, 2H, H-16), 3.08-3.16 (m, 4H, -CH₂-CH₂-CO₂H, H-14), 3.60 (s, 4H, Bn-H), 7.00 (s, 1H, H-18), 7.23-7.37 (m, 10H, Bn-H), 7.73 (d, ⁴J = 1.9, 1H, H-4), 8.01 (s, 1H, H-9), 8.67 (s, 2H, H-2, H-11).

5 Experimental

¹³C-NMR (75,5 MHz, MeOD): δ 19.54 (-CH₃), 26.35 (C-15), 28.30 (-CH₂-CH₂-NBn₂), 30.72 (-CH₂-CH₂-CO₂H), 33.02 (C-14), 33.94 (C-16), 36.24 (-CH₂-CH₂-CH₂-NBn₂), 40.10 (-CH₂-CO₂H), 53.65 (-CH₂-NBn₂), 59.63 (Bn-C) 120.13 (C-18), 128.07 (Bn-C), 129.45 (Bn-C), 130.27 (Bn-C), 133.31 (C-8), 136.28 (C-10), 137.11 (C-13), 139.18 (C-9), 140.15 (C-4), 141.11 (Bn-C), 142.77 (C-3), 144.90 (C-5), 146.22 (C-11), 147.03 (C-6), 150.03 (C-2), 151.33 (C-12), 157.96 (C-17), 158.79 (C-7), 161.62 (C-19), 169.76 (-C(O)NH₂), 171.77 (-CH₂-CH₂-CO₂H).

The product was further purified by preparative HPLC (ACN/0.1% TFA, H₂O/0.1% TFA) with the following gradient: 20% ACN to 99% ACN in H₂O in 50 minutes. **25b** eluted at t_R = 17.9 minutes and was obtained after lyophilisation as white ammonium trifluoroacetate salt.

¹H-NMR (300 MHz, MeOD): 2.31-2.37 (m, 7H, -CH₂-CH₂-NBn₂, H-15, -CH₃), 2.77-2.82 (t, ³J = 7.2, 2H, -CH₂-CO₂H), 2.93-2.97 (t, ³J = 7.1, 2H, -CH₂-NBn₂), 3.09-3.28 (m, 8H, H-14, H-16, -CH₂-CH₂-CH₂-NBn₂, -CH₂-CH₂-CO₂H), 4.43 (s, 4H, Bn-H), 7.40 (s, 1H, H-18), 7.40-7.47 (m, 10H, Bn-H), 7.87-7.88 (d, ⁴J = 1.8, 1H, H-4), 8.47-8.47 (s, 1H, H-9), 8.80-8.80 (d, ⁴J = 1.8, 2H, H-2 or H-11), 8.85-8.86 (d, ⁴J = 1.4, 2H, H-2 or H-11).

¹³C-NMR (75,5 MHz, MeOD): δ 19.16, 24.31, 26.58, 28.81, 32.71, 34.13, 34.26, 35.49, 52.28, 58.58, 121.82, 130.65, 130.76, 131.47, 132.40, 135.65, 136.14, 139.57, 140.20, 141.77, 142.52, 142.99, 147.05, 148.27, 151.66, 156.72, 158.67, 161.67, 161.90, 168.68, 175.80.

HR-MS: cal. 640.3282, exp. 640.3276 ([M+H]⁺)

ESI-MS: cal. 640.3282, exp. 640.3 ([M+H]⁺)

IR: ν [cm⁻¹] = 2922, 1722, 1671, 1197, 1086, 719, 700.

m.p. 49.3 C

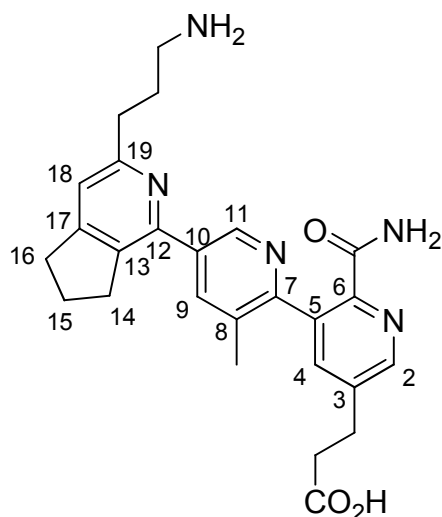
t_R (HPLC)

4.30 min

5.3.33 3-(5-(3-(3-aminopropyl)-6,7-dihydro-5H-cyclopenta[c]pyridin-1-yl)-2'carbamoyl-3-methyl-2,3'-bipyridin-5'-yl)propanoic acid (26b) and 3-(5-(3-(3-(benzylamino)propyl)-6,7-dihydro-5H-cyclopenta[c]pyridin-1-yl)-2'carbamoyl-3-methyl-2,3'-bipyridin-5'-yl)propanoic acid (26c)

An oven-dried 100 ml three-necked flask equipped with magnetic stir bar, condenser with bubbler, nitrogen inlet and rubber septum was charged with **25b** (40 mg, 0.06 mmol), ammonium formate (80 mg, 1.26 mmol) and Pd/C (12 mg, 0.02 mmol). The flask was evacuated and flushed with nitrogen three times. After addition of methanol (3 ml), the reaction mixture was heated to 70°C and was stirred at this temperature over night. After cooling down to room temperature, the reaction mixture was filtered over celite. The filtrate was dried under reduced pressure. The residue was purified by semipreparative HPLC (MeOH, H₂O) with the following gradient: 20% MeOH to 99% MeOH in H₂O in 40 minutes.

26b eluted at $t_R = 20.7$ minutes and was obtained after lyophilisation as white solid in 6% yield (2 mg) as zwitterionic salt.



¹H-NMR (300 MHz, MeOD): 2.20-2.25 (m, 4H, -CH₂-CH₂-NH₂, H-15), 2.29 (s, 3H, -CH₃), 2.83-2.88 (t, 2H, ³J = 7.1 -CH₂-CO₂H), 3.04-3.23 (m, 10H, -CH₂-CH₂-CH₂-NH₂, -CH₂-CH₂-CO₂H, H-14, H-16), 7.45 (s, 1H, H-18), 7.83 (d, ⁴J = 1.8, 1H, H-4), 8.12 (d, ⁴J = 1.7, 1H, H-9), 8.73-8.74 (d, ⁴J = 1.7, 1H, H-11), 8.75-8.76 (d, ⁴J = 1.8, 1H, H-2).

5 Experimental

¹³C-NMR (75,5 MHz, MeOD): δ 19.39 (-CH₃), 26.46 (C-15), 28.67 (-CH₂-CH₂-CO₂H), 28.82 (-CH₂-CH₂-NH₂), 32.62 (C-14), 33.96 (C-16), 34.92 (-CH₂-CH₂-CH₂-NH₂), 36.10 (-CH₂-CO₂H), 40.34 (-CH₂-NH₂), 120.64 (C-18), 133.59 (C-8), 135.51 (C-10), 136.47, 138.45 (C-5, C-13), 139.31 (C-9), 140.24 (C-4), 141.36 (C-3), 146.01 (C-11), 147.21 (C-6), 150.13 (C-2), 150.98 (C-12), 158.14 (C-7), 159.56, 159.70 (C-17, C-19), 169.87 (-C(O)NH₂).

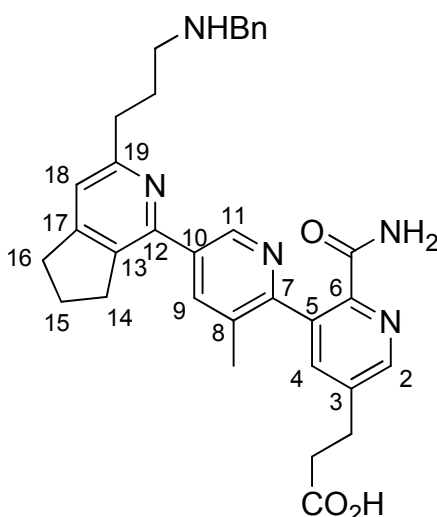
HR-MS: 460.2344, exp. 460.2343 ([M+H]⁺)

ESI-MS: cal. 460.2344, exp. 460.2 ([M+H]⁺)

IR: ν [cm⁻¹] = 2929, 1673, 1598, 1561, 1199, 1129, 720.

m.p. 99.6°C **t_R (HPLC)** 2.69 min

26c eluted at t_R = 25.7 minutes and was obtained after lyophilisation as white solid in 22% yield (7 mg).



¹H-NMR (300 MHz, d₆-DMSO): 1.87-2.10 (m, 7H, -CH₂-CH₂-NH₂, H-15, -CH₃), 2.54-2.61 (m, 2H, -CH₂-CO₂H), 2.78-2.97 (m, 8H, -CH₂-CH₂-CH₂-NH₂, -CH₂-CH₂-CO₂H, H-14), 3.07-3.12 (t, ⁴J = 1.7, 2H, H-16), 3.42 (bs, NH), 3.71 (s, 2H, Bn-H), 7.16-7.31 (m, 7H, Bn-H, H-18, -C(O)NH₂), 7.65-7.66 (d, ⁴J = 1.95, 1H, H-4), 7.98 (m, 2H, H-9, -C(O)NH₂), 8.55-8.56 (d, ⁴J = 1.92, 1H, H-2), 8.72-8.73 (d, ⁴J = 1.7, 1H, H-11).

¹³C-NMR (75,5 MHz, d₆-DMSO): δ 18.87 (-CH₃), 24.95 (C-15), 27.25 (-CH₂-CH₂-CO₂H), 29.44 (-CH₂-CH₂-NH₂), 31.24 (C-14), 32.22 (C-16), 34.07 (-CH₂-CH₂-CH₂-NH₂), 34.81 (-CH₂-CO₂H), 48.06 (-CH₂-NH₂), 52.74 (Bn-C), 117.94 (C-18), 126.49 (Bn-C), 127.96 (Bn-C), 128.02 (Bn-C), 130.38 (Bn-C), 133.80 (C-8), 134.66 (C-10), 135.35 (C-13), 136.14 (C-5), 138.71 (C-4), 144.41 (C-3), 145.24 (C-11), 147.20 (C-6), 149.51 (C-2), 153.40 (C-12), 155.47, 157.32, 159.46 (C-7, C-17, C-19), 166.91 (-C(O)NH₂), 173.57 (-CH₂-CH₂-CO₂H).

5 Experimental

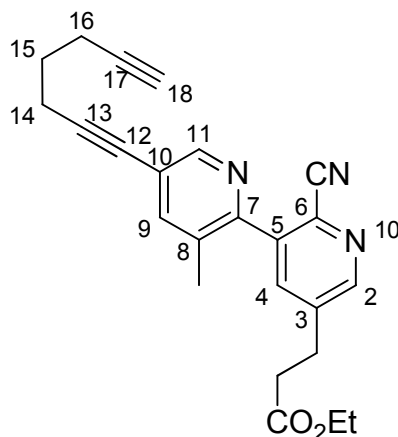
HR-MS: : cal. 550.2813, exp. 550.2808 ($[M+H]^+$)

ESI-MS: cal. 550.2813, exp. 550.2 ($[M+H]^+$)

IR: ν [cm^{-1}] = 2930, 1720, 1673, 1561, 1199, 1130, 719.

m.p. 96.9 C **t_R (HPLC)** 3.41 min

5.3.34 Ethyl 3-(2'-cyano-5-(hepta-1,6-diynyl)-3-methyl-2,3'-bipyridin-5-yl)propanoate (23a)



Procedure 1: thermal

An oven-dried 100 ml three-necked flask equipped with magnetic stir bar, nitrogen inlet, condenser with bubbler and rubber septum was charged with copper iodide (12.5 mg, 0.07 mmol), **12b** (250 mg, 0.67 mmol), triphenylphosphine (34 mg, 0.13 mmol) and palladium(II) acetate (7.5 mg, 0.03 mmol). After evacuating and purging the flask with nitrogen for at least three times, DMF (3 ml) and triethylamine (3 ml) were added and the reaction mixture was stirred at room temperature for 10 minutes. After heating the mixture to 100°C, 1,6-heptadiyne (0.1 ml, 0.8 mmol) in DMF (0.5 ml) was added to the reaction mixture dropwise via syringe. The solution was stirred for 20 more minutes at 100°C, cooled down to room temperature and diluted with brine. The aqueous phase was extracted three times with ethyl acetate. The combined organic phases were dried over MgSO₄ and the solvent was removed under reduced pressure. Column chromatography (EtOAc/hexane 1:4) gave the product in 61% yield (158 mg) as yellow oil.

Procedure 2: microwave

An oven-dried 5 ml microwave-flask equipped with magnetic stir bar was charged with copper iodide (25 mg, 0.13 mmol), **12b** (500 mg, 1.34 mmol), triphenylphosphine (68 mg, 0.26 mmol) and palladium(II) acetate (15 mg, 0.07 mmol) and was sealed with a microwave septum. The flask was evacuated and flushed with nitrogen. After addition of DMF (6 ml), triethylamine (4.5 ml) and 1,6-heptadiyne (0.2 ml, 1.6 mmol), the reaction mixture was heated in the microwave to 130°C and stirred at this

5 Experimental

temperature for 195 seconds. After cooling down to room temperature, the reaction mixture was diluted with brine. The aqueous phase was extracted three times with ethyl acetate. The combined organic phases were dried over MgSO_4 and the solvent was removed under reduced pressure. Column chromatography (EtOAc/hexane 1:4) gave the product in 67% (346 mg) yield as yellow oil.

$^1\text{H-NMR}$ (300 MHz, CDCl_3): δ 1.20-1.25 (t, $^3J = 7.18$, 3H, $-\text{CH}_2-\text{CH}_3$), 1.82-1.91 (m, 2H, H-15), 2.00-2.02 (m, $^4J = 2.6$, 1H, H-18), 2.26 (s, 3H, $-\text{CH}_3$), 2.37-2.43 (m, 2H, H-16), 2.58-2.63 (t, $^3J = 7.0$, 2H, H-14), 2.67-2.72 (t, $^3J = 7.4$, 2H, $-\text{CH}_2-\text{CO}_2\text{Et}$), 3.05-3.10 (t, $^3J = 7.4$, 2H, $-\text{CH}_2-\text{CH}_2-\text{CO}_2\text{Et}$), 4.09-4.16 (quartet, $^3J = 7.13$, 2H, $-\text{CH}_2-\text{CH}_3$), 7.68 (s, 1H, H-9), 7.70-7.71 (d, $^4J = 1.83$, 1H, H-4), 8.56 (s, 1H, H-11), 8.62 (d, $^4J = 1.86$, 1H, H-2).

$^{13}\text{C-NMR}$ (75,5 MHz, CDCl_3): δ 14.37 ($-\text{CH}_2-\text{CH}_3$), 17.87 (C-16), 18.74 (C-14), 19.02 ($-\text{CH}_3$), 27.57 (C-15), 28.20 ($-\text{CH}_2-\text{CH}_2-\text{CO}_2\text{Et}$), 34.77 ($-\text{CH}_2-\text{CO}_2\text{Et}$), 61.12 ($-\text{CH}_2-\text{CH}_3$), 69.35 (C-12), 77.70 (C-17), 83.46 (C-18), 94.18 (C-13), 116.54 ($-\text{CN}$), 121.67 (C-10), 131.36 (C-6), 131.76 (C-8), 137.87 (C-4), 140.09, 140.30 (C-3, C-5), 141.37 (C-9), 150.00 (C-11), 150.86 (C-2), 151.39 (C-7), 171.92 ($-\text{CO}_2\text{Et}$).

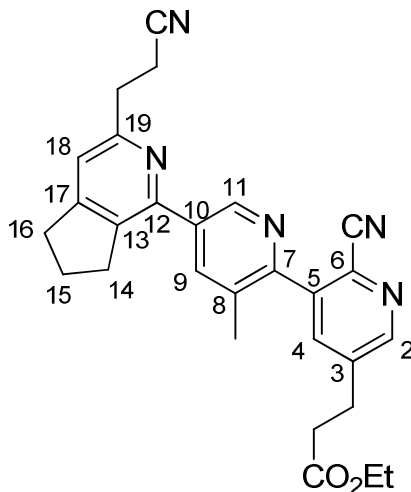
HRMS: cal. 386.1863; exp. 386.1848 ($[\text{M}+\text{H}]^+$)

ESI-MS: cal. 386.1863; exp. 386.2 ($[\text{M}+\text{H}]^+$)

IR: ν [cm^{-1}] = 2980, 2939, 2233, 1731, 1665, 1369, 1154, 946, 884.

R_f (TLC) 0.1 (EtOAc:hexane 1:4) **t_R (HPLC)** 8.46 min

5.3.35 Ethyl 3-(2'-cyano-5-(3-(2-cyanoethyl)-6,7-dihydro-5H-cyclopenta[c]pyridin-1-yl)-3-methyl-2,3'-bipyridin-5'-yl)propanoate (24a)



A 50 ml two-necked flask equipped with magnetic stir bar, nitrogen inlet and rubber septum was charged with **23a** (0.3 mg, 0.8 mmol), Cp**Ru*(cod)Cl (44 mg, 0.12 mmol) and succinonitrile (2.66 g, 31.2 mmol) under nitrogen atmosphere. The reaction mixture was heated to 110°C and stirred at this temperature for 5.5 hour. After cooling down to room temperature, the reaction mixture was partitioned between saturated NaHCO₃/CHCl₃. The aqueous phase was extracted twice with chloroform. The combined organic phases were washed with brine, dried over MgSO₄ and the solvent was removed under reduced pressure. After column chromatography (EtOAc/hexane startin at 2+1, 2% NEt₃) the product was obtained as brown oil in 13% yield (48 mg). The product was further purified by preparative HPLC (ACN/0.1% TFA, H₂O/0.1% TFA) with the following gradient: 20% ACN to 99% ACN in H₂O in 60 minutes. **24a** eluted at *t_R* = 28.5 minutes and was obtained after lyophilisation as light blue pyridinium trifluoroacetate salt.

¹H-NMR (300 MHz, CDCl₃): 1.12-1.17 (t, ³*J* = 7.1, 3H, -CH₂-CH₃), 2.05-2.15 (m, 2H, H-15), 2.33 (s, 3H, -CH₃), 2.77-2.82 (t, ³*J* = 7.4, 2H, -CH₂-CO₂Et), 2.98-3.08 (m, 6H, H-16, -CH₂-CH₂-CO₂Et, -CH₂-CN), 3.13-3.19 (m, 4H, -CH₂-CH₂-CN, H-14), 4.01-4.08 (q, ³*J* = 7.1, 2H, -CH₂-CH₃), 5.78 (bs, NH⁺), 7.41 (s, 1H, H-18), 8.11-8.12 (d, ⁴*J* = 1.9, 1H, H-4), 8.30-8.30 (d, ⁴*J* = 1.8, 1H, H-9), 8.75-8.76 (d, ⁴*J* = 1.9, 1H, H-2), 9.01 (d, ⁴*J* = 1.8, 1H, H-11).

5 Experimental

¹³C-NMR (75,5 MHz, CDCl₃): δ 14.03 (-CH₂-CH₃), 15.86 (-CH₂-CN), 18.64 (-CH₃), 24.92 (C-15), 27.27 (-CH₂-CH₂-CO₂Et), 31.38 (C-14), 31.70 (C-16), 32.43 (-CH₂-CH₂-CN), 33.62 (-CH₂-CO₂Et), 60.01 (-CH₂-CH₃), 111.94-117.25 (-CF₃), 116.82 (-CN), 119.29 (C-18), 120.47 (-CN), 129.71 (C-6), 131.71 (C-8), 134.45 (C-10), 136.82 (C-13), 137.84 (C-4), 138.27 (C-9), 139.70 (C-5), 140.51 (C-3), 146.47 (C-11), 148.29 (C-12), 150.91 (C-2), 152.37 (C-7), 155.51 (C-19), 157.44 (C-17), 158.00, 158.49 (-C(O)-CF₃), 171.78 (-CO₂Et).

HRMS: cal. 466.2238, exp. 466.2251 ([M+H]⁺)

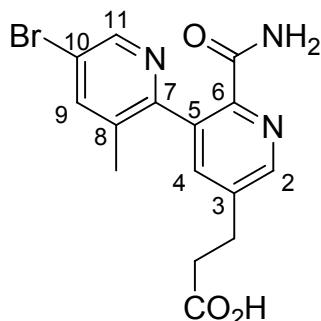
ESI-MS: cal. 466.2238, exp. 466.2 ([M+H]⁺)

IR: ν [cm⁻¹] = 2958, 2248, 2234, 1728, 1594, 1560, 1184.

R_f (TLC) 0.29 (EtOAc:hexane 2+1)

t_R (HPLC) 7.54 min

5.3.36 3-(5-bromo-2'-carbamoyl-3-methyl-2,3'-bipyridin-5'-yl)propanoic acid (12d)



Into a 50 ml one-necked flask equipped with magnetic stir bar and condenser was placed **12b** (0.14 g, 0.37 mmol) and sodium hydroxide (0.06 g, 1.5 mmol) in 70% ethanol/H₂O. The reaction mixture was refluxed for 2 hours, washed with diethyl ether and acidified with glacial acetic acid to pH 4. Part of the product precipitated; remaining product was extracted from the aqueous phase with ethyl acetate. The combined organic phases were dried over Na₂SO₄ and the solvent was removed under reduced pressure. The product was obtained as yellow solid 86% yield (116 mg).

¹H-NMR (300 MHz, d₆-DMSO): δ 2.01 (s, 3H, -CH₃), 2.61-2.66 (t, ³J = 7.38, 2H, -CH₂-CO₂H), 2.91-2.96 (t, ³J = 7.34, 2H, -CH₂-CH₂-CO₂H), 7.35 (s, 1H, -CH₂-CH₂-CO₂H), 7.62-7.63 (d, ⁴J = 2.0, 1H, H-4), 7.93-7.93 (d, ⁴J = 2.1, 1H, H-9), 7.98 (s, 1H, -CO₂H), 8.45-8.46 (d, ⁴J = 2.1, 1H, H-11), 8.56-8.56 (d, ⁴J = 2.0, 1H, H-2).

¹³C-NMR (75,5 MHz, d₆-DMSO): δ 18.50 (-CH₃), 27.04 (-CH₂-CH₂-CO₂H), 34.25 (-CH₂-CO₂H), 118.24 (C-10), 133.57 (C-8), 134.51 (C-5), 138.33 (C-4), 138.63 (C-3), 138.92 (C-9), 146.14 (C-11), 146.83 (C-6), 148.04 (C-2), 156.98 (C-7), 166.63 (-C(O)NH₂), 173.40 (-CH₂-CH₂-CO₂H).

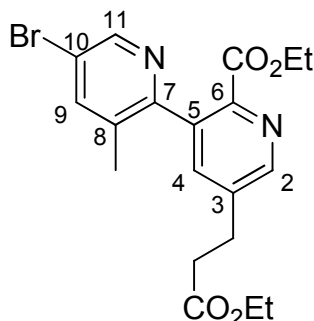
HR-MS: cal. 364.0291; exp. 364.0284 ([M+H]⁺)

ESI-MS: cal. 364.0291; exp. 364.0 ([M+H]⁺)

IR: ν [cm⁻¹] = 3437, 1701, 1646, 1558, 1390.

m.p. 230.6°C (burned) **t_R (HPLC)** 4.17 min

5.3.37 Ethyl 5-(2-(ethoxycarbonyl)ethyl)-3-(5-bromo-3-methylpyridin-2-yl)pyridine-2-carboxylate (12c)



A 100 ml one-necked flask equipped with magnetic stir bar was charged with **12d** (0.1 g, 0.34 mmol) in ethanol (5 ml). After addition of concentrated sulphuric acid (6 μ l, 0.07 mmol), the reaction mixture was warmed to 90°C and was stirred at this temperature for four hours. After concentrating the reaction mixture under reduced pressure, the mixture was diluted with saturated NaHCO₃ solution and extracted three times with ethyl acetate. The combined organic phases were dried over MgSO₄ and concentrated under reduced pressure. Column chromatography (EtOAc/hexane 1:2) gave the product as white solid in 80% yield (115 mg).

¹H-NMR (300 MHz, d₆-DMSO): δ 0.94-0.99 (t, ³J = 7.1, 3H, -CH₂-CH₃), 1.11-1.16 (t, ³J = 7.1, 3H, -CH₂-CH₃), 2.14 (s, 3H, -CH₃), 2.72-2.77 (t, ³J = 7.4, 2H, -CH₂-CO₂Et), 2.94-3.01 (t, ³J = 7.4, 2H, -CH₂-CH₂-CO₂Et), 4.00-4.07 (m, 4H, -CH₂-CH₃), 7.83-7.83 (d, ⁴J = 1.9, 1H, H-4), 8.07-8.07 (d, ⁴J = 2.0, 1H, H-9), 8.53-8.53 (d, ⁴J = 2.0, 1H, H-11), 8.61-8.61 (d, ⁴J = 1.9, 1H, H-2).

¹³C-NMR (75,5 MHz, d₆-DMSO): δ 13.53 (-CH₂-CH₃), 14.02 (-CH₂-CH₃), 18.47 (-CH₃), 27.02 (-CH₂-CH₂-CO₂Et), 33.96 (-CH₂-CO₂Et), 59.94 (-CH₂-CH₃), 61.15 (-CH₂-CH₃), 119.03 (C-10), 133.65 (C-8), 134.86 (C-5), 137.63 (C-4), 138.42 (C-3), 139.99 (C-9), 146.00 (C-6), 146.72 (C-11), 148.98 (C-2), 155.03 (C-7), 165.01 (-CO₂Et), 171.83 (-CH₂-CH₂-CO₂Et).

HRMS: cal. 421.0757; exp. 421.0731 ([M+H]⁺)

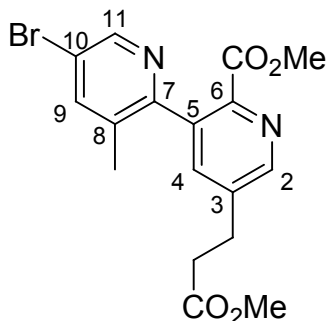
ESI-MS: cal. 421.0763; exp. 421.1 ([M+H]⁺)

IR: ν [cm⁻¹] = 2990, 1718, 1687, 943.

m.p. 39.6°C

R_f (TLC) 0.15 (EtOAc:hexane 1:2) **t_R (HPLC)** 7.35 min

5.3.38 Methyl 5-(2-(methoxycarbonyl)ethyl)-3-(5-bromo-3-methylpyridin-2-yl)pyridine-2-carboxylate (12e)



A 100 ml one-necked flask equipped with magnetic stir bar was charged with **12d** (0.1 g, 0.34 mmol) in anhydrous methanol (5 ml). After addition of concentrated sulphuric acid (6 μ l, 0.07 mmol), the reaction mixture was warmed to 70°C and was stirred at this temperature over night. After concentrating the reaction mixture under reduced pressure, the mixture was diluted with saturated NaHCO₃ solution and extracted three times with ethyl acetate. The combined organic phases were dried over MgSO₄ and concentrated under reduced pressure. Column chromatography (EtOAc/hexane 1:1, containing 1% of NEt₃) gave the product as white solid in 94% yield (125 mg).

¹H-NMR (300 MHz, d₆-DMSO): δ 2.14, (s, 3H, -CH₃), 2.74-2.79 (t, ³J = 7.38, 2H, -CH₂-CO₂Me), 2.97-3.01 (t, ³J = 7.34, 2H, -CH₂-CH₂-CO₂Me), 3.57 (s, 3H, -O-CH₃), 3.60 (s, 3H, -O-CH₃), 7.84-7.84 (d, ⁴J = 1.9, 1H, H-4), 8.07-8.07 (d, ⁴J = 1.9, 1H, H-9), 8.53-8.54 (d, ⁴J = 1.9, 1H, H-11), 8.60-8.61 (d, ⁴J = 1.9, 1H, H-2).

¹³C-NMR (75,5 MHz, d₆-DMSO): 18.55 (-CH₃), 27.01 (-CH₂-CH₂-CO₂Me), 33.74 (-CH₂-CO₂Me), 51.41 (-O-CH₃), 52.13 (-O-CH₃), 119.09 (C-10), 133.62 (C-8), 134.99 (C-5), 137.78 (C-4), 138.61 (C-3), 140.14 (C-9), 145.70 (C-6), 146.84 (C-11), 148.99 (C-2), 154.84 (C-7), 165.96 (-CO₂Me), 172.38 (-CH₂-CH₂-CO₂Me).

HRMS: cal. 393.0444; exp. 393.0447 ([M+H]⁺)

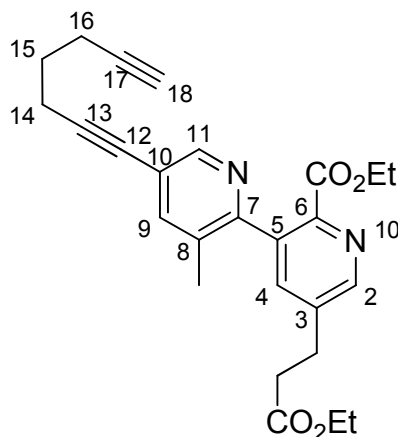
ESI-MS: cal. 393.0444; exp. 393.0 ([M+H]⁺)

m.p. 96.2°C

R_f (TLC) 0.13 (EtOAc:hexane 1:1 with 1% NEt₃)

t_R (HPLC)

6.26 min

5.3.39 Ethyl 5-(2-(ethoxycarbonyl)ethyl)-3-(5-(hepta-1,6-diynyl)-3-methylpyridin-2-yl)pyridine-2-carboxylate (23b)

An oven-dried 100 ml three-necked flask equipped with magnetic stir bar, nitrogen inlet, condenser with bubbler and rubber septum was charged with palladium(II) acetate (36 mg, 0.16 mmol), triphenylphosphine (173 mg, 0.66 mmol) and copper(I) iodide (63 mg, 0.33 mmol). The flask was evacuated and flushed with nitrogen for at least three times. After addition of 1,6-heptadiyne (0.46 ml, 4.00 mmol), DMF (9.0 ml) and NEt_3 (7.5 ml), the reaction mixture was heated to 100 °C. **12c** (1.4 g, 3.3 mmol) in DMF (3 ml) was added dropwise to the reaction mixture over 35 minutes. After 15 minutes, 1,6-heptadiyne (0.23 ml, 2.00 mmol) in NEt_3 (1.5 ml) was added dropwise to the reaction mixture over 25 minutes. The mixture was stirred for 5 more minutes at 100°C and then cooled down to room temperature. The reaction mixture was diluted with water and extracted three times with ethyl acetate. The combined organic phases were dried over MgSO_4 and concentrated under reduced pressure. Column chromatography (EtOAc/hexane 1:2 containing 1.5% NEt_3) gave the product as yellow oil in 69% yield (985 mg).

$^1\text{H-NMR}$ (300 MHz, d_6 -DMSO): δ 0.91-0.96 (t, $^3J = 7.1$, 3H, $-\text{CH}_2-\text{CH}_3$), 1.11-1.15 (t, $^3J = 7.1$, 3H, $-\text{CH}_2-\text{CH}_3$), 1.72-1.79 (m, 2H, H-15), 2.13 (s, 3H, $-\text{CH}_3$), 2.31-2.37 (m, 2H, H-16), 2.55-2.59 (t, $^3J = 7.0$, 2H, H-14), 2.72-2.76 (t, $^3J = 7.3$, 2H, $-\text{CH}_2-\text{CO}_2\text{Et}$), 2.85-2.87 (t, $^4J = 2.6$, 1H, H-18), 2.95-3.00 (t, $^3J = 7.3$, 2H, $-\text{CH}_2-\text{CH}_2-\text{CO}_2\text{Et}$), 3.97-4.06 (m, 4H, $-\text{CH}_2-\text{CH}_3$), 7.81-7.83 (m, 2H, H-4, H-9), 8.41-8.42 (d, $^4J = 1.7$, 1H, H-11), 8.59-8.59 (d, $^4J = 1.9$ 1H, H-2).

5 Experimental

¹³C-NMR (75,5 MHz, d₆-DMSO: δ 13.53 (-CH₂-CH₃), 14.02 (-CH₂-CH₃), 16.97 (C-16), 17.83 (C-14), 18.42 (-CH₃), 27.02 (-CH₂-CH₂-CO₂Et), 27.12 (C-15), 34.00 (-CH₂-CO₂Et), 59.93 (-CH₂-CH₃), 60.65 (-CH₂-CH₃), 71.80 (C-18), 77.73 (C-12), 83.57 (C-17), 93.06 (C-13), 118.99 (C-10), 130.95 (C-8), 135.22 (C-5), 137.60 (C-4), 138.23 (C-3), 139.99 (C-9), 146.29 (C-6), 148.13 (C-11), 148.80 (C-2), 154.91 (C-7), 165.47 (-CO₂Et), 171.83 (-CH₂-CH₂-CO₂Et).

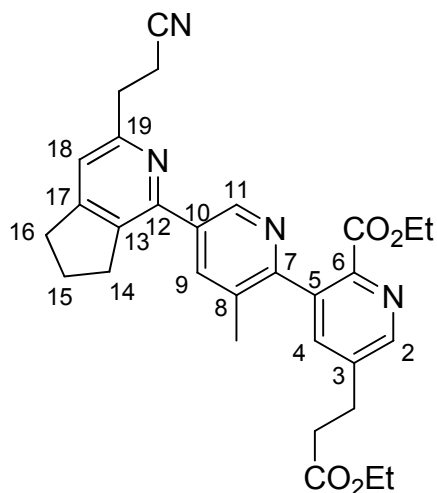
HRMS: cal. 433.2122; exp. 433.2123 ([M+H]⁺)

ESI-MS: cal. 433.2122; exp. 433.2 ([M+H]⁺)

IR: ν [cm⁻¹] = 2981, 2937, 1728, 1668, 1368, 1154, 949..

R_f (TLC) 0.10 (EtOAc:hexane 1:2) with 1.5% NEt₃ **t_R (HPLC)** 8.23 min

5.3.40 Ethyl 5-(3-(2-cyanoethyl)-6,7-dihydro-5*H*-cyclopenta[*c*]pyridin-1-yl)-5'-(3-ethoxy-3-oxopropyl)-3-methyl-2,3'-bipyridine-2'-carboxylate (**24b**)



A 50 ml two-necked flask equipped with magnetic stir bar, nitrogen inlet and rubber septum was charged with **23b** (0.48 mg, 1.1 mmol), Cp**Ru*(cod)Cl (41 mg, 0.1 mmol), succinonitrile (1.32 g, 16.5 mmol) and 1,2-dichloroethane (1 ml) under nitrogen atmosphere. The reaction mixture was heated to 110°C and stirred at this temperature for 1 hour. After cooling down to room temperature, the reaction mixture was concentrated under reduced pressure. After column chromatography (EtOAc/hexane starting from 2+3, product eluted from column at 4+1 with 5% NEt₃) the product was obtained as brown oil in 23% yield (130 mg).

¹H-NMR (300 MHz, d₆-DMSO): 0.91-0.95 (t, ³*J* = 7.1, 3H, -CH₂-CH₃), 1.12-1.17 (t, ³*J* = 7.1, 3H, -CH₂-CH₃), 2.05-2.10 (m, 2H, H-15), 2.25 (s, 3H, -CH₃), 2.74-2.79 (t, ³*J* = 7.4, 2H, -CH₂-CO₂Et), 2.93-3.03 (m, 6H, -CH₂-CH₂-CO₂Et, -CH₂-CN, H-16), 3.08-3.13 (m, 4H, -CH₂-CH₂-CN, H-14), 3.98-4.08 (m, 4H, -CH₂-CH₃), 7.30 (s, 1H, H-18), 7.89-7.90 (d, ⁴*J* = 1.9, 1H, H-4), 8.17-8.18 (d, ⁴*J* = 1.8, 1H, H-9), 8.60-8.61 (d, ⁴*J* = 1.9, 1H, H-2), 8.83-8.84 (d, ⁴*J* = 1.8, 1H, H-11).

¹³C-NMR (75,5 MHz, d₆-DMSO): δ 13.53 (-CH₂-CH₃), 14.03 (-CH₂-CH₃), 15.75 (-CH₂-CN), 18.85 (-CH₃), 24.94 (C-15), 27.06 (-CH₂-CH₂-CO₂Et), 31.48 (C-14), 32.14, 32.20 (-CH₂-CH₂-CN, C-16), 34.03 (-CH₂-CO₂Et), 59.94 (-CH₂-CH₃), 60.63 (-CH₂-CH₃), 118.61 (C-18), 120.61 (-CN), 130.61 (C-8), 134.26 (C-10), 135.54 (C-5), 135.87 (C-13), 137.28 (C-9), 137.72 (C-4), 138.16 (C-3), 145.70 (C-11), 146.58 (C-6), 148.70 (C-2), 149.32 (C-12), 155.43 (C-7), 155.76, 156.06 (C-17, C-19), 165.65 (-CO₂Et), 171.87 (-CH₂-CH₂-CO₂Et).

5 Experimental

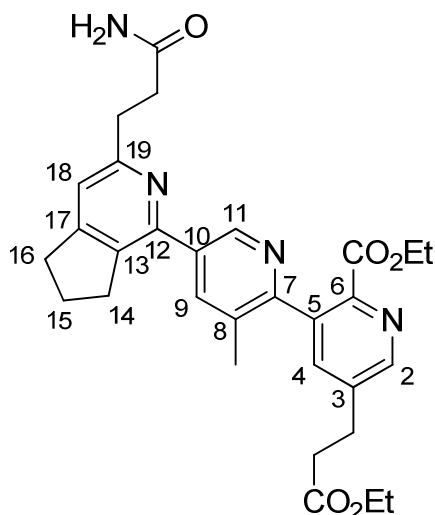
HRMS: cal. 513.2496, exp. 513.2472 ([M+H]⁺)

ESI-MS: cal. 513.2496,, exp. 513.2 ([M+H]⁺)

R_f (TLC) 0.21 (EtOAc:hexane 2:1 with 1.5% of NEt₃)

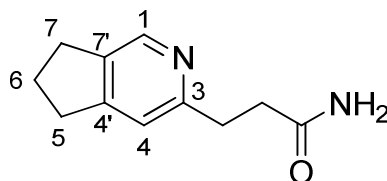
t_R (HPLC)

6.85 min

5.3.41 Ethyl 5-(3-(3-amino-3-oxopropyl)-6,7-dihydro-5H-cyclopenta[c]pyridin-1-yl)-5'-(3-ethoxy-3-oxopropyl)-3-methyl-2,3'-bipyridine-2'-carboxylate (27)

Into a 50 ml one-necked flask equipped with magnetic stir bar was placed **24b** (0.1 g, 0.2 mmol) in trifluoroacetic acid (0.8 ml). The reaction mixture was cooled in a water bath while sulphuric acid (2 ml) was added dropwise. The water bath was removed and the reaction mixture was stirred at room temperature for 5 hours until the reaction was finished. The reaction mixture was poured onto ice and alkalized to pH 9 with 10 M NaOH solution and extracted with chloroform and ethyl acetate for three times. The combined organic phases were washed with brine, dried over MgSO₄, the solvent was then removed under reduced pressure. After column chromatography and lyophilisation (EtOAc/hexane gradient, product eluted in EtOAc/5% AcOH) the product was obtained as yellow solid in 69% yield (73 mg).

¹H-NMR (300 MHz, d₆-DMSO): 0.91-0.96 (t, ³J = 7.1, 3H, -CH₂-CH₃), 1.12-1.17 (t, ³J = 7.1, 3H, -CH₂-CH₃), 2.02-2.07 (m, 2H, H-15), 2.25 (s, 3H, -CH₃), 2.50-2.57 (m, 2H, -CH₂-C(O)NH₂), 2.74-2.79 (t, ³J = 7.4, 2H, -CH₂-CO₂Et), 2.90-3.03 (m, 6H, H-16, -CH₂-CH₂-C(O)NH₂, -CH₂-CH₂-CO₂Et), 3.07-3.11 (t, ³J = 7.4, 2H, H-14), 3.98-4.08 (m, 4H, -CH₂-CH₃), 6.78 (s, 1H, C(O)NH₂), 7.20 (s, 1H, H-18), 7.38 (s, 1H, C(O)NH₂), 7.89-7.90 (d, ⁴J = 1.9, 1H, H-4), 8.12-8.13 (d, ⁴J = 1.85, 1H, H-9), 8.60-8.61 (d, ⁴J = 1.9, 1H, H-2), 8.79-8.79 (d, ⁴J = 1.83, 1H, H-11).

5.3.42 3-(6,7-dihydro-5H-cyclopenta[c]pyridi-3-yl)propanamide

Into a 50 ml one-necked flask equipped with magnetic stir bar was placed **8a** (0.1 g, 0.58 mmol) in trifluoroacetic acid (0.8 ml). The reaction mixture was cooled in a water bath while sulphuric acid (0.2 ml) was added dropwise. The water bath is removed and the reaction mixture was stirred at room temperature over night until the reaction was finished. The reaction mixture was poured onto ice and alkalized to pH 9 with 10 M NaOH solution and extracted with chloroform and ethyl acetate for three times. The combined organic phases were washed with brine, dried over MgSO₄ and the solvent was then removed under reduced pressure.

The product was purified by preparative HPLC (ACN/0.1% TFA, H₂O/0.1% TFA) with the following gradient: 5% ACN to 99% ACN in H₂O in 60 minutes. The product eluted at $t_R = 7.0$ minutes and was obtained after lyophilisation as colorless viscous liquid in 73% yield (129 mg) as trifluoroacetate salt.

¹H-NMR (300 MHz, CDCl₃): δ 2.20-2.30 (m, 2H, H-6), 2.83-2.87 (t, ³J = 6.8, 2H, -CH₂-C(O)NH₂), 3.04-3.14 (m, 4H, H-5, H-7), 3.26-3.31 (t, ³J = 6.8, 2H, -CH₂-CH₂-C(O)NH₂), 7.56 (s, 1H, H-4), 8.51 (s, 1H, H-1)

¹³C-NMR (75,5 MHz, CDCl₃): δ 25.14 (C-6), 28.56 (-CH₂-CH₂-C(O)NH₂), 30.22 (C-5 or C-7), 33.16 (-CH₂-C(O)NH₂), 33.87 (C-5 or C-7), 122.71 (C-4), 136.71 (C-1), 142.08 (C-7'), 154.16 (C-3), 165.56, (C-4'), 174.25 (-C(O)NH₂).

HRMS: cal. 191.1179, exp. 191.1176 ([M+H]⁺)

ESI-MS: cal. 191.1179, exp. 191.1 ([M+H]⁺)

t_R (HPLC) 1.48 min

5.4 Material and experimental procedures for biological assays

5.4.1 Material

5.4.1.1 Buffers

Buffers were prepared as 10x stock solution and diluted with *Aqua bidest.* prior to use, if not stated otherwise.

- **Blocking buffer**
5 % (w/v) skim milk powder
ad 500 ml with TBS-T
- **Tris-buffered saline with Tween-20 (TBS-T, 10x)**
6 g Tris (10 mM)
44 g NaCl (150 mM)
adjust to pH 7.4
5ml Tween-20
ad 1 l with *Aqua bidest.*
- **CD buffer**
3.14 g NaF (150 mM)
1.43 g Na₂HPO₄ (20 mM) ad
0.4l with *Aqua bidest.* and
0.68 g NaH₂PO₄ (20 mM) ad
0.1 l with *Aqua bidest.*
were prepared separately and
combined 4:1 to adjust pH 7.3
final volume doubled with *Aqua bidest.*
- **Phosphate-buffered saline (PBS, 10x)**
80 g NaCl (274 mM)
2 g KCl (27 mM)
2 g KH₂PO₄ (15mM)
11.5 g (Na₂HPO₄) (81 mM)
adjusted to pH 7.4, ad 1 l with
Aqua bidest., autoclaved
- **NMR phosphate buffer**
2.9 g NaCl (100 mM)
2.85 g Na₂HPO₄ (40 mM) ad
0.4l with *Aqua bidest.* and
1.25 g NaH₂PO₄ (40 mM) ad
0.1 l with *Aqua bidest.*
were prepared separately and
combined 4:1 to adjust pH 7.5
final volume doubled with *Aqua bidest.*

5.4.1.2 Peptides

Designation	Sequence
AKAP18δL314E_4-13	AELVRLSKRL
AKAP18δL314E_5-14	ELVRLSKRLV
AKAP18δL314E_6-15	LVRLSKRLVE
AKAP18δL314E_9-18	LSKRLVENAV
AKAP18δL314E_12-21	RLVENAVEKA
AKAP18δL314E_8-19	RLSKRLVENAVE
AKAP18δL314E_4-17	AELVRLSKRLVENA
AKAP18δL314E_5-18	ELVRLSKRLVENAV
AKAP18δL314E_5-18-PP	ELVRLSPPLVENAV
AKAP18δL314E_6-19	LVRLSKRLVENAVE
AKAP18δL314E_7-20	VRLSKRLVENAVEK
AKAP18δL314E_8-21	RLSKRLVENAVEKA
AKAP18δL314E_9-22	LSKRLVENAVEKAV
AKAP18δL314E_6-21	LVRLSKRLVENAVEKA
AKAP18δL314E_5-23	ELVRLSKRLVENAVEKAQ
AKAP18δL314E_3-25	DAELVRLSKRLVENAVEKAQQY
AKAP18δL314E	PEDAELVRLSKRLVENAVEKAQQY
AKAP18δL314E-PP	PEDAELVRLSKRLPENAVEKAQQY

All peptides and N-terminally stearate- or biotin-coupled versions of the peptides were synthesized by the group “peptide synthesis” (Dr. Michael Beyermann) at the FMP. Peptides were purified to > 90% (in the case of stearate-coupled peptides, lower purities were accepted), provided lyophilised and dissolved in DMSO as stock solution (10 mM or 50 mM) or dissolved directly in buffer (for CD measurements). Further dilutions were prepared in buffer as indicated.

5.4.1.3 Proteins

Catalytic subunits of PKA were obtained in a concentration of 1.66 mg/ml from Promega (Mannheim, Germany).

Bovine RII subunits (2.7 mg/ml) were purchased from Sigma-Aldrich.

Recombinant RII α subunits (PKA-RII α FL(1-404)-His) were constructed and purified by Dr. Frank Goetz.

¹⁵N-isotopically enriched recombinant RII α -D/D domain (RII α (1-44)) was purified by Dr. Frank Goetz.

5.4.1.4 Equipment

Phosphoimager Storm 830

Scintillation counter Wallac 1410

CD machine

EnSpire

NMR600 MHz

5.4.2 Experimental procedures

5.4.2.1 Peptides SPOT array synthesis

Peptide arrays were generated by Angelika Ehrlich (FMP) by automatic SPOT-synthesis on Whatman 50 cellulose membranes using standard Fmoc chemistry and the AutoSpot-Robot ASS 222 (Intavis Bioanalytical Instruments AG, Cologne, Germany) as described (Literatur-Referenzen einfügen). Control spots (approx. 50 nmol of peptide per spot) were excised from the cellulose membrane and analyzed by MALDI-TOF(matrix-assisted laser desorption ionization-time-of-flight)-MS and HPLC.

5.4.2.2 RII overlay

The RII overlay technique was established by Lohmann et al.^[206] and was conducted in a modified way as described,^[207;208] using ³²P-labelled bovine RII α . Peptide SPOT membranes were briefly equilibrated in EtOH (99.9%, RT), washed in PBS and blocked in blocking buffer for a minimum of 2 hours. Purified recombinant RII subunits (7.5 μ g) were radiolabeled by incubation with 1 μ l of purified catalytic subunit of PKA (1.66 μ g/ μ l, Promega) and 0.1 μ M [γ]³²P-ATP (6000 Ci/mmol, GE Healthcare) in 500 μ l buffer (25 mM KH₂PO₄, 10 mM MgCl₂, 10 μ M cAMP and 0.5 mM DTT). The final concentration of ATP was reached by adding 10 mM cold ATP after 10 minutes of incubation. After 50 minutes 70 μ l dextran blue (10 mg/ml) was added and the reaction was stopped by removal of cAMP and separation of radiolabeled RII subunits using gel filtration (Sephadex G-50, medium, GE Healthcare). The dextrane blue fraction contains the RII subunits. The total activity of the dextrane blue fraction

was measured and specific activity was calculated in cpm (counts per minute; Liquid scintillation counter Wallac 1410). The membranes were incubated over night with radiolabeled RII subunits in blocking buffer (specific activity of RII subunits= $(1.4 \pm 0.3) \times 10^8$ c.p.m./ μg of protein per ml of hybridisation solution), washed with blocking buffer (4x, 10 min) and twice with PBS. Signals were detected by autoradiography (Phosphoimager Storm 830) and analysed with ImageQuant software (GE healthcare).

5.4.2.3 Circular dichroism measurements

Circular dichroism (CD) measurements of peptides at the indicated concentrations were performed in CD buffer (10 mM, pH 7.4) or in a 1:1 (v/v) mixture of CD buffer/TFE (trifluoroethanol) in a 2 mm cell. Spectra were recorded between 195 and 260 nm on a J-720 spectrometer. The α -helicity of the measured peptides was determined from the mean residue ellipticity ($[\Theta]_{\text{m.r.w.}}$) at 222 nm according to the equation: $\alpha(\%) = -([\Theta]_{\text{m.r.w.}} + 2340) \times 100 / 30300$ (Referenz).

5.4.2.4 Saturation transfer difference nuclear magnetic resonance (STD-NMR)

STD-NMR experiments (reference) were carried out in collaboration with Dr. Peter Schmieder (FMP) and Brigitte Schlegel (FMP) on a Bruker spectrometer equipped with a Z-axis-gradient 5-mm TXI Cryoprobe at 300K. NMR samples for STD-NMR contained 0.1 mM of the indicated compound in NMR buffer, with a final concentration of d_6 -DMSO of 2%. Samples were measured in presence or absence of 20 μM unlabelled PKA-RII α FL(1-404)-His.

STD-NMR experiments were recorded with the carrier frequency set to -1000 (around -1 ppm) for on-resonance irradiation and about 330 ppm for off-resonance irradiation. A train of 50 Gaussian-shaped pulses at 40 ms was applied, each separated by a 1-ms delay, for a total duration of 2.05 s, to achieve selective protein saturation. Spectra acquisition was done with 32 scans in absence of protein and 256 scans in presence of protein and a relaxation delay of 1.3 s. A $T_{1\rho}$ spin lock pulse of 40 ms was used to suppress the background protein signals. The STD spectrum was obtained from the internal subtraction of the on-resonance from the off-resonance data by phase cycling.

5.4.2.5 $^1\text{H},^{15}\text{N}$ -heteronuclear single quantum coherence (HSQC)-NMR

$^1\text{H},^{15}\text{N}$ -HSQC-NMR experiments were carried out in collaboration with Dr. Peter Schmieder (FMP), Brigitte Schlegel (FMP) and Dr. Carolyn Vargas (FMP Berlin, TU Kaiserslautern) on a Bruker 600 MHz spectrometer at 300 K.

$^1\text{H},^{15}\text{N}$ -correlation experiments using with ^{15}N -isotopically enriched RII α (1-44) were recorded using a standard HSQC pulse program or an HMQC-SOFAST pulse program, both employing WATERGATE for solvent suppression.

The protein concentration employed for binding studies was in the order of 0.1 mM. The concentration of compounds used as indicated in chapter 3 (0.3 mM for compounds; 0.8 mM for peptides). Experiments were performed in NMR buffer containing 5% d_6 -DMSO. Each step was followed by recording of a new spectrum. The acquisition time in the direct dimension was restricted to 150 ms. A total of 256 increments was recorded in the indirect dimension.

6 References

- [1.] G. Pidoux, K. Tasken, *Journal of Molecular Endocrinology* **2010**, *44* 271-284.
- [2.] C. W. Dessauer, *Molecular Pharmacology* **2009**, *76* 935-941.
- [3.] J. B. Shabb, *Chemical Reviews* **2001**, *101* 2381-2411.
- [4.] A. M. Edelman, D. K. Blumenthal, E. G. Krebs, *Annual Review of Biochemistry* **1987**, *56* 567-613.
- [5.] D. Willoughby, D. M. F. Cooper, *Physiological Reviews* **2007**, *87* 965-1010.
- [6.] D. M. F. Cooper, *Biochemical Society Transactions* **2005**, *33* 1319-1322.
- [7.] J. S. Logue, J. D. Scott, *Febs Journal* **2010**, *277* 4370-4375.
- [8.] M. G. Gold, B. Lygren, P. Dokurno, N. Hoshi, G. McConnachie, K. Tasken, C. R. Carlson, J. D. Scott, D. Barford, *Molecular Cell* **2006**, *24* 383-395.
- [9.] F. S. Kinderman, C. Kim, S. von Daake, Y. L. Ma, B. Q. Pham, G. Spraggon, N. H. Xuong, P. A. Jennings, S. S. Taylor, *Molecular Cell* **2006**, *24* 397-408.
- [10.] S. S. Taylor, C. Kim, C. Y. Cheng, S. H. J. Brown, H. Wu, N. Kannan, *Biochimica et Biophysica Acta-Proteins and Proteomics* **2008**, *1784* 16-26.
- [11.] E. J. Welch, B. W. Jones, J. D. Scott, *Molecular Interventions* **2010**, *10* 86-97.
- [12.] S. Barradeau, T. Imaizumi-Scherrer, M. C. Weiss, D. M. Faust, *Trends in Cardiovascular Medicine* **2002**, *12* 235-241.
- [13.] P. Skroblin, S. Grossmann, G. Schafer, W. Rosenthal, E. Klussmann, *International Review of Cell and Molecular Biology, Vol 283* **2010**, 235-330.
- [14.] P. Skroblin, C. Hundsrucker, F. Christian, H. M. Zenn, F. W. Herberg, W. Rosenthal, E. Klussmann, *Naunyn-Schmiedeberg's Archives of Pharmacology* **2009**, 379 116.
- [15.] C. Hundsrucker, P. Skroblin, F. Christian, H. M. Zenn, V. Popara, M. Joshi, J. Eichhorst, B. Wiesner, F. W. Herberg, B. Reif, W. Rosenthal, E. Klussmann, *Journal of Biological Chemistry* **2010**, *285* 5507-5521.
- [16.] D. W. Carr, R. E. Stofko-Hahn, I. D. Fraser, S. M. Bishop, T. S. Acott, R. G. Brennan, J. D. Scott, *Journal of Biological Chemistry* **1991**, *266* 14188-14192.
- [17.] M. G. Newlon, M. Roy, D. Morikis, Z. E. Hausken, V. Coghlan, J. D. Scott, P. A. Jennings, *Nature Structural Biology* **1999**, *6* 222-227.
- [18.] M. G. Newlon, M. Roy, D. Morikis, D. W. Carr, R. Westphal, J. D. Scott, P. A. Jennings, *EMBO J* **2001**, *20* 1651-1662.
- [19.] M. L. Ruehr, M. A. Russell, M. Bond, *Journal of Molecular and Cellular Cardiology* **2004**, *37* 653-665.
- [20.] M. G. Gold, F. D. Smith, J. D. Scott, D. Barford, *Journal of Molecular Biology* **2008**, *375* 1329-1343.
- [21.] C. Hundsrucker, G. Krause, M. Beyermann, A. Prinz, B. Zimmermann, O. Diekmann, D. Lorenz, E. Stefan, P. Nedvetsky, M. Dathe, F. Christian, T. McSorley, E. Krause, G. McConnachie, F. W. Herberg, J. D. Scott, W. Rosenthal, E. Klussmann, *Biochemical Journal* **2006**, *396* 297-306.
- [22.] C. Hundsrucker, W. Rosenthal, E. Klussmann, *Biochemical Society Transactions* **2006**, *34* 472-473.
- [23.] J. T. Hulme, T. W. C. Lin, R. E. Westenbroek, T. Scheuer, W. A. Catterall, *Proceedings of the National Academy of Sciences of the United States of America* **2003**, *100* 13093-13098.
- [24.] C. Hundsrucker, E. Klussmann, in *Protein-Protein Interactions as New Drug Targets*, Springer Berlin Heidelberg, **2008**, p. pp. 483-503.
- [25.] E. A. Torheim, E. Jarnaess, B. Lygren, K. Tasken, *Biochemical Journal* **2009**, *424* 69-78.

-
- [26.] J. K. Murray, S. H. Gellman, *Biopolymers* **2007**, *88* 657-686.
- [27.] F. Christian, M. Szaszak, S. Friedl, S. Drewianka, D. Lorenz, A. Goncalves, J. Furkert, C. Vargas, P. Schmieder, F. Gotz, K. Zuhlke, M. Moutty, H. Gottert, M. Joshi, B. Reif, H. Haase, I. Morano, S. Grossmann, A. Klukovits, J. Verli, G. Robert, C. Noack, M. Bergmann, R. Kass, K. Hampel, D. Kashin, H. G. Genieser, F. W. Herberg, D. Willoughby, D. M. F. Cooper, G. S. Baillie, M. D. Houslay, J. P. von Kries, B. Zimmermann, W. Rosenthal, E. Klussmann, *Journal of Biological Chemistry* **2011**, *286* 9079-9096.
- [28.] A. J. Wilson, *Chem.Soc.Rev.* **2009**, *38* 3289-3300.
- [29.] M. R. Arkin, J. A. Wells, *Nature Reviews Drug Discovery* **2004**, *3* 301-317.
- [30.] A. G. Cochran, *Chemistry & Biology* **2000**, *7* R85-R94.
- [31.] C. G. Cummings, A. D. Hamilton, *Current Opinion in Chemical Biology* **2010**, *14* 341-346.
- [32.] W. L. Delano, *Current Opinion in Structural Biology* **2002**, *12* 14-20.
- [33.] J. M. Davis, L. K. Tsou, A. D. Hamilton, *Chem.Soc.Rev.* **2007**, *36* 326-334.
- [34.] N. T. Ross, W. P. Katt, A. D. Hamilton, *Philosophical Transactions of the Royal Society A-Mathematical Physical and Engineering Sciences* **2010**, *368* 989-1008.
- [35.] D. C. Rees, M. Congreve, C. W. Murray, R. Carr, *Nature Reviews Drug Discovery* **2004**, *3* 660-672.
- [36.] C. W. Murray, D. C. Rees, *Nature Chemistry* **2009**, *1* 187-192.
- [37.] M. van Dongen, J. Weigelt, J. Uppenberg, J. Schultz, M. Wikstrom, *Drug Discovery Today* **2002**, *7* 471-478.
- [38.] S. Fletcher, A. D. Hamilton, *Current Opinion in Chemical Biology* **2005**, *9* 632-638.
- [39.] J. Garner, M. M. Harding, *Organic & Biomolecular Chemistry* **2007**, *5* 3577-3585.
- [40.] L. L. Burns, J. M. Canaves, J. K. Pennypacker, D. K. Blumenthal, S. S. Taylor, *Biochemistry* **2003**, *42* 5754-5763.
- [41.] L. L. Burns-Hamuro, Y. Ma, S. Kammerer, U. Reineke, C. Self, C. Cook, G. L. Olson, C. R. Cantor, A. Braun, S. S. Taylor, *Proceedings of the National Academy of Sciences of the United States of America* **2003**, *100* 4072-4077.
- [42.] L. L. Burns-Hamuro, Y. Hamuro, J. S. Kim, P. Sigala, R. Fayos, D. D. Stranz, P. A. Jennings, S. S. Taylor, V. L. Woods, *Protein Science* **2005**, *14* 2982-2992.
- [43.] H. E. Blackwell, R. H. Grubbs, *Angewandte Chemie-International Edition* **1998**, *37* 3281-3284.
- [44.] C. E. Schafmeister, J. Po, G. L. Verdine, *Journal of the American Chemical Society* **2000**, *122* 5891-5892.
- [45.] L. D. Walensky, A. L. Kung, I. Escher, T. J. Malia, S. Barbutto, R. D. Wright, G. Wagner, G. L. Verdine, S. J. Korsmeyer, *Science* **2004**, *305* 1466-1470.
- [46.] F. Bernal, A. F. Tyler, S. J. Korsmeyer, L. D. Walensky, G. L. Verdine, *Journal of the American Chemical Society* **2007**, *129* 5298.
- [47.] R. Fasan, R. L. A. Dias, K. Moehle, O. Zerbe, J. W. Vrijbloed, D. Obrecht, J. A. Robinson, *Angewandte Chemie-International Edition* **2004**, *43* 2109-2112.
- [48.] J. A. Kritzer, N. W. Luedtke, E. A. Harker, A. Schepartz, *Journal of the American Chemical Society* **2005**, *127* 14584-14585.
- [49.] J. D. Sadowsky, W. D. Fairlie, E. B. Hadley, H. S. Lee, N. Umezawa, Z. Nikolovska-Coleska, S. M. Wang, D. C. S. Huang, Y. Tomita, S. H. Gellman, *Journal of the American Chemical Society* **2007**, *129* 139-154.
- [50.] B. P. Orner, J. T. Ernst, A. D. Hamilton, *Journal of the American Chemical Society* **2001**, *123* 5382-5383.

6 References

- [51.] O. Kutzki, H. S. Park, J. T. Ernst, B. P. Orner, H. Yin, A. D. Hamilton, *Journal of the American Chemical Society* **2002**, *124* 11838-11839.
- [52.] J. M. Davis, A. Truong, A. D. Hamilton, *Organic Letters* **2005**, *7* 5405-5408.
- [53.] H. Yin, G. i. Lee, K. A. Sedey, J. M. Rodriguez, H. G. Wang, S. M. Sebti, A. D. Hamilton, *Journal of the American Chemical Society* **2005**, *127* 5463-5468.
- [54.] H. Yin, G. i. Lee, K. A. Sedey, O. Kutzki, H. S. Park, B. P. Orner, J. T. Ernst, H. G. Wang, S. M. Sebti, A. D. Hamilton, *Journal of the American Chemical Society* **2005**, *127* 10191-10196.
- [55.] L. H. Chen, H. Yin, B. Farooqi, S. Sebti, A. D. Hamilton, J. D. Chen, *Molecular Cancer Therapeutics* **2005**, *4* 1019-1025.
- [56.] J. Rodriguez, A. Hamilton, *Angewandte Chemie International Edition* **2007**, *46* 8614-8617.
- [57.] I. C. Kim, A. D. Hamilton, *Organic Letters* **2006**, *8* 1751-1754.
- [58.] J. M. Rodriguez, L. Nevola, N. T. Ross, G. I. Lee, A. D. Hamilton, *ChemBiochem* **2009**, *10* 829-833.
- [59.] C. G. Cummings, N. T. Ross, W. P. Katt, A. D. Hamilton, *Organic Letters* **2009**, *11* 25-28.
- [60.] A. Volonterio, L. Moisan, J. Rebek, *Organic Letters* **2007**, *9* 3733-3736.
- [61.] S. M. Biro, L. Moisan, E. Mann, A. Carella, D. Zhai, J. C. Reed, J. Rebek, *Bioorganic & Medicinal Chemistry Letters* **2007**, *17* 4641-4645.
- [62.] Y. Che, B. R. Brooks, G. R. Marshall, *Biopolymers* **2007**, *86* 288-297.
- [63.] P. Restorp, J. Rebek, *Bioorganic & Medicinal Chemistry Letters* **2008**, *18* 5909-5911.
- [64.] J. H. Lee, Q. Zhang, S. Jo, S. C. Chai, M. Oh, W. Im, H. Lu, H. S. Lim, *Journal of the American Chemical Society* **2011**, *133* 676-679.
- [65.] I. Saraogi, J. A. Hebda, J. Becerril, L. A. Estroff, A. D. Miranker, A. D. Hamilton, *Angewandte Chemie-International Edition* **2010**, *49* 736-739.
- [66.] J. P. Plante, T. Burnley, B. Malkova, M. E. Webb, S. L. Warriner, T. A. Edwards, A. J. Wilson, *Chemical Communications* **2009**, 5091-5093.
- [67.] I. Saraogi, C. D. Incarvito, A. D. Hamilton, *Angewandte Chemie-International Edition* **2008**, *47* 9691-9694.
- [68.] J. M. Ahn, S. Y. Han, *Tetrahedron Letters* **2007**, *48* 3543-3547.
- [69.] F. Campbell, J. P. Plante, T. A. Edwards, S. L. Warriner, A. J. Wilson, *Organic & Biomolecular Chemistry* **2010**, *8* 2344-2351.
- [70.] E. Ko, J. Liu, L. M. Perez, G. L. Lu, A. Schaefer, K. Burgess, *Journal of the American Chemical Society* **2011**, *133* 462-477.
- [71.] N. M. Alto, S. H. Soderling, N. Hoshi, L. K. Langeberg, R. Fayos, P. A. Jennings, J. D. Scott, *Proceedings of the National Academy of Sciences of the United States of America* **2003**, *100* 4445-4450.
- [72.] J. K. Myers, C. N. Pace, J. M. Scholtz, *Protein Science* **1998**, *7* 383-388.
- [73.] M. K. Luidens, J. Figge, K. Breese, S. Vajda, *Biopolymers* **1996**, *39* 367-376.
- [74.] M. Pellecchia, I. Bertini, D. Cowburn, C. Dalvit, E. Giralto, W. Jahnke, T. L. James, S. W. Homans, H. Kessler, C. Luchinat, B. Meyer, H. Oschkinat, J. Peng, H. Schwalbe, G. Siegal, *Nature Reviews Drug Discovery* **2008**, *7* 738-745.
- [75.] B. Meyer, T. Peters, *Angewandte Chemie-International Edition* **2003**, *42* 864-890.
- [76.] X. Q. Shen, G. O. Jones, D. A. Watson, B. Bhayana, S. L. Buchwald, *Journal of the American Chemical Society* **2010**, *132* 11278-11287.

-
- [77.] T. Eicher, S. Hauptmann, A. Speicher, *Systematic Nomenclature of Heterocyclic Compounds*, Wiley-VCH Verlag GmbH & Co. KGaA, **2003**, pp. 5-16.
- [78.] T. Eicher, S. Hauptmann, A. Speicher, *Six-Membered Heterocycles* Wiley-VCH Verlag GmbH & Co. KGaA, **2003**, pp. 257-310.
- [79.] G. D. Henry, *Tetrahedron* **2004**, *60* 6043-6061.
- [80.] B. Heller, M. Hapke, *Chem.Soc.Rev.* **2007**, *36* 1085-1094.
- [81.] J. A. Varela, C. Saa, *Chemical Reviews* **2003**, *103* 3787-3801.
- [82.] I. Eryazici, C. N. Moorefield, G. R. Newkome, *Chemical Reviews* **2008**, *108* 1834-1895.
- [83.] M. Hapke, L. Brandt, A. Lutzen, *Chem.Soc.Rev.* **2008**, *37* 2782-2797.
- [84.] Y. A. Getmanenko, R. J. Twieg, *The Journal of Organic Chemistry* **2008**, *73* 830-839.
- [85.] A. S. Voisin-Chiret, A. Bouillon, G. Burzicki, M. Celant, R. Legay, H. El-Kashef, S. Rault, *Tetrahedron* **2009**, *65* 607-612.
- [86.] A. Bouillon, A. S. Voisin, A. Robic, J. C. Lancelot, V. Collot, S. Rault, *Journal of Organic Chemistry* **2003**, *68* 10178-10180.
- [87.] A. Goswami, K. Ohtaki, K. Kase, T. Ito, S. Okamoto, *Adv.Synth.Catal.* **2008**, *350* 143-152.
- [88.] A. Puglisi, M. Benaglia, G. Roncan, *Eur.J.Org.Chem.* **2003**, 1552-1558.
- [89.] M. Heller, U. S. Schubert, *Journal of Organic Chemistry* **2002**, *67* 8269-8272.
- [90.] G. Burzicki, A. S. Voisin-Chiret, J. S. D. Santos, S. Rault, *Tetrahedron* **2009**, *65* 5413-5417.
- [91.] N. Kudo, M. Perseghini, G. C. Fu, *Angewandte Chemie-International Edition* **2006**, *45* 1282-1284.
- [92.] K. L. Billingsley, T. E. Barder, S. L. Buchwald, *Angewandte Chemie-International Edition* **2007**, *46* 5359-5363.
- [93.] K. Billingsley, S. L. Buchwald, *Journal of the American Chemical Society* **2007**, *129* 3358-3366.
- [94.] A. Gutnov, B. Heller, C. Fischer, H. J. Drexler, A. Spannenberg, B. Sundermann, C. Sundermann, *Angewandte Chemie-International Edition* **2004**, *43* 3795-3797.
- [95.] A. S. Voisin-Chiret, M. Muraglia, G. Burzicki, S. Perato, F. Corbo, J. S. D. Santos, C. Franchini, S. Rault, *Tetrahedron* **2010**, *66* 8000-8005.
- [96.] L. C. Campeau, K. Fagnou, *Chem.Soc.Rev.* **2007**, *36* 1058-1068.
- [97.] I. J. S. Fairlamb, *Chem.Soc.Rev.* **2007**, *36* 1036-1045.
- [98.] N. Miyaura, A. Suzuki, *Chemical Reviews* **1995**, *95* 2457-2483.
- [99.] K. C. Nicolaou, P. G. Bulger, D. Sarlah, *Angewandte Chemie-International Edition* **2005**, *44* 4442-4489.
- [100.] M. Heller, U. S. Schubert, *Eur.J.Org.Chem.* **2003**, 947-961.
- [101.] A. F. Littke, G. C. Fu, *Angewandte Chemie-International Edition* **2002**, *41* 4176-4211.
- [102.] A. E. Smith, K. M. Clapham, A. S. Batsanov, M. R. Bryce, B. Tarbit, *Eur.J.Org.Chem.* **2008**, 1458-1463.
- [103.] K. L. Billingsley, S. L. Buchwald, *Angewandte Chemie-International Edition* **2008**, *47* 4695-4698.
- [104.] P. B. Hodgson, F. H. Salingue, *Tetrahedron Letters* **2004**, *45* 685-687.
- [105.] Becker, Heinz G. O. Organikum. Berger, W., Domschke, G., Fanghänel, E., Faust, J., Fischer, M., Gentz, F., Gewalt, K., Gluch, R., Mayer, R., Müller, K., Pavel, D., Schmidt, H., Schollberg, K., Schwetlick, K., Seiler, E., Zeppenfeld,

- G., Beckert, R., Habicher, W. D., and Metz, P. *Organisch-chemisches Grundpraktikum*. [22. Auflage]. 2004.
- [106.] Wuts, P. G. M. and Greene, T. W. *Greene's Protective Groups in Organic Synthesis*. [Fourth Edition]. 2007.
- [107.] G. Battistuzzi, S. Cacchi, G. Fabrizi, R. Bernini, *Synlett* **2003**, 1133-1136.
- [108.] F. Mongin, G. Queguiner, *Tetrahedron* **2001**, 57 5897.
- [109.] M. Schlosser, F. Mongin, *Chem.Soc.Rev.* **2007**, 36 1161-1172.
- [110.] F. Mongin, F. Trecourt, G. Queguiner, *Tetrahedron Letters* **1999**, 40 5483-5486.
- [111.] J. Lazaar, A. S. Rebstock, F. Mongin, A. Godard, F. Trecourt, F. Marsais, G. Queguiner, *Tetrahedron* **2002**, 58 6723-6728.
- [112.] F. Trecourt, M. Mallet, F. Marsais, G. Queguiner, *The Journal of Organic Chemistry* **1988**, 53 1367-1371.
- [113.] S. Choppin, P. Gros, Y. Fort, *Organic Letters* **2000**, 2 803-805.
- [114.] T. Cailly, F. Fabis, A. Bouillon, S. Lemaitre, J. Sopkova, O. de Santos, S. Rault, *Synlett* **2006**, 53-56.
- [115.] T. Cailly, F. Fabis, S. Lemaitre, A. Bouillon, S. Rault, *Tetrahedron Letters* **2005**, 46 135-137.
- [116.] R. W. Hoffmann, K. Ditrich, S. Froch, *Liebigs Annalen der Chemie* **1987**, 977-985.
- [117.] D. S. Matteson, *Journal of Organometallic Chemistry* **1999**, 581 51-65.
- [118.] E. M. Kaiser, *Tetrahedron* **1983**, 39 2055-2064.
- [119.] R. R. Fraser, T. S. Mansour, S. Savard, *The Journal of Organic Chemistry* **1985**, 50 3232-3234.
- [120.] Wrackmeyer B. 119Sn-NMR Parameters. *Annual Reports on NMR Spectroscopy* 16, 73-186. 1985.
- [121.] M. Alessi, A. L. Larkin, K. A. Ogilvie, L. A. Green, S. Lai, S. Lopez, V. Snieckus, *The Journal of Organic Chemistry* **2007**, 72 1588-1594.
- [122.] K. Akiba, Y. Iseki, M. Wada, *Bulletin of the Chemical Society of Japan* **1984**, 57 1994-1999.
- [123.] D. L. Comins, A. H. Abdullah, *Journal of Organic Chemistry* **1982**, 47 4315-4319.
- [124.] K. Akiba, Y. Iseki, M. Wada, *Tetrahedron Letters* **1982**, 23 3935-3936.
- [125.] P. N. W. Baxter, *Chemistry-A European Journal* **2003**, 9 2531-2541.
- [126.] A. Numata, Y. Kondo, T. Sakamoto, *Synthesis-Stuttgart* **1999**, 306-311.
- [127.] M. L. Davis, B. J. Wakefield, J. A. Wardell, *Tetrahedron* **1992**, 48 939-952.
- [128.] T. Klis, S. Lulinski, J. Serwatowski, *Current Organic Chemistry* **2008**, 12 1479-1501.
- [129.] P. Caubere, *Chemical Reviews* **1993**, 93 2317-2334.
- [130.] Y. Yamamoto, K. Kinpara, R. Ogawa, H. Nishiyama, K. Itoh, *Chem.Eur.J.* **2006**, 12 5618-5631.
- [131.] Y. Yamamoto, *Current Organic Chemistry* **2005**, 9 503-519.
- [132.] Y. Yamamoto, K. Kinpara, H. Nishiyama, K. Itoh, *Adv.Synth.Catal.* **2005**, 347 1913-1916.
- [133.] R. T. Skerlj, Y. Zhou, T. Wilson, G. J. Bridger, *The Journal of Organic Chemistry* **2002**, 67 1407-1410.
- [134.] M. Schlosser, *Angewandte Chemie-International Edition* **2005**, 44 376-393.
- [135.] C. F. Purchase, O. P. Goel, *Journal of Organic Chemistry* **1991**, 56 457-459.
- [136.] P. C. Gros, Y. Fort, *Eur.J.Org.Chem.* **2009**, 4199-4209.
- [137.] J. Mathieu, P. Gros, Y. Fort, *Chemical Communications* **2000**, 951-952.
- [138.] T. Kaminski, P. Gros, Y. Fort, *Eur.J.Org.Chem.* **2003**, 3855-3860.

-
- [139.] P. Gros, Y. Fort, P. Caubere, *Journal of the Chemical Society-Perkin Transactions 1* **1997**, 3597-3600.
- [140.] P. Gros, Y. Fort, *Eur.J.Org.Chem.* **2002**, 3375-3383.
- [141.] P. Gros, U. Viney, Y. Fort, *Synlett* **2002**, 628-630.
- [142.] H. K. Khartabil, P. C. Gros, Y. Fort, M. F. Ruiz-Lopez, *Journal of the American Chemical Society* **2010**, 132 2410-2416.
- [143.] D. Rojas, A. M. Garcia, A. Vega, Y. Moreno, D. Venegas-Yazigi, M. T. Garland, J. Manzur, *Inorganic Chemistry* **2004**, 43 6324-6330.
- [144.] B. D. Gray, P. W. Jeffs, *Journal of the Chemical Society-Chemical Communications* **1987**, 1329-1330.
- [145.] P. Mal, U. Lourderaj, Parveen, P. Venugopalan, J. N. Moorthy, N. Sathyamurthy, *The Journal of Organic Chemistry* **2003**, 68 3446-3453.
- [146.] R. J. Bergeron, J. S. Mcmanis, *Journal of Organic Chemistry* **1988**, 53 3108-3111.
- [147.] L. F. Tietze, C. Schneider, A. Grote, *Chemistry-A European Journal* **1996**, 2 139-148.
- [148.] P. Gros, S. Choppin, Y. Fort, *Journal of Organic Chemistry* **2003**, 68 2243-2247.
- [149.] T. W. Bell, L. Y. Hu, S. V. Patel, *Journal of Organic Chemistry* **1987**, 52 3847-3850.
- [150.] I. Kondolff, H. Doucet, M. Santelli, *Tetrahedron* **2004**, 60 3813-3818.
- [151.] F. Trecourt, M. Mallet, O. Mongin, B. Gervais, G. Queguiner, *Tetrahedron* **1993**, 49 8373-8380.
- [152.] D. L. Comins, D. H. Lamunyon, *Tetrahedron Letters* **1988**, 29 773-776.
- [153.] F. Marsais, G. Lenard, G. Queguiner, *Synthesis-Stuttgart* **1982**, 235-237.
- [154.] M. C. Venuti, B. E. Loe, G. H. Jones, J. M. Young, *Journal of Medicinal Chemistry* **1988**, 31 2132-2136.
- [155.] E. J. Corey, R. K. Bakshi, *Tetrahedron Letters* **1990**, 31 611-614.
- [156.] Carey, F. A. and Sundberg R.J. *Advanced Organic Chemistry - Part B: Reaction and Synthesis.* 2007.
- [157.] T. Ishiyama, Y. Itoh, T. Kitano, N. Miyaura, *Tetrahedron Letters* **1997**, 38 3447-3450.
- [158.] T. Ishiyama, N. Miyaura, *Chemical Record* **2004**, 3 271-280.
- [159.] M. Murata, T. Oyama, S. Watanabe, Y. Masuda, *Journal of Organic Chemistry* **2000**, 65 164-168.
- [160.] K. L. Billingsley, S. L. Buchwald, *Journal of Organic Chemistry* **2008**, 73 5589-5591.
- [161.] G. B. Smith, G. C. Dezeny, D. L. Hughes, A. O. King, T. R. Verhoeven, *Journal of Organic Chemistry* **1994**, 59 8151-8156.
- [162.] R. Martin, S. L. Buchwald, *Accounts of Chemical Research* **2008**, 41 1461-1473.
- [163.] Sven Schroter, Christoph Stock Thorsten Bach. *Tetrahedron* **2005**, 61 2245-2267.
- [164.] Y. Yamamoto, Y. Azuma, H. Mitoh, *Synthesis-Stuttgart* **1986**, 564-565.
- [165.] T. E. Barder, S. D. Walker, J. R. Martinelli, S. L. Buchwald, *Journal of the American Chemical Society* **2005**, 127 4685-4696.
- [166.] J. A. Marshall, *Chemical Reviews* **2000**, 100 3163-3185.
Marshall, JA, Univ Virginia, Dept Chem, McCormick Rd, Charlottesville, VA 22904 USA
- [167.] T. Ishiyama, K. Ishida, N. Miyaura, *Tetrahedron* **2001**, 57 9813-9816.

-
- [168.] A. Bouillon, J. C. Lancelot, V. Collot, P. R. Bovy, S. Rault, *Tetrahedron* **2002**, 58 2885-2890.
- [169.] Y. Leblanc, P. Cerat, *Synthetic Communications* **2008**, 38 2775-2781.
- [170.] M. Miura, T. Koike, T. Ishihara, S. Sakamoto, M. Okada, M. Ohta, S. I. Tsukamoto, *Synthetic Communications* **2007**, 37 667-674.
- [171.] A. Giroux, Y. X. Han, P. Prasit, *Tetrahedron Letters* **1997**, 38 3841-3844.
- [172.] B. Avitia, E. MacIntosh, S. Muhia, E. Kelson, *Tetrahedron Letters* **2011**, 52 1631-1634.
- [173.] K. L. Billingsley, K. W. Anderson, S. L. Buchwald, *Angewandte Chemie-International Edition* **2006**, 45 3484-3488.
- [174.] Tierney, J. P. and Lidstrom P. Microwave Assisted Organic Synthesis. **2004**.
- [175.] C. O. Kappe, *Angewandte Chemie-International Edition* **2004**, 43 6250-6284.
- [176.] N. E. Leadbeater, *Chemical Communications* **2005**, 2881-2902.
- [177.] A. Furstner, G. Seidel, *Organic Letters* **2002**, 4 541-543.
- [178.] E. A. B. Kantchev, C. J. O'Brien, M. G. Organ, *Angewandte Chemie-International Edition* **2007**, 46 2768-2813.
- [179.] A. F. Littke, C. Y. Dai, G. C. Fu, *Journal of the American Chemical Society* **2000**, 122 4020-4028.
- [180.] I. P. Beletskaya, A. V. Cheprakov, *Chemical Reviews* **2000**, 100 3009-3066.
- [181.] U. Christmann, R. Vilar, *Angewandte Chemie-International Edition* **2005**, 44 366-374.
- [182.] G. C. Fu, *Accounts of Chemical Research* **2008**, 41 1555-1564.
- [183.] T. E. Barder, S. L. Buchwald, *Journal of the American Chemical Society* **2007**, 129 5096-5101.
- [184.] E. C. Jorgense, G. C. Windridg, T. C. Lel, *Journal of Medicinal Chemistry* **1970**, 13 352-&.
- [185.] K. Sonogashira, Y. Tohda, N. Hagihara, *Tetrahedron Letters* **1975**, 4467-4470.
- [186.] R. Chinchilla, C. Najera, *Chemical Reviews* **2007**, 107 874-922.
- [187.] M. Lautens, M. Yoshida, *Journal of Organic Chemistry* **2003**, 68 762-769.
- [188.] R. Hrdina, A. Kadlcikova, I. Valterova, J. Hodacova, M. Kotora, *Tetrahedron-Asymmetry* **2006**, 17 3185-3191.
- [189.] R. Hrdina, I. G. Stara, L. Dufkova, S. Mitchel, I. Cisarova, M. Kotora, *Tetrahedron* **2006**, 62 968-976.
- [190.] Y. Yamamoto, R. Ogawa, K. Itoh, *Journal of the American Chemical Society* **2001**, 123 6189-6190.
- [191.] J. A. Varela, L. Castedo, C. Saa, *Journal of Organic Chemistry* **2003**, 68 8595-8598.
- [192.] B. Heller, B. Sundermann, H. Buschmann, H. J. Drexler, J. S. You, U. Holzgrabe, E. Heller, G. Oehme, *Journal of Organic Chemistry* **2002**, 67 4414-4422.
- [193.] Y. Yamamoto, K. Kinpara, F. Saigoku, H. Takagishi, S. Okuda, H. Nishiyama, K. Itoh, *Journal of the American Chemical Society* **2005**, 127 605-613.
- [194.] L. Severa, J. Vavra, A. Kohoutova, M. Cizkova, T. Salova, J. Hyvl, D. Saman, R. Pohl, L. Adriaenssens, F. Tepy, *Tetrahedron Letters* **2009**, 50 4526-4528.
- [195.] K. Kase, A. Goswami, K. Ohtaki, E. Tanabe, N. Saino, S. Okamoto, *Organic Letters* **2007**, 9 931-934.
- [196.] L. Garcia, A. Pla-Quintana, A. Roglans, T. Parella, *Eur.J.Org.Chem.* **2010**, 3407-3415.
- [197.] K. Tanaka, *Synlett* **2007**, 1977-1993.
- [198.] K. Tanaka, H. Hara, G. Nishida, M. Hirano, *Organic Letters* **2007**, 9 1907-1910.
- [199.] K. Sonogashira, *Journal of Organometallic Chemistry* **2002**, 653 46-49.

6 References

- [200.] Y. Yamamoto, K. Kinpara, R. Ogawa, H. Nishiyama, K. Itoh, *Chemistry-A European Journal* **2006**, *12* 5618-5631.
- [201.] A. Gaucher, Y. Zuliani, D. Cabaret, M. Wakselman, J. P. Mazaleyrat, *Tetrahedron-Asymmetry* **2001**, *12* 2571-2580.
- [202.] F. Miyake, M. Hashimoto, S. Tonsiengsom, K. Yakushijin, D. A. Horne, *Tetrahedron* **2010**, *66* 4888-4893.
- [203.] Y. Yamamoto, K. Hattori, H. Nishiyama, *Journal of the American Chemical Society* **2006**, *128* 8336-8340.
- [204.] Y. Yamamoto, K. Hattori, *Tetrahedron* **2008**, *64* 847-855.
- [205.] N. R. Krishna, V. Jayalakshmi, *Progress in Nuclear Magnetic Resonance Spectroscopy* **2006**, *49* 1-25.
- [206.] S. M. Lohmann, P. Decamilli, I. Einig, U. Walter, *Proceedings of the National Academy of Sciences of the United States of America-Biological Sciences* **1984**, *81* 6723-6727.
- [207.] D. B. Bregman, N. Bhattacharyya, C. S. Rubin, *Journal of Biological Chemistry* **1989**, *264* 4648-4656.
- [208.] E. Klusmann, K. Maric, B. Wiesner, M. Beyermann, W. Rosenthal, *Journal of Biological Chemistry* **1999**, *274* 4934-4938.

List of figures

Figure 1.1: Schematic representation of the structure of an R subunit protomer.....	1
Figure 1.2: A schematic view on top of the AKAP-binding site of the D/D domain of RII α	4
Figure 1.3: Models derived from the corresponding x-ray structures showing the D/D domain from RII α with different AKAP peptides.....	5
Figure 1.4: A schematic representation of potential H-bonding interactions (depicted in shaded light grey) and salt bridges (depicted in dark grey) between the RIIBD of AKAP18 and the D/D domain of RII α	6
Figure 1.5: A schematic representation of potential H-bonding interactions (depicted in shaded light grey) and salt bridges (depicted in dark grey) between the peptide AKAP18 δ -L314E and the D/D domain of RII α	7
Figure 1.6: Schematic representation of the terphenyl scaffold that has been employed as α -helix-mimic.....	12
Figure 1.7: Backbone scaffolds that were proposed as potential mimetics of the peptidic α -helix.....	13
Figure 1.8: Backbone scaffolds that were proposed as potential mimetics of the peptidic α -helix with lower hydrophobicity as compared to the terphenyl scaffold. ...	14
Figure 1.9: Backbone scaffolds that were proposed as potential mimetics of the peptidic α -helix with proposed better synthetic accessibility as compared to the terphenyl scaffold.	15
Figure 2.1: Proposed mimic of the RIIBD of AKAP18.....	16
Figure 3.1: Results of autoradiography of 14-mer peptides after incubation with 32 P-labeled RII α	19
Figure 3.2: Results of autoradiography of 10-mer peptides after incubation with 32 P-labeled RII α	19
Figure 3.3: Depiction of circular dichroism spectra of selected AKAP18 δ L314E-derived peptides in CD buffer/TFE (1:1, v/v).....	21
Figure 3.4: HSQC spectra of D/D domain.....	23
Figure 3.5: HSQC spectra of D/D domain.....	24
Figure 3.6: View of ligand 2a docked into the D/D domain of the RII α -subunit of PKA.....	26

List of figures

Figure 3.7: Schematic view of the proposed interaction of ligand 2a and its binding site within the D/D domain of the RII α -subunit of PKA.....	27
Figure 3.8: Quaterpyridine ligands 2a and derivative 2b.	27
Figure 3.9: Nomenclature of pyridine and cyclopenta[c]pyridine derivatives..	29
Figure 3.10: Schematic overview of sequential Bohlmann-Rahtz heteroannulation reaction towards oligopyridines.	31
Figure 3.11: Scheme of the general catalytic cycle of Pd-catalyzed cross-couplings of aryls.....	32
Figure 3.12: Commonly utilized Pd-catalysed cross-coupling reactions for oligopyridine synthesis.	32
Figure 3.13: Schematic overview of the retrosynthesis of quaterpyridine 2b.....	34
Figure 3.14: Retrosynthetic analysis of the quaterpyridine 2b.....	35
Figure 3.15: Retrosynthetic analysis of the quaterpyridine 2b.....	36
Figure 3.16: Scheme of the retrosynthetic analysis of building block 6.	37
Figure 3.17: General scheme of <i>ortho</i> -directed metalation of pyridine derivatives. ...	38
Figure 3.18: General scheme of the transmetalation of pyridyl lithium derivatives. ...	38
Figure 3.19: Scheme of the synthesis of pyridyl boronic acid and esters from 2-cyanopyridine. ^[56;57]	39
Figure 3.20: Proposed intermediate 18 during the functionalization of 6b.....	39
Figure 3.21: Scheme of the synthesis of 6b.....	40
Figure 3.22: Scheme of the functionalization of 6b.....	40
Figure 3.23: Pyridyl stannanes 6c and 6d.....	40
Figure 3.24: LC chromatogram of crude 6c (254nm).....	41
Figure 3.25: ¹ H-NMR spectrum of trimethylstannane 6c in d ₆ -DMSO.....	42
Figure 3.26: Magnified view of sections of the 2D-spectra of 6c.	42
Figure 3.27: Scheme of the synthesis of pinacol pyridyl boronic acid ester 6f.....	43
Figure 3.28: ¹ H-NMR spectrum of crude 6f in CDCl ₃ after lyophilization in H ₂ O/ACN.	44
Figure 3.29: LC chromatogram of crude 6f (254nm). 5.84: 6f. 6.25: 6b.....	44
Figure 3.30: Retrosynthetic analysis of building block 7.	45
Figure 3.31: Scheme of the proposed synthesis of pyridinium salt 20.....	46
Figure 3.32: Scheme of the proposed synthesis of pyridyl iodide 7c.....	47
Figure 3.33: ¹ H-NMR spectrum of 7c after preparative HPLC in d ₆ -DMSO.	48
Figure 3.34: Scheme of the synthesis of 2,5-dibromo-3,4-dimethylpyridine 7d.	49

List of figures

Figure 3.35: Enlarged sections of the ^{13}C -NMR spectra of 2,5-dibromo-3-methylpyridine 7a (top) and product 7d (bottom) in CDCl_3	49
Figure 3.36: Enlarged sections of the HMBC spectra of 2,5-dibromo-3-methylpyridine (left) and product 7d (right).	50
Figure 3.37: Scheme depicting the retrosynthetic analysis of building block 8.	53
Figure 3.38: Scheme of the synthesis of 8a.....	54
Figure 3.39: Scheme of the synthesis of amine 8b.....	55
Figure 3.40: Scheme of the retrosynthetic analysis of building block 8.	55
Figure 3.41: Simplified view of the composition of $n\text{BuLi/LiDMAE}$ aggregates and potential activation of the aggregate with an acidic reactant R-H . ^[82]	56
Figure 3.42: Scheme of the proposed mechanism of C-2 lithiation of pyridine by chelate formation. ^[51]	56
Figure 3.43: Scheme of the synthesis of halides 8d and 8e.	58
Figure 3.44: ^1H -NMR spectrum of chloride 8e in d_6 -DMSO.	59
Figure 3.45: Compound 8l.	61
Figure 3.46: ^1H -NMR spectrum of 8l in CDCl_3	61
Figure 3.47: Scheme of a potential one-pot borylation-Suzuki coupling procedure with 8k.....	62
Figure 3.48: Scheme of the retrosynthetic analysis of dihalo-pyridine 8k.	63
Figure 3.49: Scheme of the synthesis of 8g.....	64
Figure 3.50: Scheme of the synthesis of 8i.....	65
Figure 3.51: Scheme of the synthesis of 8k.....	65
Figure 3.52 ^1H -NMR spectrum of pyridine 8k recorded in d_6 -DMSO.	65
Figure 3.53: Retrosynthetic analysis of building block 9.	67
Figure 3.54: Scheme of the synthesis of benzyloxyether 9c.....	68
Figure 3.55: Scheme of the synthesis of pyridine 9d.	69
Figure 3.56: Scheme of the synthesis of bromide 9f and chloride 9g.	70
Figure 3.57: ^1H -NMR spectrum of chloride 9g in d_6 -DMSO.	71
Figure 3.58: Zoom into the HMBC-spectrum of aromatic carbon atoms of chloride 9g.	71
Figure 3.59: Scheme of the synthesis of 9e.....	72
Figure 3.60: LC-spectrum of crude 9e at 280nm.	73
Figure 3.61: Scheme of the synthesis of bromide 9h and chloride 9i.	74
Figure 3.62: ^1H -NMR spectrum of chloride 9i in d_6 -DMSO.	75

List of figures

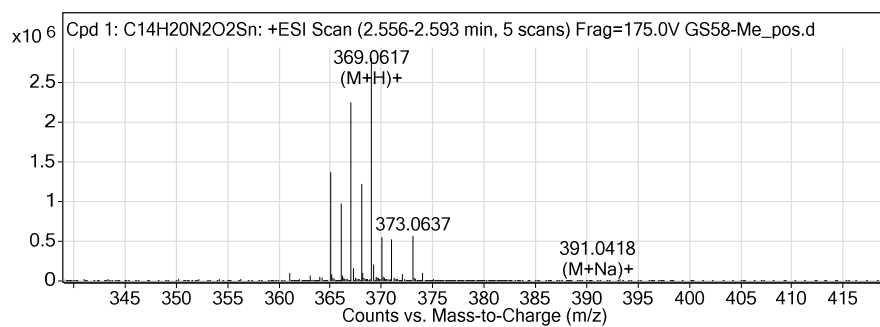
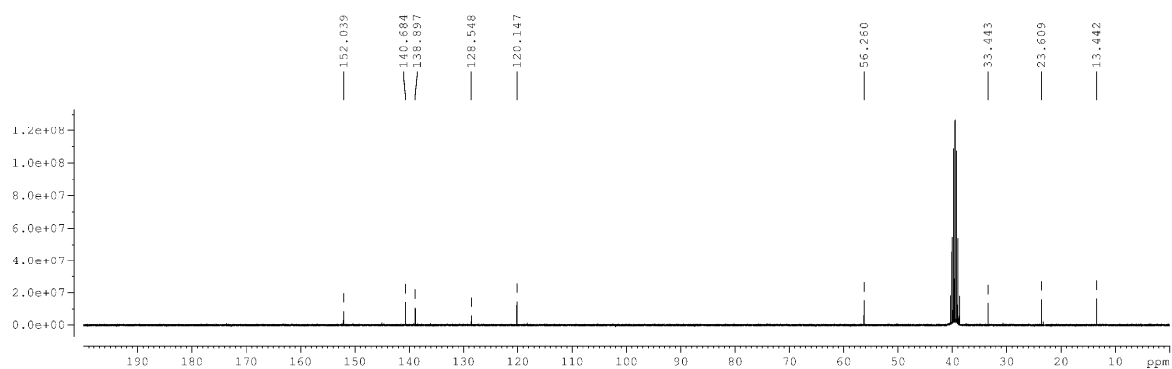
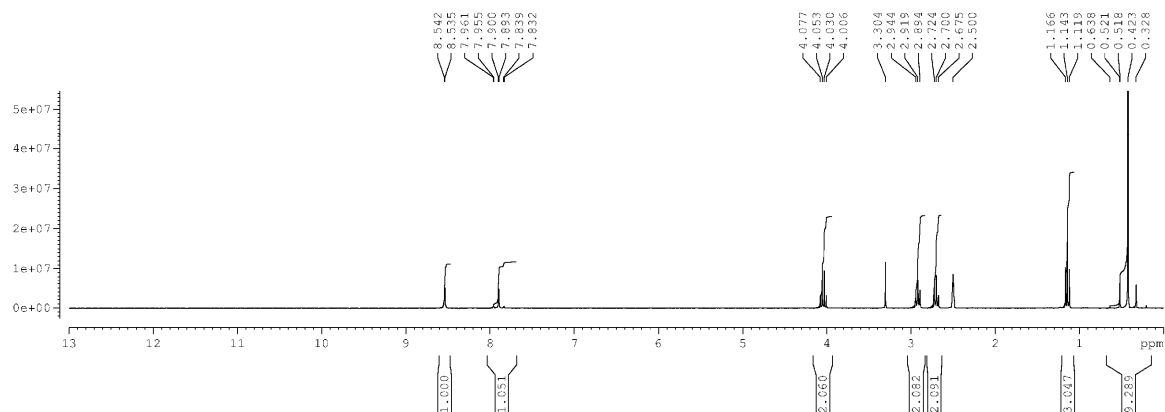
Figure 3.63: Scheme of successfully synthesized single pyridine building blocks.	76
Figure 3.64: Terpyridine derivatives 14a and 14b.	77
Figure 3.65: Overview of proposed synthesis of terpyridines 22a and 22b.	78
Figure 3.66: General scheme of proposed synthesis of terpyridines <i>via</i> [2+2+2] cycloaddition.	78
Figure 3.67: Scheme of proposed Pd-catalyzed cross-coupling of building blocks 6 and 7.	80
Figure 3.68: Scheme of the synthesis of bipyridine 12a by Suzuki-Miyaura coupling.	81
Figure 3.69: Scheme of the synthesis of bipyridine 12b by Suzuki-Miyaura coupling.	83
Figure 3.70: Schemes of the catalytic cycles that are proposed to be involved in Pd-catalyzed borylation of aryl halides. ^[40]	84
Figure 3.71; Scheme of the synthesis of boronate esters 21a and 21b.	85
Figure 3.72: Schematic representation of the synthesis of terpyridine 22b from boronate ester 21b and bromide 8d.	86
Figure 3.73: LC-chromatogram of crude 22b.	87
Figure 3.74: Scheme of the two-step one-pot procedure for the synthesis of terpyridine 22b.	88
Figure 3.75: Scheme of the two-step one-pot protocol for the synthesis of terpyridine 22b with chloride 8e as coupling partner.	90
Figure 3.76: Phosphine ligands L1-L4.	92
Figure 3.77: Scheme of the synthesis of terpyridine 22a.	96
Figure 3.78: ¹ H-NMR spectrum of 22a recorded in MeOD.	96
Figure 3.79: Scheme of the synthesis of terpyridine 22c.	97
Figure 3.80: Scheme of the synthesis of terpyridines 25a and 25b.	99
Figure 3.81: ¹ H-NMR spectrum of terpyridine 25b in MeOD.	100
Figure 3.82: Scheme of the synthesis of amine 26b and <i>N</i> -benzylamine 26c.	100
Figure 3.83: ¹ H-NMR spectrum of 26b recorded in MeOD.	102
Figure 3.84: ¹ H-NMR spectrum of 26c recorded in d ₆ -DMSO.	102
Figure 3.85: Scheme of the retrosynthesis of terpyridines 24a and 24b via [2+2+2] cycloaddition/Sonogashira coupling.	103
Figure 3.86: General scheme of the Sonogashira reaction. Adapted from ^[41]	104

List of figures

Figure 3.87: Proposed mechanism of Co-catalysed (left) and Ru-catalysed pyridines synthesis by [2+2+2] cycloaddition.	106
Figure 3.88: Scheme of the synthesis of nitrile 8a and proposed synthesis of terpyridine derivatives by [2+2+2] cycloaddition.	107
Figure 3.89: Scheme of the synthesis of diyne 23a.	109
Figure 3.90: Scheme of the synthesis of terpyridine 24a.	110
Figure 3.91: ¹ H-NMR spectrum of terpyridine 24a (obtained as pyridinium salt after HPLC purification) in d ₆ -DMSO.	111
Figure 3.92: Scheme of the synthesis of 12c-e.	112
Figure 3.93: Scheme of the synthesis of diynes 23b and 23c.	113
Figure 3.94: LC spectra of crude diyne 23a (left) and crude diyne 23b (right).	115
Figure 3.95: LC spectrum of the reaction mixture from the synthesis of methylester-diyne 23c.	115
Figure 3.96: Scheme of the synthesis of terpyridine 24b.	117
Figure 3.97: ¹ H-NMR spectrum of terpyridine 24b recorded in d ₆ -DMSO.	118
Figure 3.98: Scheme of the synthesis of amide 27.	120
Figure 3.99: ¹ H-NMR spectra from STD measurements of Rllalf-His with indicated compound.	123
Figure 3.100: HSQC spectra of D/D domain.	124
Figure 3.101: HSQC spectra of D/D domain.	124
Figure 4.1: Quaterpyridines 2c and 2d.	127
Figure 4.2: Scheme of the one-pot borylation/Suzuki coupling procedure.	128
Figure 4.3: Scheme of the [2+2+2] cycloaddition reaction for the synthesis of terpyridines.	129
Figure 4.4: Compounds 25a, 25b and Compounds 26b, 26c.	130
Figure 4.5: Scheme of the synthesis of di-halo building block 8k.	131

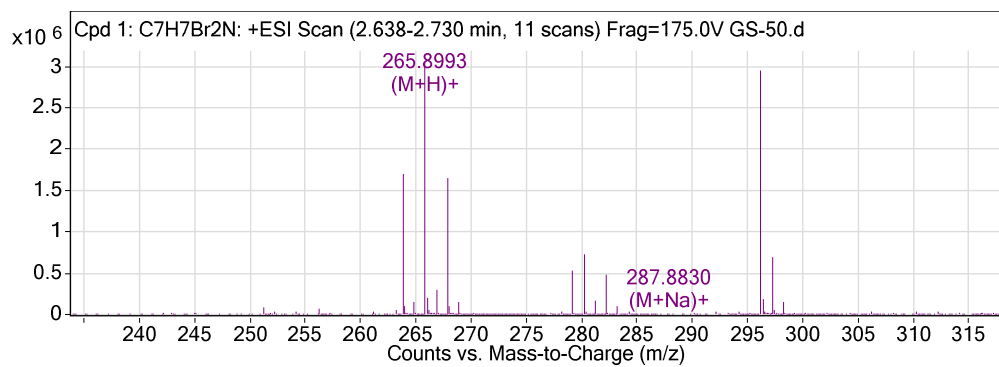
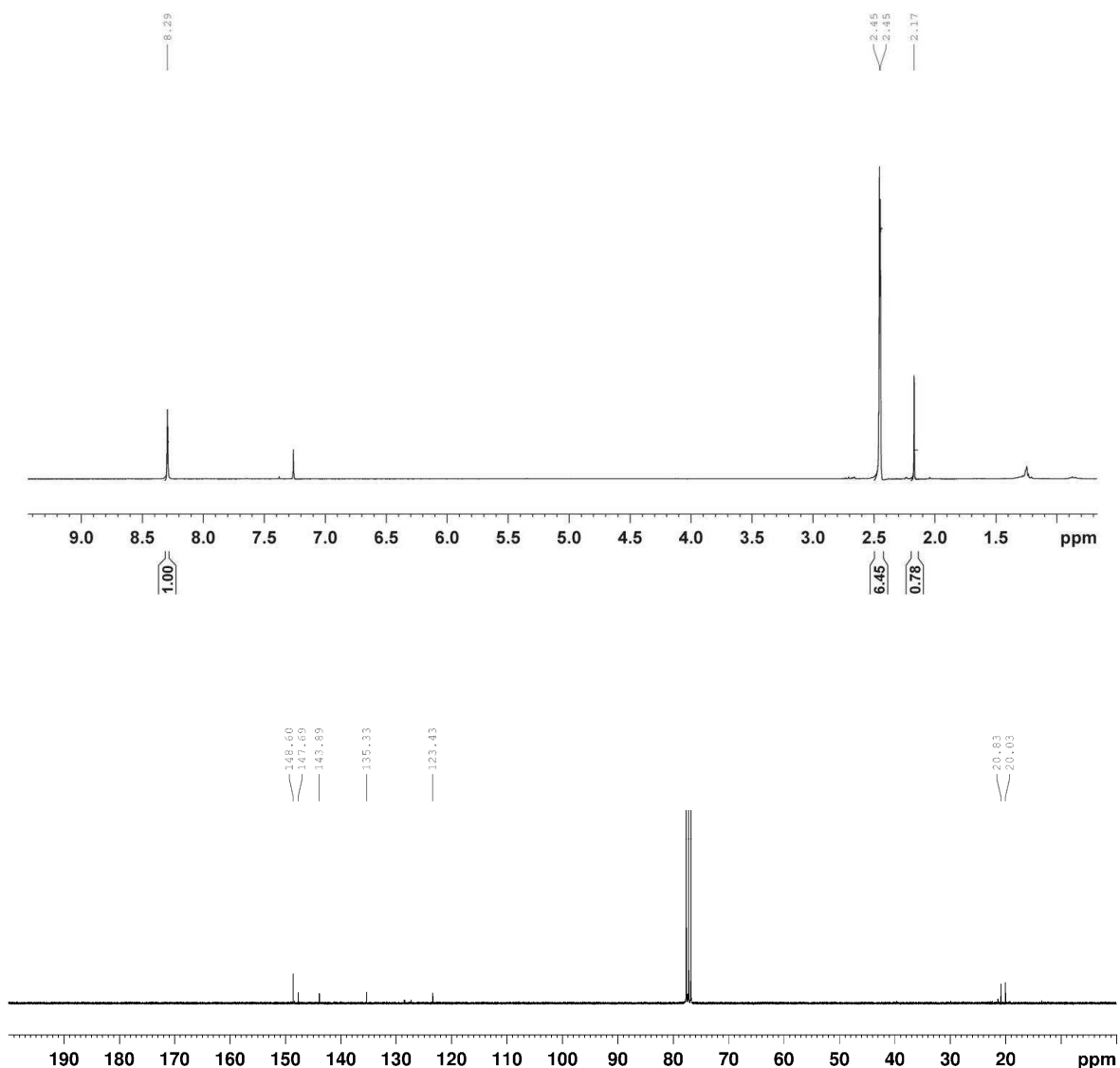
Attachment

6c: $^1\text{H-NMR}$ spectrum, $^{13}\text{C-NMR}$ spectrum (both in $\text{d}_6\text{-DMSO}$) and HRMS spectrum.



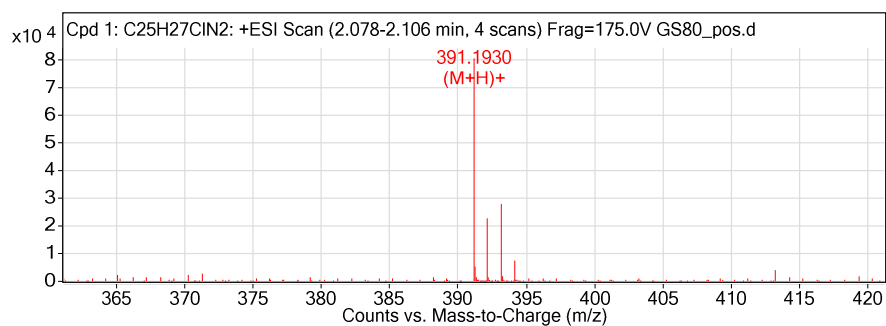
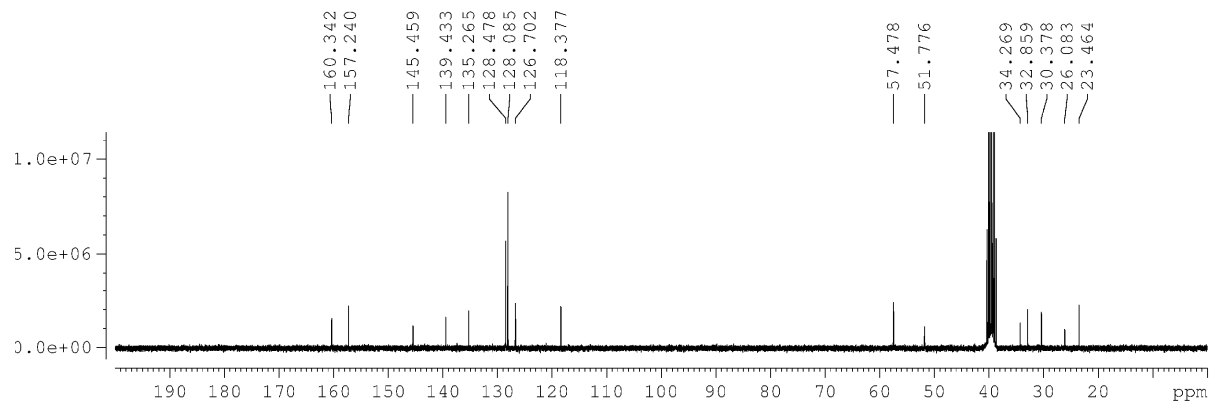
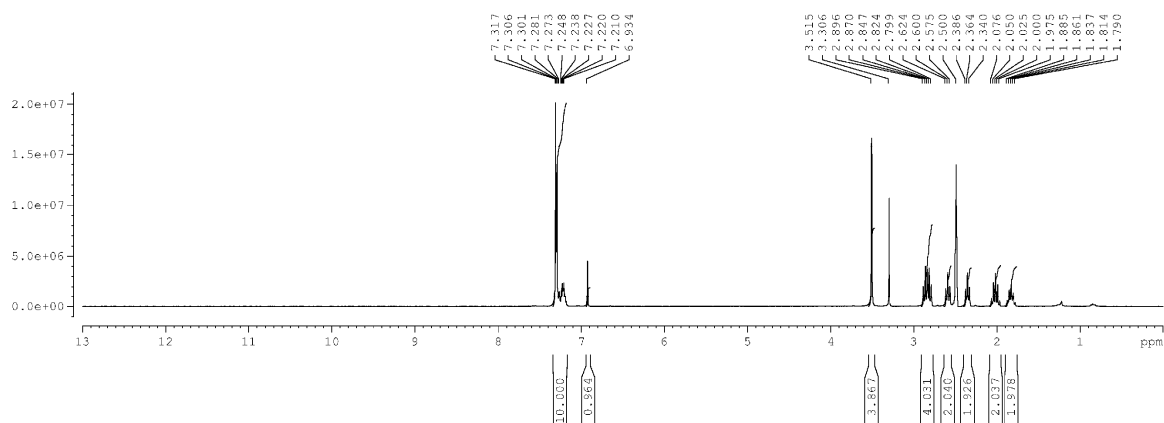
Attachment

7d: $^1\text{H-NMR}$ spectrum, $^{13}\text{C-NMR}$ spectrum (both in CDCl_3) and HRMS spectrum.



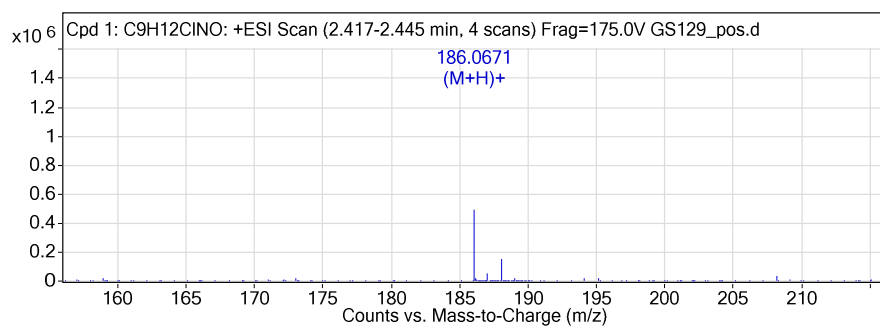
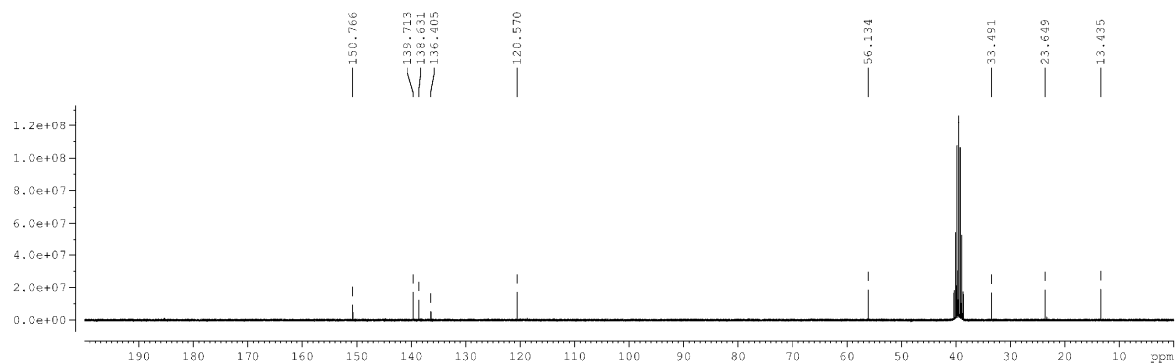
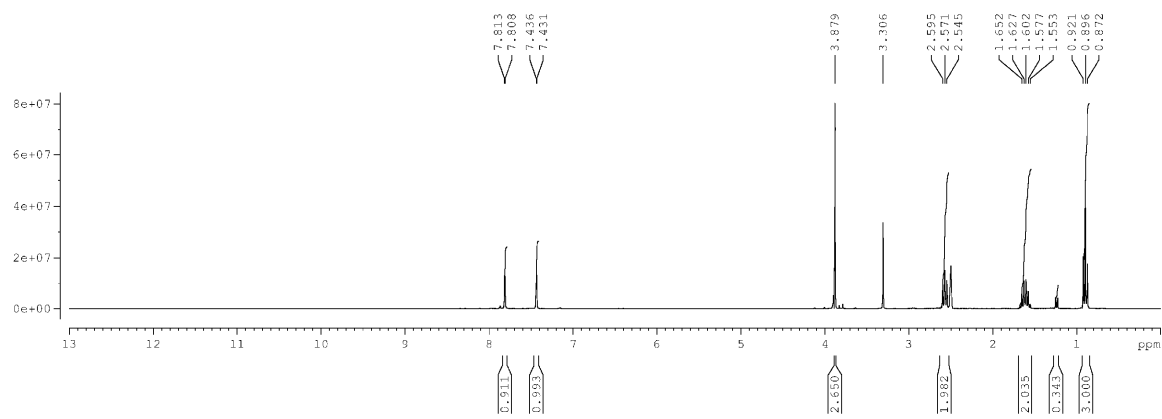
Attachment

8e: ^1H -NMR spectrum, ^{13}C -NMR spectrum (both in d_6 -DMSO) and HRMS spectrum.



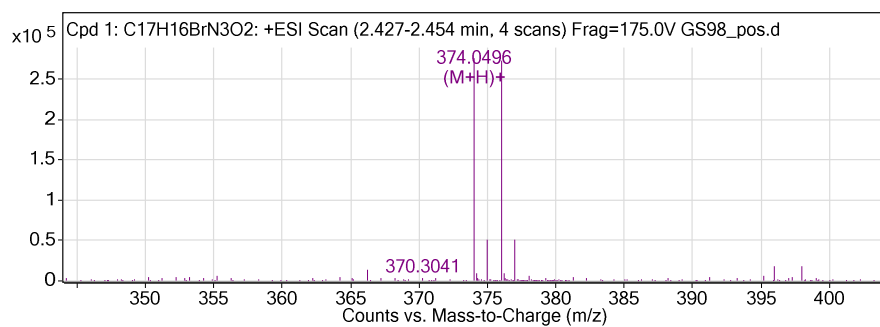
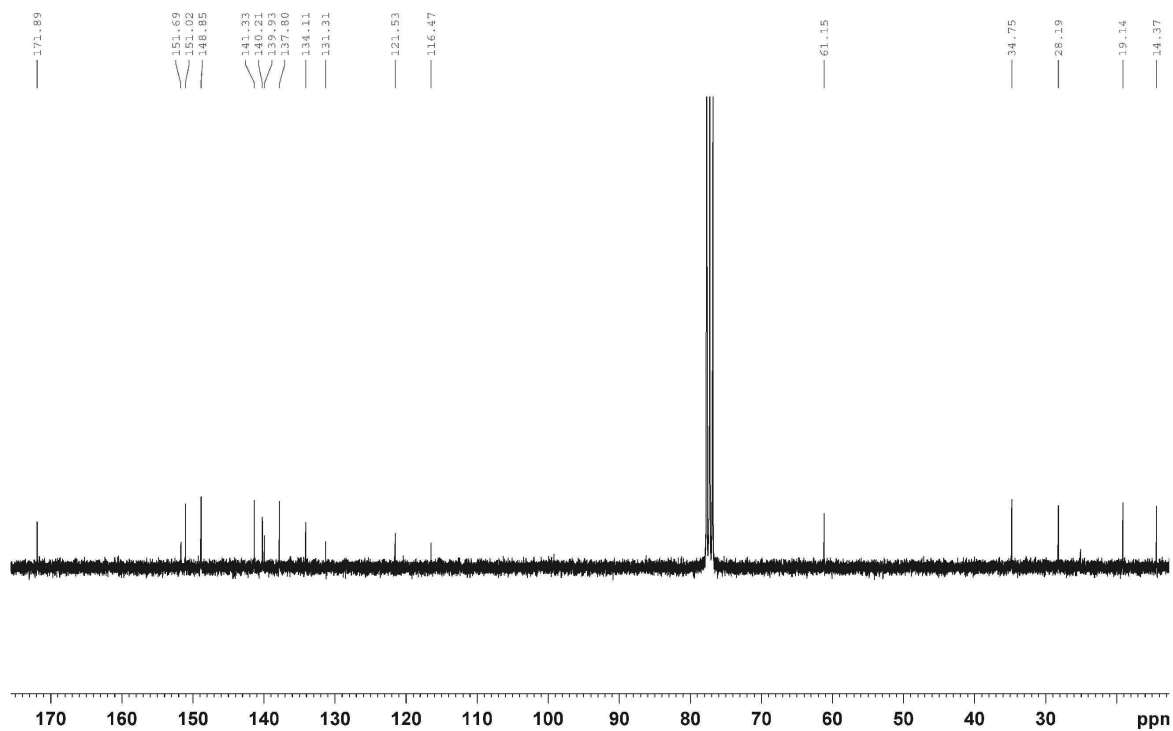
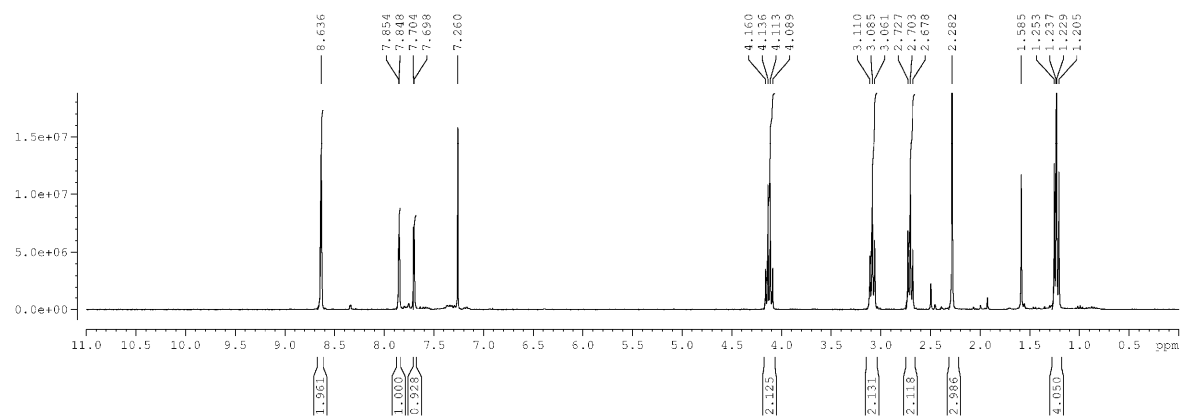
Attachment

9i: $^1\text{H-NMR}$ spectrum, $^{13}\text{C-NMR}$ spectrum (both in $\text{d}_6\text{-DMSO}$) and HRMS spectrum.



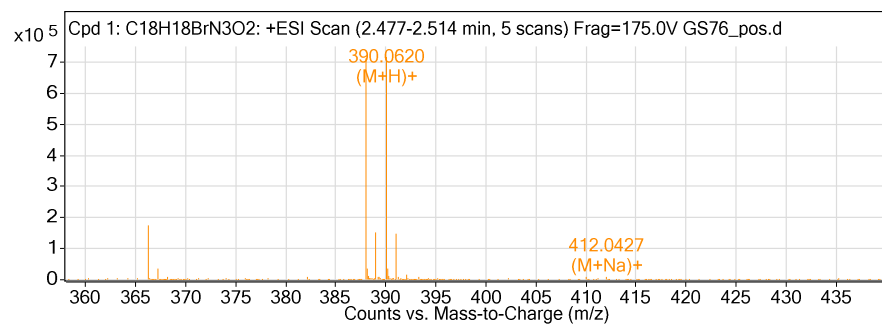
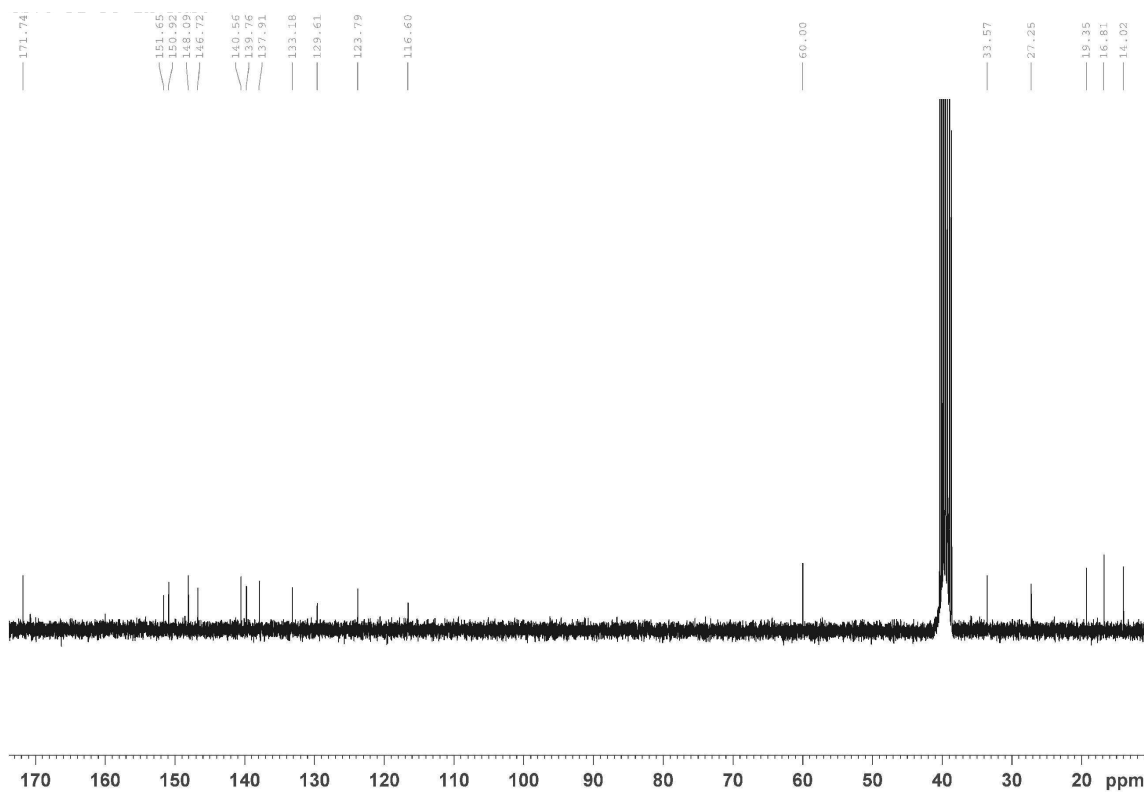
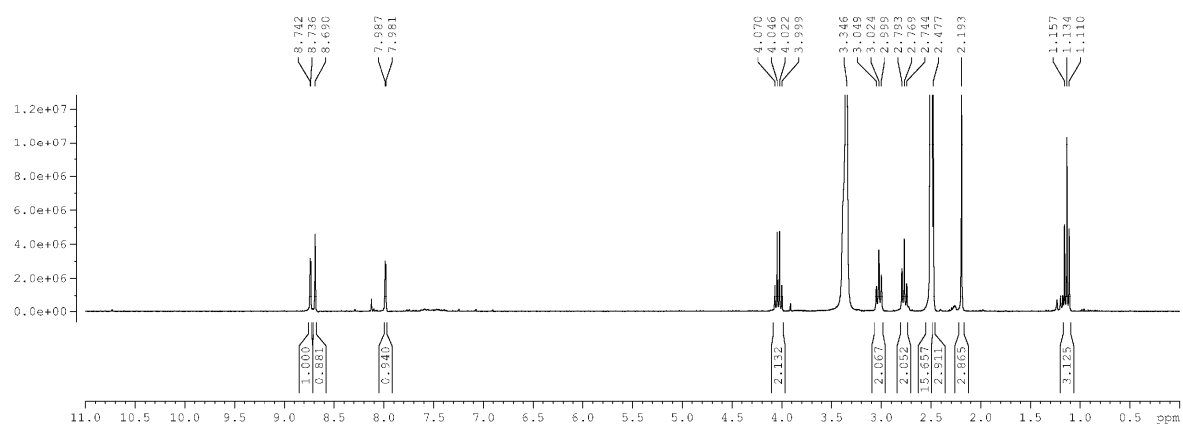
Attachment

12b: $^1\text{H-NMR}$ spectrum (in $\text{d}_6\text{-DMSO}$), $^{13}\text{C-NMR}$ spectrum (in CDCl_3) and HRMS spectrum.



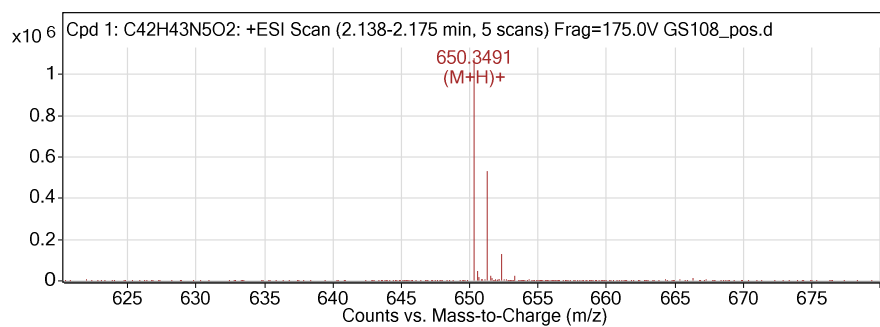
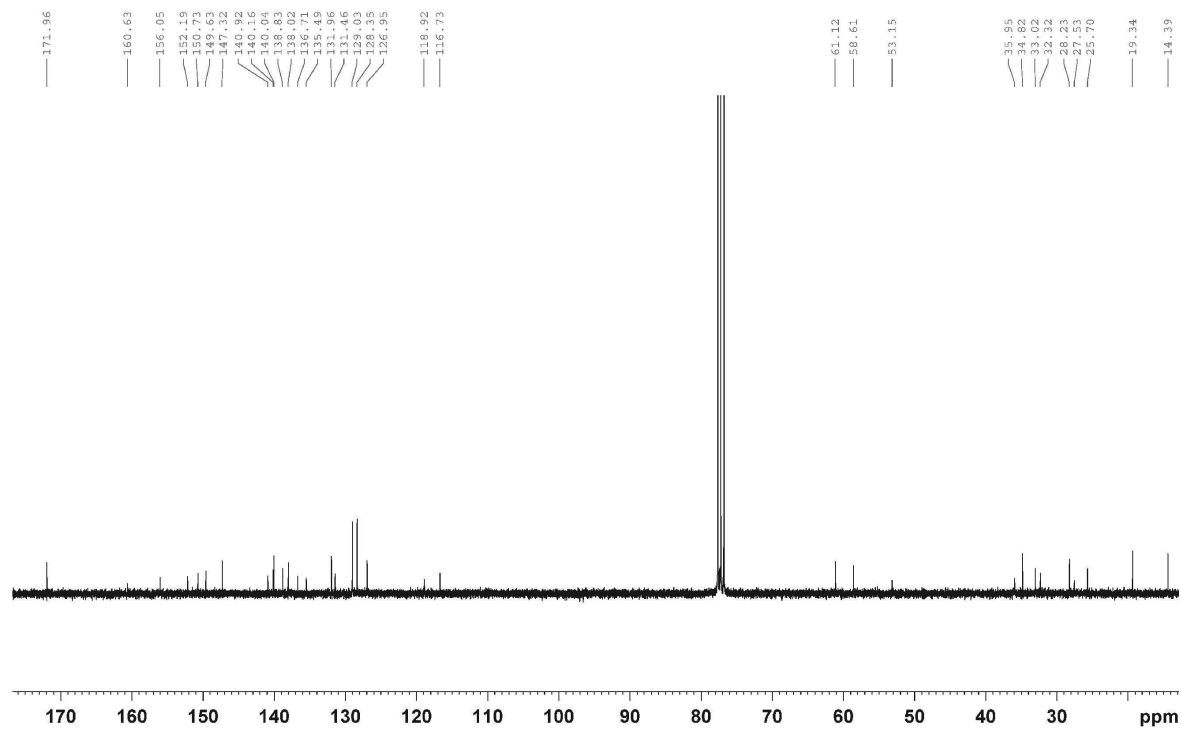
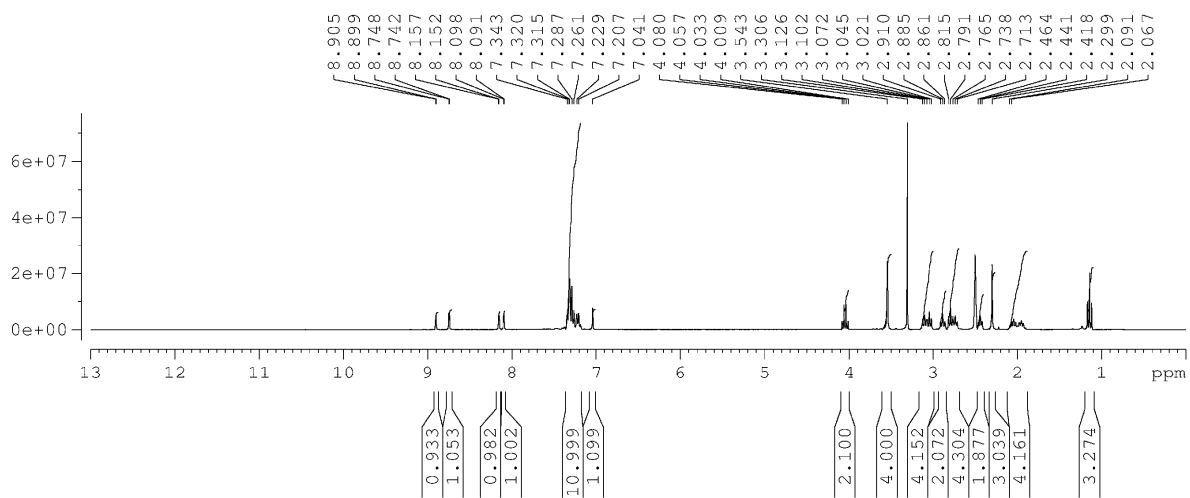
Attachment

12a: ¹H-NMR spectrum, ¹³C-NMR spectrum (both in d₆-DMSO) and HRMS spectrum.



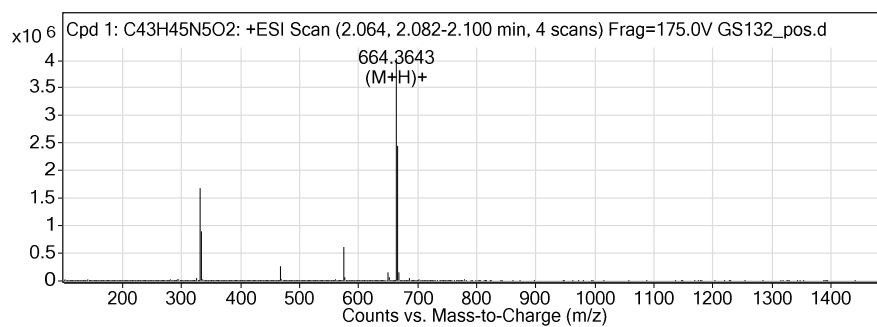
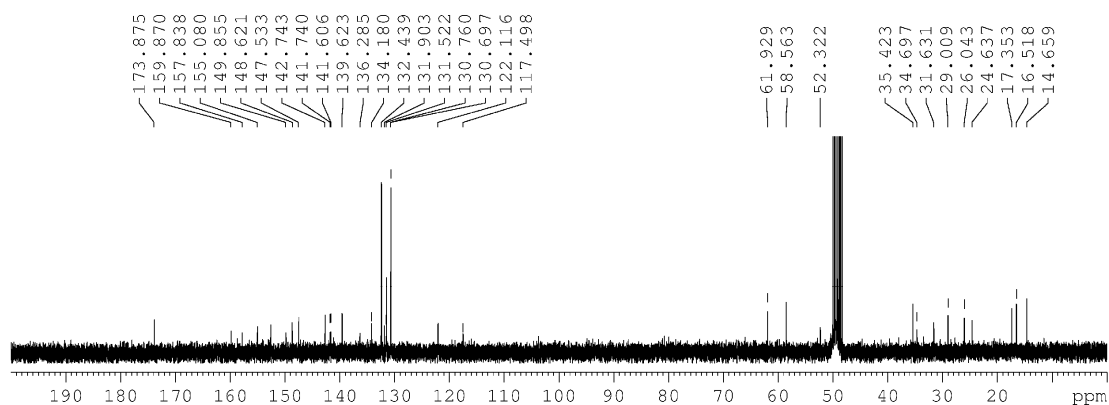
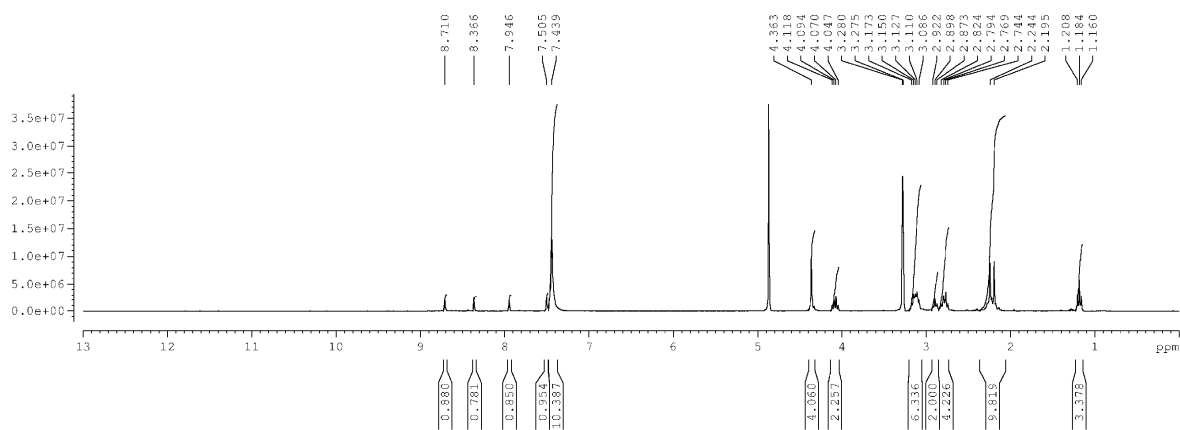
Attachment

22b: $^1\text{H-NMR}$ spectrum, $^{13}\text{C-NMR}$ spectrum (both in CDCl_3) and HRMS spectrum.



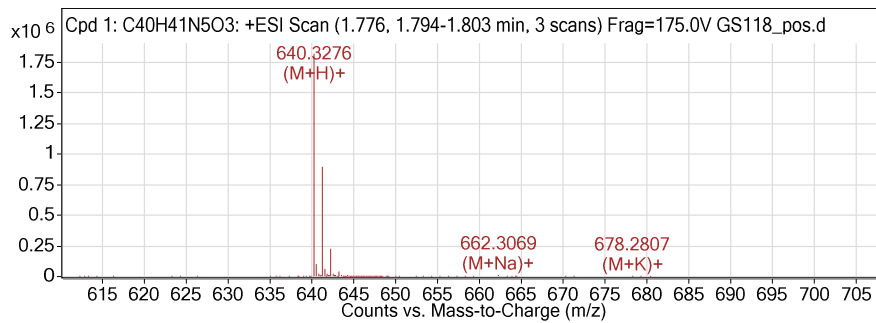
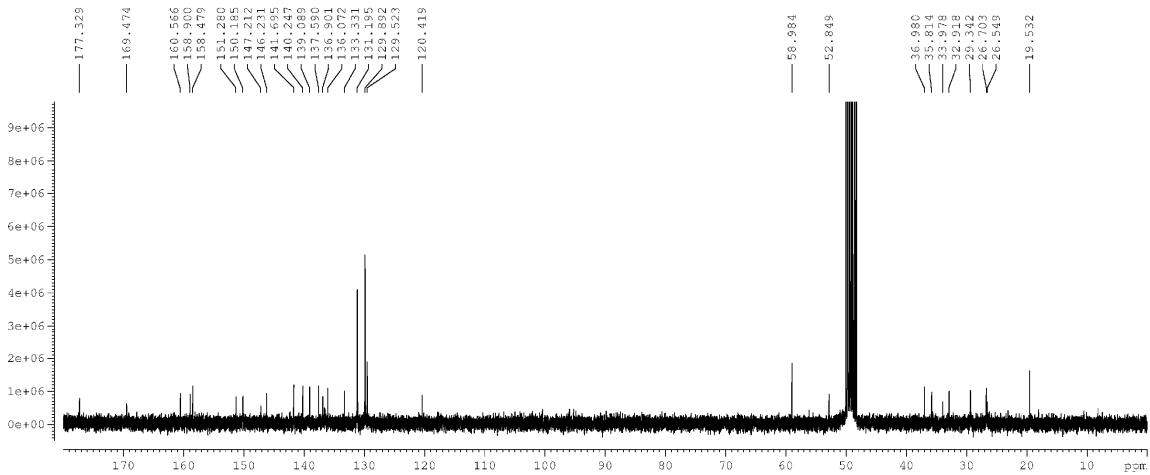
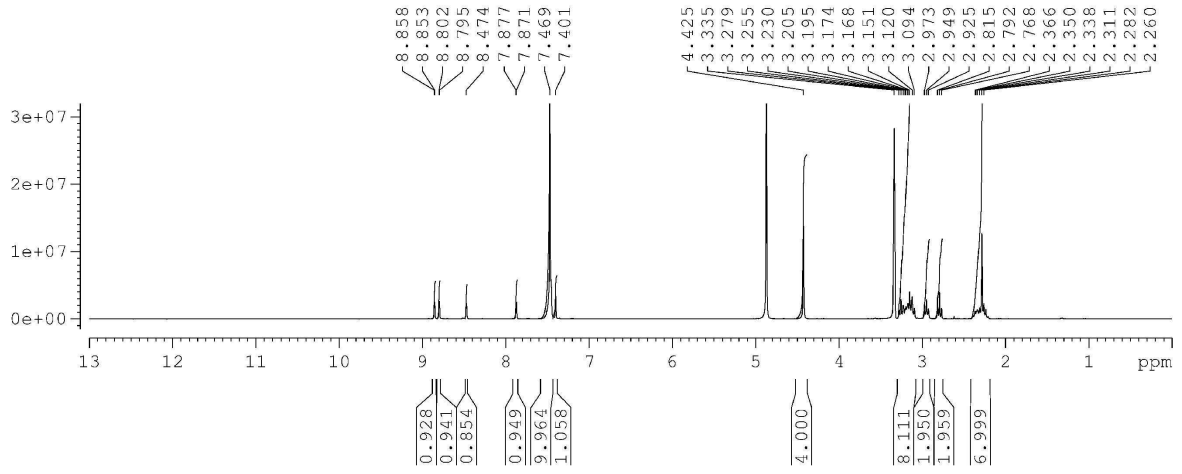
Attachment

22a: ¹H-NMR spectrum, ¹³C-NMR spectrum (both in MeOD) and HRMS spectrum.



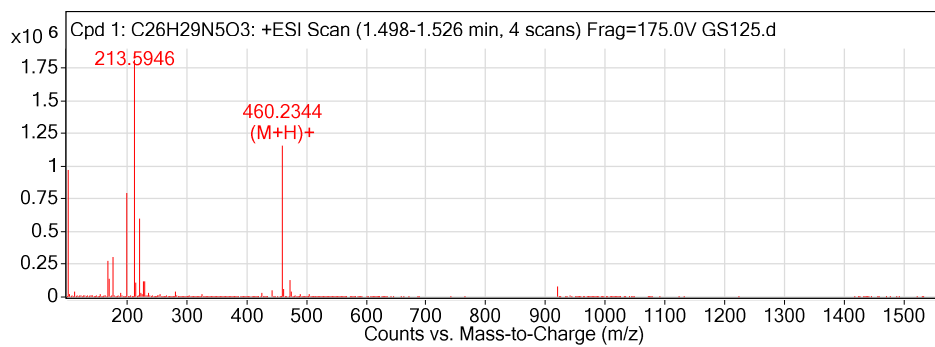
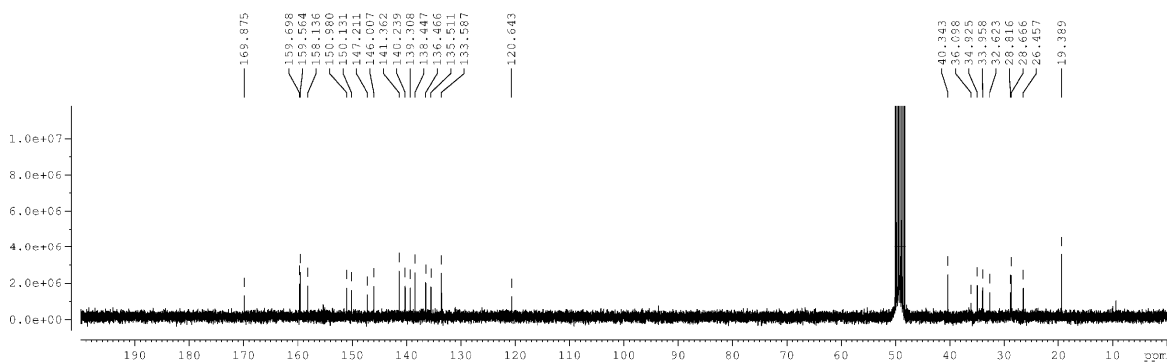
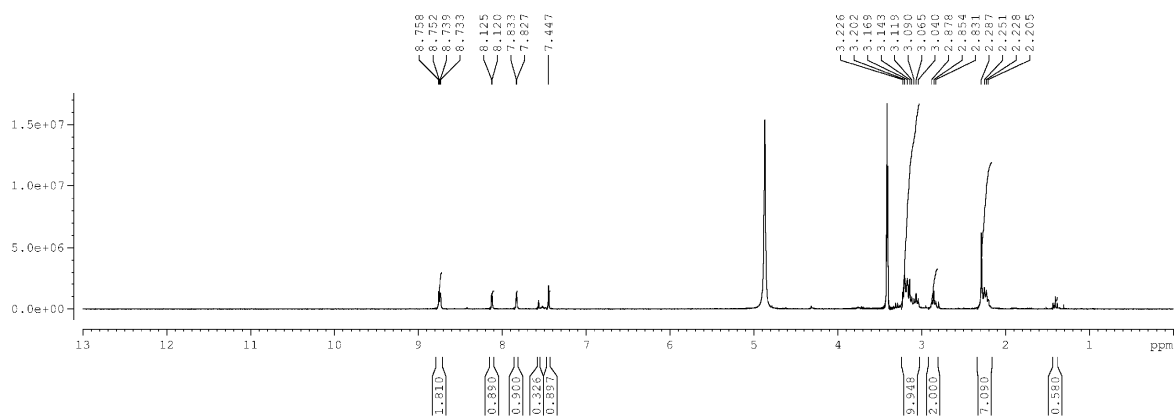
Attachment

25b: $^1\text{H-NMR}$ spectrum, $^{13}\text{C-NMR}$ spectrum (both TFA-salt in MeOD) and HRMS spectrum.



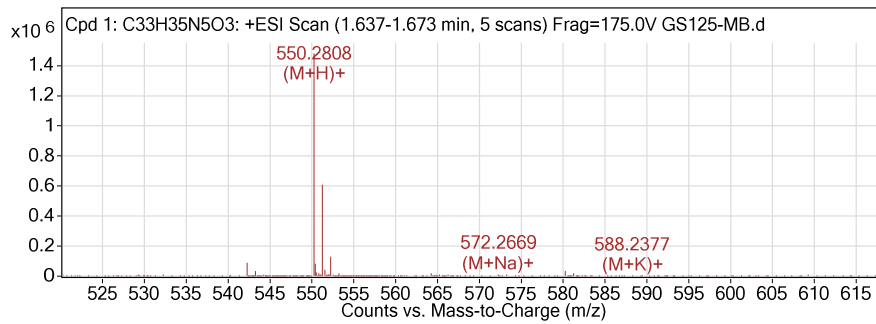
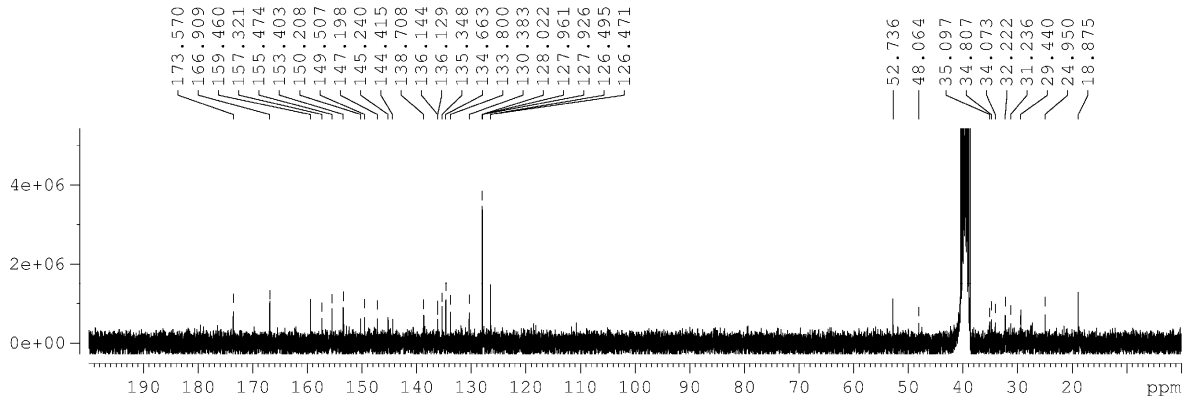
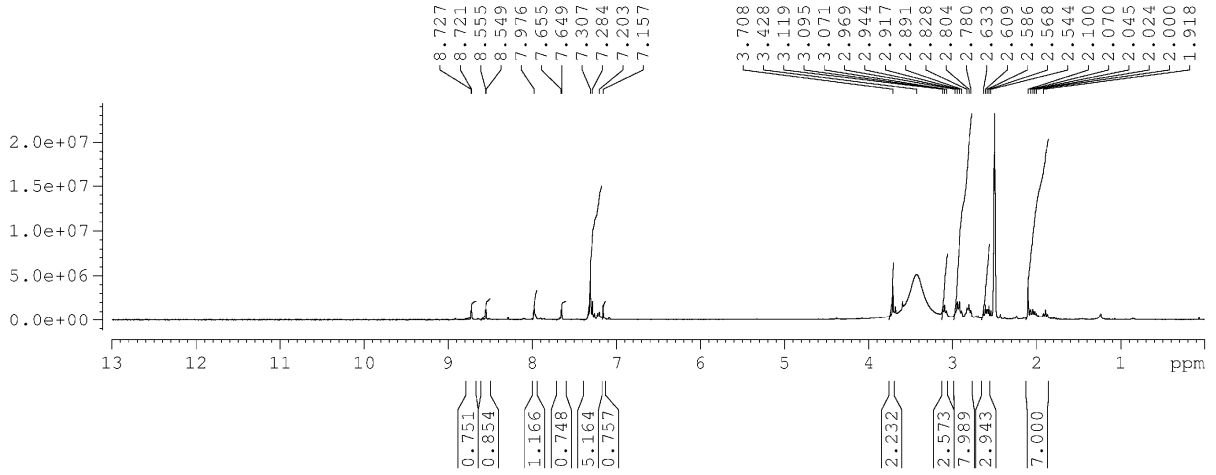
Attachment

26b: ^1H -NMR spectrum, ^{13}C -NMR spectrum (both in MeOD) and HRMS spectrum.



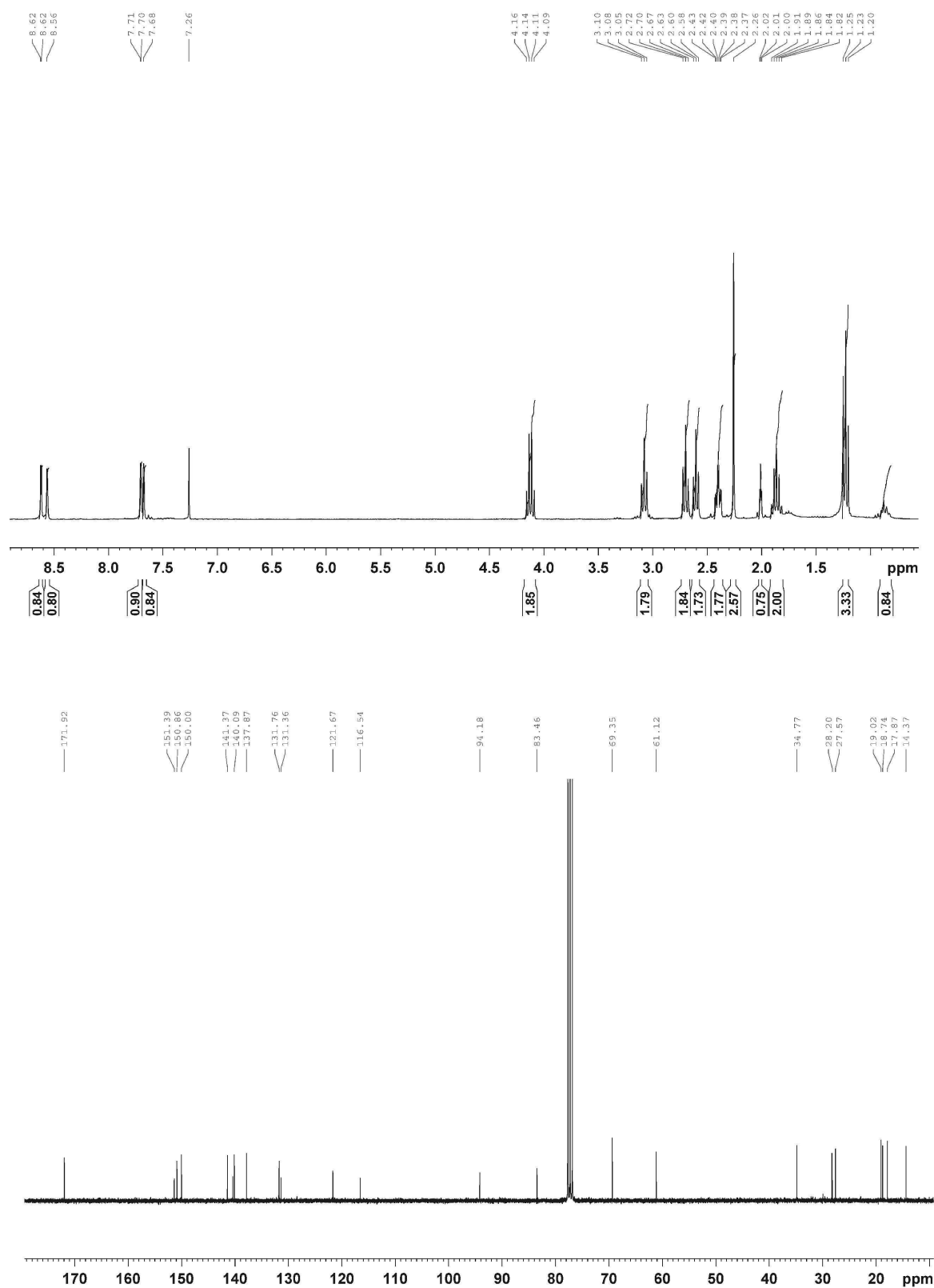
Attachment

26c: ^1H -NMR spectrum, ^{13}C -NMR (both in d_6 -DMSO) and HRMS spectrum.



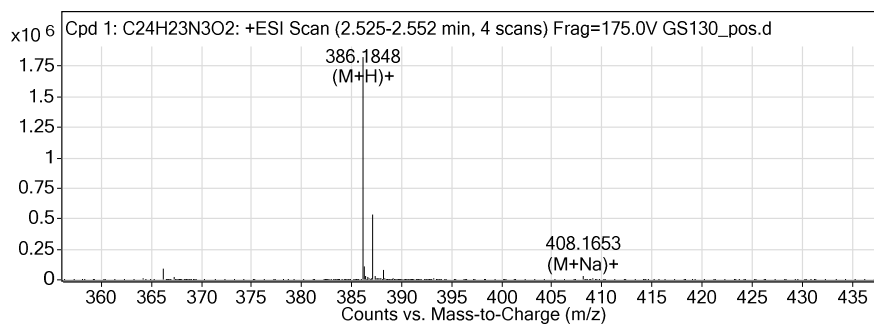
Attachment

23a: $^1\text{H-NMR}$ spectrum and $^{13}\text{C-NMR}$ spectrum (both in CDCl_3).



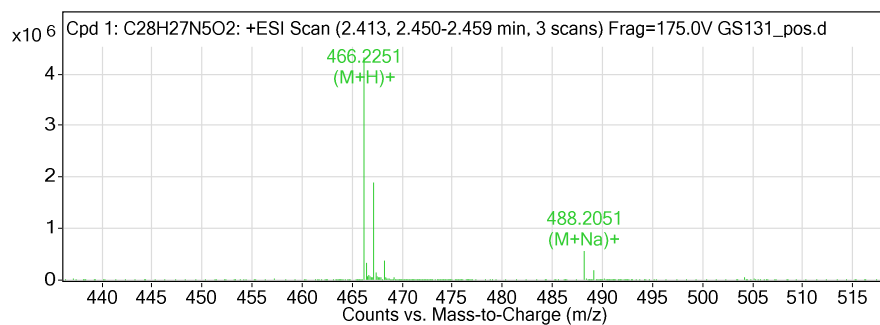
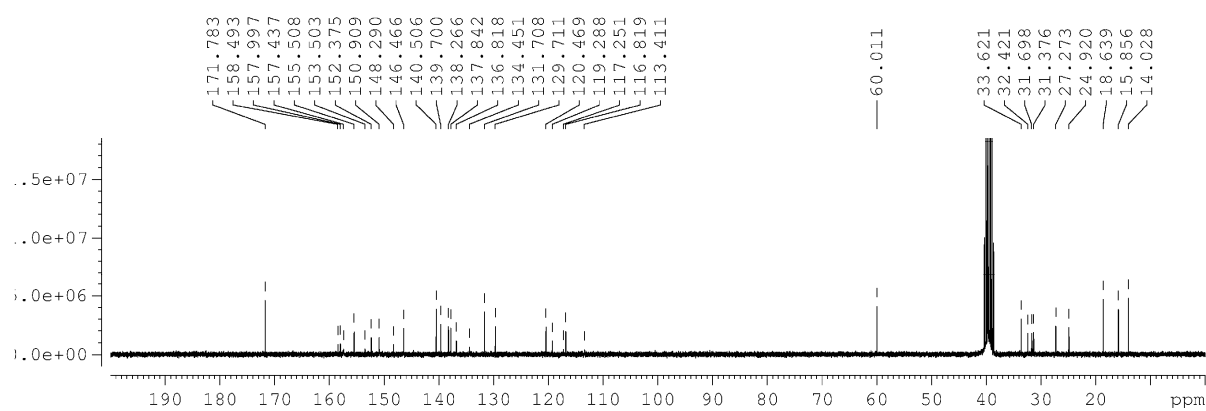
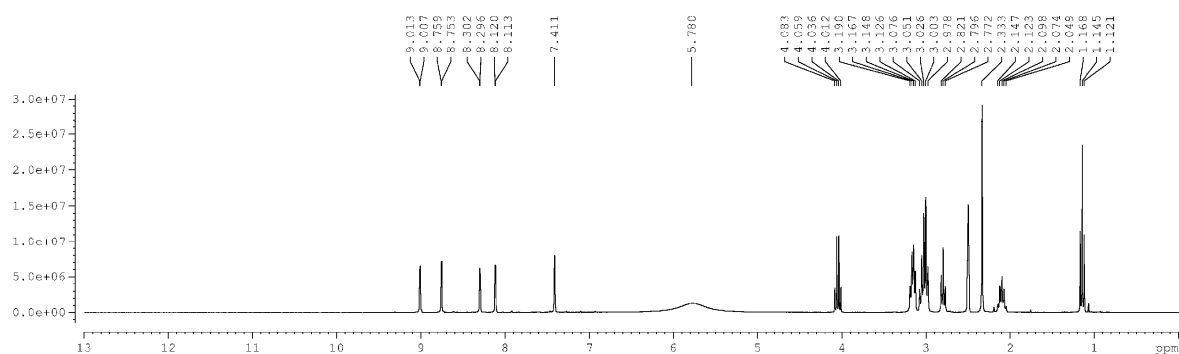
Attachment

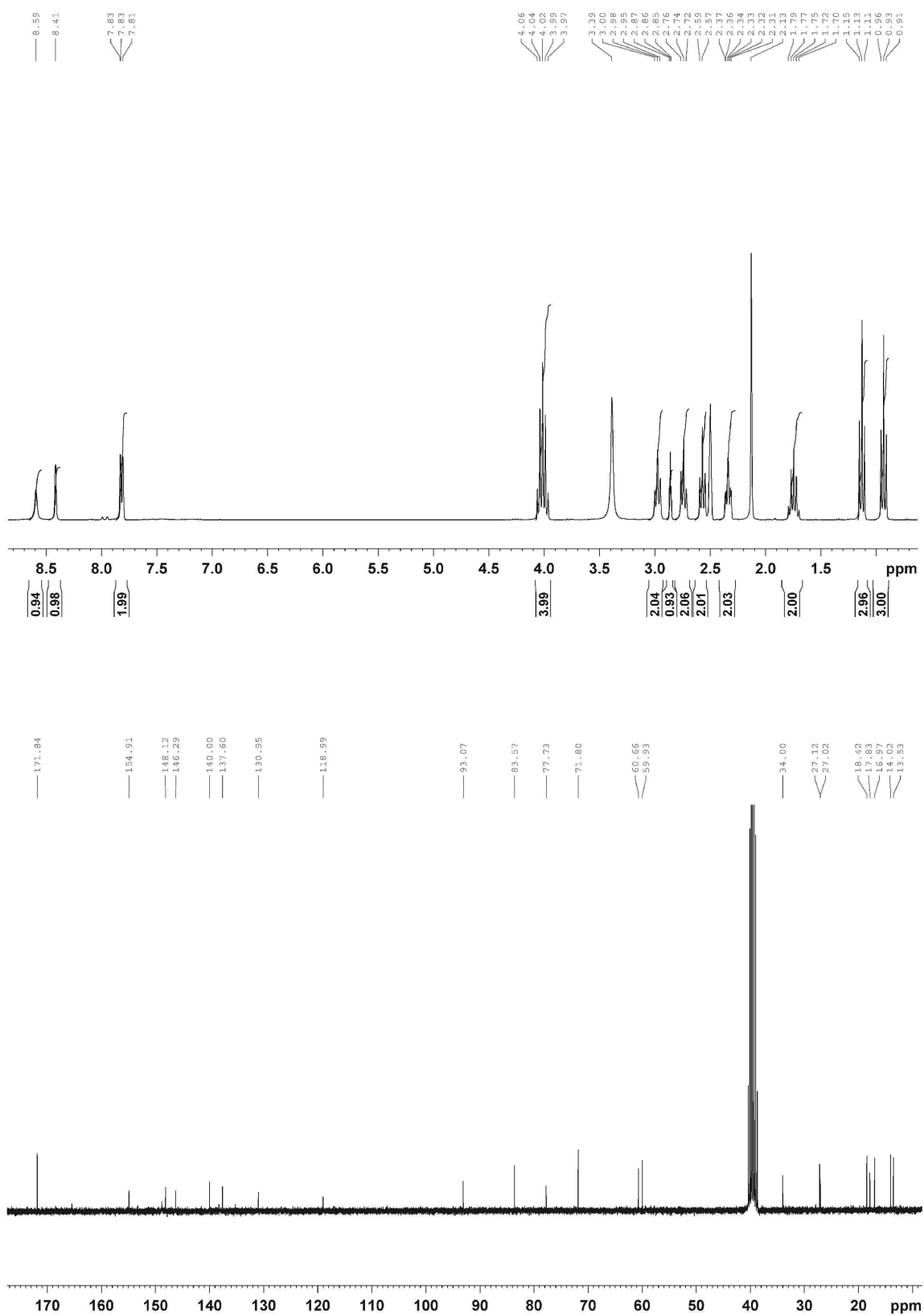
23a: HRMS spectrum.



Attachment

24a: $^1\text{H-NMR}$ spectrum, $^{13}\text{C-NMR}$ spectrum (both in $\text{d}_6\text{-DMSO}$) and HRMS spectrum.



23b: ^1H -NMR spectrum and ^{13}C -NMR spectrum (both in d_6 -DMSO).

23b: HRMS spectrum

